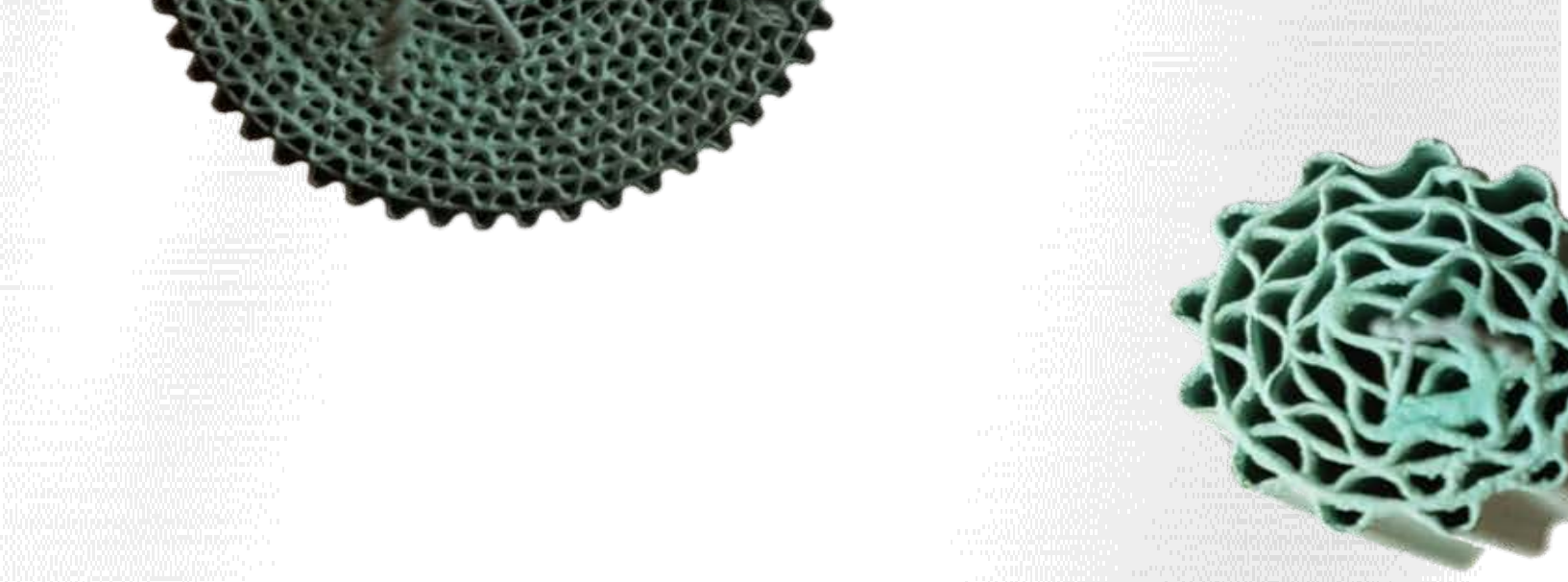

Direct synthesis of dimethyl ether from syngas in structured reactors

Iñigo Pérez Miqueo

Grupo de Ingeniería Química

Departamento de Química Aplicada

Facultad de Químicas, Donostia-San Sebastián

Donostia-San Sebastián, Octubre 2019

eman ta zabal zazu

Universidad del País Vasco
Euskal Herriko Unibertsitatea
The University of the Basque Country

eman ta zabal zazu

Universidad del País Vasco
Euskal Herriko Unibertsitatea

Direct synthesis of dimethyl ether from syngas in structured reactors

Grupo de Ingeniería Química

Departamento de Química Aplicada

Facultad de Químicas, Donostia-San Sebastián

Donostia-San Sebastián

Octubre 2019

Memoria presentada para optar al Grado de Doctor en Química por

Iñigo Pérez Miqueo

Bajo la dirección de

Prof. Mario Montes Ramírez y Oihane Sanz Iturralde

General Index

Resumen

El dimetil éter (DME) ha adquirido gran interés en las últimas décadas debido a su elevado índice de cetano (55-60) y a la reducción en la emisión de partículas y NOx en su combustión, presentándose como una alternativa limpia al diésel.

El DME puede sintetizarse a partir de gas de síntesis proveniente de fuentes de energía abundantes como el carbón y el gas natural pudiendo reducir la dependencia con el mercado del petróleo. Además, este compuesto también puede sintetizarse a partir de gas de síntesis proveniente de fuentes renovable como la biomasa, resaltando su interés en el desarrollo de biocombustibles de segunda generación (combustible verde).

La producción de DME a partir de gas de síntesis se ha llevado a cabo tradicionalmente mediante el método de dos etapas: en primer lugar, se sintetiza metanol a partir de gas de síntesis para posteriormente deshidratar ese metanol formado a DME.

Síntesis de metanol:	$2 \cdot CO + H_2 \longleftrightarrow CH_3OH$	($\Delta H° = -91$ kJ/mol)
Deshidratación de metanol:	$2 \cdot CH_3OH \longleftrightarrow CH_3OCH_3 + H_2O$	($\Delta H° = -23$ kJ/mol)
Reacción Water Gas Shift:	$CO + H_2O \longleftrightarrow H_2 + CO_2$	($\Delta H° = -41$ kJ/mol)
Reacción global:	$3 \cdot CO + 3 \cdot H_2 \longleftrightarrow CH_3OCH_3 + CO_2$	($\Delta H° = -246$ kJ/mol)

En el siglo XXI, la producción de DME a partir de gas de síntesis en una única etapa o síntesis directa de DME ha adquirido notoriedad. De esta manera, se obtiene un sistema más sencillo y económico al emplear un único reactor para llevar a cabo las dos reacciones (síntesis de metanol + deshidratación de metanol). Pero, sobre todo, se elimina la limitación del equilibrio termodinámico de formación de metanol al ir deshidratando éste conforme se genera, obteniendo un sistema más eficiente.

El carácter exotérmico de la síntesis directa de DME requiere de sistemas con un adecuado control de la temperatura que eviten disparos térmicos que aumenten la peligrosidad de los sistemas de reacción. Además, el empleo común de catalizadores basados en cobre para la etapa de síntesis de metanol, aumenta

la necesidad de un buen control de la temperatura en el reactor para evitar problemas de sinterizado del cobre.

Los reactores estructurados metálicos pueden resultar interesantes para la síntesis directa de DME. La fina capa de catalizador depositada en los canales del sustrato estructurado, junto con la elevada conductividad proporcionada por el propio sustrato metálico pueden mejorar la transferencia de materia y calor en el sistema. Además, la geometría de canales abiertos en los que se basan estos sustratos permite trabajar con flujos elevados con bajas pérdidas de carga. Sin embargo, la obtención de buenas adherencias de la capa catalítica al sustrato metálico puede ser compleja. En el método de recubrimiento por inmersión (o washcoating), la preparación de la suspensión es una de las etapas más importantes, requiriendo comúnmente del empleo de aditivos para obtener unas propiedades de recubrimiento adecuadas, que en ocasiones pueden alterar también las propiedades catalíticas del catalizador de partida.

En la presente tesis doctoral, se han preparado diferentes formulaciones para las suspensiones de los dos catalizadores necesarios para la síntesis directa de DME: el catalizador de síntesis de metanol ($Cu/ZnO/Al_2O_3$, CZA) y el catalizador de deshidratación de metanol (zeolita ZSM-5), tanto de forma separada como mezclados conjuntamente en una misma suspensión. De este modo, se pudieron obtener las formulaciones apropiadas para poder estudiar el comportamiento de los catalizadores estructurados en la síntesis directa de DME.

Catalizador de síntesis de metanol, CZA

Con el fin de mejorar las propiedades de recubrimiento de las suspensiones del catalizador, se emplearon diferentes coloides inorgánicos como aditivos: Al_2O_3, ZnO y SiO_2.

Los resultados mostraron la necesidad del empleo de coloides inorgánicos como aditivos para obtener unos recubrimientos homogéneos y adherentes. Estos coloides permiten generar puntos de anclaje tanto entre las propias partículas del catalizador (cohesión), como entre la capa catalítica y el sustrato (adhesión). El efecto positivo se ve mejorado cuanto mayor es la cantidad de coloide empleada.

No obstante, la adición de estos coloides inorgánicos al catalizador inicial modifica las propiedades catalíticas del sólido resultante. La superficie metálica de cobre se vio notablemente reducida con la adición de los coloides debido a un

incremento del tamaño de cristal de Cu^0 cuando se aumentaba su contenido. Por otro lado, el carácter ácido de la alúmina genera una deshidratación del metanol a DME, disminuyendo la selectividad del primero, al igual que ocurre con la adición de SiO_2 coloidal, aunque en mucha menor medida.

La utilización de ZnO coloidal, por el contrario, disminuyó la poca cantidad de DME generada por el catalizador CZA, incrementando ligeramente la selectividad a metanol. No obstante, este coloide modifica en mayor medida la superficie de cobre disponible, disminuyendo la actividad global del catalizador final.

Por lo tanto, en la búsqueda de un compromiso entre obtener buenas adherencias y mantener las propiedades catalíticas del catalizador de partida, la formulación con un 10% de alúmina coloidal fue la que mejor resultado mostró.

Catalizador de deshidratación de metanol, zeolita ZSM-5

Como catalizador ácido para la deshidratación de metanol se empleó una zeolita comercial ZSM-5. Debido a la acidez requerida para deshidratar el metanol a DME, en dicha reacción se estudió el efecto del estado en el que era suspendida la zeolita (amoniacal o protónico) y la temperatura a la que debía ser calcinada para obtener su fase protónica (forma ácida).

Los resultados indicaron la necesidad de suspender la zeolita en su estado protónico o bien calcinarla a 500 °C, ya que a temperaturas inferiores y/o suspendida en estado amoniacal, se mostró un descenso de la actividad. Según análisis termogravimétricos y de TPD de NH_3, se pudo observar como el polivinil alcohol (PVA), que se adiciona a la suspensión para mejorar sus propiedades reológicas y el secado, no se elimina totalmente a 400 °C y esto podría generar un impedimento del cambio de fase (de amoniacal a protónico) a la hora de realizar el tratamiento térmico.

Mezcla de los catalizadores CZA + ZSM-5

El contacto de las dos fases activas en la síntesis directa de DME es un factor a tener en cuenta. Se estudiaron diferentes arquitecturas de los catalizadores en el lecho (sub-lechos de diferente composición y lechos uniformes) y diferentes métodos de mezcla (mezcla física y en suspensión). Los resultados mostraron el

mejor contacto de la mezcla en suspensión frente a la mezcla física y las diferentes arquitecturas estudiadas.

De esta manera, al igual que se realizó con el catalizador CZA, se estudiaron diferentes formulaciones de la suspensión conjunta de los catalizadores CZA y HZSM-5 empleando como aditivos diferentes coloides inorgánicos (Al_2O_3, SiO_2 y ZnO) y contenidos de los mismos.

Con el conocimiento de los estudios realizado con la estructuración de los catalizadores por separado se seleccionaron las formulaciones a estudiar, siendo aquellas con las que se obtuvieron las mejores adherencias. Todas estas formulaciones presentaron buenas adherencias (>80%). Sin embargo, se manifestaron cambios significativos en la actividad catalítica de la síntesis directa de DME.

La adición de óxido de zinc mostró una notable reducción de la acidez de la zeolita lo que se tradujo en una desactivación del catalizador ácido, reduciendo la deshidratación de metanol a DME y en consecuencia el desplazamiento del equilibrio de formación de metanol (reduciéndose la X_{CO}).

Por otro lado, la presencia de SiO_2 coloidal produjo selectividades similares al catalizador de referencia, pero con menor conversión de CO. Un estudio de la cantidad adicionada de SiO_2 coloidal mostró una mejora de la conversión con la disminución de la cantidad de sílice empleada debido a un menor cambio de las propiedades fisicoquímicas del catalizador inicial. No obstante, dicha reducción de la cantidad de coloide suponía una reducción drástica de la adherencia (≈40%).

Sin embargo, el empleo de Al_2O_3 coloidal como aditivo mostraba unos resultados satisfactorios en actividad. La adición de Al_2O_3 coloidal no modifica en gran medida las propiedades catalíticas finales del catalizador. Por lo tanto, se obtuvieron unos rendimientos similares al catalizador de partida (sin coloides inorgánicos) tanto en la conversión de CO como en las selectividades. Además, la buena adherencia mostrada por este coloide permitió emplear menores cantidades del coloide en la formulación con adherencias igualmente adecuadas (> 80%).

Catalizadores estructurados para la síntesis directa de DME

Tras conocer las formulaciones más apropiadas para la estructuración de los catalizadores de la síntesis directa de DME, se prepararon diferentes catalizadores estructurados variando la geometría (monolitos de canal longitudinal de diferente densidad de celda y espumas de porosidad abierta) y la aleación del sustrato (FeCrAl, latón y aluminio).

Con ello se pudo observar que ni la forma ni la aleación del sustrato modificaban sensiblemente la conversión de CO y las selectividades obtenidas. El buen comportamiento de los sustratos metálicos permitió trabajar en condiciones prácticamente isotermas con todas las aleaciones usadas y con diferentes fracciones huecas. Tampoco se apreciaron problemas de difusión interna con el cambio de espesor de capa ni modificaciones en la actividad catalítica con un cambio de régimen de flujo.

Por otro lado, gracias a la gran versatilidad del método de recubrimiento por inmersión, se prepararon diferentes arquitecturas de los catalizadores sobre los monolitos (capas independientes de los catalizadores). Sorprendentemente, la disposición de la capa del catalizador de síntesis de metanol (CZA) sobre el catalizador ácido (HZSM-5) mostró los mejores resultados, similares a la mezcla en suspensión de ambos catalizadores. El recubrimiento de la capa de zeolita sobre la del catalizador de síntesis de metanol produjo un descenso de la conversión de CO y un aumento de la selectividad a sub-productos (hidrocarburos), agravándose dicho comportamiento con el incremento del espesor de las capas.

Finalmente, valiéndonos de la conductividad térmica de los monolitos de latón, se pudo incrementar la productividad volumétrica de DME (intensificación) variando condiciones en el sistema como la carga volumétrica de catalizador en el monolito y las condiciones de reacción (temperatura de reacción y velocidad espacial). La productividad de DME se incrementó 4 veces con respecto a los monolitos de partida (con una carga volumétrica de 0,16 cm^3/g, T=260 ºC y velocidad espacial de 1,7 $L_{syn}/g_{cat}·h$) empleando una carga volumétrica del doble (0,33 g/cm^3) y una temperatura de 300 ºC y una velocidad espacial de 3,4 $L_{syn}/g_{cat}·h$. Mayores temperaturas de reacción producían un incremento de la deshidratación a sub-productos (hidrocarburos).

Síntesis de catalizadores bifuncionales

Se estudió la preparación de nuevos catalizadores bifuncionales para la síntesis directa de DME, en colaboración con la estancia realizada en el laboratorio del Prof. Andrei Khodakov (Universidad de Lille). Se estudiaron diferentes métodos de síntesis basados en la dispersión de partículas de cobre en una matriz de un sustrato ácido.

Aunque se consiguió sintetizar zeolita alrededor de partículas de cobre mediante 3 métodos diferentes, los catalizadores obtenidos presentaron una muy

baja superficie metálica de cobre que producía actividades bajas o casi nulas en la hidrogenación de CO.

El confinamiento de partículas de cobre en SBA-15, por el contrario, permitió obtener partículas de cobre bien dispersas con buenos resultados de actividad en la síntesis de metanol. Sin embargo, la necesidad de centros ácidos en el sustrato para deshidratar el metanol generado requiere una modificación en el mismo. La modificación de SBA-15 con aluminio proporcionó una acidez al soporte, permitiendo deshidratar el metanol generado a DME. Sin embargo, la dispersión de cobre sobre el soporte ácido no fue satisfactoria y la superficie metálica de cobre se vio notablemente alterada, produciendo bajas conversiones de CO.

Abstract

Dimethyl ether (DME) is a promising alternative to diesel fuel due to its high cetane number and the reduction of pollutant emission to the atmosphere in the combustion such as particle matters and NO_x. The traditional way of synthesising DME from syngas has been carried out via two-step method in which the methanol is first synthesised from syngas to finally dehydrate it to DME. However, in the last century the synthesis of DME from syngas via one-step, also referred to as direct synthesis of DME, has acquired interest. This synthesis route consist of an easier and cheaper system than the traditional two-step route due to the requirement of one reactor instead of two, but above all, the reaction yield is improved due to the removal of the thermodynamic equilibrium limitation of methanol synthesis reaction.

The metallic structured reactors can be interesting for this exothermic reaction, in which the temperature control of the system is an essential factor to take into account due to the use of Cu-based catalysts, which are sensitive to sintering. The thin layer of the catalyst in the substrate and the conductivity of the metallic substrate itself may improve the mass and heat transfer of the system as well as they allow to work with high flows with low pressure drops.

Nevertheless, the adherence of the catalytic layer on a metallic substrate could be challenging. In this work, numerous slurry formulation were studied achieving good coating properties for structured catalysts preparation of the two catalysts involved in the direct synthesis of DME ($Cu/ZnO/Al_2O_3$ catalysts (CZA) and ZSM-5 zeolite) separately, as mixed in the same slurry. The inorganic oxide colloids (Al_2O_3, ZnO, SiO_2) act as a binder and the results showed the need of using them in slurry formulation to obtain good adherence between the catalyst layer and the substrate in all cases. However, the use of additives in the slurry formulation produced changes in the catalytic properties of the parent catalyst. This effect is worsened by increasing the amount of colloid added. The colloidal alumina was the colloid that presents the best performance between maintaining catalytic properties of the parent catalysts and obtaining good adherence with lower contents.

Moreover, it was shown that an intimate contact between catalysts (CZA catalysts and ZSM-5 zeolite) is needed for achieving good performances in the direct synthesis of DME. Structured catalysts were successfully prepared with

different geometry and alloy substrates. Similar reaction yield to the powder catalysts were obtained with a good control of the system, working in almost isotherm reactor. Due to this good performance of structured catalysts, the DME volumetric productivity was increased 4 times in the brass monoliths (intensification) by changing the catalyst load and reaction conditions (temperature and space velocity).

Finally, in the 3-month-stay in University of Lille different bifunctional Cu-based catalysts synthesis methods were carried out. However, the synthesised catalysts presented low copper surface area (both due to loss of active phase and low metal dispersion) that make the method unsuitable for the reaction.

Table List

Figure List

CHAPTER 4

CHAPTER 6

APPENDIX

CHAPTER 1

Introducción general

ÍNDICE

1.1. Antecedentes

El crecimiento del sector industrial y el progreso de los países en vías de desarrollo están generando un continuo incremento de la demanda energética. La Agencia Internacional de Energía (AIE) estima que la demanda de energía aumente en un 30% de aquí al 2040 [1]. El agotamiento de los yacimientos de petróleo junto con la dependencia de su mercado, impulsan la búsqueda y desarrollo de fuentes alternativas al petróleo para poder abastecer las futuras demandas energéticas. Tal como se muestra en la *Figura 1.1* el uso de combustibles líquidos sintéticos va a ir tomando una gran relevancia con el paso del tiempo para poder cumplir con dicha demanda.

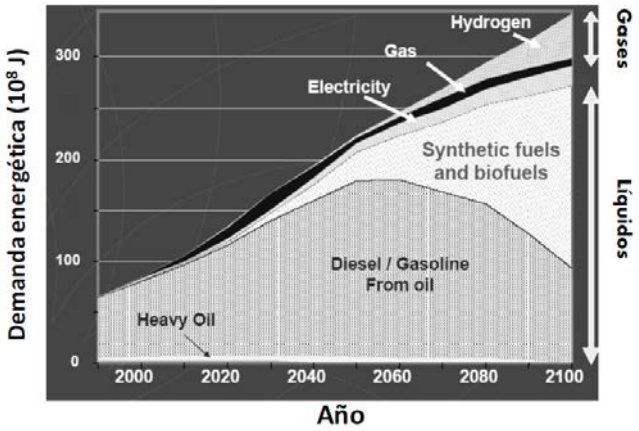

Figure 1.1. Previsión de la demanda de combustibles a lo largo del siglo XXI [2]

Además, ese incremento del consumo energético, conllevará también un aumento en las emisiones de gases efecto invernadero. Si unimos a esto la mayor conciencia social sobre la protección del ambiente, todo ello nos lleva a la búsqueda o desarrollo de fuentes de energía alternativas a los combustibles fósiles que reduzcan las emisiones contaminantes haciendo uso de las conocidas como energías renovables. Por ejemplo, en la Unión Europea el consumo de energía renovable se duplicó de un 8,5% en 2004 a un 17% en 2016, valores que se prevee que sigan aumentando con los años [3].

Uno de los sectores que más consumo energético supone, es el sector transporte. En Europa este sector consume entorno a un 33,2% de la energía utilizada, mientras que en España el sector transponte supuso el 42,4% del

consumo en 2016 [4]. Todo ello, por lo tanto, también lo hace ser uno de los sectores con mayor responsabilidad en las emisiones de gases de efecto invernadero a la atmósfera. En Europa, las emisiones provenientes del sector transporte en 2016 fueron del 26,3% del total emitido, y de un 30,9% en España [4].

La producción de combustibles sintéticos a partir de gas de síntesis (mezcla constituida principalmente por H_2 y CO) presenta actualmente una posible alternativa a los combustibles convencionales provenientes del petróleo. El gas de síntesis es el punto de partida en la obtención de diversos compuestos de interés tanto energético como industrial (Figura 1.2), donde resaltan los combustibles líquidos (gasolina, diésel, olefinas, metanol…) y otros como el dimetil éter, propuesto en los últimos años como un combustible alternativo de interés [5-8].

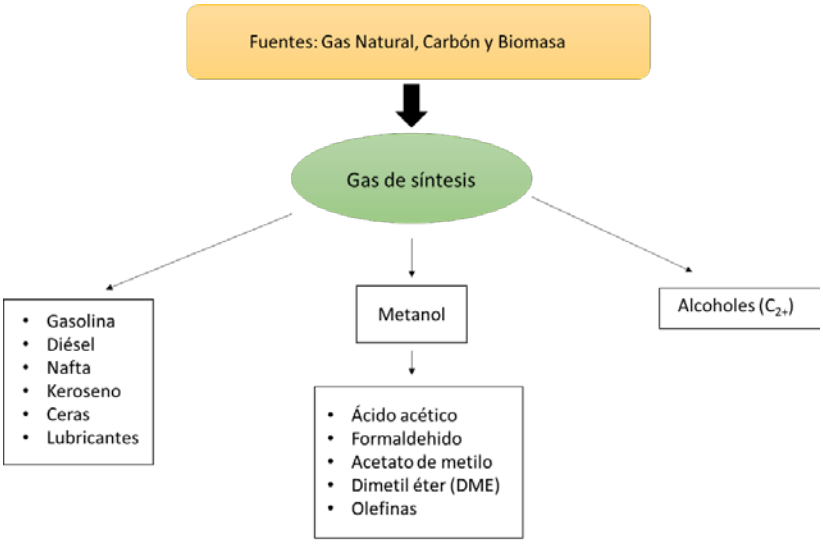

Figura 1.2. Esquema de las rutas de producción de diferentes productos a partir de gas de síntesis.

Al poder producirse gas de síntesis a partir de fuentes abundantes como el gas natural y el carbón, hace a estos combustibles sintéticos una alternativa al crudo, flexible en cuanto a disponibilidad y requerimientos del mercado. El gas natural ha sido considerado una alternativa a la transición del uso del petróleo a energías renovables debido a la gran cantidad de reservas disponibles en el mundo [9]. En

enero del 2018 la EIA (*Energy Information Administration*) estimó una reservas mundiales de gas natural de 7.124 billones de pies cúbicos (~200 trillones de m^3) [10] de los cuales el 42% de las reservas se localiza en Europa y en la antigua URSS [9].

El principal problema de utilizar estas fuentes es que se mantiene la dependencia de las fuentes de energía fósiles que no cumplirían con los requisitos ambientales para poder reducir las emisiones a la atmósfera. Sin embargo, aparte de las fuentes abundantes anteriormente citadas como el carbón y el gas natural, el gas de síntesis también puede obtenerse de fuentes renovables como la biomasa. De esta manera, los combustibles provenientes de estas fuentes supondrían menores emisiones de CO_2 a la atmósfera (*Figura 1.3*), considerando que el CO_2 emitido en su combustión equivaldría al consumido en el crecimiento del recurso empleado (balance neutro de carbono) [11,12].

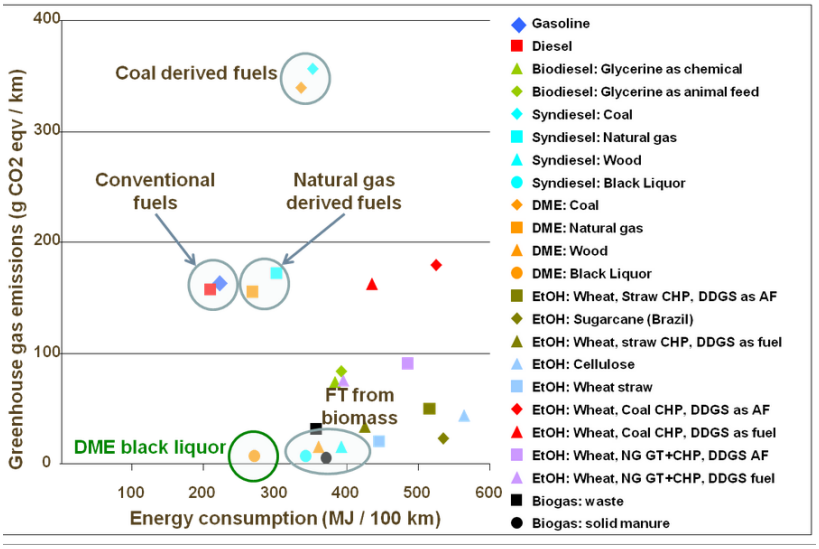

Figura 1.3. Reducción de las emisiones de CO_2 en función de la fuente de energía empleada [13].

Entre los diferentes combustibles líquidos sintéticos derivados del gas de síntesis (gasolina, diésel,...), en especial, el dimetil éter ha mostrado en el siglo XXI un gran potencial como sustituto de los actuales combustibles derivados del

petróleo, al presentar buenos rendimientos en su combustión como en la reducción de las emisiones contaminantes [5,7,8,14,13]

1.2. Dimetil éter (DME): combustible alternativo

El dimetil éter, abreviado como DME, es un compuesto oxigenado de amplia utilidad en la industria. Es considerado un compuesto no tóxico, no cancerígeno ni mutagénico [5], siendo en sus inicios usado como agente anestésico [15] y que no produce efectos negativos en la capa de ozono, lo que ha llevado a su utilización en aerosoles (pintura, agricultura, y cosmética) con el fin de evitar los compuestos clorofluorocarbonos (CFC) [8,16], perjudiciales para la atmósfera. Además, debido a su facilidad de licuefacción (a 6 atm o -25 ºC a presión atmosférica), lo hace atractivo también para equipos de refrigeración [8]. No obstante, en las últimas décadas el DME ha adquirido gran interés como alternativa a los combustibles derivados del petróleo.

El DME es el éter más simple sin enlaces C-C y con un elevado porcentaje de oxígeno (alrededor de 35% en masa), lo que permite una mejor combustión y reduce la formación de partículas y NO_x, pudiendo alcanzar unos límites de emisión inferiores a los de los vehículos de baja emisión (Ultra low emission vehicle – ULEV) [7,16,17]. Además, es un combustible libre de azufre (no emite SO_x) y que puede provenir de fuentes renovables como la biomasa o el licor negro del proceso Kraft que reducirían significativamente las emisiones de CO_2 a la atmosfera [18,19].

Por otro lado, sus propiedades similares a los LPG (Liquid Petrol Gas) como el butano y el propano (Tabla 1.1), lo hacen un sustituto perfecto para los mismos. Esto hace que las infraestructuras ya existentes para los LPG puedan servir sin ninguna modificación cuando se emplean mezclas de hasta el 20% de DME con los LPG, o con modificaciones mínimas en las bombas o juntas empleadas debidas a su naturaleza corrosiva y menor viscosidad [5,15]. Por lo que la transición a DME generaría una menor inversión que la construcción completa de una nueva infraestructura como podría ocurrir con otros combustibles alternativos como el hidrógeno, dónde se estimó una inversión de 18 mil millones de dólares (US$) frente a los 4 mil millones de dólares estimados para el DME [5,20].

Tabla 1.1. Comparación de las propiedades de diferentes combustibles [5,8]

	Metano	Metanol	DME	LPG	Etanol	Gasolina	Diésel
Peso molecular (g/mol)	16,04	32,04	46,07	44,1	46,07	100,2	198,4
Densidad (g/cm^3)	0,00072	0,792	0,661	0,54	0,785	0,737	0,856
Punto de Ebullición (ºC)	-162	64	-24,9	-30	78	38-204	125-400
LHV (KJ/g)	47,79	19,99	28,62	46,3	26,87	43,47	41,66
Contenido en C (% peso)	74	37,5	52,2	82	52,2	85,5	87
Contenido en azufre (% peso)	~7-25	0	0	~10-50	0	~200	~250

Sobre todo, el elevado índice de centano (55-60) que proporciona este compuesto, similar al del diésel, junto con las ventajas ambientales anteriormente citadas, ha resaltado su posible empleo como sustituto del combustible diésel. El motor de inyección para el combustible diésel actualmente existente tampoco necesitaría grandes cambios, salvo los citados anteriormente relacionados con sus propiedades físico-químicas (viscosidad y corrosión) que generalmente podrían solucionarse con el uso de juntas más resistentes a la corrosión como las de politetrafluoroetileno (PTFE) y el empleo de aditivos (los comúnmente empelados en el diésel reformulado) que mejoren la viscosidad y lubricidad del combustible [5,15,21,22]. Incluso, su bajo punto de ebullición permite una rápida vaporización de los sistemas de inyección, reduciendo las presiones de inyección requeridas con el empleo del diésel de 1200 a 220 bar aproximadamente [8]. No obstante, debido a su baja densidad energética requiere del empleo de un depósito de combustible de aproximadamente el doble de volumen para obtener el mismo rendimiento energético que el diésel [5,8,21,].

Asia es el continente que parece haber mostrado hasta ahora mayor interés en este compuesto como combustible, lo que llevó en 2009, al desarrollo de un proyecto de autobuses urbanos en Shanghái (China) abastecidos con DME. Diez vehículos fueron puestos en circulación junto con la construcción de una estación de servicio. El proyecto mostró unos buenos resultados con más de 220.000 km recorridos por estos vehículos y con buenos resultados en cuanto a emisiones y operación (sin problemas técnicos), existiendo hoy día 3 autobuses con licencia

en Shanghái y continuando con el estudio de su uso en vehículos como taxis y camiones [23,24].

No obstante, en Europa el DME también ha llamado la atención en países como Suecia, donde la compañía Haldar Topsøe junto con Volvo también realizaron pruebas de campo con camiones de bio-DME proveniente de licor negro proveniente del proceso Kraft. El uso de DME proveniente de energías renovables generaría una reducción del 95% de emisiones de CO_2 y mayor eficiencia energética que otros biocombustibles [25,26]. También, en Estados Unidos, en colaboración con el Departamento Sanitario de Nueva York (DSNY) y Oberon Fuels, se comenzó con estudios del empleo de DME en un modelo de camión de Volvo en 2017. Tras 3 meses de estudio bajo diferentes condiciones atmosféricas, los resultados mostraron un buen rendimiento general y aceleración de los camiones, siendo su manejo similar al de un camión diésel, incluso operando el motor adecuadamente en climas frios (- 7 ºC) [27,28].

1.3. Producción de DME

El gas de síntesis necesario para la producción de DME puede provenir de diferentes fuentes como el gas natural, carbón o fuentes renovables. La producción de DME a partir de este gas de síntesis puede llevarse a cabo mediante dos rutas diferentes. La primera ruta consiste en dos etapas separadas, en la que el gas de síntesis se transforma en metanol inicialmente, para posteriormente, ese metanol deshidratarlo a DME. Por otro lado, existe también una segunda vía directa conocida como síntesis directa de DME en el que el gas de síntesis es transformado a DME en una única etapa o reactor.

1.3.1. Proceso convencional en dos etapas

Tradicionalmente, la producción de DME se ha llevado a cabo mediante el proceso en dos etapas. Compañías como Haldor-Topsøe, Lurgi, Toyo Engineering Corporation, Mitsubishi Gas Chemical Company, Uhde, China Southwestern Research Institute of Chemical Industry y China Energy (Jiutai Group) poseen esta tecnología [29].

Esta ruta indirecta consta de dos etapas catalíticas independientes: síntesis de metanol + deshidratación de metanol a DME.

- Síntesis de metanol

El metanol es uno de los intermediarios químicos más demandados mundialmente, y supuso una producción 85 millones de toneladas en 2016, pudiendo alcanzar los 100 millones de toneladas en 2020 [30,31]. Presenta un amplio uso en la industria química como materia prima para la producción de numerosos compuestos oxigenados como el formaldehido, el ácido acético, el DME, el metil-terbutil éter (MTBE)… y diferentes disolventes (Figura 1.4). Además, también puede utilizarse para sintetizar hidrocarburos (especialmente olefinas en el método conocido como "methanol-to-olefins" (MTO)), y como combustible en sí mismo [32,33].

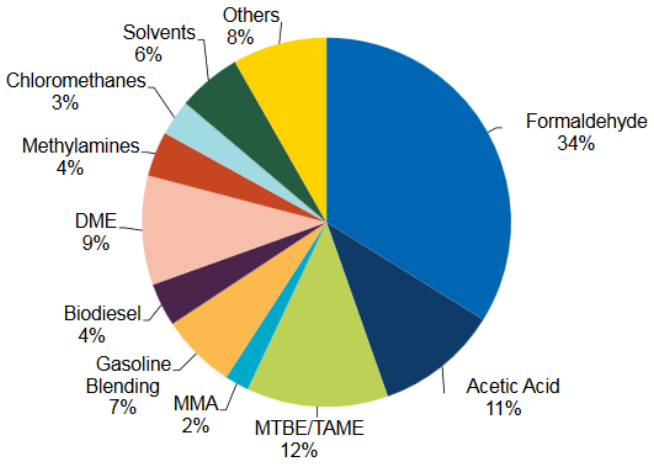

Figura 1. 4. Empleo de la demanda mundial de metanol en 2016 [34]

En la actualidad, la producción de metanol es uno de los procesos químicos más conocidos a nivel industrial, donde a partir de gas de síntesis se obtienen metanol según las siguientes reacciones químicas.

$$CO + 2\ H_2 \longleftrightarrow CH_3OH \quad (1.1)$$

$$CO_2 + 3\ H_2 \longleftrightarrow CH_3OH + H_2O \quad (1.2)$$

Apareciendo la reacción de desplazamiento de agua o comúnmente conocida como Water Gas Shift (WGS) como reacción secundaria por los productos y condiciones a las que se trabaja

$$CO + H_2O \longleftrightarrow CO_2 + H_2 \quad (1.3)$$

Debido al carácter exotérmico de la reacción y la reducción en el volumen de la mezcla reactiva esta reacción se ve favorecida a bajas temperaturas y elevadas presiones. Sin embargo, la reacción de síntesis de metanol presenta una fuerte restricción termodinámica, generando bajas conversiones en cada paso por el reactor y obligando a trabajar con elevadas relaciones de recirculación.

La compañía BASF fue la primera en producir a nivel industrial metanol a partir de gas de síntesis. Ésta se llevaba a cabo a altas presiones (> 300 bar) y temperaturas de 300-400 ºC empleando un catalizador de cromo (Cr_2O_3-ZnO). Sin embargo, en 1960 la compañía ICI (*Imperial Chemical Industries*) desarrolló un proceso de producción más viable económicamente al diseñar un catalizador más activo capaz de trabajar en unas condiciones menos severas (< 100 bar), sustituyendo así el proceso anterior [31,35].

- Deshidratación de metanol

La deshidratación del metanol a DME, se lleva a cabo generalmente sin muchas dificultades con un catalizador ácido (Al_2O_3, zeolitas, sílice-alúminas…), de forma que dos moléculas de metanol se convierten en una de DME perdiendo una molécula de agua.

$$2\ CH_3OH \longleftrightarrow CH_3OCH_3 + H_2O \quad (1.4)$$

No obstante, una variación de los catalizadores (naturaleza y fuerza ácida), y sobre todo, de las condiciones de reacción (altas temperaturas favorecen la formación de hidrocarburos) pueden originar una excesiva deshidratación a hidrocarburos [36,37].

$$2\ CH_3OH \longleftrightarrow CH_3OCH_3 \longrightarrow \text{Hidrocarburos (parafinas, olefinas, aromáticos…)} \quad (1.5)$$

La deshidratación de metanol a DME es una reacción relativamente sencilla (y rápida). Sin embargo, la naturaleza del centro ácido (Brønsted o Lewis) que toma parte en esta reacción da lugar a discrepancias entre diferentes autores [38-45]. El grupo del Prof. A. Martínez [46] achacan esta falta de precisión a estudios con condiciones de reacción diferentes en bibliografía que junto con la caracterización incompleta (la mayoría de los estudios solo emplean TPD de amoniaco) no ayuda a dilucidar dicho problema. Aun así, en bibliografía existe bastante acuerdo (independientemente del tipo de centro) en que una acidez débil y moderada son suficientes para deshidratar el metanol a DME (primera etapa de deshidratación), mientras que centros ácidos más fuertes son los responsables de la producción de hidrocarburos [39,43,44,47-51].

1.3.2. Proceso en una etapa o síntesis directa de DME

Más recientemente, el desarrollo del proceso de síntesis de DME a partir de gas de síntesis en una única etapa ha adquirido gran interés. En este proceso las reacciones de síntesis de metanol y deshidratación de éste a DME se llevan a cabo en un único reactor, lo que permite un sistema más sencillo y económico. Pero, sobre todo, al deshidratar el metanol conforme este se genera, se consigue eliminar la limitación termodinámica de formación de metanol. Este efecto conduce a una mayor conversión de los reactivos por paso, disminuyendo la relación de recirculación en el mismo, y en general, dando lugar a un sistema más eficiente.

Compañías como Haldor Topsøe, JFE y Korea Gas Corporation (KOGAS) han desarrollado tecnologías para la síntesis directa de DME. Haldor Topsøe fue una de las primeras en desarrollar la tecnología en la que se sintetizaba DME a partir

de gas de síntesis [2,52]. Posteriormente, en el 2002-2006, gracias al apoyo del gobierno japonés y diferentes empresas como Toyota Tsusho, INPEX, JAPEX y Total, la compañía JFE diseñó una planta piloto para la síntesis directa de DME con una capacidad de producción de 100 toneladas diarias (Figura 1.5) [53,54].

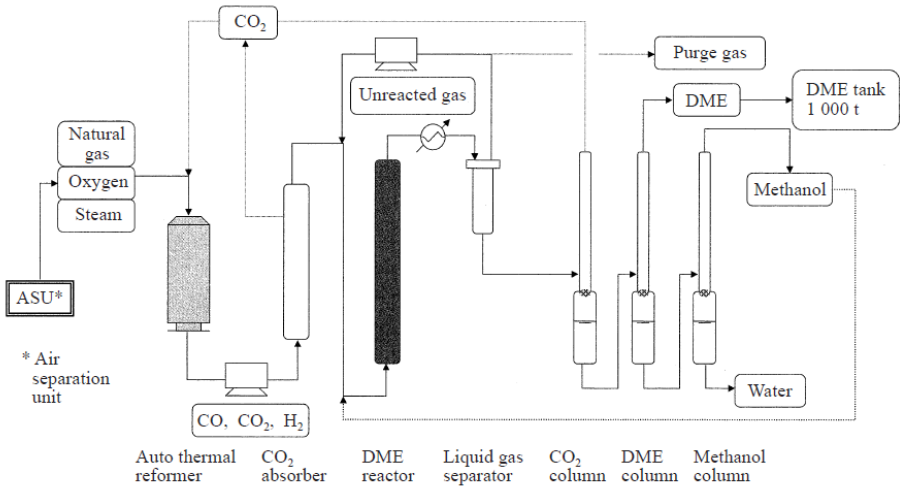

Figura 1. 5. Diagrama de flujo de la planta de 100 toneladas/día desarrollada por JFE [54]

La reacción global de la síntesis directa de DME se obtiene de la suma de las reacciones involucradas. El catalizador ácido empleado produce la formación de DME (1.7.) a partir del metanol generado (1.6.), lo que lleva a la aparición de agua en el sistema, que es responsable de la reacción WGS (1.8.), que consume agua del medio para generar CO_2.

Síntesis de metanol: $CO + H_2 \longleftrightarrow CH_3OH$ ($\Delta H = -91$ KJ/mol) (1.6)

Deshidratación: $2 \cdot CH_3OH \longleftrightarrow CH_3OCH_3 + H_2O$ ($\Delta H = -23$ KJ/mol) (1.7)

WGS: $CO + H_2O \longleftrightarrow CO_2 + H_2$ ($\Delta H = -41$ KJ/mol) (1.8)

Reacción Global: $CO + H_2 \longleftrightarrow CH_3OCH_3 + CO_2$ ($\Delta H = -246$ KJ/mol) (1.9)

1.4. Catalizadores para la síntesis directa de DME

Los catalizadores para la síntesis directa de DME deben ser catalizadores bifuncionales/híbridos compuestos por la función de síntesis de metanol y la función de deshidratación de metanol.

Como se ha indicado previamente, la síntesis de metanol en sus inicios se llevaba a cabo con catalizadores basados en cromo que requerían operar en condiciones severas (> 100 bar y 300-400 ºC) [31,55]. Sin embargo, desde que en 1965 la compañía ICI [56] diseñara un catalizador basado en cobre, zinc y aluminio ($Cu/ZnO/Al_2O_3$ o CZA de forma abreviada) es el catalizador comúnmente empleado para dicha reacción. De esta manera, los buenos rendimientos de los catalizadores basados en cobre han llevado a la mayoría de las investigaciones dedicadas a la síntesis directa de DME, a elegirlo como catalizador de síntesis de metanol [42,47,57-61].

La superficie metálica de cobre presentada por el catalizador es el factor determinante de la conversión obtenida en dicha reacción. El óxido de zinc es ampliamente conocido como un promotor en la dispersión del cobre, incrementando el número de centros activos expuestos [62,63]. La adición de otros óxidos de metales como (Al, Zr o Mn) busca aumentar la superficie específica del catalizador y mejorar, por tanto, la dispersión del cobre con el fin de evitar su sinterizado bajo las condiciones de operación [16,63,64]. F. Song *y cols.* [65], por ejemplo, observaron como una adición de <5% de Zr en la preparación del catalizador CZA por coprecipitación mejoraba la dispersión del cobre y la reducibilidad del mismo, con el consiguiente incremento de la conversión. Incluso, la adición de ZrO_2 en el catalizador CZA también produjo una mayor estabilidad

[66]. Del mismo modo, Y. Tan *y cols.* [67], estudiaron el efecto de la modificación del catalizador CZA con Mn, observando una mejora de la reducibilidad y estabilidad con respecto al catalizador CZA sin este promotor.

En cuanto al catalizador de deshidratación, se han estudiado un gran número de catalizadores ácidos para obtener DME: alúmina [42,49,65,68], sílice-alúmina [39] o zeolitas (ZSM-5 [42,69], MOR [49], FER [69,70], Beta [71], Y [72,73], SAPO [48,74],...).

La reacción de deshidratación de metanol se lleva a cabo gracias a la presencia de centros ácidos (Lewis y Brønsted) característicos de los sólidos anteriores [36]. La naturaleza y fuerza de los centros juegan un papel importante en la reacción de deshidratación. M. Stiefel *y cols.* [49] observaron la importancia de la acidez en la síntesis directa de DME, observando un mayor rendimiento de la reacción con catalizadores más ácidos como la zeolita ZSM-5. Sin embargo, demasiada acidez en el catalizador de deshidratación también mostró un incremento de productos indeseados a expensas de la selectividad a DME. Como se comentó anteriormente, a pesar de la incertidumbre existente en bibliografía que rodea a la naturaleza de los centros [38-46], hay un amplio acuerdo en que la reacción de deshidratación de metanol a DME tiene lugar en centros con una acidez débil y/o moderada, mientras que centros ácidos más fuertes están asociados al posible desplazamiento de la reacción a productos indeseados como hidrocarburos [39,43,44,49,75-78]. Es por ello que autores como D. Mao *y cols.* [47] estudiaron la modificación de catalizadores de síntesis de metanol, como la zeolita HZSM-5, con óxido de antimonio (Sb_2O_3) con el fin de reducir la acidez fuerte presentada por la zeolita, reduciendo el desplazamiento de la reacción a compuestos indeseados y mejorando la selectividad a DME.

La alúmina es una opción interesante por su bajo coste y su alta estabilidad y resistencia térmica y mecánica, además de presentar una elevada selectividad a DME. Sin embargo, es conocida la menor actividad de la alúmina frente a las zeolitas, lo que ha llevado a determinados autores a estudiar la modificación de la alúmina con sulfatos con el fin de incrementar su acidez [51,79,80]. Aun así, la alúmina requiere del empleo de mayores temperaturas de trabajo para mejorar su actividad de deshidratación [44,81]. La síntesis directa de DME se suele realizar a temperaturas comprendidas entre 240-280 ºC, ya que a mayores temperaturas esta reacción exotérmica no está favorecida termodinámicamente, además el empleo de catalizadores de cobre limita el uso de elevadas temperaturas debido a su desactivación por sinterizado. Por otro lado, los centros ácidos de la Al_2O_3 son sensibles a la presencia de agua en el sistema, desactivándolos y dirigiendo a

catalizadores menos estables [44,49,81]. Así, las zeolitas han sido ampliamente utilizadas en la síntesis directa de DME al permitir operar a menores temperaturas con un mayor rendimiento. En particular, la zeolita HZSM-5 ha mostrado unos resultados de actividad y estabilidad mayores que los de la alúmina, siendo el catalizador ácido más interesante para la síntesis directa de DME [39,46].

Ahora bien, en la síntesis directa de DME estas dos fases activas deben situarse en un mismo reactor. El método de preparación de los catalizadores híbridos va a jugar un papel importante en el rendimiento de la reacción. La mejora en el rendimiento de esta reacción frente a la ruta indirecta radica en la eliminación del equilibrio termodinámico de formación de metanol, deshidratando este conforme se genera, por lo que "a priori", una mezcla intima de las fases favorecería el contacto de los centros para poder llevar a cabo eficientemente este proceso en serie.

El grupo del Prof. J. Bilbao [82-84] cita la mezcla conjunta de los dos catalizadores en medio acuoso como el mejor método para la preparación del catalizador favoreciendo el contacto entre fases. Con él obtuvieron unos buenos resultados de conversión, selectividad y rendimiento a DME. Del mismo modo, Q. Ge *y cols.* [85] y J.H. Flores *y cols.* [70] tras estudiar diferentes formas de preparación del catalizador híbrido, observaron que la mezcla de los componentes en medio acuoso, a la que denominaron "método de coprecipitación sedimentación", mostraba una mayor actividad. No obstante, determinados autores sugieren que un contacto excesivamente íntimo de las fases puede generar interacciones perjudiciales que desactiven el catalizador. A. García-Trenco *y cols.* [86] concluyeron que un excesivo contacto de las fases llevaba a un deterioro del rendimiento del catalizador híbrido CZA/HZSM-5 por un bloqueo de los microporos de la zeolita y la migración parcial de los iones Cu^{2+} (aunque tampoco descartaron una posible migración los Zn^{2+}) al catalizador ácido, sufriendo una notable disminución de los centros ácidos Brønsted. Del mismo modo, J. H. Flores *y cols.* [70] tras observar cambios en la acidez de catalizadores híbridos preparados de diferente forma, sugirieron un posible bloqueo de los centros ácidos de la zeolita por los óxidos metálicos debido a un mayor contacto.

1.5. Reactores para la producción de DME

1.5.1. Reactores convencionales

El diseño de los reactores es uno de los factores importantes a tener en cuenta al llevar a cabo una reacción catalítica. En la actualidad la producción de DME a escala industrial se lleva a cabo con el proceso en dos etapas, produciendo el DME a partir de metanol con el empleo de catalizadores ácidos en un reactor convencional de lecho fijo [2,87,88]. Aun así, como se ha comentado con anterioridad en las últimas décadas surgió el interés por llevar a cabo la producción de DME a partir de gas de síntesis en una única etapa debido a sus ventajas económicas. Así diversas compañías invirtieron en el desarrollo de plantas para la síntesis directa de DME con reactores convencionales como los reactores de lecho fijo o reactores de lodo (slurry) [29,52,54,89].

El reactor de lecho fijo es el reactor comúnmente empleado en las plantas piloto o a escala de laboratorio para las diferentes reacciones catalíticas por su simplicidad y bajo coste. En este tipo de reactores, un lecho de partículas de catalizador es colocado en el reactor tubular, proporcionando un buen contacto gas-sólido que favorece la trasferencia de materia en el sistema. Sin embargo, este tipo de reactores dificulta el control térmico en el mismo cuando se llevan a cabo reacciones altamente exo- o endotérmicas, lo que puede llevar a problemas de inestabilidad térmica en los ciclos de encendido y apagado o reducción de la vida útil de los catalizadores por sinterizado. Es por ello, que a fin de evitar esta serie de problemas, en este tipo de sistemas se suele operar con bajas conversiones por paso para evitar elevadas temperaturas, lo que obliga a trabajar con elevadas relaciones de recirculación [16,90-92].

Haldor Topsøe y KOGAS ofrecen sistemas para la producción de DME en una etapa mediante el empleo de reactores de lecho fijo, dónde esta última empresa utiliza un reactor de lecho fijo multitubular con el que se permite un mayor control de la temperatura al circular agua alrededor del catalizador (Figura 1.6) [52,29] y así poder mitigar los problemas anteriormente citados.

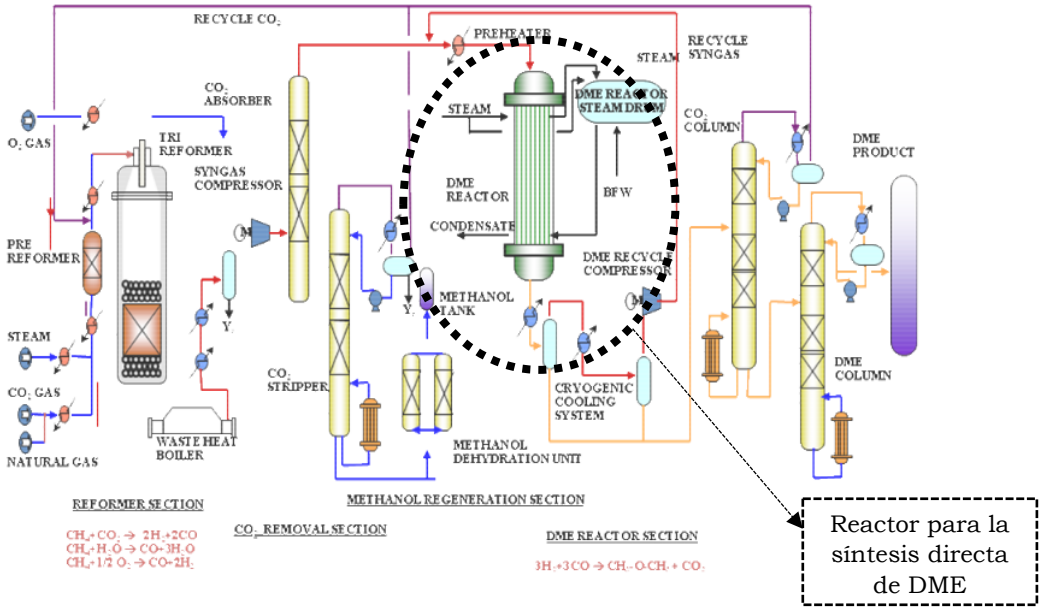

Figura 1. 6. Diagrama de la planta de producción de DME por vía directa en un reactor multitubular de lecho fijo propuesta por Korean Gas Corporation (KOGAS) [29]

Otra alternativa para el control de temperatura en la síntesis directa de DME, fue el reactor de lodos, empleado, por ejemplo, en las plantas de la compañía JFE o Air Products [52,54,89,93]. Con estos sistemas catalíticos, el catalizador se suspende en un disolvente y el reactivo es burbujeado a través del mismo, permitiendo un control óptimo de la temperatura. Sin embargo, la necesidad de que los reactivos gaseosos a difundir por el disolvente para llegar a las partículas de catalizador genera problemas de transferencia de materia. Además, la pérdida de catalizador causada por la fricción entre las partículas, junto con la mayor complejidad de este sistema, que requiere un sistema de separación gas-líquido, incrementa la inversión [16,90,91,94].

Por otro lado, en estos últimos años, el uso de reactores fluidizados es otra de las alternativas que ha sido planteada en el ámbito de la investigación [16]. En estos reactores el lecho es suspendido en el medio fluido obteniendo un buen control de la temperatura por el movimiento libre de las partículas en el lecho y, a diferencia del reactor de lodos (slurry), mejora la difusión de los reactivos por la mezcla forzada del catalizador con el gas reactante. No obstante, la fricción sufrida por las partículas fluidizadas entre ellas mismas y con la pared del reactor pueden causar la pérdida del catalizador [90,95].

1.5.2. Reactores estructurados

En los sistemas convencionales de lecho fijo se emplean pellets de un cierto tamaño para poder superar los problemas de pérdida de carga y poder operar así con flujos elevados. Pero ese elevado tamaño de las partículas puede originar problemas de difusión intraparticular afectando a la eficiencia de la reacción global. Numerosos diseños de pellets han sido desarrollados para reducir esas pérdidas de carga y aumentar la superficie externa de las partículas, desde partículas cilíndricas, esféricas, cilindros huecos, etc. Sin embargo, estas estructuras tienden a presentar una menor resistencia mecánica (resistencia a la abrasión y compresión). Su erosión puede generar partículas finas en el sistema que producen problemas de obstrucciones en el sistema [96]. De esta manera, los reactores estructurados han sido planteados como solución a estos problemas.

Los reactores estructurados pueden ser además una alternativa de interés para las reacciones altamente exo o endotérmicas. Los sustratos estructurados son estructuras rígidas formados por canales o poros de gran tamaño por los que se permite el paso de los fluidos con menor pérdida de carga que en los reactores convencionales. Además, la fina capa de catalizador generalmente depositada en la superficie del sustrato, facilita la transferencia de materia y calor intraparticular en el sistema [97-99].

La aplicación a escala comercial de este tipo de sistemas en los tubos de escape de los automóviles para tratar las emisiones ha producido un gran desarrollo de estos sistemas, también aplicados en otros procesos ambientales donde se requiere operar con elevados flujos [100].

La forma o geometría de los sustratos estructurados puede ser muy variada como se muestra en la *Figura 1.7*. [96]

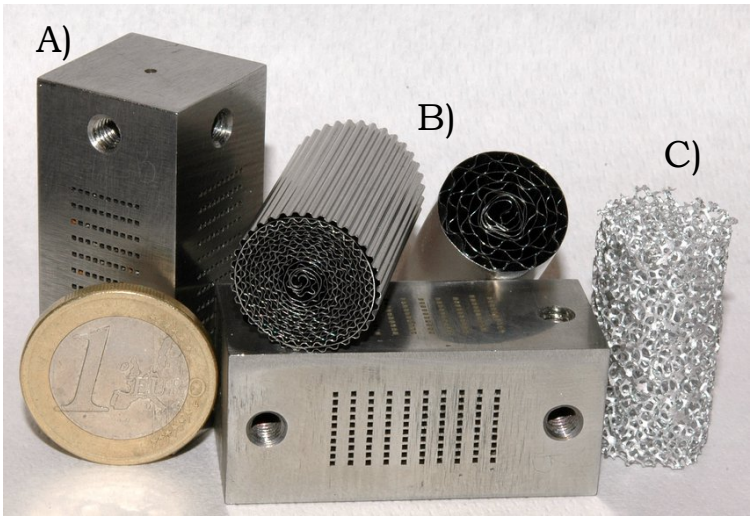

Figura 1.7. Diferentes tipos de sustratos metálicos A) reactor de microcanales B) monolito de canal longitudinal y C) espuma metálica.

Los sistemas estructurados se pueden clasificar en los siguientes bloques:

- *Canales longitudinales paralelos*: Los comúnmente conocidos como monolitos, se tratan de estructuras con canales longitudinales paralelos (*Figura 1.7B*). También son conocidos por el nombre de 'honeycomb' (panel de abeja) debido a la forma hexagonal de los canales que presentaban los monolitos inicialmente producidos. Los grandes canales reducen notablemente la perdida de carga en el sistema, además de presentar una elevada relación superficie/volumen que permite depositar finas capas de catalizador mejorando la transferencia de materia intraparticular [98,99]. Por otro lado, operan bajo un régimen de flujo laminar disminuyendo la posibilidad de canales preferenciales. Sin embargo, este régimen de flujo conlleva a una menor mezcla de los fluidos, requiriendo un mezclado y distribución de los fluidos previos a entrar al canal [96].

  Desde que a mediados de 1970 se comenzara a aplicar esta tecnología en la industria automovilística debido a su alta eficiencia, se ha estudiado el empleo de estos sistemas en diversas reacciones como la combustión de

metano, oxidación catalítica, hidrogenación de compuestos aromáticos, producción de hidrógeno, etc. [101]

Una variación de los monolitos son los reactores de microcanales. Estos sistemas consisten en unidades con canales de un tamaño comprendido entre 10 y 1000 μm (*Figura 1.7A*) lo que proporciona una elevada relación superficie/volumen que potencia las velocidades de trasferencia de calor y materia [98,102]. Además, la posibilidad que ofrecen estos sistemas de replicar cuantas unidades sean necesarias, ofrece una flexibilidad de uso al poder adaptarse a cambios en la capacidad de producción utilizando más o menos bloques conectados en paralelo, operando siempre en condiciones óptimas y evitando los problemas asociados al cambio de escala.

En la síntesis directa de DME esta nueva tecnología permitiría adaptarse a la gran variedad de recursos existentes para su producción, como los yacimientos de gas de pequeño tamaño o alejado de las redes de gas (*stranded gas*) que requieran un aprovechamiento 'in situ' o la biomasa cuyo coste de transporte a grandes instalaciones puede ser elevado. De esta manera con esta tecnología, se podrían diseñar unos sistemas más compactos adaptados a esa capacidad de producción y de fácil desplazamiento que permitan aprovechar todas esas fuentes. Existen trabajos en la bibliografía que exploran el potencial de la tecnología de microcanales en la síntesis directa de DME, mostrando que dicha tecnología es altamente prometedora al permitir un excelente control de la temperatura, punto clave de este proceso, una buena estabilidad del catalizador y una mayor productividad volumétrica que la tecnología convencional [57,103,104].

- *Espumas*: Las espumas son sustratos con una elevada porosidad y tortuosidad formadas por celdas unitarias poliédricas, que unidas entre sí, constituyen una red tridimensional (*Figura 1.7C*)[105]. Éstas se definen por su tamaño de poro, factor relacionado con la densidad de poro y expresado en poros por pulgada lineal (ppi – pore per inch). La alta tortuosidad de las mismas, generan un régimen de flujo turbulento en comparación con los monolitos de canal longitudinal, lo que mejora la mezcla de los componentes en el flujo reduciendo posibles problemas difusivos a la par que mejoran la transferencia de calor por convección en el reactor [106,107]. Además, su baja densidad y alta resistencia mecánica hacen a

las espumas unos sistemas interesantes para el diseño de componentes ligeros y robustos [105].

Aunque en la actualidad no hay muchas aplicaciones industriales en el campo de la catálisis en las que se empleen este tipo de sistemas [106], se está investigando en diversos grupos su aplicación en diferentes reacciones catalíticas [96]. Por ejemplo, el grupo del Prof. E. Tronconi estudiaron ampliamente las propiedades de conductividad térmica de las espumas metálicas [106,108], y en estudios recientes, mostraron su aplicación en la síntesis de metanol [109]. En comparación con el reactor multitubular relleno de pellets de catalizador comúnmente empleado en esta reacción, el empleo de espumas metálicas recubiertas con el catalizador permitía un diseño de sistemas más compactos, al permitir reducir la longitud de los tubos gracias a la mejor conductividad térmica mostrada por los mismos.

- *Mallas*: Este material consiste en un conjunto de hilos entrecruzados formando una malla. Este tipo de sustratos también aportarían una excelente transferencia de calor y materia a los sistemas, con unos coeficientes de transferencia de calor y materia 10 veces superiores a los proporcionados por los monolitos de canal longitudinal [110,111]. La empresa Precision Combustion, Inc. (PCI) comercializa hoy día con este tipo de sistemas ofreciendo tecnologías con ventajas frente a los sistemas convencionales para reformado, adsorción, oxidación… [112-114]

1.5.2.1. Reactores estructurados metálicos

Los sustratos estructurados pueden ser de diferentes materiales, siendo los más importantes los sustratos cerámicos y metálicos. Los sustratos cerámicos son comúnmente preparados por extrusión, siendo la cordierita el material más utilizado [100]. Sin embargo, los materiales metálicos ofrecen la posibilidad de obtener sustratos con espesores más delgados (laminado de los metales) con alta resistencia mecánica a la par que proporcionan una mayor conductividad térmica al sistema. Además, la maleabilidad ofrecida por los metales, la cual permite modificar la forma de los canales, dota a estos sustratos de una elevada versatilidad [99,96].

La fabricación de los monolitos metálicos se basa en el enrollamiento o apilado de placas lisas y onduladas (corrugadas) del metal de forma alterna. En función del corrugado realizado a las placas, el tamaño del canal obtenido varía, pudiendo obtenerse un amplio abanico de densidades de celda [100]. Además, la versatilidad de estos materiales que permiten realizar cortes o relieves transversales al flujo puede permitir el diseño de geometrías más complejas que interconecte los canales entre sí [100].

No obstante, es bien conocida la menor adherencia a la capa catalítica mostrada por los metales en comparación con los sustratos cerámicos por su diferente composición química y rugosidad superficial. Numerosas aleaciones han sido estudiadas en la preparación de reactores metálicos, aceros inoxidables [115-117], aluminio [107,118], latón [119,120], cobre [121,122], etc., pero la superficie extremadamente lisa que suelen presentar requiere un tratamiento previo para generar una cascarilla con la naturaleza y la rugosidad apropiada en la superficie de las aleaciones con el fin de mejorar sus propiedades adherentes.

Los aceros ferríticos con Al, los materiales más utilizados para la preparación de estos sistemas, son capaces de generar una capa de alúmina en su superficie tras un tratamiento térmico que le protege de la ulterior oxidación. Mediante este tratamiento térmico, el aluminio de la aleación es capaz de migrar a la superficie formando una capa de α-alúmina con forma de agujas (whisker) que proporcionan puntos de anclaje para el catalizador [123]. Del mismo modo, otras aleaciones han sido tratadas térmicamente con el fin de obtener superficies rugosas. Por ejemplo, el latón o el cobre, formando una capa de óxido de cobre modificando la rugosidad original de las placas [124,125].

Por otro lado, el aluminio es un material atractivo para la preparación de reactores estructurados debido a su elevada conductividad térmica, lo que favorecería el control de temperatura en dichos sistemas. En este caso, con el fin de obtener esa rugosidad apropiada para mejorar las propiedades adherentes del sustrato, los tratamientos comúnmente empleados son el anodizado [126,127] o ataque químico [128,129] del aluminio.

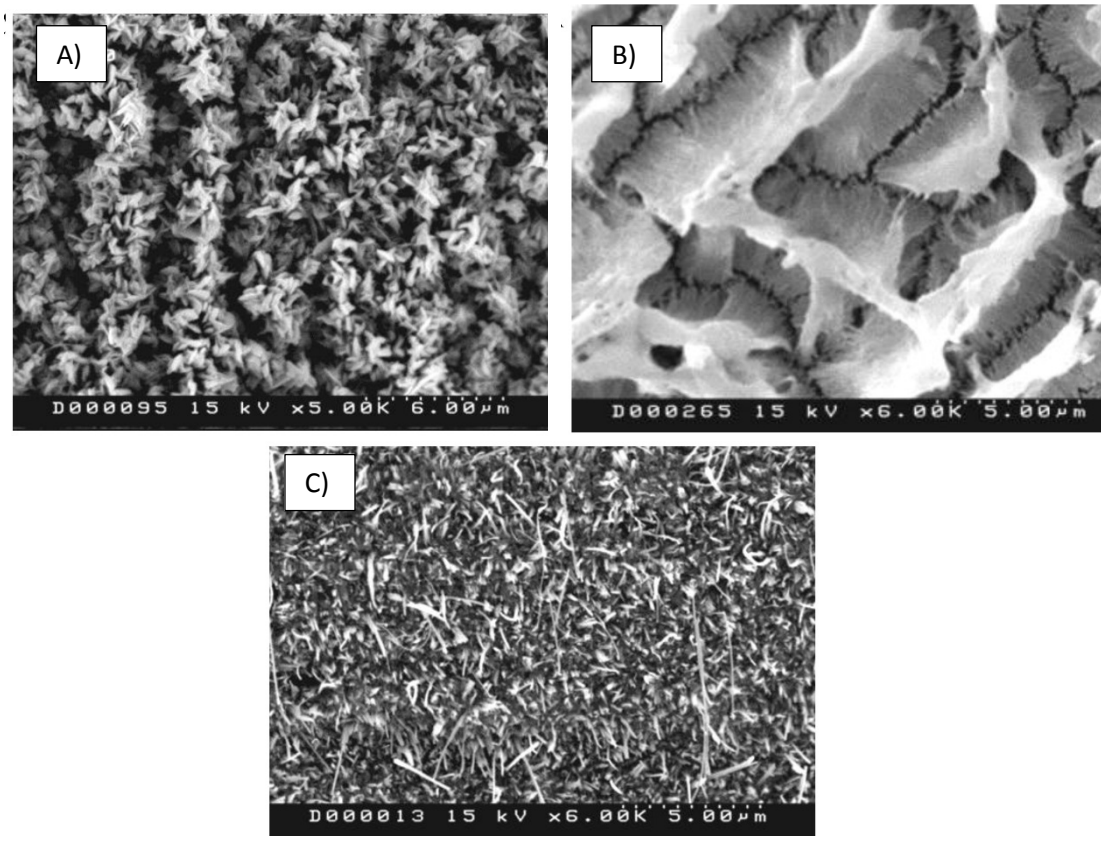

Figura 1.8. Imágenes de SEM de las diferentes rugosidades obtenidas tras el pretratamiento de los sustratos A) Fecralloy B) Aluminio y C) Latón [119]

1.5.2.2. Método de recubrimiento por inmersión

Uno de los métodos más empleados en el depósito de catalizadores en los sustratos estructurados es el método de recubrimiento por inmersión (también conocido como washcoating o dip coating) [97]. Este método consiste en sumergir el sustrato en una suspensión del catalizador a una velocidad controlada, mantenerlo sumergido un corto periodo de tiempo para volver a sacarlo a una velocidad controlada, y finalmente eliminar el exceso que ha podido quedar ocluido en los canales, secarlo y calcinarlo para generar una capa adherente. Por lo tanto, el hecho de poder aplicar este método a casi cualquier suspensión de un

catalizador o su precursor [99120], genera una gran versatilidad que favorece su utilización.

El resultado final del recubrimiento depende, de este modo, tanto del procedimiento de recubrimiento como de las propiedades de la suspensión y del sustrato [98,99]. La finalidad de este proceso es la obtención de unos recubrimientos homogéneos y adherentes, donde las propiedades de la suspensión van a jugar un papel relevante, ya que se requiere que sea estable y que moje bien el sustrato para que sea capaz de fluir por los canales generando una película homogénea (sin acumulaciones), pero que a su vez produzca una capa del catalizador con buenas propiedades cohesivas y adhesivas.

Las propiedades de recubrimiento del fluido van a depender de parámetros de la suspensión como estabilidad, viscosidad, tensión superficial, etc., que son parámetros bastante relacionados entre sí, lo que dificulta la modificación de uno de ellos sin alterar otros. Estos parámetros pueden ser modificados con diferentes variables [100,130]:

- *Propiedades de las partículas en suspensión*. El tamaño de partícula empleada en la suspensión afecta a la estabilidad de la misma. Partículas de elevado tamaño precipitan con mayor facilidad, por lo que tamaños medios de partícula inferiores a 10 μm suelen emplearse con el fin de evitar la sedimentación [131-133]. Tamaños de partícula demasiado pequeños (por debajo de 1 micra) no son aconsejables porque propician una excesiva interacción entre partículas que promueve la floculación de la suspensión. Por otro lado, el potencial zeta es otro parámetro que define la estabilidad de las suspensiones. Mediante el ajuste de pH puede maximizarse la repulsión entre partículas y por ende mejorar la estabilidad de la suspensión [98,134].

- *Propiedades del disolvente*. El empleo de agua o alcoholes permite obtener suspensiones con diferentes propiedades como la tensión superficial, siendo los alcoholes los que proporcionan suspensiones con menor tensión superficial que mejora la mojabilidad del sustrato con la suspensión [130]. Sin embargo, el empleo de alcoholes puede proporcionar una mala dispersión de las partículas en el medio, formando agregados que dan lugar a recubrimientos poco homogéneos y con baja adherencia [135].

- *Contenido en sólidos*. El porcentaje en peso de sólidos define la capacidad de carga catalítica por cada ciclo de recubrimiento, es decir, el número de inmersiones requeridas para depositar la carga deseada. Altos contenidos en sólido, que suponen elevadas viscosidades, reducen el número de inmersiones requeridas, pero valores demasiado altos pueden originar un mal flujo de la suspensión por los canales (generando acumulaciones y por ende recubrimientos heterogéneos) y taponamientos de los mismos [98,99].
- *Aditivos*. Para modificar las propiedades de la suspensión también se pueden utilizar diferentes aditivos con propiedades estabilizadoras, ligantes, espesantes, etc. Estos aditivos pueden ser orgánicos (polivinil alcohol, polietilenglicol, metil hidroxietil celulosa…) o inorgánicos (generalmente coloides de Al_2O_3, ZnO, SiO_2…) [99,136,137].

1.6. Objetivo de la tesis

El principal objetivo de este trabajo es el estudio de la estructuración conjunta de los dos catalizadores necesarios para la síntesis directa de DME. Para cumplir con dicho objetivo los pasos seguidos fueron los siguientes:

1. Búsqueda de la formulación de la suspensión adecuada para estructurar los catalizadores de la síntesis directa de DME (catalizador de síntesis de metanol y catalizador de deshidratación de metanol) de forma separada sin alterar las propiedades catalíticas del catalizador de partida, obteniendo unos recubrimientos homogéneos y adherentes.

2. Búsqueda de la formulación de la suspensión adecuada para estructurar los dos catalizadores conjuntamente con el empleo de una única suspensión (mezcla en suspensión de ambos catalizadores) sin alterar las propiedades catalíticas del catalizador de partida, obteniendo unos recubrimientos adherentes y homogéneos.

3. Estudio del comportamiento catalítico de la síntesis directa de DME en sustratos metálicos.

    - Estudio de la influencia de diferentes geometrías y aleaciones
    - Estudio de las diferentes arquitecturas de los catalizadores en el monolito. Disposición por capas separadas o como mezcla conjunta de ambos catalizadores.
    - Estudio de la intensificación de los monolitos metálicos con el fin de incrementar la productividad volumétrica de DME.

4. Estudio de la síntesis de nuevos catalizadores bifuncionales basados en el encapsulamiento de Cu en un sustrato ácido.

1.7. Estructura de la tesis

La presente tesis doctoral se ha dividido en siete capítulos.

En el Capítulo 1, se presenta una breve introducción general. Cada uno de los capítulos de resultados llevará una introducción más específica los aspectos trabajados en ese capítulo. En este primer capítulo se abarca desde una visión global del dimetil éter (DME) como alternativa a los combustibles derivados del petróleo, pasando por las diferentes vías de síntesis de DME a partir de gas de síntesis, hasta llegar a las ventajas que aporta el uso de sistemas estructurados.

En el Capítulo 2, se resumen los métodos y técnicas experimentales utilizados para la síntesis, caracterización y evaluación catalítica de los diferentes catalizadores y suspensiones.

El Capítulo 3 se recogen los resultados del estudio de las diferentes formulaciones de la suspensión para el catalizador de síntesis de metanol, el catalizador $Cu/ZnO/Al_2O_3$ (CZA), y para el catalizador de deshidratación de metanol, una zeolita comercial ZSM-5. En este apartado se presentan los resultados de caracterización y de evaluación catalítica de las diferentes suspensiones secas y calcinadas (*slurried catalysts*), seguidos de la caracterización de sus propiedades de recubrimiento (potencial zeta, tamaño de partícula, adherencia…).

El capítulo 4 recoge, en primer lugar, los resultados de diferentes formas de contacto de los catalizadores en polvo necesarios para la síntesis directa de DME en un reactor de lecho fijo. Y finalmente, el estudio se centra en la estructuración de la mezcla en suspensión conjunta de estos catalizadores. Este apartado recoge tanto la caracterización y evaluación catalítica, como el estudio de las propiedades de recubrimiento, empleando diferentes coloides inorgánicos y cantidades de los mismos como aditivo.

En el Capítulo 5 se presentan los resultados del test catalítico del estudio de los catalizadores estructurados para la síntesis directa de DME. Este capítulo se divide en tres grandes bloques: uno primero en el que se estudian diferentes formas y aleaciones de los sustratos con la mezcla en suspensión de ambas fases; otro segundo donde se observa el efecto de diferentes arquitecturas de los catalizadores en los monolitos (mezcla en suspensión o por capas); finalmente se estudia la variación de diferentes parámetros para incrementar la productividad volumétrica de DME.

El Capítulo 6 presenta los resultados obtenidos en la estancia de 3 meses realizada en la Universidad de Lille (Francia) bajo la supervisión del Prof. Andrei Khodakov. Este trabajo recoge los resultados de diferentes métodos de encapsulamiento de cobre para la preparación de catalizadores bifuncionales.

Y en el Capítulo 7, se presentan las conclusiones más relevantes del trabajo.

1.8. Referencias

[1] Página Web: El País 14 Nov 2017 disponible en Junio de 2019 en https://elpais.com/economia/2017/11/14/actualidad/1510661591_352717.html.

[2] A. García-Trenco. *Tesis Doctoral* (2013) Universidad Politécnica de Valencia (UPV).

[3] Página Web: Eurostat – Statistics Explained disponible en Junio de 2019 en https://ec.europa.eu/eurostat/statistics-explained/index.php?title=Renewable_energy_statistics/es.

[4] Informe anual 2018 del Observatorio del transporte y logística en ESPAÑA (OTLE). Marzo de 2019.

[5] T.H. Fleisch, A. Basu, M.J. Gradassi, J.G. Masin. Studies in Surface Science and Catalysis 107 (1997) 117-125.

[6] T.A. Semelsberger, R.L. Borup, H.L. Greene. *Journal of Power Sources* 156 (2006) 497-511.

[7] E.S. Yoon, C. Han. *PSE2009 Computer Aided Chemical Engineering* 27 (2009) 169-175.

[8] H. Erdener, A. Arinan, S. Orman. *International Journal of Renewable Energy Research* 1 (2011) 252-258.

[9] S. Mokhatab, W.A. Poe, J.Y. Mak. *Handbook of Natural Gas Transmission and Processing*. Ed. S. Mokhatab, W.A. Poe and J.Y. Mak (Gulf Professional Publishing - Elsevier) Estados Unidos (2019) 1-35.

[10] Página Web: Independent Statistics & Analysis U.S. Energy Information Administration disponible en Julio de 2019 en https://www.eia.gov/tools/faqs/faq.php?id=52&t=8.

[11] S.C. Bhatia. *Advanced Renewable Energy Systems*. Ed. S.C. Bhatia (Woodhead Publishing India PVT LTD) Nueva Delhi (2014) 688-718.

[12] Página Web: Hardwood Biofuels disponible en Julio de 2019 en https://hardwoodbiofuels.org/news-and-events/feature-stories/understanding-the-carbon-balance-of-biofuel-production/.

[13] Página Web: BioDME disponible en Junio de 2019 en http://www.biodme.eu/about-dme/.

[14] C. Arcoumanis, C. Bae, R. Crookes, E. Kinoshita. *Fuel* 87 (2008) 1014-1030.

[15] E.D. Larson, H. Yang. *Energy for Suitainable Development* 8 (2004) 115-126.

[16] Z. Azizi, M. Rezaeimanesh, T. Tohidian, M.R. Rahimpour. *Chemical Engineering and Processing* 2 (2014) 150-172.

[17] M. Deepak Kumar, M. Karthick, D. Dineshbabu, P. Srikanth, M.G. Ramachandran. ICMEET 2015 International Journal of Innovative Research in Science, *Engineering and Technology* 4 (2015) 401-407.

[18] Página Web: Bio-DME disponible en Junio de 2019 en www.biodme.eu.

[19] Página Web: Disponible en Junio de 2019 en https://marketing-accion.com/news/si-el-diesel-se-reemplazara-por-el-bio-dme-las-emisiones-de-co2-se-reducirian-en-un-95/.

[20] S. Jones. Hydrogen Distribution and Transmission. *UK Hydrogen Energy Network-Hydrogen Storage Workshop*, 2005.

[21] S.C. Sorenson. *Journal of engineering for gas turbines and power* 123 (2001) 652-658.

[22] S.H. Park, C.S. Lee. *Process in Energy and Combustion Science* 39 (2013) 147-168.

[23] Z. Huang, W. Zhang, J. Fang, X. Qiao. *4th International DME Conference* (2010) Stockholm – Sweden.

[24] B. Prabowo, M. Yan, M. Syamsiro, R.H. Setyobudi, M.K.Biddinika. *Proceeding of the Pakistan Academy of Science. Pakitan Academy of Sciences B. Life and Environmental Sciences* 54 (2017) 29-39.

[25] Brochure of Volvo. Volvo Bio-DME Unique field test in comercial operations, 2010-2012. Disponible en Junio de 2019 en

https://www.aboutdme.org/aboutdme/files/ccLibraryFiles/Filename/000000002392/BioDME_Volvo_brochure.pdf.

[26] P. Salomonsson. BioDME. *5th International DME Conference* (2013), Ann Arbor (EEUU).

[27] Página Web: Volvo Group disponible en Junio de 2019 en

https://www.volvogroup.com/en-en/news/2017/jan/mack-trucks-tests-alternative-fuel-dme.html.

[28] Página Web: aboutdme.org. New York City Reports on First Customer Demonstration of DME-Powered Mack Truck. New York City 2 de octubre de 2017. Disponible en Junio de 2019 en https://www.aboutdme.org/index.asp?sid=97.

[29] S-H. Lee, W. Cho, T. Song, Y-J. Ra. Scale up study of DME direct synthesis technology. *24th World Gas Conference* (2009) Buenos Aire, Argentina.

[30] M. Berggren. Global Methanol: Demand Grows as Margins Atrophy. *19th IMPCA Asian Methanol Conference* (2016) Singapore.

[31] D. Sheldon. *Johnson Matthey Technology Review*. 61 (2017) 172-182.

[32] A. Montebelli, C. G. Visconti, G. Groppi, E. Tronconi, S. Kohler, H. J. Venvik, R. Myrstad. *Applied Catalysis A: General* 481 (2014) 96-103.

[33] X. K. Phan, H. Bakhtiary-Davijany, R. Myrstad, P. Pfeifer, H. J. Venvik, A. Holmen. *Applied Catalysis A: General* 405 (2011) 1-7.

[34] M. Alvarado. Global Methanol Outlook. The source for Critical Information and Insight. Febrero 2016. Disponible en Junio de 2019 en http://www.methanol.org/wp-content/uploads/2016/07/Marc-Alvarado-Global-Methanol-February-2016-IMPCA-for-upload-to-website.pdf.

[35] J.H. Edwards, N.R. Foster. *Fuel Science and Technology International* 4 (1986) 365-390.

[36] J.J. Spivey. *Chemical Engineering Communications* 110 (1991) 123-142.

[37] C.D. Chang, C.T-W. Chu, R.F. Socha. *Journal of catalysis* 86 (1984) 289-296.

[38] É. Sarkadi-Pribóczki, N. Kumar, T. Salmi, Z. Kovács, D.Y. Murzin. *Catalysis Letters* 93 (2004) 101-107.

[39] T. Takeguchi, K. Yanagisawa, T. Inui, M. Inoue. *Applied Catalysis A: General* 192 (2000) 201-209.

[40] J. Xia, D. Mao, W. Tao, Q. Chen, Y. Zhang, Y. Tang. *Microporous and Mesoporous Materials* 91 (2006) 33-39.

[41] M. Stöcker. *Microporous and Mesoporous Materials* 29 (1999) 3-48.

[42] F.S. Ramos, A.M. Duarte de Farias, L.E.P. Borge, J.L. Monteiro, M.A. Fraga, E.F. Sousa-Aguiar, L.G. Appel. *Catalysis Today* 101 (2005) 39-44.

[43] D. Mao, W. Yang, J. Xia, B. Zhang, Q. Song, Q. Chen. *Journal of catalysis* 230 (2005) 140-149.

[44] M. Xu, J.H. Lunsford, D.W. Goodman, A. Bhattacharyya. *Applied Catalysis A: General* 149 (1997) 289-301.

[45] S.N. Khadzhiev, M.V. Magomedova, E.G. Peresypkina. *Petroleum Chemistry* 54 (2014) 245-269.

[46] A. García-Trenco, A. Martínez. *Applied Catalysis A: General* 411-412 (2012) 170-179.

[47] D. Mao, J. Xia, B. Zhang, G. Lu. *Energy conversion and Management* 51 (2010) 1134-1139.

[48] K.S. Yoo, J-H. Kim, M-J. Park, S-J. Kim, O.S. Joo, K.D. Jung. *Applied catalysis A: General* 330 (2007) 57-62.

[49] M. Stiefel, R. Ahmad, U. Arnold, M. Döring. *Fuel Processing Technology* 92 (2011) 1466-1474.

[50] J.M. Campelo, F. Lafont, J.M. Marinas, M. Ojeda. *Applied Catalysis A: General* 192 (2000) 85-96.

[51] D. Mao, W. Yang, J. Xia, B. Zhang, G. Lu. *Journal of Molecular Catalysis A: Chemical* 250 (2006) 138-144.

[52] T.H. Fleisch, A. Basu, R.A. Sills. *Journal of Natural Gas Science and Engineering* 9 (2012) 94-107.

[53] Japan DME Association (http://japan-dme.or.jp/english/dme/production.html).

[54] Y. Ohno, M. Yoshida, T. Shikada, O. Inokoshi, T. Ogawa, N. Inoue. *JFE Technical Report*. JFE GIHO 6 (2004) 70-75.

[55] M.C.J. Bradford, M.V. Konduru, D.X. Fuentes. *Fuel Processing Technology* 83 (2003) 11-25.

[56] P. Davis, F.F. Snowdon, G.W. Bridger, D.O. Hughes, P.W. Young. UK *Patent 1010871 (1965).*

[57] M. Stiefel, R. Ahmad, U. Arnold, M. Döring. *Fuel Processing Technology* 92 (2011) 1466-1474.

[58] A.S. Rocha, A.M. da S. Forrester, E.R. Lachter, E.F. Sousa-Aguiar. *Catalysis Today* 192 (2012) 104-111.

[59] J. Chang, Y. Fu, Z. Luo. *Biomass and Bioenergy* 39 (2012) 67-72.

[60] Y. Wang, W-L. Wang, Y-X. Chen, J-J. Zheng, R-F. Li. *Journal of Duel Chemistry and Technology* 41 (2013) 873-882.

[61] F. Hayer, H. Bakhtiary-Davijany, R. Myrstad, A. Holmen, P. Pfeifer, H. J. Venvik. *Chemical Engineering Journal* 167 (2011) 610-615.

[62] R. Tavares Figueiredo, A. Martínez-Arias, M. López Granados, J.L. Fierro. *Journal of Catalysis* 178 (1998) 146-152.

[63] C. Baltes, S. Vukojevic, F. Schuth. *Journal of catalysis* 258 (2008) 334-344.

[64] K. Saravanan, H. Ham, N. Tsubaki, J.W. Bae. *Applied Catalysis B: Environmental* 217 (2017) 494-522.

[65] F. Song, Y. Tan, H. Xie, Q. Zhang, Y. Han. *Fuel Processing Technology* 126 (2014) 88-94.

[66] C. Li, X. Yuan, K. Fujimoto. *Applied catalysis A: General* 469 (2014) 306-311.

[67] Y. Tan, H. Xie, H. Cui, Y. Han, B. Zhong. *Catalysis Today* 104 (2005) 25-29.

[68] Z. Li, J. Li, M. Dai, Y. Liu, D. Han, J. Wu. *Fuel* 121 (2014) 173-177.

[69] A. García-Trenco, S. Valencia, A. Martínez. *Applied catalysis A: General* 468 (2013) 102-111.

[70] J. Huertas Flores, M.I. Pais da Silva. *Catalysis Letter* 146 (2016) 1505-1516.

[71] E. Catizzone, A. Aloise, M. Migliori, G. Giordano. *Applied catalysis A: General* 502 (2015) 215-220.

[72] J. Fei, Z. Hou, B. Zhu, H. Lou, X. Zheng. *Applied Catalysis A: General* 304 (2006) 49-54.

[73] D. Jin, B. Zhu, Z. Hou, J. Fei, H. Lou, X. Zheng. *Fuel* 86 (2007) 2707-2713.

[74] A. Ateka, P. Pérez-Uriarte, M. Sanchez-Contador, J. Ereña, A.T. Aguayo, J. Bilbao. *International Journal of Hydrogen Energy* 41 (2016) 18015-18026.

[75] D. Mao, J. Xia, B. Zhang, G. Lu. *Energy conversion and Management* 51 (2010) 1134-1139.

[76] K.S. Yoo, J-H. Kim, M-J. Park, S-J. Kim, O.S. Joo, K.D. Jung. *Applied catalysis A: General* 330 (2007) 57-62.

[77] J.M. Campelo, F. Lafont, J.M. Marinas, M. Ojeda. *Applied Catalysis A: General* 192 (2000) 85-96.

[78] D. Mao, W. Yang, J. Xia, B. Zhang, G. Lu. J*ournal of Molecular Catalysis A: Chemical* 250 (2006) 138-144.

[79] P. Berteau, B. Delmon, *Cataysis Today* 5 (1989) 121-137.

[80] T. Curtin, J.B. McMonagle, B.K. Hodnett, *Applied Catalysis A: General* 93 (1992) 75-89.

[81] F. Raoof, M. Taghizadeh, A. Eliassi, F. Yaripour. *Fuel* 87 (2008) 2967-2971.

[82] R. Garoña*, Tesis Doctoral* (2005) Universidad del País Vasco (UPV/EHU).

[83] A.T. Aguayo, J. Ereña, I. Sierra, M. Olazar, J. Bilbao. *Catalysis Today* 106 (2005) 265-270.

[84] J. Ereña, R. Garoña, J.M. Arandes, A.T. Aguayo, J. Bilbao. *International Journal of Chemical Reactor Engineering* 3 (2005) 1-15.

[85] Q. Ge, Y. Huang, F. Qiu, S. Li. *Applied Catalysis A: General* 167 (1998) 23-30.

[86] A. García, Trenco, A. Vidal-Moya, A. Martínez. *Catalysis Today* 179 (2012) 43-51 .

[87] S. Papari, M. Kazemeini, M. Fattahi. *Journal of Natural Gas Chemistry* 21 (2012) 148-157.

[88] D. Liu, X. Hua, D. Fang. *Journal of Natural Gas Chemistry* 16 (2007) 193-199.

[89] T. Ogawa, N. Inoue, T. Shikada, Y. Ohno. *Journal of Natural Gas Chemistry* 12 (2003) 219-227.

[90] H.S. Fogler. *Elements of Chemical Reaction Engineering*. 3rd Edition (1999) Prentice Hall.

[91] W.Z. Lu, L-H. Teng, W-D. Xiao. *Chemical Engineering Science* 59 (2004) 5455-5464.

[92] J. Ereña, R. Garoña. J.M. Arandes, A.T. Aguayo, J. Bilbao. *Catalysis Today* 107 (2005) 467-473.

[93] D.M. Brown, B.L. Bhatt, T.H. Hsiung, J.J. Lewnard, F.J. Waller. *Catalysis Today* 8 (1991) 279-304.

[94] D. Liu, X. Hua, D. Fang. *Journal of Natural Gas Chemistry* 16 (2007) 193-199.

[95] Y.C. Ray, T.S. Jiang, C.Y. Wen. *Power Technology* 49 (1987) 193-206.

[96] P. Ávila, T. Garetto, M. Montes. *Eliminación de emisiones atmosféricas de COVs por catálisis y adsorción. Capítulo 8*. Ed. T. Garetto, I. Legorburu y M. Montes (CYTED) España (2008) 63-83.

[97] V. Meille. Applied Catalysis A: General 315 (2006) 1-17.

[98] O.H. Laguna, M.I. Domínguez, M.A. Centeno, J.A. Odriozola. *New Materials for Catalysis Applications. Capítulo 4*. Ed. V.I. Parvulescu y E. Kemnitz (Elsevier) Amsterdam (2016) 81-120.

[99] O. Sanz, F.J. Echave, F. Romero-Sarria, J.A. Odriozola, M. Montes. *Renewable Hydrogen Technologies. Capítulo 9*. Ed. L.M. Gandía, G. Arzamendi y P.M. Diéguez (Elsevier) Amsterdam (2013) 201-224.

[100] P. Ávila, M. Montes, E.E. Miró. Chemical Engineering Journal 109 (2005) 11-36.

[101] M.M. Manfe, K.S. Kulkarni, A.D. Kulkarni. *International Journal of Advanced Engineering Research and Studies* 1 (2011) 1-3.

[102] I. Velasco Ortiz. Tesis Doctoral (2015) Universidad del País Vasco (UPV/EHU).

[103] J. Hu, Y. Wang, C. Cao, D.C. Elliot, D.J. Stevens, J.F. White. *Industrial & Engineering Chemistry Research* 44 (2005) 1722-1727.

[104] F. Hayer, H. Bakhtiary-Davijany, R. Myrstad, A. Holmen, P. Pfeifer, H. J. Venvik. *Chemical Engineering and Processing* 70 (2013) 77-85.

[105] L. Giani, C. Cristiani, G. Groppi, E. Tronconi. *Applied Catalysis B: Environmental* 62 (2006) 121-131.

[106] E. Bianchi, T. Heidig, C.G. Visconti, G. Groppi, H. Freund, E. Tronconi. *Catalysis Today* 216 (2013) 121-134.

[107] A. Egaña, O. Sanz, D. Merino, X. Moriones, M. Montes. I*ndustrial & Engineering Chemistry Research* 57 (2018) 10187-10197.

[108] E. Bianchi, T. Heidig, C.G. Visconti, G. Groppi, H. Freund, E. Tronconi. *Chemical Engineering Journal* 198-199 (2012) 512-528.

[109] C.G. Visconti, A. Montebelli, G. Groppi, E. Tromconi, S. Kohler. *Methanol Science and Engineering. Capítulo 19.* Ed. A. Basile y F. Dalena (Elsevier) Amsterdam (2018) 519-538.

[110] A. Kolodziej, J. Lojewska. *Catalysis Today* 105 (2005) 378-384.

[111] O. Sanz, E.D. Banús, A. Goya, H. Larumbe, J.J. Delgado, A. Monzón, M. Montes. *Catalysis Today* 296 (2017) 76-83.

[112] Página Web: Precision Combustion, Inc. disponible en Julio de 2019 en https://www.precision-combustion.com/technologies/microlith-technologies.

[113] S.A. Vilekar, K. Hawley, C. Junaedi, B. Crowder, J. Prada, R. Mastanduno. *47th International Conference on Environmental Systems 16-20* July 2017, Charleston, South Carolina.

[114] M. Castaldi, M. Lyubovsky, R. LaPierre, W.C. Pfefferle, S. Roychoudhury. *Society of Automotive Engineers*, Inc. 2003.

[115] Z. Shan, W.E.J. Van Kooten, O.L. Oudshoorn, J.C. Jansen, H. Van Bekkum, C.M. Van den Bleek, H.P.A. Calis. *Microporous and Mesoporous Materials*. 81-91.

[116] N. R. Peela, A. Mubayi, D. Kunzru. *Catalysis Today,* 147S (2009) S17-S23.

[117] V.G. Milt, S. Ivanova, O Sanz, M.I. Dominguez, A. Corrales, J.A. Odriozola, M.A. Centeno. *Applied Surface Science*, 270 (2013) 169-177.

[118] G. Groppi, E. Tronconi, C. Cortelli, R. Leanza. *Industrial & Engineering Chemistry Research* 51 (2012) 7590-7596.

[119] F.J. Echave, O. Sanz, I. Velasco, J.A. Odriozola, M. Montes. *Catalysis Today* 213 (2013) 145-154.

[120] O. Sanz, S.A. Cruz, J.C. Millán, M. Montes, J.A. Odriozola. *Studies in Surface Science and Catalysis* 175 (2010) 661-664.

[121] E. Tronconi, G. Groppi, T. Boger, A. Heibel. *Chemical Engineering Science* 59 (2004) 4941-4949.

[122] A. Montebelli, C.G. Visconti, G. Groppi, E. Tronconi, S. Kohler, H.J. Venvik, R. Myrstad. *Applied Catalysis A: General* 481 (2014) 96-103.

[123] L.R. Chapman, Powell, Tenn (1982) *U.S. Patent No. 4,318,828.*

[124] M. Kaur, K.P. Methe, S.K. DEspande, S. Choudhury, J.B. Singh, N. Verma, S.K. Gupta, J.V. Yakhmi. *Journal of Crystal Growth* 289 (2006) 670-675.

[125] Y. Diaz, A. Sevilla, A. Mónaco, F.J. Méndez, P. Rosales, L. García, J.L. Brito. *Fuel* 110 (2013) 235-248.

[126] O. Sanz, F.J. Echave, J.A. Odriozola, M. Montes. *Industrial & Engineering Chemistry Research* 50 (2011) 2117-2125.

[127] J.A. Santander, D.E. Boldrini, M.N. Pedernera, G.M. Tonetto. *The Canadian Journal of Chemical Engineering* 95 (2017) 1554-1561.

[128] B. Balamurugan, B. Mehta, S. Shivaprasad. *Applied Physics Letters* 79 (2001) 3176-3178.

[129] D. Merino Bella. *Tesis Doctoral* (2016) Universidad del País Vasco (UPV/EHU).

[130] F.J. Echave, O. Sanz, M. Montes. *Applied Catalysis A: General* 474 (2014) 159-167.

[131] C. Agrafiotis, A. Tsetsekou. *Journal of the European Ceramic Society* 20 (2000) 815-824.

[132] J.R. González-Velasco, M.A. Gutierrez-Ortiz, J.L. Marc, J.A. Botas, M.P. González-Marcos, G. Blanchard. *Industrial & Engineering Chemistry Research*, 42 (2003) 311-317.

[133] T.A. Nijhuis, A.E. W. Beers, T. Vergunst, I. Hoek, F. Kapteijn, J.A. Moulijn *Preparation of monolithic catalysts, Catalysis Reviews*, 43:4 (2001) 345-380.

[134] S. Vallar, D. Houivet, J. El Fallah, D. Kervadec, J.M. Haussonne. *Journal of the European Ceramic Society* 19 (1999) 1017-1021.

[135] J.M. Zamaro, M. A. Ulla, E.E. Miró. *Catalysis Today*, 107-108 (2005) 86-93.

[136] G. Germani, A. Stefanescu, Y. Schuurman, A.C. van Veen. *Chemical Engineering Science,* 62 (2007) 5084-5091.

[137] A.K. Mogalicherla, D. Kunzru. The *Canadian Journal of Chemical Engineering*, 88 (2010) 367-375.

CHAPTER 2

Experimental Part

INDEX

2.1. Introduction

This chapter is divided in three parts. First, the catalyst preparation methods are described. Then, all characterization techniques are explained. Finally, the set-up for activity tests is described.

2.2. Catalysts preparation

In this part, a detailed description of the synthesis of all the catalysts used is presented. Catalysts can be divided in 3 main groups: powder, slurried or structured catalysts.

2.2.1. Powder Catalyst preparation

Different catalysts were tested for each reaction. A $Cu/ZnO/Al_2O_3$ catalyst was used for methanol synthesis reaction and methanol dehydration was carried out with a ZSM-5 zeolite.

On the other hand, different ways of synthesis based on copper encapsulation were studied to prepare Cu-based catalysts for direct synthesis of DME.

2.2.1.1. $Cu/ZnO/Al_2O_3$ (CZA)

Methanol synthesis catalyst, $Cu/ZnO/Al_2O_3$ (CZA), was synthesised by a conventional co-precipitation method [1]. A 1 M solution of metallic precursors such as $Cu(NO_3)\cdot 3H_2O$ (≥99.5% for analysis, Merk), $ZnO(NO_3)\cdot 6\cdot H_2O$ (reagent grade ≥98%, Sigma Aldrich) and $Al(NO_3)_3\cdot 9H_2O$ (ACS reagent ≥98%, Sigma Aldrich) was slowly dropped into a closed vessel with water at 70 ºC. The solution was prepared to obtain a molar ratio of Cu:Zn:Al of 6:3:1 in the final catalyst. 1 M of Na_2CO_3 (Panreac, anhydrous for analysis ACS) solution was simultaneously added to maintain the pH at 7.

After the addition of the metallic precursors solution, the mixture was aged 1 h at 70 ºC and pH 7. Finally, the generated solid was filtered and washed until all Na^+ was removed, dried at 100 ºC for 12 h and calcined at 400 ºC (2 ºC/min) 3 h.

2.2.1.2. ZSM-5 zeolite

In this work, a commercial ammonium ZSM-5 zeolite (CBV2314 provided by Zeolyst International) was used as solid acid. To obtain the H-type zeolite, it was thermally treated at 500 ºC (2 ºC/min) during 5 h under air atmosphere.

2.2.1.3. Cu encapsulation

Different copper encapsulation methods were synthesised.

2.2.1.3.1. Sacrificial Template

The encapsulation of copper by the sacrificial template method consists of using multi-walled carbon nanotubes (CNT) as sacrificial template. The metal salt used as precursor is dispersed on the CNT's surface by impregnation. Then, the zeolite is grown around these CNT's following a hydrothermal treatment (*Figure 2.1*). During calcination, the CNT's are removed and a porous structure is generated, causing the encapsulation of copper particles inside the zeolite structure [2,3].

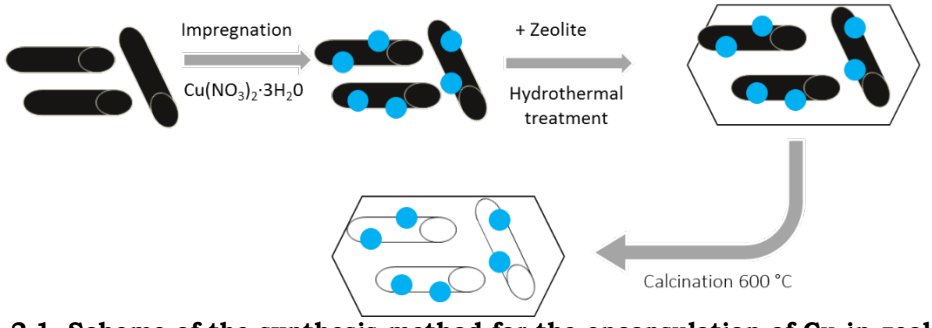

Figure 2.1. Scheme of the synthesis method for the encapsulation of Cu in zeolite by sacrificial template.

The synthesis steps are:

1. *Functionalization of carbon nanotubes*: CNT's (IoLiTec nanomaterials) with different sizes (O.D.: 10-20 and 20-40 nm) were functionalised by means of nitric acid oxidation. 3 g of CNT's were treated in 210 g of HNO_3 (65% technical grade, Panreac) at 140 ºC for 14 h. Then, CNT's were filtered and washed until a pH value of 7.0 was attained. Finally, samples were dried at 100 ºC overnight.

2. *Copper impregnation:* Functionalised CNT's were impregnated with a $Cu(NO_3)\cdot 3H_2O$ solution to obtain a metal content of 20% Cu in the CNT's. 1.5 g of CNT's were sonicated during 30 minutes in a solution with 30 g of water and 1.4 g of $Cu(NO_3)\cdot 3H_2O$. Then the mixture was dried at 80 ºC overnight and treated thermally in inert flow (N_2) at 400 ºC (5 ºC/min) for 4 h. Samples were referred to as 20%Cu/CNT with the size of CNT's used in brackets.

3. *Refunctionalisation of 20%Cu/CNT*: this process was carried out to generate again hydroxyl groups on the CNT's surface and to improve the hydrophilic character of CNT's. A mixture of H_2O_2:H_2O (1:1, mass ratio) was added dropwise onto 20%Cu/CNT. The mixture was sonicated during 30 min and dried at 80 ºC overnight.

4. *Zeolite surface growth*: ZSM-5 zeolite was synthesised on the 20%Cu/CNT sample. 380 mg of NaCl (Scharlau), 3 g of TPAOH (tetrapropilammonium hydroxide solution 1 M, Sigma Aldrich), 40 mg of $NaAl_2O$ (Sodium aluminate technical anhydrous, Sigma Aldrich), 30 g of deionised water, 2.8 g of TEOS (tetraethyl orthosilicate ≥99%, Sigma Aldrich) and 0.3 g of 20%Cu/CNT were transferred to a Teflon lined autoclave and stirred for 1 h. Then, the autoclave was closed, and the mixture was treated at 170 ºC for 24 h. The solid was filtered and washed until pH = 7. Then, the solid was dried at 80 ºC and calcined at 600 ºC (5 ºC/min) during 4 h. Samples were referred to as Cu@NaZSM-5 with the size of CNT's in nm used in brackets.
   Samples without CNT's (Zeolite ZSM-5) or with CNT's without copper (@ZSM-5) were also synthesised. Samples without CNT's were synthesised

with 380 mg of NaCl, 3 g of TPAOH, 40 mg of $NaAl_2O$, 30 g of deionised water and 2.8 g of TEOS. Lastly, samples with CNT's without copper were prepared using 380 mg of NaCl, 3 g of TPAOH, 40 mg of $NaAl_2O$, 30 g of deionised water, 2.8 g of TEOS and 0.3 g of CNT's. Then, the same procedure as that described above for Cu@NaZSM-5 was followed.

5. *Ion exchange*: The synthesised zeolite was obtained in sodium form. An ion exchange was conducted to obtain the ammonium-form zeolite. The sample was mixed with 50 mL of 2 M NH_4NO_3 (≥99.5%, Sigma Aldrich) at 80 ºC for 1 h. Then, the solid was filtered and dried at 80 ºC for 2 h. This procedure was repeated twice.

6. *Calcination*: the final solid was calcined at 450 ºC (5º C/min) during 4 h to obtain the H-type zeolite. The samples were called as Cu@HZSM-5 with the size of CNT's used in brackets.

2.2.1.3.2. Carbon spheres

This method is based on the generation of a carbon layer around copper nanoparticles with glucose. Then, the zeolite is grown around these carbon spheres and, after calcination, the carbon layer is removed. As a result, copper nanoparticles are dispersed in a zeolite matrix (*Figure 2.2*).

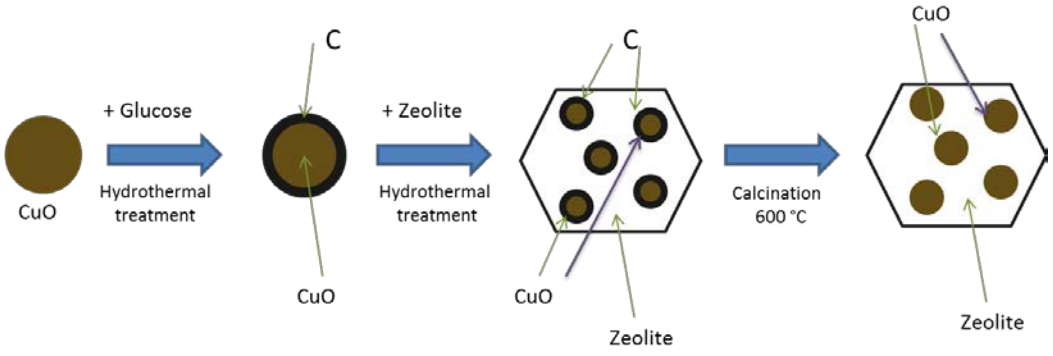

Figure 2.2. Scheme of the synthesis method for encapsulation of Cu in zeolite by carbon spheres.

The procedure was:

1. *Carbon spheres synthesis*: 0.5 g of CuO (Alfa Aesar 30-50nm APS powder) was mixed in 30 g of 0.1 M glucose solution. The mixture was dried in a closed autoclave to grow on the copper particles a carbon layer at 130 ºC for 24 hours. The powder was washed with deionised water by centrifugation and dried at 80 ºC overnight. The obtained powder was referred to as Cu@C.

2. *Zeolite growth*: the ZSM-5 zeolite was synthesised by mixing 0.2 g of Cu@C, 380 mg of NaCl (Scharlau), 3 g of TPAOH (1 M, Sigma Aldrich), 40 mg of $NaAl_2O$ (Sodium aluminate technical anhydrous, Sigma Aldrich), 30 g of deionised water and 2.8 g of TEOS (≥99%, Sigma Aldrich). The mixture was stirred for 1 h and thermally treated in autoclave at 170 ºC for 24 h.

3. *Calcination*: the obtained powder was washed thoroughly and calcined at 600 ºC (5 ºC/min) during 4h.

4. *Ion exchange*: the synthesised zeolite was obtained in sodium form. This process was made to obtain the ammonium-form zeolite. The sample was mixed with 50 mL of 2 M NH_4NO_3 (≥99.5%, Sigma Aldrich) at 80 ºC 1 h. Then the solid was filtered and dried at 80 ºC for 2 h. This procedure was repeated twice.

5. *Calcination*: The final solid was calcined at 450 ºC (5º C/min) during 4 h to obtain the H-type zeolite.

2.2.1.3.3. Nanoreactors

The nanoreactors method consists of preparing copper nanoparticles by an emulsion (every emulsion drop is considered a nanoreactor) and covering them with a layer of SiO_2, which is used as silicon source for zeolite synthesis [4] (*Figure 2.3*).

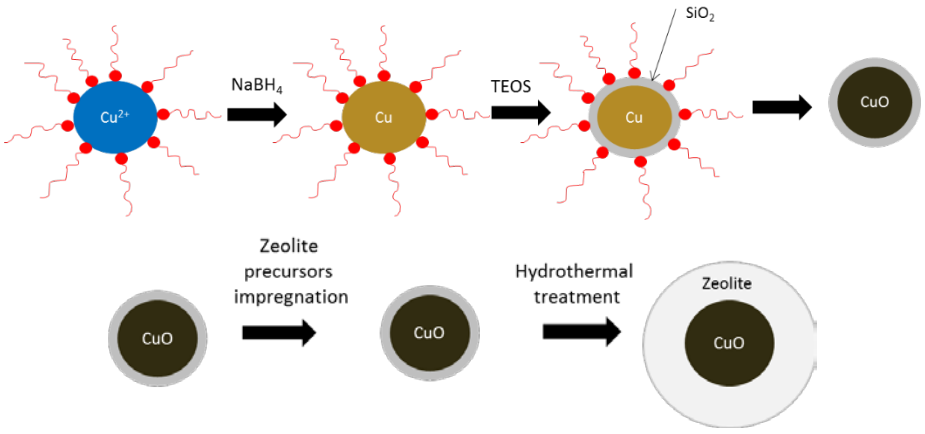

Figure 2.3. Scheme of the synthesis method for encapsulation of Cu in zeolite by the nanoreactors method.

The synthesis steps are:

1. An inverse microemulsion (water in oil) was prepared by mixing 12 g of CTAB (hexadecyltrimethylammonium bromide ≥99%, Sigma Aldrich), 20 g of 1-hexanol (anhydrous ≥99%, Sigma Aldrich) and 8 g of a 0.4 M $Cu(NO_3)\cdot 3H_2O$ solution (Emulsion A).

2. Another emulsion (Emulsion B) was prepared with 6 g of CTAB, 10 g of 1-hexanol, 4 g of deionised water and 0.44 g of $NaBH_4$ (≥96%, Sigma Aldrich).

3. Emulsion B is slowly dropped onto Emulsion A thus forming Emulsion C.

4. pH of the Emulsion C was adjusted to 9 using an ammonia solution.

5. 5 g of TEOS (≥99%, Sigma Aldrich) were added to Emulsion C and stirred during 5 h.

6. After hydrolysis time, the solid was filtered and washed by centrifugation with ethanol and deionised water.

7. The final powder was dried at 80 °C overnight and calcined at 450 °C (5 °C/min) for 4 h. The sample was referred to as Cu@SiO_2-xh, where x is the hydrolysis time in hours.

8. Finally, the zeolite was synthesised. 0.066 g NaOH (Fluka), 0.032 g $NaAl_2O$ (technical anhydrous, Sigma Aldrich) and 6 g of TPAOH (1 M, Sigma Aldrich) per g of SiO_2 was added to Cu@SiO_2. The mixture was stirred 30 min to generate a gel and dried at 60 °C overnight.

   The powder was milled and put in a small vessel inside the Teflon autoclave (*Figure 2.4*). This small vessel was placed inside the autoclave with 15 g of water, as shown in *Figure 2.4*. This arrangement allows the solid not to be in direct contact with liquid water but with its vapor.

Figure 2.4. Autoclave and Teflon vessels used for zeolite synthesis with Cu@SiO_2 nanoreactors.

9. The autoclave was closed and put in the oven for 3 days at 170 °C. The final solid was filtered and washed thoroughly, dried at 80 °C overnight and calcined at 450 °C (5 °C/min) for 4 h.

10. The zeolite was synthesised in sodium-form. An ion exchange treatment was carried out to obtain the ammonium-form zeolite. The sample was mixed with 50 mL of 2 M NH_4NO_3 (≥99.5%, Sigma Aldrich) at 80 ºC for 1 h. Then, the solid was filtered and dried at 80 ºC 2 h. This procedure was repeated twice.

11. The final solid was calcined at 450 ºC (5º C/min) for 4 h to obtain the H-type zeolite.

2.2.1.3.4. Confinement of CuZn in SBA-15

Copper and zinc particles were confined in the mesopores of SBA-15 substrates. First, two different substrates with SBA-15 structures were synthesised: one conventional SBA-15 siliceous substrate and another substrate with greater acidity by incorporating aluminium to the SBA-15 structure. Finally, copper and zinc were impregnated on the substrates.

2.2.1.3.4.1. SBA-15

First, SBA-15 was synthesised following the method proposed by H. Pérez *et al.* [5]. Briefly, 9.6 g of Pluronic® P-123 (poly(ethylene glycol)-block-poly(propylene glycol)-block-poly(ethylene glycol) Mn~5800, Sigma Aldrich) were dissolved in 225 g of deionised water in a polypropylene autoclave (Nalgene®). Then, 150 g of 0.5 M HNO_3 (65% technical grade, Panreac) were added and the mixture was stirred during 4 h at 35 ºC. Once this dwell time elapsed, 5 g of TEOS (98%, Acros organics) were added to the vessel and the mixture was stirred at 35 ºC during 24 h. Finally, the vessel was closed and thermally treated in an oven at 80 ºC for 72 h. The obtained powder was filtered and washed until a pH value of 7 was attained. The solid was calcined at 500 ºC (2 ºC/min) for 6 h.

2.2.1.3.4.2. Al incorporation to SBA-15

Incorporation of aluminium was carried out following a similar method to the "pH-adjusting" method proposed by S. Wu *et al.* [6]. In a polypropylene closed vessel (Nalgene®) 9.6 g of Pluronic® P-123 (poly(ethylene glycol)-block-poly(propylene glycol)-block-poly(ethylene glycol) Mn~5800, Sigma Aldrich) were dissolved with 225 g of distillate water. 150 g of 0.5 M HNO_3 (65% technical grade, Panreac) were added and stirred during 4 h at 35 ºC. Then, 5 g of TEOS (98%, Acros Organics) and the required amount of $Al(NO_3)_3 \cdot 9H_2O$ (ACS reagent ≥98%, Sigma Aldrich) to obtain a Si/Al ratio of 5 were added. The solution was stirred for 24 h at 35 ºC. Once this time had passed, the vessel was closed and put in the oven at 80 ºC for 72 h.

After the first hydrothermal treatment, the product was cooled down to room temperature and the pH was fixed to 7.5 to favour Al condensation. Then, it was hydrothermally treated again at 80 ºC for 24 h.

The obtained solid was filtered and washed until pH = 7.0 and dried at room temperature overnight. The final powder was calcined at 500 ºC (2 ºC/min) for 6 h.

2.2.1.3.4.3. Ammonia-driving deposition-precipitation method

To confine copper in the characteristic porous structure of the siliceous SBA-15 support, an ammonia-driving deposition-precipitation method was used [7,8]. A 0.4 M solution of $Cu(NO_3) \cdot 3H_2O$ (≥99.5% for analysis, Merk) and $Zn(NO_3) \cdot 6H_2O$ (reagent grade ≥98%, Sigma Aldrich) was prepared with a Cu/Zn mass ratio of 2. This solution was mixed with the siliceous support and stirred during 10 min to obtain a catalyst with 25% of CuZn. Then, ammonia solution (20% extra pure, Scharlau) was added in the necessary amount to have a $(Cu+Zn)/NH_3$ molar ration of ¼ , and stirred at 40 ºC during 4 h. Then, the solvent was evaporated in a rotary evaporator at 40 ºC. The obtained solid was dried at 100 ºC overnight and calcined at 550 ºC (1 ºC/min) for 4 h.

2.2.2. Structured catalyst preparation

Structured catalyst preparation by washcoating consisted of three main steps: structured substrate preparation, slurry preparation and washcoating.

2.2.2.1. Structured substrate preparation

Different metallic substrates were prepared: monoliths and open cell foams (*Figure 2.5*). The characteristics of the metallic substrates are summarised in *Table 2.1*.

Table 2.1. Characteristics of different alloys used for monoliths preparation (Data from manufacturers).

Alloy	Chemical composition	Thickness (μm)	Melting point (ºC)	Thermal conductivity (W/(m·K))
Fecralloy®	72.8% Fe, 22.0% Cr, 5.0% Al, 0.1% Y, 0.1% Zr	50	1380-1490	16-26
Brass 63Cu/37Zn	61.5-64.0% Cu Zn balance	50	916	109-121
Aluminium Al 8079	0.05-0.30% Si, 0.70-1.30% Fe, 0.05% Cu, 0.10% Zn, Al balance	80	660	200-235

Figure 2.5. Metallic structured substrates used for structured catalysts preparation.

A) Monoliths

Monoliths with longitudinal channels were manufactured by rolling up corrugated and flat metal foils.

Monoliths of 16 mm outer diameter and 30 mm of height with different cell densities were prepared (*Table 2.2*). First, they were cleaned with water and soap followed by acetone rinsing. After cleaning, the longest foil was corrugated (*Figure 2.6*). Then, the corrugated and flat foils were assembled and rolled up (*Figure 2.7*). The obtained monoliths were cleaned with soap and water followed by acetone rinsing in ultrasound for 30 min.

Table 2.2. Characteristic dimensions of the different monoliths prepared.

Name	Cell density (cpsi)	Foil length (cm)		Lateral surface (cm^2)
		Flat	Corrugated	
R1	2360	36	52.0	528
R4	289	15	20.5	213

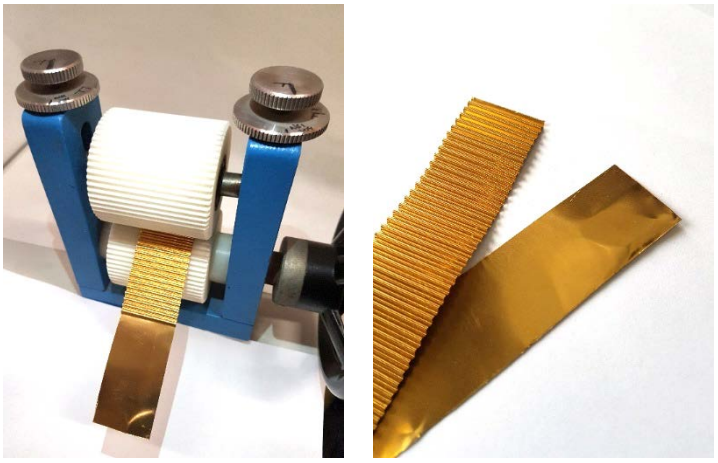

Figure 2.6. Equipment for corrugation (Left) and detailed image of corrugated and flat brass foils (right).

Figure 2.7. Equipment for rolling (left) and detailed image of two foils (corrugated and flat) assembled and rolled up (right).

Monoliths were pretreated depending on the alloy to form roughness in the surface. Fecralloy monoliths were thermally treated at 900 ºC (10ºC/min) for 22 h [9]. Brass monoliths were thermally treated at 550 ºC (10ºC/min) during 18h [10]. As for aluminium monoliths, they were chemically treated: first, monoliths were immersed in a soapy solution having 1500 g of deionised water and a half of a dishwasher detergent tablet (8 g approx. of Finish Quantum, Reckitt Benckiser Ltd.) at 70 ºC for 40 min; finally, aluminium monoliths were rinsed with water, dried at 120 ºC during 30 min and calcined at 500 ºC (10 ºC/min) for 2 h [11].

B) Metallic foams

FeCrAl foams (BRC2005-08 Metpore®) were provided by Selee Co. and aluminium foams (Duocel®) were provided by ERG Aerospace. FeCrAl foams with 25.4 mm of height and aluminium foams with 30 mm of height, both with 16 mm of outer diameter, were obtained by cutting them with OPTIdrill B 23Pro (Optimum Maschinen Gmbh, Germany) (*Figure 2.8*). Finally, FeCrAl foams were thermally treated at 900 ºC (10 ºC/min) for 22 h and aluminium foams were calcined at 500 ºC during 2 h with a heating ramp of 10 ºC/min [12].

Figure 2.8. Photograph of OPTIdrill B 23Pro which is used to cut the cylindrical foam samples.

2.2.2.2. Slurry preparation

Slurry preparation consists of mixing the catalysts in aqueous media with different additives to improve coating properties and obtain homogeneous and adherent coatings.

Commonly, PVA (Sigma-Aldrich Mowiol® 4-88 Mw~31,000) was dissolved in water at 60-70 °C. After cooling, the catalyst and inorganic oxide colloid were added sequentially to the solution under stirring. The mixture was sonicated during 10 min, and then stirred for 24 h before the coating process.

- **Methanol synthesis catalyst**

Slurries were prepared with the dried CZA catalyst. Different slurries with 20% solid content were prepared by varying the CZA/colloid ratio (*Table 2.3*). In all the formulations, the CZA/PVA mass ratio was maintained at 21.5 approximately.

Table 2.3. Slurry formulations for methanol synthesis catalysts, CZA

Sample	CZA (%)	Colloid (%)	PVA (%)	H_2O (%)	Colloid
CZA_0%C*	19.1	0.0	0.9	80	-
CZA_10%C*	17.3	1.9	0.8	80	Al_2O_3
CZA_17.7%C*	15.9	3.4	0.7	80	Al_2O_3 ZnO SiO_2
CZA_33.3%C*	12.9	6.5	0.6	80	Al_2O_3 ZnO SiO_2

*C= Colloid used (Al_2O_3, ZnO or SiO_2)

- **Dehydration catalyst**

Slurries of ZSM-5 zeolite (CBV2314) were prepared with formulations previously developed in our lab (*Table 2.4*) [13]. Slurries were prepared with the zeolite in ammonium and proton forms.

Table 2.4. Slurry formulations for dehydration catalysts, ZSM-5 zeolite.

Sample	ZSM-5 (%)	Colloid (%)		PVA (%)	H_2O (%)
		SiO_2	Al_2O_3		
ZSM-5	35.0	0.0	0.0	0.0	65
ZSM-5_SiO_2	29.8	4.0	0.0	1.2	65
ZSM-5_Al_2O_3	31.6	0.0	2.1	1.3	65

- **Direct synthesis of DME catalyst**

Different formulations of slurries containing mixtures of both catalysts (CZA and HZSM-5) and with different colloids were prepared (*Table 2.5*). Formulations of 20 % of total solid content were prepared to get a CZA/HZSM-5 mass ratio equal to 2.

The formulation presenting the best adherence for each colloid was selected:

1. Methanol synthesis catalyst, CZA:

   - CZA_17.7%Al_2O_3
   - CZA_33.3%ZnO
   - CZA_33.3%SiO_2

2. Dehydration catalyst, HZSM-5: ZSM-5_11.8%SiO_2

Table 2.5. Slurry formulations of catalysts mixtures, CZA+HZSM-5, with different colloids.

Sample	CZA (%)	HZSM-5 (%)	Colloid (%)			PVA (%)
			Al_2O_3	ZnO	SiO_2	
C-Z	12.7	6.4	0.0	0.0	0.0	0.9
C-Z_ZnO	9.3	4.7	0.0	5.3	0.0	0.7
C-Z_ZnO+SiO_2	9.3	4.7	0.0	4.6	0.7	0.7
C-Z_SiO_2	9.3	4.7	0.0	0.0	5.3	0.7
C-Z_Al_2O_3+SiO_2	10.8	5.4	2.4	0	0.7	0.7
C-Z_Al_2O_3	10.8	5.4	3.1	0	0	0.7

For example, to prepare the C-Z_ZnO+SiO_2 sample:

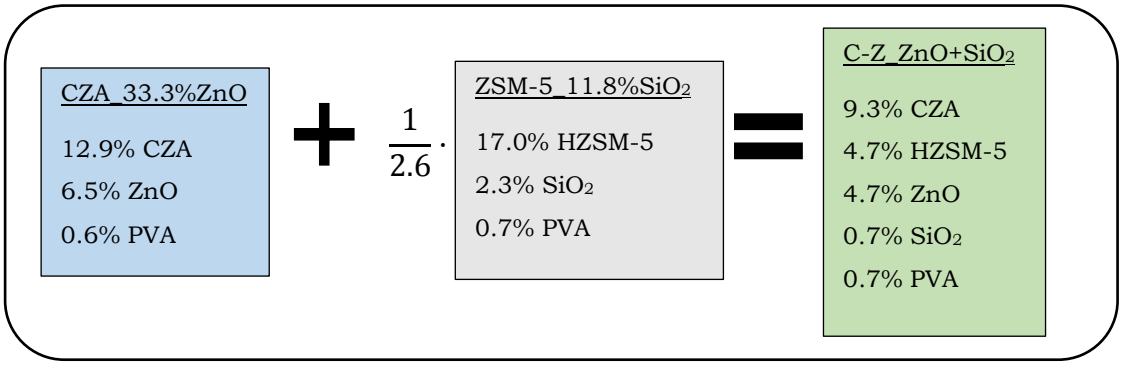

Furthermore, slurries of catalysts mixtures with different colloidal Al_2O_3 and SiO_2 contents were prepared (*Table 2.6*). The same CZA/zeolite = 2 and CZA+HZSM-5/PVA = 22.4 mass ratios were maintained.

Table 2.6. Slurry formulations of catalysts mixtures, CZA+HZSM-5, with different colloidal Al_2O_3 and SiO_2 content.

Sample	CZA (%)	HZSM-5 (%)	Colloid (%)		PVA (%)	H_2O (%)
			Al_2O_3	SiO_2		
C-Z	12.7	6.4	-	-	0.9	80
C-Z_6.8%Al_2O_3	11.9	6.0	1.3	-	0.8	80
C-Z_8.9%Al_2O_3	11.7	5.8	1.7	-	0.8	80
C-Z_12.5%Al_2O_3	11.2	5.6	2.4	-	0.8	80
C-Z_15.8%Al_2O_3	10.8	5.4	3.1	-	0.7	80
C-Z_15.2%SiO_2	10.9	5.4	-	2.9	0.8	80
C-Z_27.6%SiO_2	9.3	4.7	-	5.3	0.7	80

2.2.2.3. Washcoating method

The washcoating method consists of dipping the structured substrate into the slurry at controlled speed.

Structured substrates were dipped into the slurries at a rate of 3 cm/min. The substrates were immersed into the slurry and held for 1 min. Then, they were withdrawn from the suspension at a 3 cm/min rate. The excess of the slurry inside the channels was removed by centrifugation at 400 rpm (100 rcf) during 1 min. If there remained any channels blocked, these were blown with compressed air. Then, the monolith was dried at 120 ºC for 30 minutes and the procedure was repeated until the desired catalyst loading was coated. Finally, the coated monoliths were calcined at 400, 450 or 500 ºC (2 ºC/min) for 3h.

2.2.3. Slurried catalysts

Slurried catalysts were prepared by drying and calcining slurries at the same conditions as the structured catalysts. The drying step was always the same, 120 ºC overnight, but different calcination conditions were used:

- Methanol synthesis catalyst: 400 ºC (2 ºC/min) 3 h
- Dehydration catalyst: 400-500 ºC (2 ºC/min) 3 h
- Direct synthesis of DME catalyst: 400 ºC (2 ºC/min) 3 h

2.3. Characterisation

2.3.1. N_2 Adsorption

N_2 adsorption technique is based on the adsorption-desorption phenomena between gases and solids. The adsorption is given by a weak interaction between the gas and the surface of the solid that is known as physical adsorption or physisorption, and it is caused by van der Waals forces. This technique gives information related to the textural properties of the solid. By interpreting the adsorption-desorption isotherms and using different mathematical models, different textural parameters can be calculated, such as BET surface area, pore volume and pore size distribution.

A Micromeritics ASAP 2020 apparatus was used to analyse the samples. The degasification conditions were 10 °C/min, 240 °C, 5 h in all cases, and N_2 adsorption-desorption was performed at 77 K. The measurement of powder samples was carried out in conventional physisorption sample holders (*Figure 2.9-A*), whereas a special sample holder was used for structured substrates (*Figure 2.9-B*).

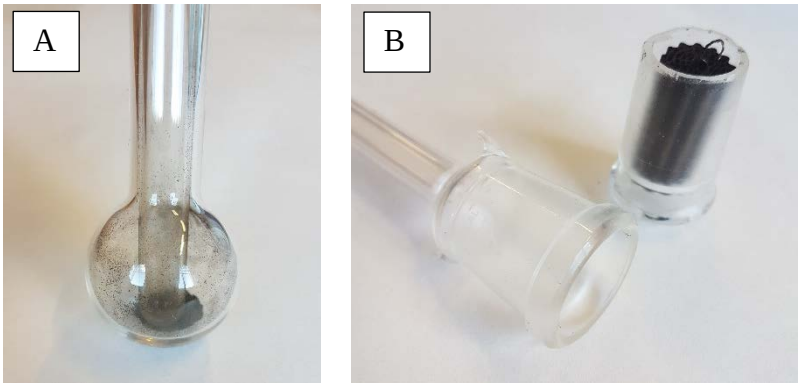

Figure 2.9. Samples holders for a) powder catalyst and b) structured catalysts.

Surface area of samples was calculated by the Brunauer-Emmet-Teller (BET) method. The total pore volume was determined at P/P_0 near to 0.995. The pore size distribution was obtained by Barrett-Joyner-Halenda (BJH) model using

the desorption isotherm. The equivalent cylindrical pore size was estimated by Eq. 2.1.

$$Average\ pore\ size = \frac{4 \cdot Total\ pore\ volume}{BET\ surface\ area} \qquad \text{(Eq. 2.1.)}$$

2.3.2. Reactive frontal chromatography of N_2O (RFC-N_2O)

Copper surface area of Cu-based catalysts is usually measured by Reactive Frontal Chromatography (RFC-N_2O). This technique is based on the decomposition of N_2O molecules on the Cu^0 surface at temperatures below 100 ºC as follows [14]:

$$2{\cdot}Cu^0\ (s) + N_2O\ (g) \longrightarrow Cu_2O\ (s) + N_2\ (g)$$

Measurements were carried out in an AutoChem II 2920 (Micromeritics). Different sample tubes were used depending on the physical shape of the sample: powder or structured catalysts (*Figure 2.10*).

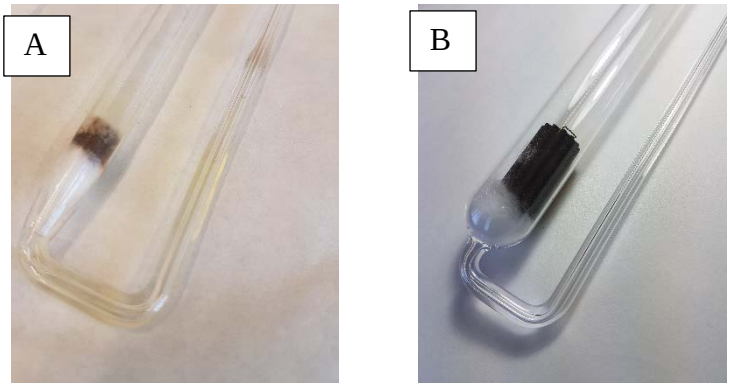

Figure 10. Autochem II sample tubes for a) powder catalysts and b) structured catalysts.

First, samples (100-150 mg) are reduced at 245 °C (2 °C/min) during 4 h with 10% H_2/Ar flow. Then, samples are cooled down to 60 ºC with He, and N_2O pulses are introduced into the U-shaped tube reactor at the same

temperature to oxidize the copper surface. A cool trap made with liquid nitrogen and acetone (-80 °C approx.) was placed downstream from the reactor to trap unreacted N_2O. The Cu surface area was calculated by quantifying the N_2 produced by the N_2O decomposition according to Eq. 2.2. The signal was recorded by a thermal conductivity detector (TCD), which was calibrated for N_2.

$$Cu\ surface\ (m^2/g) = V_{N_2}\left(\frac{cm^3}{g}\right)\cdot\frac{1\ mol}{22400\ cm^3}\cdot\frac{2\ mol}{1\ mol}\cdot N_A\left(\frac{atom}{mol}\right)\cdot a\left(\frac{nm^2}{atom}\right)\cdot\frac{1\ m^2}{10^{-18}nm^2} \quad \text{(Eq. 2.2)}$$

Where:

V_{N_2} = Volume of N_2 produced

N_A = Avogadro number

a = Copper atomic area (0.068 nm^2)

2.3.3. Temperature programmed reduction (TPR)

Temperature programmed reduction with hydrogen (H_2-TPR) is a widely used technique to study the reducibility of different metallic oxides. By increasing the temperature in a linear programmed way under a reducing atmosphere (H_2), metallic oxides such as CuO tend to reduce:

$$CuO + H_2 \longrightarrow Cu + H_2O$$

The measurement was carried out in a Micromeritics Autochem II 2920. 80-120 mg of catalyst were treated in 10% H_2/Ar flow from 40 to 450 °C following a 10 °C/min heating ramp. An ice/salt bath (-18 °C aprox.) was used downstream from the reactor to trap the water produced in the reduction. The signal was monitored by a thermal conductivity detector (TCD), which was previously calibrated to calculate the H_2 consumption.

2.3.4. Temperature programmed desorption of Ammonia (NH_3-TPD)

Temperature programmed desorption of ammonia (NH_3-TPD) is commonly used to study the acid strength of different solid acids. Acid sites are able to adsorb ammonia molecules, which are desorbed at different temperatures depending on the strength of these acid sites. It is accepted that ammonia molecules desorb in increasing order of sites acid strength while the temperature is increased.

A Micromeritics Autochem II 2920 was used to carry out NH_3-TPD. The analysis conditions were chosen after a previous study (*Appendix A.2*). Briefly, 100-150 mg of catalyst were pretreated in air flow at 350 ºC (10 ºC/min) during 30 min to remove any possible impurities such as water inside the pores. Then, the sample is cooled down to 130 ºC in He flow. After that, 10%NH_3/He was flown through the sample for 15 min to saturate the sample surface with ammonia. Then, the sample is purged with He for 60 min to avoid physisorbed ammonia. TPD profiles were obtained by raising temperature from 130 to 700 ºC with a heating ramp of 10 ºC/min. The equipment was connected to a Balzers Omnistar mass spectrometer (MS) and the 15, 17 and 18 m/z signal was monitored.

2.3.5. X-Ray diffraction (XRD)

X ray diffraction provides information about the crystalline phases and allows for an estimation of the average crystal sizes. The technique is based on the diffraction of a monochromatic X-ray beam on a crystalline sample. This phenomenon could be described with the Bragg's law, which predicts the direction of the X-ray beams in the constructive interferences of a crystalline sample according to the expression shown in Eq. 2.3.

$$n\,\lambda = 2d\,sin\theta \qquad \text{Eq. 2.3}$$

where λ is the wavelength of the beam, θ is the angle between incident beam and the surface of the crystal, d is the spacing between diffracting planes. The constructive interference occurs when n is an integer.

The Scherrer equation (Equation 2.4) is widely used to estimate the crystal size. According to this equation, the crystal size is inversely related to broadening of the reflection.

$$d_{crystal} = \frac{k \cdot \lambda}{\beta \cdot cos\theta} \qquad \text{Eq. 2.4}$$

Where d is the mean size of the crystal, k is the dimensionless shape factor which is normally assumed to be 0.9 for spherical particles, β is the line broadening at half maximum intensity and θ is the Bragg's angle in degrees.

XRD diffractograms were obtained in a Bruker D8 Advanced with monochromatic radiation (40 kV/30 mA) of CuKα, λ = 0.154 nm. Measurements were made in the 2θ interval between 5º and 85º with step size of 0.05° and step time of 5 s. CuO crystal size was estimated by the Scherrer equation at 38.8 º. In this case, measurements were made in the 2θ interval between 27º and 42º with a step size of 0.01° and a step time of 1 s.

2.3.6. Zeta potential

The zeta potential magnitude is used to obtain information about particles repulsion in slurry or colloidal systems. Particles in suspension develop surface charges that generate electrostatic forces between contiguous particles in the system. In this way, the slurry stability can be improved by maximising repulsive forces, *id est*, avoiding their attraction, and consequently, their sedimentation.

The theory of the double layer explains the behaviour of charges surrounding the particles. This theory indicates that particles are surrounded by two layers of ions (charges). One is called the Stern layer and it consists of counter-ions (ions with opposite charge to that of the particle surface), concentrated close to the particle surface. Additional counter-ions are still attracted to the particle, but they are also repulsed by the Stern layer as well as by other counter-ions

that try to get closer to the particle. This less firmly attached second layer of ions is called diffuse layer (*Figure 2.11*). The boundary between the Stern layer and the diffuse layer is the point of interest, where the electrical potential that exists in this boundary gives the zeta potential. This boundary is called the surface of hydrodynamic shear or slipping plane [15].

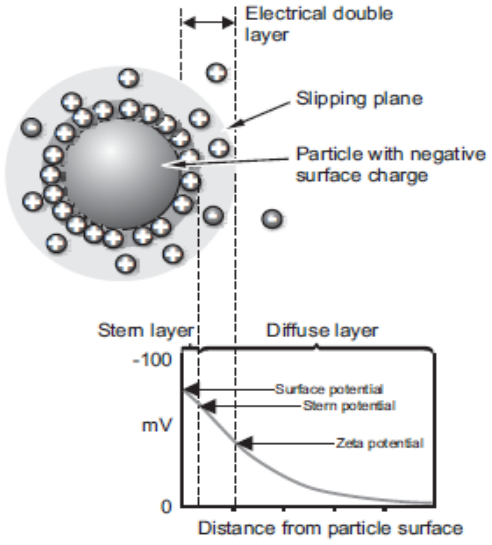

Figure 2.11. Schematic representation of the electrical double layer.

Zeta potential is measured by electrophoretic mobility (μe), which is defined as expressed by Eq. 2.5:

$$\mu_e = {}^{V_e}/_{\bar{E}} \qquad \text{Eq. 2.5}$$

Where *Ve* is the velocity of the particles and $\bar{E}$ is the applied electric field. Then, the value of zeta potential is calculated by the Henry equation (Eq. 2.6):

$$\mu_e = \frac{2 \cdot \varepsilon \cdot z \cdot f(k_a)}{3 \cdot \eta} \qquad \text{Eq. 2.6}$$

Where ε is the dielectric constant, z is the zeta potential, η is the viscosity and *f(ka)* is a factor that depends on the model used. In aqueous media the Smoluchowski model is used and f(ka) is 1.5.

Therefore, the zeta potential gives information about the stability of a slurry or colloidal system. Large positive or negative values of zeta potential (/<20 mV/) lead to stable slurries in which particles repeal each other. Nevertheless, if the particles have a low zeta potential or the value reaches to zero (the so-called isoelectric point) there is not enough force to prevent particles from flocculating [16].

Measurements were performed in a Zetasizer Nano ZS. For sample preparation, 20 mg of the samples were dispersed in 50 g of 1 mM NaCl and they were sonicated for 1 h (at room temperature) in order to obtain highly dispersed solutions. Then, 6 solutions were prepared for each sample to cover the entire pH range. pH was adjusted to 2, 4, 6, 8, 10 or 12 with HNO_3 or NH_4OH. Finally, the solutions were stirred overnight to ensure a stable pH before performing the measurement.

2.3.7. Particle size

The particle size distribution in aqueous medium was measured by laser diffraction technique. This technique is based on the different scattering of the light with varying particle size. It is widely known that large particles scatter light at small angles and small particles at large angles. By measuring the angular variation in intensity, the particle size distribution can be obtained.

The measurement was made in a Mastersizer 2000 (Malvern). For powder samples, 100 mg were dispersed in 20 g of water. In the case of slurries, the required amount of the slurry to obtain the same concentration (0.5% solid content) was mixed with water. The suspensions were adjusted to the desired pH, and then sonicated for 2 h at room temperature. Finally, the sample was measured by adding dropwise the required amount of solution to the apparatus.

The particle size was defined by supposing that all particles are spherical:

- D[4,3]: Volume weighted mean
- D(0,9): It is the value that define the particle size bellow which the 90% of the sample lies

2.3.8. Viscosity

Viscosity is defined as material´s resistance to flow. Fluids can be classified as Newtonian or non-Newtonian depending on their viscosity behaviour as a function of the shear rate. Newtonian fluids are independent of the shear rate. However, most fluids are non-Newtonian (like the slurries studied in this work) and they are dependent on shear rate.

In the washcoating method, this factor gives information about the ability of slurries to flow through the channels. Due to its non-Newtonian behaviour, slurries will not flow in the same way through a channel at different immersion rates. Moreover, viscosity also affects the coating loading since this loading increases when the viscosity of the suspension increases [12,17].

The viscosity was measured by means of a TA instrument (AR 1500ex model) with concentric cylinder geometry. The flow experiments were performed from 0 to 3600 s^{-1} at 25 ºC. Aiming to predict the flow behaviour when channels are centrifuged or flowed with air to remove the excess of slurry in the washcoating method (*Section 2.2.2.3. Washcoating method*, see above), the viscosity was studied at shear rates of 1000 s^{-1} [12].

2.3.9. Adherence

One essential property of a coating catalyst layer is its ability to remain on the structured substrate during reaction and handling. The adhesion of the catalyst layer on structured substrates is measured by the weight loss of the coated monolith after being exposed to sonication [18].

The coated monolith was immersed in petroleum ether solution (OPPAC) and was sonicated for 30 min. Then, the monolith was dried 30 min at 120 ºC in an

oven and calcined at the same calcination temperature used to prepare the structured catalyst. The adherence was calculated by weight loss as follows:

$$Adherence\ (\%) = \frac{grams\ of\ coating\ after\ adherent\ test}{grams\ of\ coating\ before\ adherence\ test} \cdot 100 \qquad \text{Eq. 2.7}$$

2.3.10. Hg Porosimetry

Mercury intrusion porosimetry is a widely used technique to measure the porosity of the solids, especially macroporosity (> 50 nm), since gas adsorption is not able to measure this range. Moreover, with this technique the envelope or bulk density of a solid can be estimated, which is of interest in order to predict the catalyst layer thickness on the monolith.

Due to the high surface tension of mercury (485 dyne/cm^2), it presents poor wettability (high contact angle θ>90º) in most surfaces. Therefore, mercury will not enter in the pores of the solid by capillarity. An external force such as pressure is needed to fill in the pores, and the force applied is inversely proportional to the pore diameter [19]. At low pressures, the pores of the sample are not filled, and mercury is just covering the solid (envelope or bulk). At high pressures, mercury enters in gradually smaller pores of the solid (skeleton).

The Washburn equation (Eq. 2.8) relates the applied pressure with pore diameter:

$$D = \frac{-4 \cdot \gamma \cdot cos\theta}{P} \qquad \text{Eq. 2.8}$$

Where:

D is the pore diameter

γ is surface tension of mercury

θ is the contact angle

P is the applied pressure

The measurement was carried out in a Micromeritics Autopore IV. Monoliths with dimensions of the penetrometer bulb were prepared (15x15 mm, *Figure 2.12*). Prior to the measurement, the sample was placed in the penetrometer and degassed until 50 μm Hg for 5 minutes. Then, mercury was introduced in two steps, first at low pressure, and then at high pressure. The total range used to perform the analysis was from 0.1 to 30,000 Psia, which provides a wide pore volume and pore size distribution.

Figure 2.12. Autopore IV penetrometer for solid samples (5 cm³ - Part No. 950-61707-00) and monolith with the required dimensions.

The catalyst layer thickness was estimated by measuring the amount of mercury intruded in the sample. Weighing the penetrometer empty with the sample (W_s) and filled with mercury (W), the volume of the intruded mercury (V_{Hg}) was obtained as shown in Eq. 2.9:

$$V_{Hg} = \frac{W - W_S}{Hg\ density} \qquad \text{Eq. 2.9}$$

The volumes of intruded mercury in a coated monolith and an empty monolith were measured. Therefore, the volume of the layer is calculated following Eq. 2.10.

$$V_{layer} = V_{Hg\ empty\ monolith} - V_{Hg\ coated\ monolith} \quad \text{Eq. 2.10}$$

By knowing the amount of coated catalyst in the monolith (W_{cat}), the density of the catalytic layer (ρ_{layer}) was determined by means of Eq. 2.11:

$$\rho_{layer} = \frac{W_{cat}}{V_{layer}} \quad \text{Eq. 2.11}$$

Therefore, for the catalyst layer, the thickness of the layer (t_{layer}) is dependent on the coated amount and the lateral surface area ($S_{lateral}$) of the monolith (Eq. 2.12):

$$t_{layer} = \frac{W_{cat}}{\rho_{layer} \cdot S_{lateral}} \quad \text{Eq. 2.12}$$

2.3.11. Thermogravimetric analysis (TGA)

In thermogravimetric analysis, the weight change of the sample is monitored as a function of temperature in a controlled atmosphere. In this study, this technique gives information about the minimum temperature required to eliminate precursors and additives from the catalyst, such as nitrates, PVA, etc.

Experiments were carried out in a TA instruments TGA Q500. The sample (~10 mg) was heated from 40 to 800 °C, with a heating rate of 10 °C/min, in a flow of inert (N_2) or oxidant gas (Air).

2.4. Activity Tests

2.4.1. Set-up description

The reactions were carried out in a laboratory-scale set-up, which consists of three main parts: feed section, reaction section and analysis section:

- The feed section presents gas cylinders (N_2, H_2 and syngas) connected to different Mass Flow Controllers (MFC) that supply gases to the reaction section. Moreover, for methanol dehydration, liquid methanol was fed into a evaporator and then to a reactor by a high-performance liquid chromatography (HPLC) pump (Gilson 307).

- The reaction section consists of a Microativity Reference lab reactor (PID Eng&Tech). This reactor is controlled by a software called Process@, which allows to program the reaction sessions with all the steps for the reaction.

  The reactor is heated by an electric furnace and the gases can flow through the reactor or avoid to pass through the reactor by a bypass 6-port valve. The pressure in the system is controlled by a pressure controller. All these parts are place inside a hot box (at 160 ºC) that helps preheating inlet gases as well as avoiding possible condensation of different compounds. In addition, an evaporator is also located inside the hotbox to evaporate the liquid methanol pumped to the lab reactor in methanol dehydration reactions, as it was said before.

- Two different tubular reactors were used in this work. The tubular reactor used in the fixed bed reactor configuration is made of stainless steel (SS316) and has an internal diameter of 9 mm, whereas the tubular reactor used for structured catalysts is made of Hastelloy® and has an internal diameter of 17 mm. Gases circulate in a downward direction. The catalysts were placed in the reactors depending on their morphology:

- Powder or slurried catalysts: 3 cm of catalytic bed were placed inside the tubular reactor. Mainly, 1 g of catalyst with a particle size distribution of 300-500 μm were diluted with 2 g of SiC (Carborondum, 500 μm) in the study of the direct synthesis of dimethyl ether and in methanol synthesis. In the case of methanol dehydration, 50 mg of solid acid with a particle size distribution of 300-500 μm were diluted with 2.9 g of SiC (Carborondum 500 μm). Then, the mixture was placed inside the reactor above a porous plate of Fecralloy® and a thin layer of quartz wool to support the catalytic bed, and the temperature thermocouple was placed at the bottom of the bed (*Figure 2.13*).
- Structured catalysts: Coated monoliths or foams loaded with 1-2 g of catalyst were placed inside the Hastelloy reactor. In this case, the reaction temperature was monitored by 3 thermocouples set in 3 different positions as shown in *Figure 2.14*. Monoliths were placed in the reactor and held by these thermocouples as shown in *Figure 2.14*.

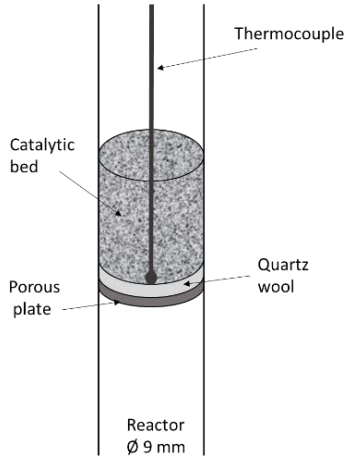

Figure 2.13. Scheme of the fixed bed reactor.

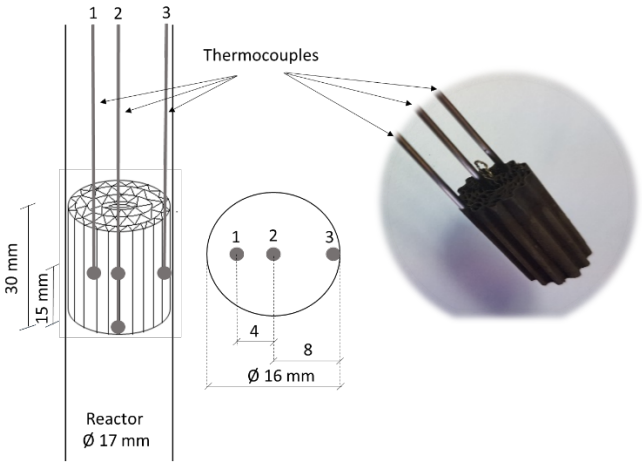

Figure 2.14. Scheme of the structured catalyst reactor with thermocouples positions.

- Finally, the products are online analysed in a GC (Agilent 7890A). The products were taken out through a thermostatic line from the reactor

and were analysed by TCD (HP-PLOT/Q and HP-MOLESIEVE columns) and FID (HP-PLOT/Q column) detectors.

2.4.2. Reaction conditions

The stages of the start-up of standard runs for the direct synthesis of dimethyl ether and methanol synthesis reactions are:

1. Leak test of the reactor at 44 bar carried out with N_2.
2. Reactor purge with N_2 flow for 10 min (at atmospheric pressure).
3. Sample reduction at 245 ºC for 4 h (ramp 2 ºC/min) in a 5% H_2/N_2 flow.
4. Reactor cooling down to 85 ºC with the same diluted H_2 flow.
5. Feeding of the syngas (Mixture of 60:30:10 H_2:CO:N_2) to the reactor and pressurization to 40 bar. Space velocities of 2.55 L of syngas/(g_{CZA}·h) were used.
6. When the desired pressure is achieved, the reactor is heated to the reaction temperature (260 ºC, 4 ºC/min). The starting time of the reaction is defined as the time when the reactor reaches the selected reaction temperature. In this work, all the CO conversions were presented at 10 h of reaction time.

For Methanol dehydration:

1. Leak test of the reactor at 10 bar is done with N_2.
2. Reactor purge with N_2 flow (at room temperature and atmospheric pressure) for 10 min.
3. Thermal pretreatment of the catalyst with 60 mL/min N_2 at 300 ºC (ramp 10 ºC/min) for 1 h to remove any possible impurities such as water in pores.
4. Reactor cooling down to 260 ºC (reaction temperature).
5. Switching N_2 to 30 % MeOH in N_2. At this moment, the reaction starting time is computed. The results were given at 5 h of reaction with a space velocity of 10 L/($g_{zeolite}$·h).

2.5. References

[1] C. Baltes, S. Vukojević, F. Schüth. *Journal of catalysis* 258 (2008) 334-344.

[2] C. Flores, N. Batalha, V.V. Ordomsky, V.L. Zholobenko, W. Baaziz, N.R. Marcilio, A.Y. Khodakov. *ChemCatChem* 10 (2018) 2291-2299.

[3] C. Manrique, A. Guzmán, J. Pérez-Pariente, C. Márquez-Álvarez, A. Echevarría. *Fuel* 182 (2016) 236-247.

[4] V. Subramanian, K. Cheng, C. Lancelot, S. Heyte, S. Paul, S. Moldovan, O. Ersen, M. Marinova, V.V. Ordomsky, A.Y. Khodakov. *ACS Catalysis* 6 (2016) 1785-1792.

[5] Hermicenda Pérez Vidal. *PhD Thesis* (2009). University of the Basque Country

[6] S. Wu, Y. Han, Y-C. Zou, J-W. Song, L. Zhao, Y. Di, S-Z. Liu, F-S Xiao. *Chemistry of materials* 16 (2004) 486-492.

[7] X. Guo, A. Yin, W-L. Dai, K. Fan. *Catalysis Letter* 132 (2009) 22-27.

[8] A. García-Trenco. A. Martínez. *Catalysis Today* 215 (2013) 152-161.

[9] Lloyd R. Chapman, Powell, Tenn (1982) *U.S. Patent No. 4,318,828.*

[10] Y. Diaz, A. Sevilla, A. Mónaco, F.J. Méndez, P. Rosales, L. García, J.L. Brito. *Fuel* 110 (2013) 235-248.

[11] David Merino Bella. *PhD Thesis* (2017). University of the Basque Country.

[12] A. Egaña, O. Sanz, D. Merino, X. Moriones, M. Montes. *Industrial & Engineering Chemistry Research* 57 (2018) 10187-10197.

[13] Asier Eleta López. *PhD Thesis* 2008. University of the Basque Country.

[14] G.C. Chinchen, C.M. Hay, H.D. Vandervell, K.C. Waugh. *Journal of Catalysis* 103 (1987) 79-86.

[15] Zetasizer Nano Series *User Manual.*

[16] S. Vallar, D. Houivet, J. El Fallah, D, Kervadec, J-M. Haussonne. *Journal of European Ceramic Society*, 19 (1999) 1017-1021.

[17] C. Cristiani, M. Valentini, M. Merazzi, S. Neglia, P. Forzatti, *Catalysis Today* 105 (2005) 492-498.

[18] S. Yasaki, Y. Yoshino, K. Ihara, K. Ohkubo, *US Patent* 5,208,206 (1993).

[19] P.A. Webb, C. Orr, R.W. Camp, J.P. Oliver, Y.S. Yunes. *Analytical methods in fine particle technology*. Micromeritics Instrument Corp (U.S.A.). ISBN 0-9656783-0-X.

CHAPTER 3

Single-phase catalysts

INDEX

3.1. Introduction

The washcoating method or dip coating method is one of the most employed method for structured catalyst preparation due to its simplicity and versatility [1- 6]. The method consists of depositing a thin layer of the catalyst on the structured substrate surface by dipping the latter in a catalyst slurry and subsequent withdrawing under controlled speed. The coating process is repeated several times using the same slurry with a drying step between coatings, until the target catalyst load is achieved. Finally, the coated structured substrate is calcined to anchorage the catalyst layer properly.

In a way of obtaining stable slurries, three variables must be taken into account: solvent properties, properties of the solid particles and solid content (%wt.) [3]. These variables are responsible for determining properties of the slurry such as viscosity, surface tension, concentration, etc., which are essential to control the stability of the slurries and the homogeneity of the coatings.

For catalyst slurry preparation, the catalyst could be dispersed in aqueous or organic medium. Aqueous slurries are more common: water produces a good catalyst dispersion. In aqueous solutions, repulsion between particles can be altered by modifying the pH [3-6]. By polarization of the particles surface, there are pH values where the interaction between particles is enough to repel each other and avoid aggregates. At the isoelectric point (cero repulsion between particles), particles tend to flocculate and settle. Getting away from this point, stable dispersions could be prepared by reaching values of zeta potential higher than /± 20 mV/ [7]. However, catalysts can interact with water (e.g. leaching) and change some properties (activity, selectivity, stability) of the initial catalyst [8].

Organic solvents might present less interaction with the catalyst and could also be used to change the viscosity, vapour pressure and dispersion capacity [8,9]. Nevertheless, the use of alcoholic medium might not be always the best option. J.M. Zamaro *et al.* [9] observed a low dispersion of zeolite in alcohol due to generation of catalyst particles aggregates. Hence, poor catalyst coating adherence was obtained in comparison to water dispersions. Moreover, particle size of the catalysts is also vital to obtain good adherence of catalytic coatings. A particle size smaller than the cracks of the roughness on structured substrate surface is needed to occlude the catalyst and promote a mechanical anchorage of the coating [10].

The used catalyst particle size also affects the stability of the slurry [4,5,11,12]. To obtain stable slurries small particles are required. Many authors suggest that particle size should be below 10 μm to obtain good stability [4,11,12]. C. Agrafiotis *et al.* [5] studied the particle size of alumina in slurries, and concluded that particle size of 5 μm is highly recommended due to the fact that bigger particles tend to settle fast, but excessively small particles could result in flocculation.

The solid content of the slurry also influences the coating properties. High solid content in slurries increases their viscosity. Hence, more stable slurries would be obtained. Moreover, viscosity is probably one of the main parameter controlling coating procedure. Low viscosity lead to obtain homogeneous coatings but it increases the number of immersion required to load the monolith [4,6]. However, too high viscosity values might reduce its ability to flow through the channel of the structured substrate and it also could generate accumulations that may produce poor adherence or channels blocking [4,6,12,13].

Additives are an alternative to improve coating properties of slurries acting as stabilizer, binder, viscosity controller, surfactants etc. [3-6,12,14,15]. Some organic or inorganic compounds are commonly added to the slurry formulation to enhance the homogeneity and coating adherence [16]. Furthermore, it is widely accepted that the difficulty to coat catalysts on metallic substrate is higher than on ceramic ones due to the difference in porosity and surface roughness [3]. Consequently, more additives are frequently used to obtain good performances in metallic structured catalyst preparation [17-20].

These additives could also change properties such as viscosity or surface tension. G. Germani *et al.* [15] studied the effect of three organic compounds as binder in microchannel coatings: namely, polyvinyl alcohol (PVA), methylhydroxyethyl cellulose (Tylose®) and polyethylene glycol (PEG). Improvement in the homogeneity of the coatings were shown with the use of these binders, without cracking in the catalytic layer. However, large amount of these binders decreases the BET surface area of the parent catalyst [15,16]. Moreover, the use of high content of these binders could also create cracks in the coatings due to the formation of large amount of gases during calcination [16].

Inorganic additives, such as inorganic oxide colloids can be also a good option to increase adherence of the catalyst layer [18,20]. Apart from stabilising the slurry, these colloidal nanoparticles are used as a binder to improve the cohesion of the catalyst layer and the adhesion between the catalyst and the substrate. Due to the small size of the colloidal particles, during the drying process of the layer,

these small particles are drawn by capillary forces to intraparticular points of the main catalyst (larger ones) [6,12]. Hence, they create anchoring points between particles and the substrate. J. M. Zamaro *et al.* [21] showed an improvement in adherence using colloidal SiO_2 to coat different zeolites (ZSM-5, mordenite, ferrierite). With an addition of 3% wt. (with respect to zeolite), an increase of 10-20% in adherence was shown. Therefore, many researchers use these inorganic oxide colloids for slurry preparation [8,16,22-25].

The nature of the colloid to be employed depends on its compatibility with the catalyst to be deposited and the substrate alloy employed. Therefore, it is important to know the chemical composition of the metallic surface. Different treatments are used to generate roughness in the metallic surface such as thermal, electrochemical or chemical treatments [2,3]. Depending on the treatment and the used material, different oxides layers are generated. In this sense, F. J. Echave *et al.* [8] used colloidal ZnO to deposit PdZnO catalyst and H. Pérez *et al.* [24] used colloidal SiO_2 to deposit SBA-15 on Fecralloy® monoliths, while R. Peela *et al.* [16] coated alumina in SS304 employing colloidal alumina. On the other hand, V.G. Milt *et al.* [25] coated Au/TiO_2 catalyst using colloidal alumina into Aluchrom YHf monoliths, which presented whiskers of α-alumina in its surface after the proper treatment. Nevertheless, not only do the use of these additives change the coating properties, but also they could change the main properties of the parent catalyst such as activity, selectivity and stability [3,8].

In this chapter, the structuration of methanol synthesis catalyst ($Cu/ZnO/Al_2O_3$) and methanol dehydration catalyst (ZSM-5) was studied. The effect of the nature of the colloid, colloid content used and final calcination temperature were studied in physicochemical and coating properties.

3.2. Methanol synthesis catalyst

In this section, different catalyst slurry formulations were studied (*see Table 3.1*). First, the effect of the additives incorporation to the methanol synthesis catalyst ($Cu/ZnO/Al_2O_3$) slurry was analysed after drying and calcining the slurries (slurried catalyst). Then, coating process by washcoating method was studied with these slurry formulations. Finally, taking into account the best formulation (coating adherence and methanol yield), structured catalysts were prepared and characterised.

Table 3.1. Studied slurry formulations

Sample	CZA (%)	Colloid (%)	PVA (%)	H_2O (%)	pH
CZA_0% colloid	19.1	0	0.9	80	6.5
CZA_10% Al_2O_3	17.3	1.9	0.8	80	6.2
CZA_17.7% Al_2O_3					5.7
CZA_17.7% ZnO	15.9	3.4	0.7	80	8.3
CZA_17.7% SiO_2					7.5
CZA_33.3% Al_2O_3					5.3
CZA_33.3% ZnO	12.9	6.5	0.6	80	8.5
CZA_33.3% SiO_2					7.5

Slurried catalysts samples were referred to as CZA_X%C, where CZA is the catalyst employed ($Cu/ZnO/Al_2O_3$), X is the colloid percent in the slurried catalyst and C is the colloid used (Al_2O_3, ZnO or SiO_2). The structured catalysts were referred to as R4 and R1 for substrates (monoliths) with 289 and 2360 cpsi respectively, followed by the thickness of the layer. For example R4_46.5μm.

3.2.1. Results

3.2.1.1. Slurried catalysts

All the slurried catalyst and colloids were characterised after drying at 120 ºC overnight and calcining at 400 ºC (2 ºC/min) during 3 h with the following techniques.

The main physicochemical properties of the slurried catalysts are presented in *Table 2*.

Table 3.2. Characterization of different slurried catalysts

	N_2-Adsoption			N_2O-RFC	H_2-TPR	XRD	
Sample Name	BET surface area (m^2/g)	Total pore volume (cm^3/g)	Equivalent pore diameter (nm)	Cu surface area (m^2/g_{CZA})	Reducibility (%)	CuO crystal size (nm)	Cu crystal size (nm)
Parent catalyst	100	0.62	24.5	35.9	100	3.8	-
CZA_0%colloid	80	0.52	25.7	30.7	101	4.0	6.9
CZA_10%Al_2O_3	86	0.50	23.3	27.5	104	4.3	7.8
CZA_17.7%Al_2O_3	101	0.54	21.4	26.5	90	4.6	-
CZA_33.3%Al_2O_3	127	0.51	16.0	23.0	88	4.4	8.7
CZA_17.7%ZnO	55	0.38	27.3	21.3	85	4.6	-
CZA_33.3%ZnO	46	0.29	24.8	17.4	76	4.2	12.0
CZA_17.7%SiO_2	75	0.48	25.3	27.4	92	3.9	-
CZA_33.3%SiO_2	80	0.44	21.9	25.6	85	4.4	7.3
Colloidal Al_2O_3	204	0.31	6.2	-	-	-	-
Colloidal ZnO	19	0.11	24.2	-	-	-	-
Colloidal SiO_2	114	0.22	7.6	-	-	-	-

- **Textural Properties**

The textural properties of the slurried catalysts were measured by N_2 adsorption. The adsorption-desorption isotherms are presented in *Figure 3.1*. It can be seen that all the samples presented type IV isotherm. BET surface area, total pore volume and equivalent pore diameter calculated from these isotherms are summarised in *Table 3.2*.

It can be seen a decrease in the BET surface area of CZA catalyst with respect to the parent catalyst when it is dispersed in water (0% colloid), as well as, a decrease in total pore volume (*Table 3.3* and *Figure 3.1A*). However, a similar pore size distribution was shown, in which a pore size around 20 nm is showed (*Figure 3.1B).*

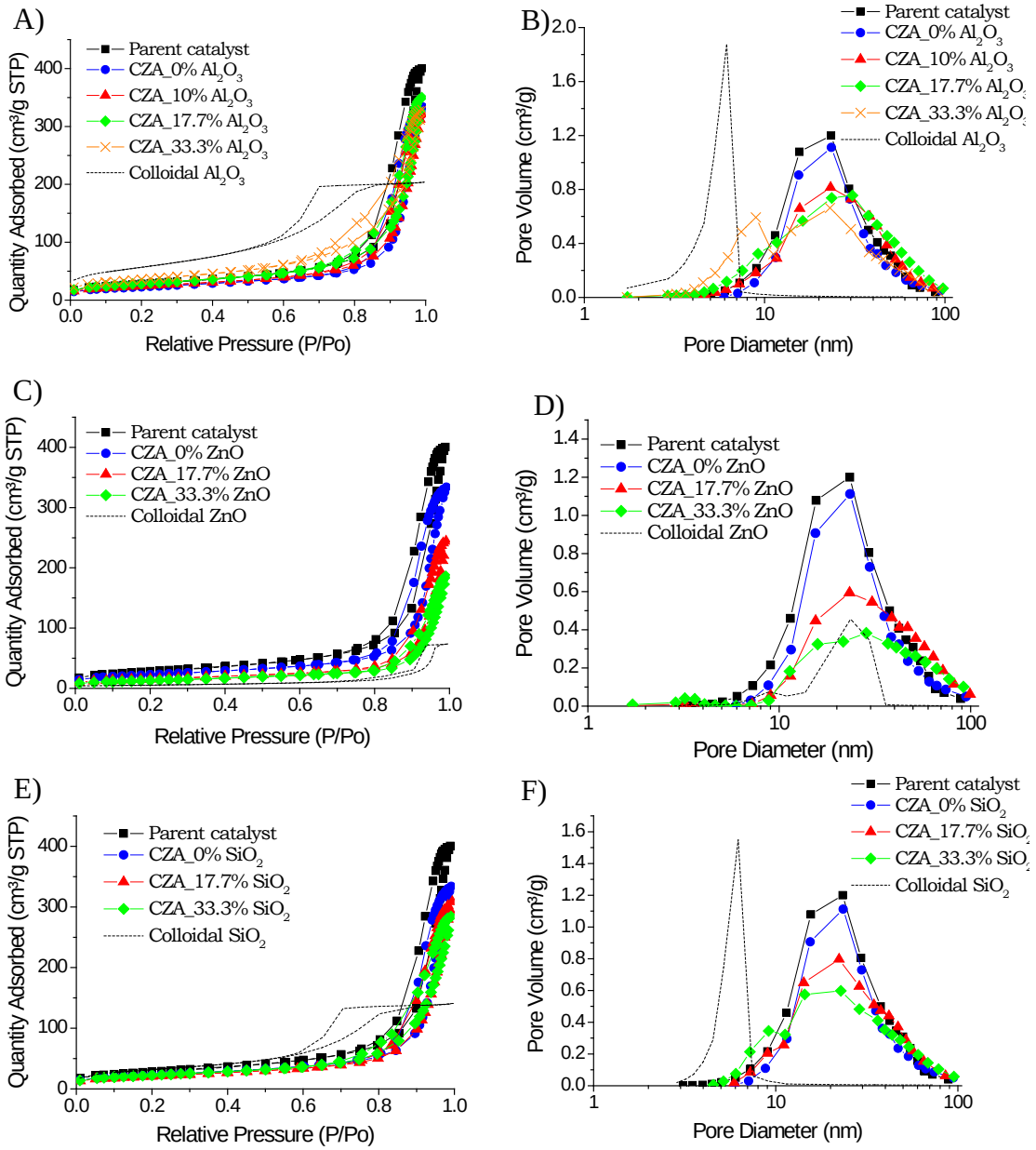

Figure 3.1. N_2 isotherms (left) and pore size distribution (right) of different slurried catalyst.

When the colloidal Al_2O_3 was added to the slurry, the slurried catalysts showed intermediate textural properties between the CZA catalyst and the colloidal Al_2O_3 (*Table 3.2 and Figure 3.1A-B*). The increase of the Al_2O_3 content produced an

increase in the BET surface area and a decrease in the pore diameter (*Table 3.2*). As it is shown in *Figure 3.1A,* the addition of colloidal alumina increased the quantity adsorbed in the range of P/P_0 0.05-0.3. Furthermore, the pore size distribution showed pores of the slurried catalysts centred around 20 nm, whereas, the colloidal Al_2O_3 presented smaller pores at 6 nm. Moreover, new pores at around 9 nm appeared in the sample with the highest colloid content (CZA_33.3% of Al_2O_3), that tend to be closer to those of the colloidal Al_2O_3 (*Figure 3.1B*).

The addition of colloidal ZnO in the slurried catalyst also produced intermediate textural properties between that of the CZA catalyst and the colloid (*Table 3.2 and Figure 3.1C-D*). Due to the lower surface area and pore volume of the ZnO, the textural properties of the slurried catalyst with this colloid such as BET surface area and total pore volume decreased as the content of ZnO increases (*Table 3.2 and Figure 3.1C-D*).

On the other hand, the colloidal SiO_2 exhibited slightly higher BET surface area than the CZA catalyst (*Table 3.2 and Figure 3.1E-F*). The addition of colloidal SiO_2 showed a slight increase in the BET surface area with the colloid content (*Table 3.2* and *Figure 3.1E*). Nevertheless, the surface area of the slurried catalysts presented similar values to the slurried catalyst with 0% SiO_2 (CZA_0%colloid) around 80 m^2/g. Furthermore, a decrease in the total pore volume and the pore diameter was shown when the silica content increased and the pore size distribution underwent to a bimodal distribution appearing new pores that bring closer to the pores of colloidal SiO_2 (*Figure 3.1F*).

For the same colloid content, BET surface area and pore volume increased in this order $ZnO < SiO_2 < Al_2O_3$.

- **Copper metal surface area**

The copper metal surface area was measured by RFC of N_2O and the results are presented in *Table 3.2*.

The slurried catalyst without colloids addition (CZA_0% colloid) showed a decrease in the Cu metal surface area from 35 to 30 m^2/g_{CZA} in comparison to the parent catalyst (*Table 3.2*). Moreover, the addition of colloids produced a decrease in the Cu surface area (*Table 3.2*). However, it was noticeable that the addition of colloidal ZnO presented higher decrease in the Cu surface area. On the other

hand, an increase in the content of different colloids also produced a decrease in the Cu metal surface area.

- **Reducibility**

The reducibility of catalysts was measured by H_2-TPR. The H_2 consumption was calculated by integrating the peaks of the TCD signal and this value was used to determine the reducibility percent of the catalyst. The results are shown in *Table 3.2 and Figure 3.2*.

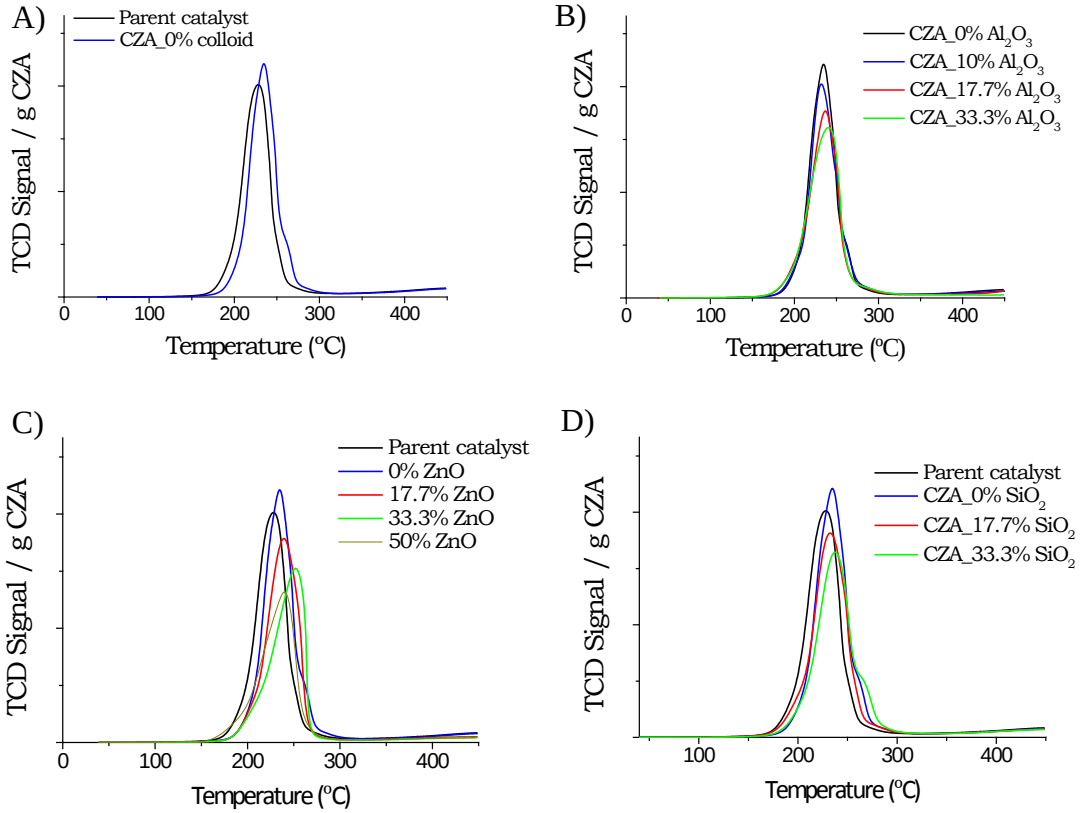

Figure 3.2. H_2-TPR analysis of the slurried catalyst with different colloid added: A) parent catalyst vs slurried catalyst B) colloidal Al_2O_3 C) colloidal ZnO and D) colloidal SiO_2

It can be observed that the dispersion of the CZA catalyst in water (CZA_0%colloid) did not present changes from the parent catalyst (*Table 3.2 and Figure 3.2A*). Similar reducibility and maximum reduction peak were exhibited.

The slurried catalyst prepared with the colloidal Al_2O_3 showed similar reducibility to the parent catalyst when low colloid content was added (CZA_10%Al_2O_3) (*Table 3.2* and Figure 3.2B). However, at increasing alumina content a decrease in H_2 consumption was observed (*Table 3.2* and Figure 3.2B). Something similar happens with colloidal ZnO and SiO_2: increasing the colloid content in the slurried catalysts, the reducibility decreases (*Table 3.2 and Figure 3.2C-D*). However, this effect is more intense with ZnO. Moreover, there is no change in the maximum reduction temperature (around 225 ºC) with the addition of all the colloids (*Figure 3.2*).

- **Crystallinity**

The crystallinity of the samples were measured by XRD and the results are shown in *Figure 3.3*. The Scherrer equation was used to estimate the CuO crystal size at 38.8 ° and the results are also presented in *Table 3.2*.

The results of the synthesised CZA catalyst (Parent catalyst, in *Figure 3.3A*) showed the peaks related to the CuO (Tenorite) and ZnO (Zincite) phase, which indicate the formation of mixed oxides successfully. Moreover, the dispersion of the CZA catalyst in water without inorganic oxide colloids (CZA_0%colloid) presented similar XRD patterns to the parent catalyst and CuO particle size (*Figure 3.3 and Table 3.2*).

Figure 3.3 also shows the effect of the colloids addition in the crystallinity of the catalyst. The addition of alumina in the slurried catalyst (*Figure 3.3B*) did not show changes in the XRD patterns at low Al_2O_3 content (<17.7%). However, with 33.3% of colloidal Al_2O_3, peaks of this alumina can be seen at 14.7, 28.4, 38.6 and 49.5° (*Figure 3.3B*). The slurried catalysts with colloidal ZnO and SiO_2 showed new peaks at 17.7% and 33.3% content. Peaks of ZnO appeared at 31.8, 34.3, 36.5, 47.6, 57.2, 63.2 and 67.9° (*Figure 3.3C*) and the amorphous form of silica could be shown at 15-30° approximately (*Figure 3.3D*).

However, the CuO crystal size measured by XRD did not change significantly when the colloids were added (*Table 3.2*).

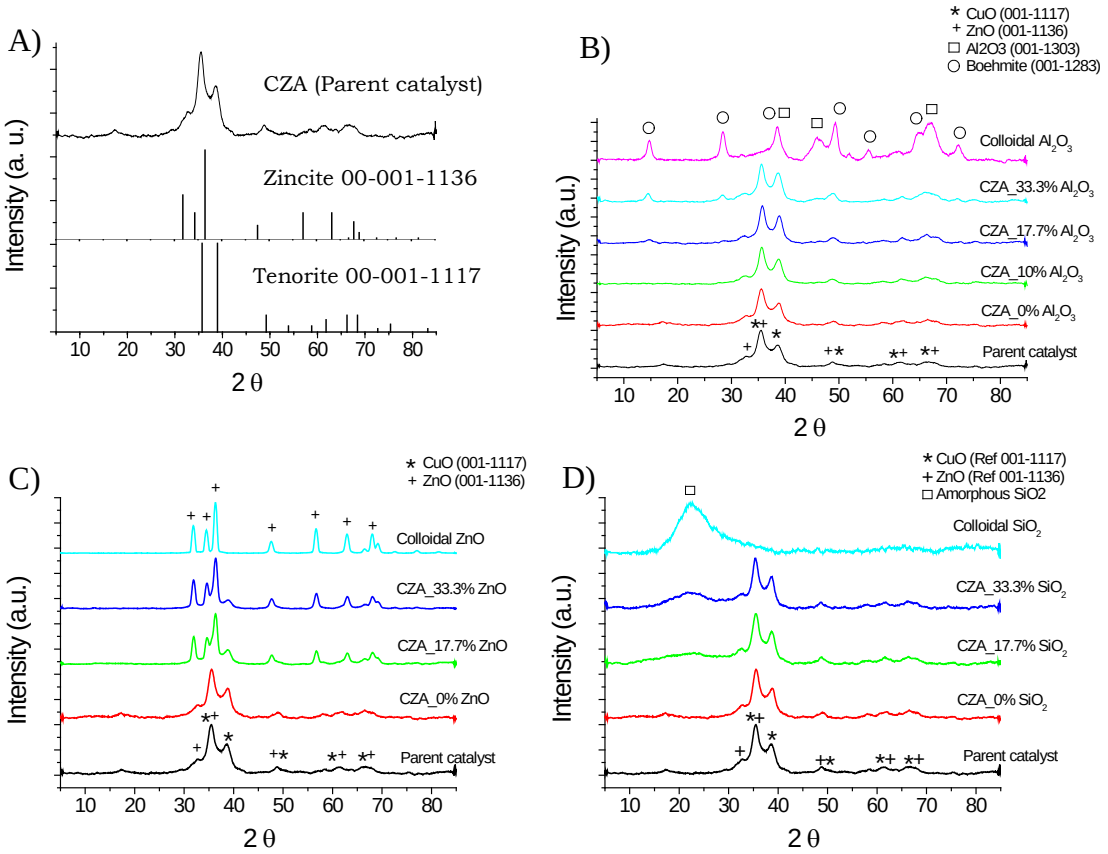

Figure 3.3. XRD results for parent catalyst (A) and different slurried catalysts with different Al_2O_3 (B), ZnO (C) and SiO_2 (D) content.

Supplementary studies were carried out to evaluate the copper crystal size in the samples reduced by in-situ XRD analysis in the group of Prof. J.A. Odriozola (University of Sevilla). The results showed the complete reduction of CuO to Cu (*Figure 3.4*). However, colloids still remains in the XRD patterns without changes in structure (Boehmite, amorphous SiO_2 and ZnO). On the other hand, crystal size of Cu was estimated by Scherrer equation at 43.3 °. The results showed an increase in the crystal size when colloids were used (*Table 3.2*). The increase in the Al_2O_3 content produced an increase in the crystal size. Moreover, the addition of ZnO produced the highest increase in the Cu crystal size.

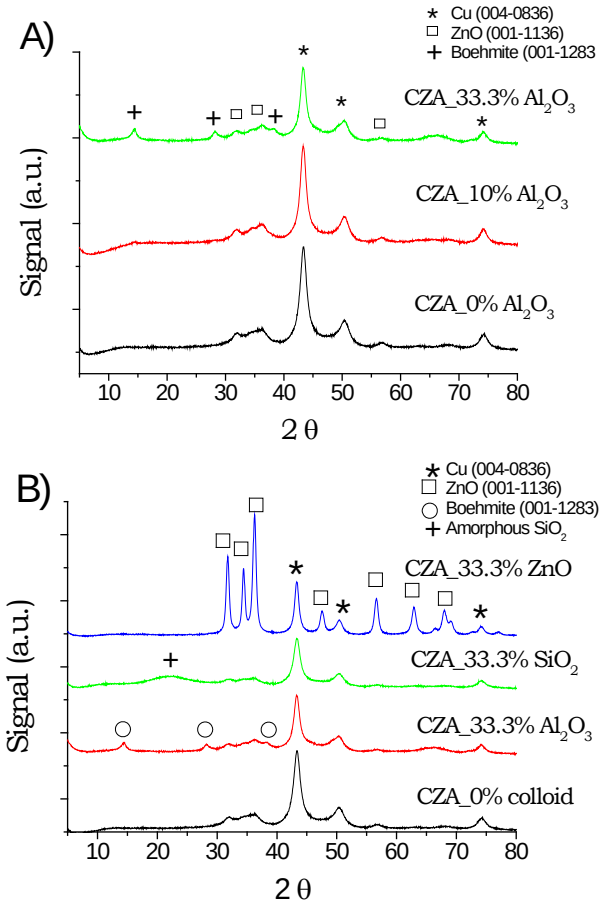

Figure 3.4. XRD patterns of the reduced samples with a) different colloidal Al_2O_3 content and b) different colloid

- **Acidity**

The acid strength of the slurried catalysts were measured by NH_3-TPD monitored by mass spectrometer (*Figure 3.5 and 3.6*). The desorbed ammonia signal was commonly followed by 17 m/z, which presents the highest intensity to ammonia (*Figure 3.5A*). The results with colloidal Al_2O_3 showed a peak between 400-500 ºC that increased with colloid content (*Figure 3.5A*). However, after a blank analysis (temperature programme without NH_3 saturation), the results showed that the peak at 400-500 °C also appear in this blank analysis (*Figure 3.5B*), so this peak was not due to ammonia desorption. The signal was related to

water decomposition (mass 18 m/z in *Figure 3.5C*) of the phase change from boehmite to γ-alumina (*see Thermogravimetric analysis in section 3.2.1.2*). Therefore, to avoid signal distortion mass 15 m/z was followed when colloids were added. The results are presented in *Figure 3.6*.

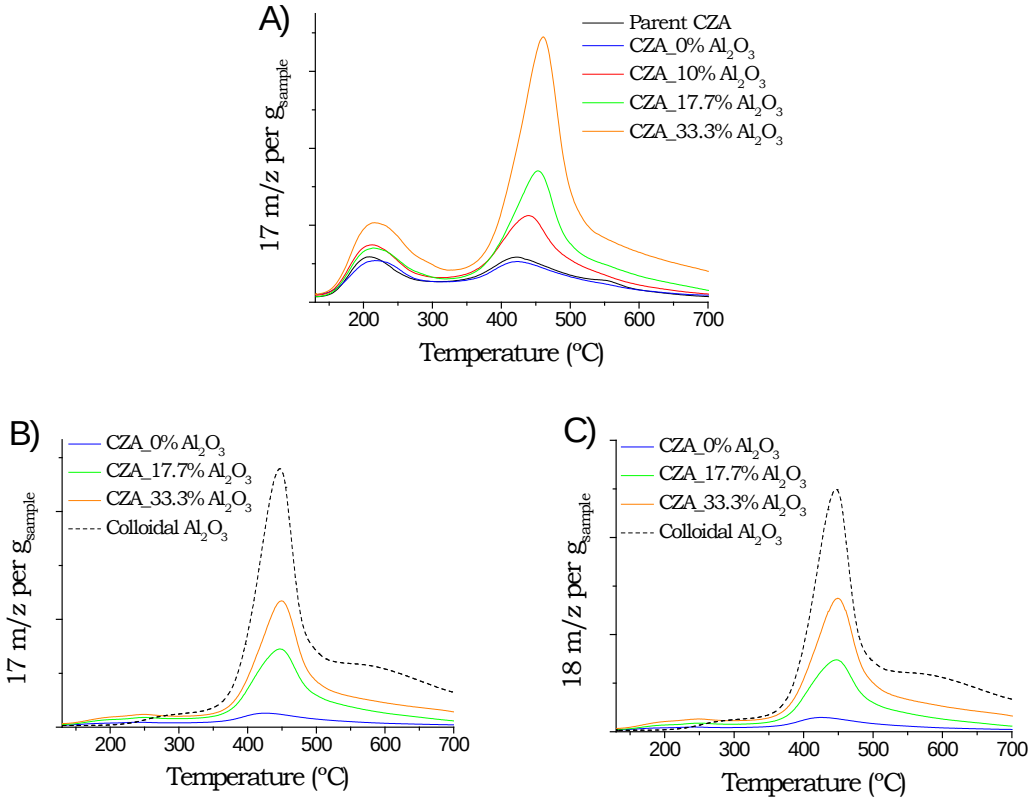

Figure 3.5. Results of a) NH_3-TPD and b) blank analysis of 17 m/z and c) blank analysis of 18 m/z when colloidal Al_2O_3 is added to CZA catalyst

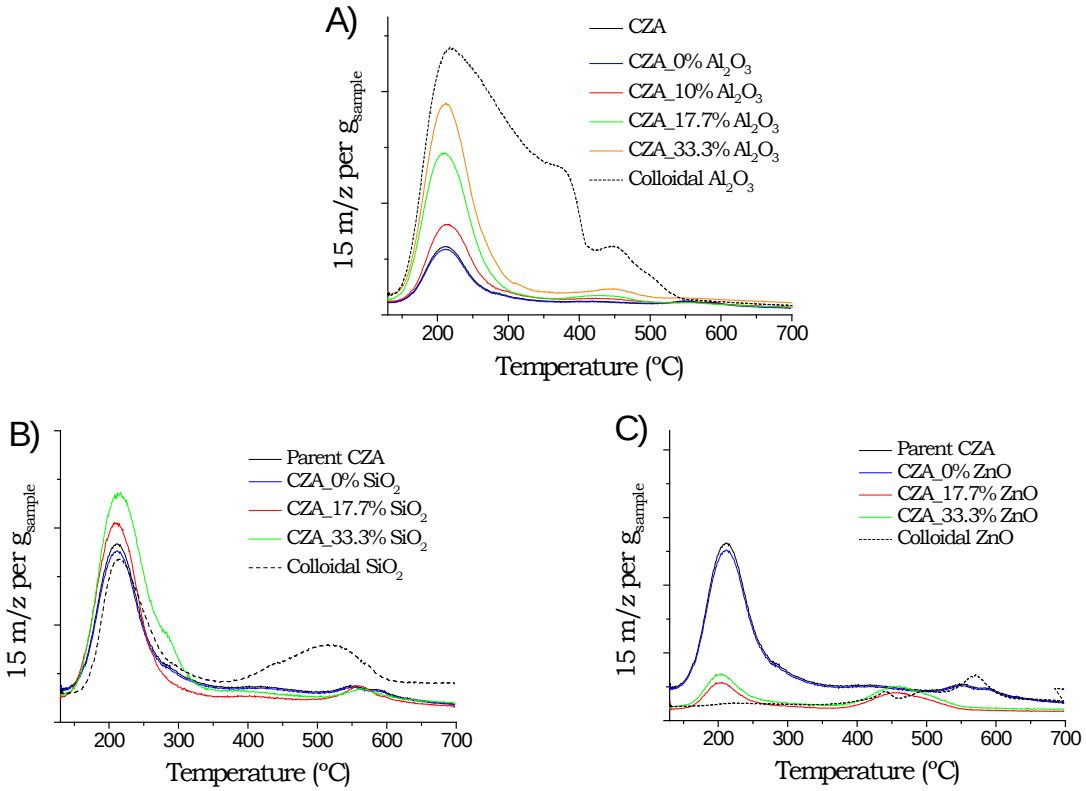

Figure 3.6. NH_3-TPD curves monitored with 15 m/s by MS of samples with (a) Al_2O_3, (b) ZnO and (c) SiO_2 addition.

The results showed that the parent catalyst and the slurried catalyst without colloids (CZA_0%colloid) presented similar acidity (*Figure 3.6*). The colloidal alumina presented higher acidity than the CZA catalyst (*Figure 3.6A)*. The addition of colloidal Al_2O_3 to the CZA catalyst presented an increase in the acidity of the slurried catalyst. Increasing the Al_2O_3 content, an increase in the peak signal can be observed. The colloidal ZnO, in contrast, presented negligible acidity. The use of ZnO produced a decrease in the desorbed ammonia (*Figure 3.6B*). Finally, the colloidal silica presented a slightly higher acidity than the CZA catalyst. The addition of colloidal SiO_2 to the CZA catalysts produced a slight increase in the overall acidity (*Figure 3.6C*).

- **Activity Test**

Finally, the activity test of different slurried catalysts was measured. The effect of colloid addition (Al_2O_3, ZnO and SiO_2) was studied in the methanol synthesis reaction, in a fixed bed reactor at 260 ºC and 40 bar.

a) Slurried catalysts prepared with colloidal alumina (Al_2O_3)

First of all, it can be observed that there were no changes neither in the conversion nor in the selectivity when the parent catalyst was slurried without colloids (*Figure 3.7*).

The effect of the addition of colloidal alumina is shown in *Figure 3.7*. The increase of the Al_2O_3 content in the slurried catalyst resulted in an increase in CO conversion, but it was accompanied by a decrease in the selectivity to methanol. Moreover, the selectivity to dimethyl ether (DME) and CO_2 increase when the content of this acid oxide increases.

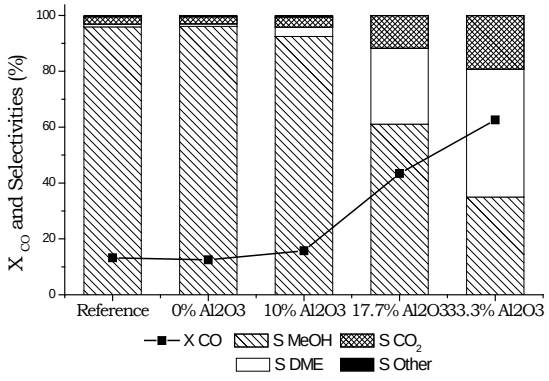

Figure 3.7. Effect of the addition of colloidal alumina to the slurry formulation in catalytic test. Methanol synthesis reaction was carried out at 260 ºC and 40 bar with space velocity of 2.55 Lsyn/g_{CZA}·h.

The increase in the CO conversion and selectivity to DME can be thought to be produced by the acidity of the added alumina. Indeed, the alumina acidity favours the methanol dehydration to DME and the disappearance of methanol favours the increase of the CO conversion due to a shift of the equilibrium in the methanol synthesis reaction.

In order to see the separate influence of alumina on copper but without modifying the overall acidity of the catalyst, the addition of a compound that neutralizes this acidity was considered. One of the compound used in the literature to kill the acidity of alumina is boric acid [26-28]. When H_3BO_3 was added to this slurry formulation with the colloidal Al_2O_3 (CZA_17.7%Al_2O_3), the selectivity to DME decreased with the H_3BO_3 content (*Figure 3.8*). Moreover, the CO conversion also decreased with the addition of H_3BO_3 (*Figure 3.8*). However, the selectivity of the sample with the highest H_3BO_3 content used (17.4 mmol H_3BO_3/g Al_2O_3 added to the slurry), which showed a selectivity to DME of 3.4 %, did not reach to the DME selectivity value of the parent catalyst (≈1 %).

On the other hand, the addition of H_3BO_3 to the slurry formulation showed a sharp decrease of the Cu metal surface area (*Figure 3.9*). Consequently, this strategy was abandoned because it produced alterations in the catalyst as important or more than the changes due to the acidity of the alumina that were intended to be avoided.

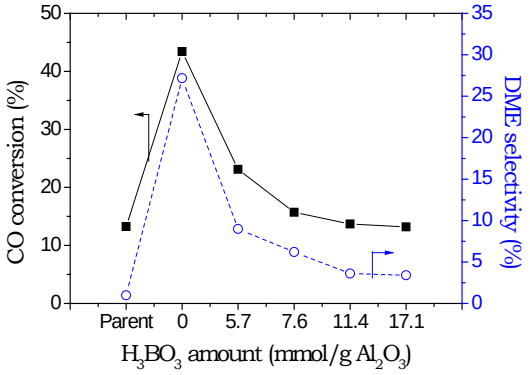

Figure 3.8. CO conversion of CZA_17.7%Al_2O_3 with different H_3BO_3 content.

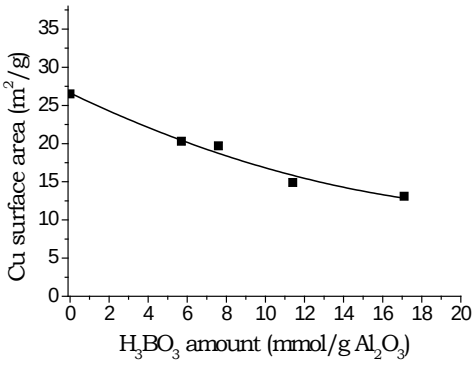

Figure 3.9. Cu metal surface area of CZA_17.7%Al_2O_3 with different H_3BO_3 content.

b) Slurried catalysts preparation with colloidal zinc oxide (ZnO)

The addition of colloidal zinc oxide produced slight changes in activity (*Figure 3.10*). The use of this colloid resulted in a slight decrease in the CO conversion. However, the three-studied ZnO contents produced similar CO conversion. According to selectivities, the increase in the ZnO added in the slurry formulation resulted also in a slight decrease in the selectivity to DME. The catalyst with 17.7, 33.3 and 50% of ZnO produced a 0.4, 0.15 and 0.1 % of DME respectively. The

reference catalyst and the slurried catalyst (0% colloid) presented a selectivity of 0.9-1% to this compound.

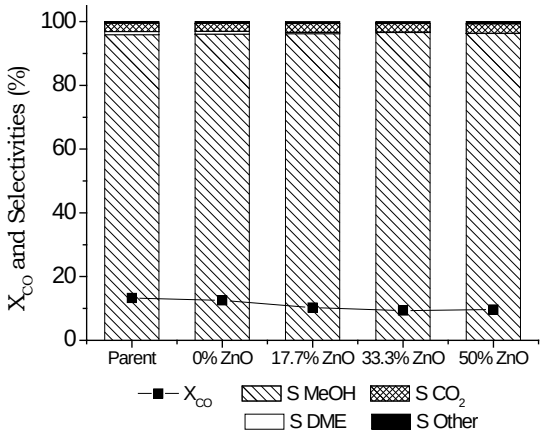

Figure 3.10. Catalytic test of the sample with colloidal ZnO as additive. Reaction conditions: 260 ºC, 40 bar and 2.55 Lsyn/g_{CZA}·h.

This similarity in the CO conversion was also observed at different space velocities (*Table 3.3*). However, increasing the space velocity a decrease in the CO conversion was observed. Furthermore, a slight decrease in the DME selectivity and other compounds (mainly light hydrocarbons) was also shown when the space velocity increased.

Table 3.3. CO conversion and selectivities for methanol synthesis of the catalyst with different colloidal ZnO content at different space velocities.

Sample	WHSV (L_{syn}/g_{CZA}·h)	X_{CO} (%)	Selectivity (%)			
			MeOH	DME	CO_2	Other
CZA_17.7%ZnO	1.2	17.6	96.0	0.53	2.7	0.73
	2.55	10.3	96.2	0.40	2.8	0.58
	5	5.2	96.2	0.31	3.0	0.57
CZA_33.3%ZnO	1.2	15.6	96.3	0.17	2.8	0.74
	2.55	9.3	96.6	0.14	2.7	0.57
	5	4.9	96.4	0.15	2.9	0.51
CZA_50%ZnO	1.2	16.2	95.9	0.17	3.0	0.87
	2.55	9.7	96.2	0.10	3.0	0.63
	5	5.5	96.4	0.14	2.9	0.55

Trying to understand the effect of the presence of colloidal ZnO in the slurried catalysts, a study of different interaction between the CZA catalyst and colloidal ZnO was made (33.3% of ZnO in CZA). Mixtures of both compounds (CZA and ZnO) were prepared by different contact methods: namely, physical mixture (powder of both compounds pressed, grinded and sieved separately to the desired size, and finally mixed), mechanical mixture (powder of both compounds mixed together and then pressed, grinded and sieved) and slurried mixture (powder of both compounds dispersed in water, dried and calcined, pressed and sieved).

The Cu metal surface area, which was measured by N_2O-RFC, is presented in *Figure 3.11* and the results of activity test of these mixtures in a fixed bed reactor are presented in *Figure 3.12*.

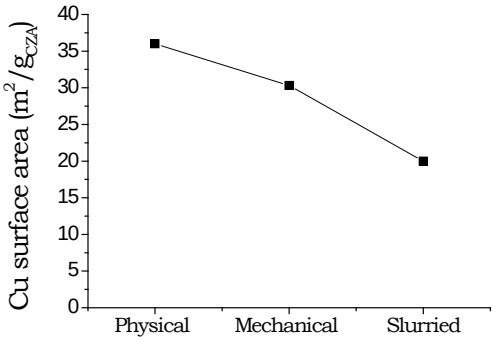

Figure 3.11. Effect in Cu metal surface area with the contact of CZA catalyst and colloidal ZnO

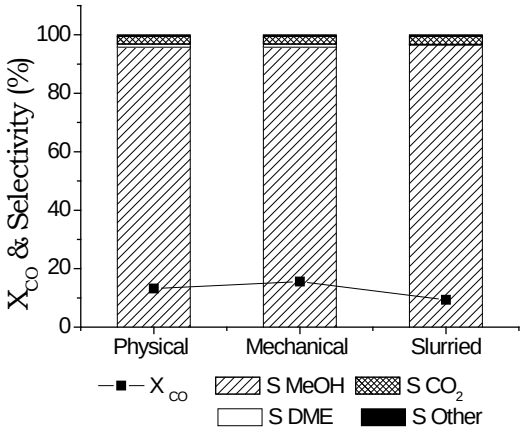

Figure 3.12. Activity test of CZA catalyst with 33.3% of colloidal ZnO prepared with different mixtures.

The results showed a decrease in the Cu metal surface area when both compounds are mixed mechanically and a higher decrease was exhibited by the slurried mixture (*Figure 3.9*). The methanol synthesis activity test showed a slight increase of the CO conversion of the mechanical mixture in comparison to that of the physical mixture (*Figure 3.10*). However, the slurried mixture presented a decrease of CO conversion. Moreover, the DME selectivity of the slurried mixture (0.15%) is much lower than that of the physical and the mechanical mixture (which present similar values of 1.1 % approximately).

c) Slurried catalysts preparation with colloidal silica (SiO_2)

The effect of the addition of colloidal silica to the slurried catalyst is shown in *Figure 3.13*. In these samples, a slight increase in CO conversion was observed when silica was used. Furthermore, the selectivity to methanol decreased with the silica content as well as the selectivity to DME and CO_2 increased.

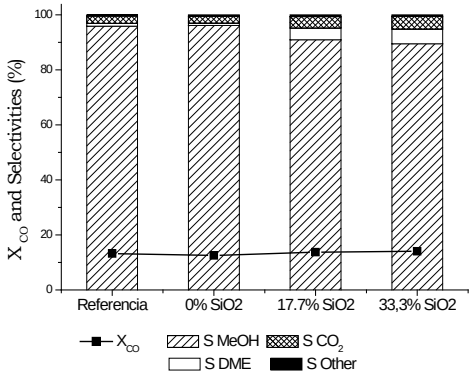

Figure 3.13. Catalytic test as a function of the colloidal silica employed. Reaction conditions: 260 ºC, 40 bar and 2.55 Lsyn/g_{CZA}·h.

3.2.1.2. Coating properties

Slurry properties were characterised by different techniques.

- **Zeta Potential**

The slurries of the catalysts were prepared in aqueous media. Therefore, trying to obtain stable slurries, the zeta potential of the slurries was monitored (*Figure 3.14*).

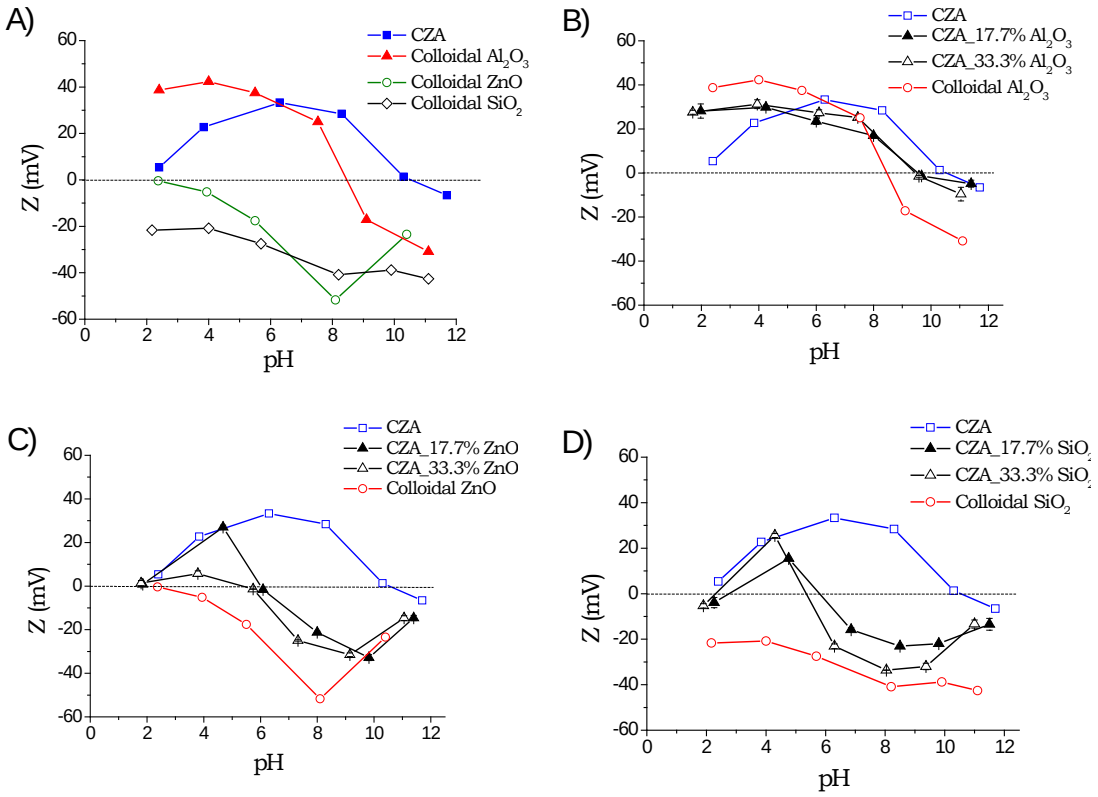

Figure 3.14. Zeta potential at different pH values of a) CZA catalyst and colloids employed and the slurries with different colloids b) Al_2O_3, c) ZnO and d) SiO_2

The CZA catalyst showed an isoelectric point at pH values around 10 and a high zeta potential value at pH 6 (*Figure 3.14A*). However, pH changes must be carefully analysed when Cu-based catalysts are used. At it is shown in *Figure 3.15*, acid solution (pH<4) lead to the dissolution of the copper [29] and the suspension become transparent. However, the use of large amount of ammonia (pH > 11) generate a copper coordination complex and the solution becomes dark blue [30,31].

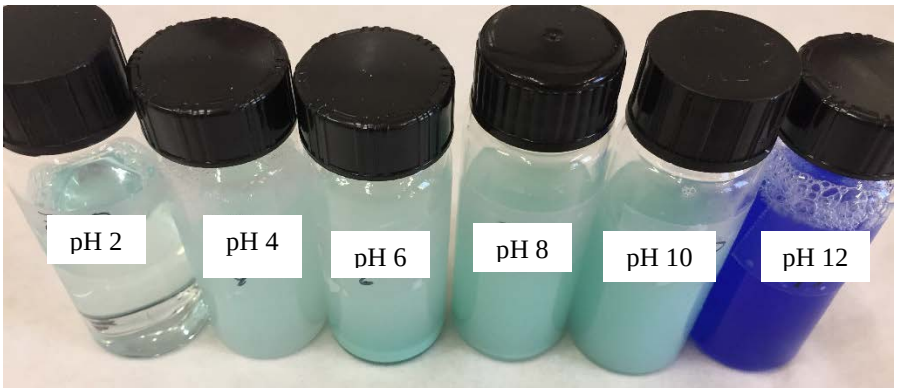

Figure 3.15. Photograph of solutions of slurry CZA_17.7%ZnO at different pH.

The inorganic oxide colloids presented different zeta potential curves (*Figure 3.14A*). While the colloidal alumina presented the isoelectric point at pH 8.5 approximately, the colloidal ZnO present this value at pH 2 (*Figure 3.14A*). However, the colloidal SiO_2 tend to present zeta potential values lower than -20 mV in all the studied pH range (*Figure 3.14A*). Moreover, the colloidal ZnO and SiO_2 exhibited a zeta potential negative in all the studied range, while the CZA catalyst and the colloidal Al_2O_3 presented more similar zeta potential with positive values at pH lower than 10 and 8.5 respectively and negatives at higher values.

The zeta potential of the different slurry formulation (*Table 3.1*) are also presented in *Figure 3.14*. It has been taken into account that mixing two solids with different charges (positive and negative) could generate aggregates when they are mixed due to an attraction of charges. In *Figures 3.14B to 12D* the zeta potential of the CZA catalysts slurries with different colloids and colloid content were shown. The results showed that the addition of colloidal Al_2O_3 to the slurry generated an intermediate behaviour between the two solids. On the contrary, the use of the colloidal ZnO and SiO_2, which presented opposite charge to the CZA catalyst, presented a behaviour close to that of the colloids. This may be because the colloidal particles are surrounding the CZA particles especially at pH>6.

During the slurry preparation, the measured pH's of all formulations presented values corresponding to high zeta potential (*Table 3.1*). Therefore, pH was not modified for slurries trying to avoid changes in the acidity of the catalyst (especially in the case of zeolite in later sections).

- **Particle size distribution**

The particle size distribution of the CZA catalyst in aqueous media (*Figure 3.16*) was measured by light scattering. The results, showed a D[4,3] value of 4.2 μm and d(0.9) of 8.2 μm, which is adequate for obtaining stable slurries without requiring additional milling [5,6,11].

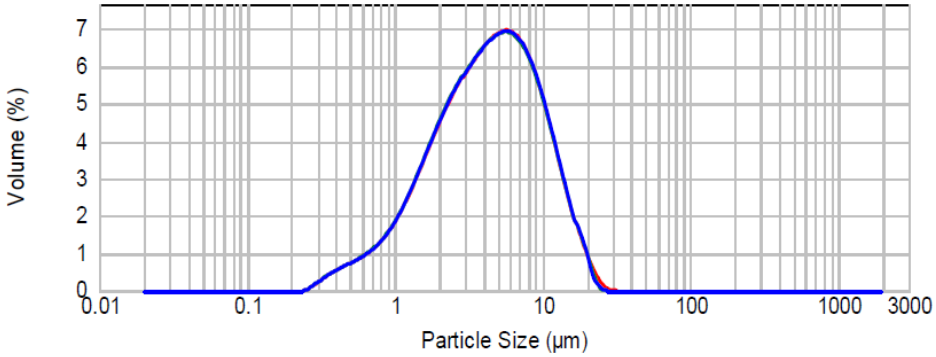

Figure 3.16. Particle size distribution of CZA catalyst

Furthermore, in *Table 3.4* the results of particle size measurement of the slurries were presented. The results showed that the particle size measured of the different slurries is adequate and they presented good stability at the pH values in which they are prepared

Table 3.4. Particle size and zeta potential of slurries

	Slurry pH	Zeta Potential (mV)	Particle size (μm)
CZA parent	6.5	+ 32	4.2
CZA_17.7%Al_2O_3	5.7	+ 24	6.6
CZA_17.7%ZnO	8.3	- 23	5.3
CZA_17.7%SiO_2	7.5	- 19	7.0

- **Viscosity**

The viscosity of different slurry formulations was also measured (*Table 3.5*). The results showed an increase in the viscosity with the colloid content. Moreover, the nature of the colloid affects the viscosity. The use of colloidal alumina produced the highest values of this parameter and the addition of colloidal SiO_2 the lowest value, even lower than the slurry without colloid.

Table 3.5. Viscosity of different slurry formulation

Sample	CZA (%)	Colloid (%)	PVA (%)	H_2O (%)	Colloid type	Viscosity (mPa·s) 1000 s^{-1}
CZA_0%C*	19.1	0.0	0.9	80	-	7.0
CZA_10%C*	17.3	1.9	0.8	80	Al_2O_3	8.7
CZA_17.7%C*	15.9	3.4	0.7	80	Al_2O_3 ZnO SiO_2	11.9 8.3 4.8
CZA_33.3%C*	12.9	6.5	0.6	80	Al_2O_3 ZnO SiO_2	16.2 10.2 5.2
Al_2O_3 Colloid	-	20.0	-	80	Al_2O_3	14.0
SiO_2 Colloid	-	20.0	-	80	ZnO	8.9
ZnO Colloid	-	34.0	-	66	SiO_2	4.8

*C = Employed colloid; namely, Al_2O_3, ZnO and SiO_2.

- **Washcoating process**

Metallic monoliths were coated with different slurries by the washcoating method. The catalyst amount coated in each immersion is presented in *Figure 3.17*. Results showed the gradual increase of the total amount of catalyst loaded as a function of the immersions number. However, viscosity affects the coating process and more immersions number were required to deposit the same amount of catalyst when the colloidal SiO_2 was used, which presents the lowest viscosity (*Table 3.5*). Moreover, all the studied formulations showed homogeneous coatings without plugged channels (*Figure 3.18*).

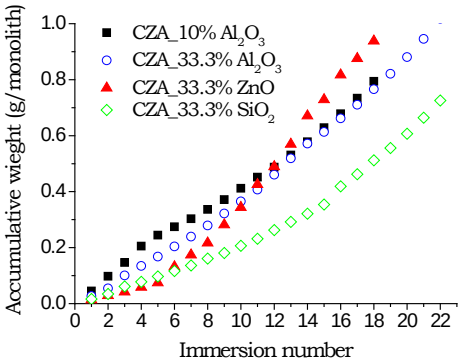

Figure 3.17. Graph of catalyst amount coated vs. immersions

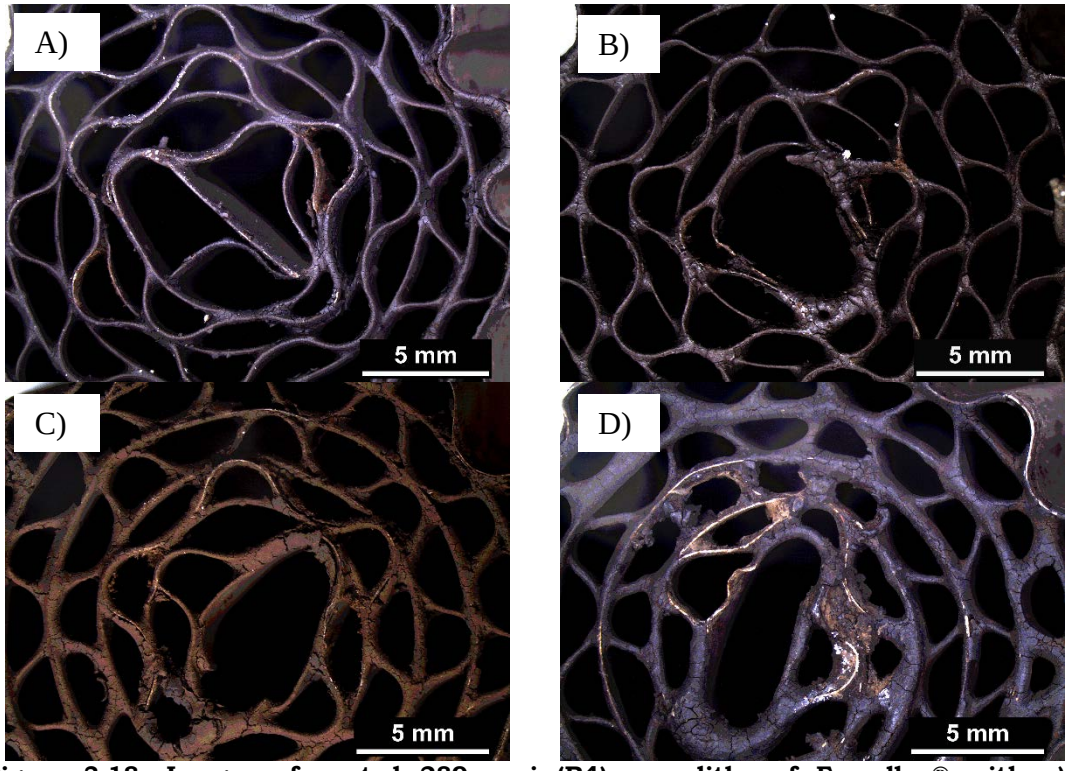

Figure 3.18. Images of coated 289 cpsi (R4) monoliths of Fecralloy® with a) CZA_10%Al_2O_3 b) CZA_33.3%Al_2O_3 c) CZA_33.3%ZnO and D) 33.3% SiO_2.

- **Adherence Test**

The adherence produced by the different slurry formulations was measured by the sonication method of the coated monolith. The adherence of the catalyst layer in Fecralloy® substrates as function of the colloid employed and the calcination temperature is shown in *Figure 3.19*.

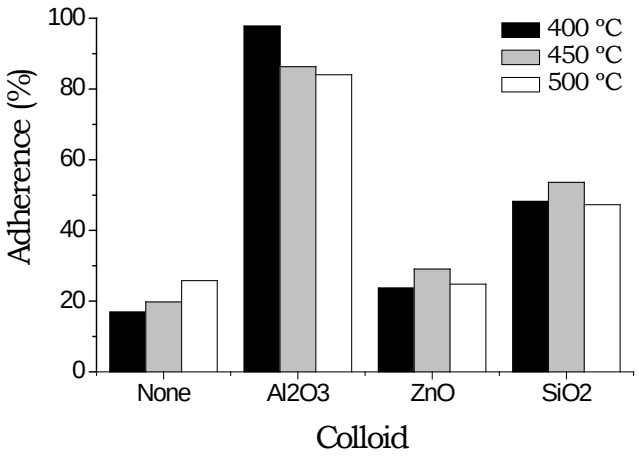

Figure 3.19. Adherence obtained with different colloids employed with the same content of them (17.7% of colloid) and calcined at different temperatures.

The results showed remarkable differences in the adherence obtained with the nature of the colloid employed in the formulation. No use of colloid resulted in poor adherence, around 20% (*Figure 3.19*). The use of colloidal ZnO did not show an increase in adherence. Nevertheless, the colloidal SiO_2 and Al_2O_3 improved the adherence. Colloidal Al_2O_3 showed the best results with good adherence, above 80%. Regarding the calcination temperature, there was not a clear trend in the adherence.

Figure 3.20 shows the adherence obtained with the different colloids as a function of their content. The increase in colloid content led to an increase in the adherence in all cases. However, the content required for good adherence (>80%) is lower with Al_2O_3 than with the other ones. Moreover, a decrease in the adherence was shown increasing the calcination temperature with the use of colloidal Al_2O_3. Nevertheless, there was no appreciable effect in adherence with calcination temperature employing colloidal ZnO and SiO_2. Therefore, for the activity test lower calcination temperature (400 ºC) was selected due to possible sintering of Cu-based catalysts at high temperatures [32-34].

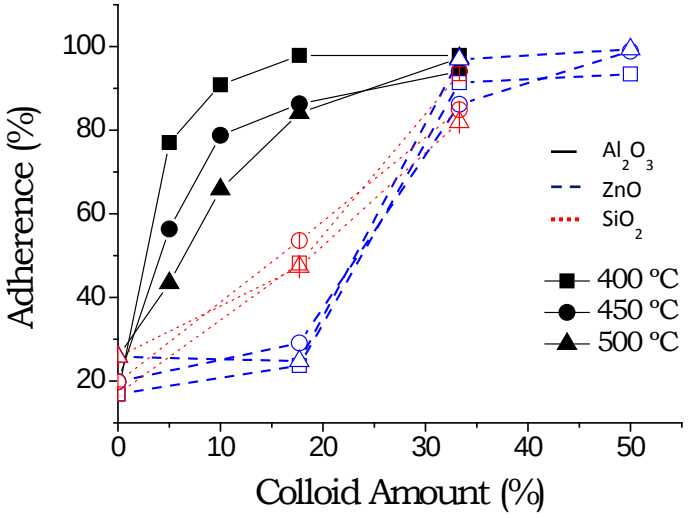

Figure 3.20. Adherence obtained with different content of the studied colloids: Al_2O_3 (solid), ZnO (dot) and SiO_2 (Dash); and different calcination temperatures: 400 (square), 450 (circle) and 500 ºC (triangle).

- **Thermogravimetric analysis of additives**

A thermogravimetric analysis was done to all the additives used in the slurry formulations: namely, polyvinyl alcohol (PVA) and inorganic oxide colloids (Al_2O_3, ZnO and SiO_2) (*Figure 3.21*).

All the slurry formulation were prepared with PVA as additive (*Table 3.1*). A TG analysis of this organic compound showed that it is completely remove at 500 ºC (*Figure 3.21A*). Moreover, when the TG analysis was made to the different colloids (*Figure 3.21B*), the results showed that colloidal SiO_2 and ZnO did not have weight-loss in the range of 400-500 ºC, the calcination temperature studied. However, the colloidal Al_2O_3 presented an important weight-loss in this range.

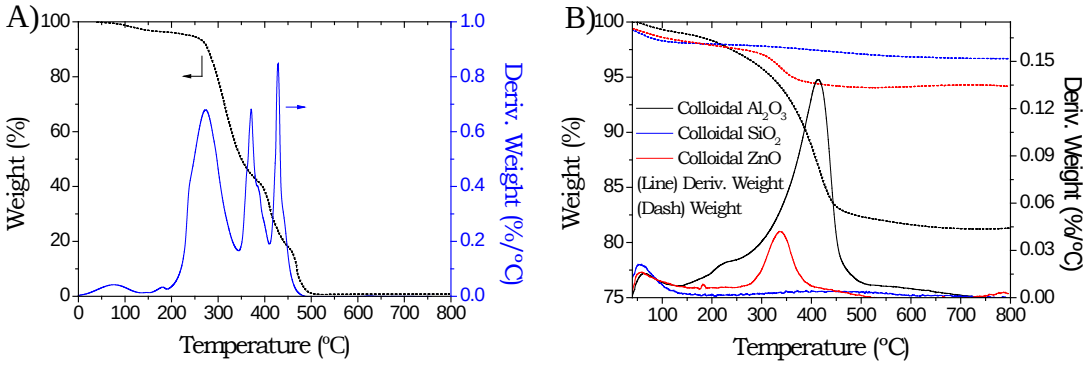

Figure 3.21. TG analysis of A) polyvinil alcohol (PVA) and B) different colloids (Al_2O_3, SiO_2, ZnO).

A TG analysis was done to the colloidal Al_2O_3 calcined at different temperatures, and the results exhibited a decrease in weight-loss with calcination temperature (*Figure 3.22A*). Furthermore, the differences with calcination temperature were also detected by XRD (*Figure 3.22B*). The diffractograms presented a structural change of the Al_2O_3. The commercial colloid (dried) exhibited the presence of boehmite that was completely transformed to γ-alumina at 500 °C.

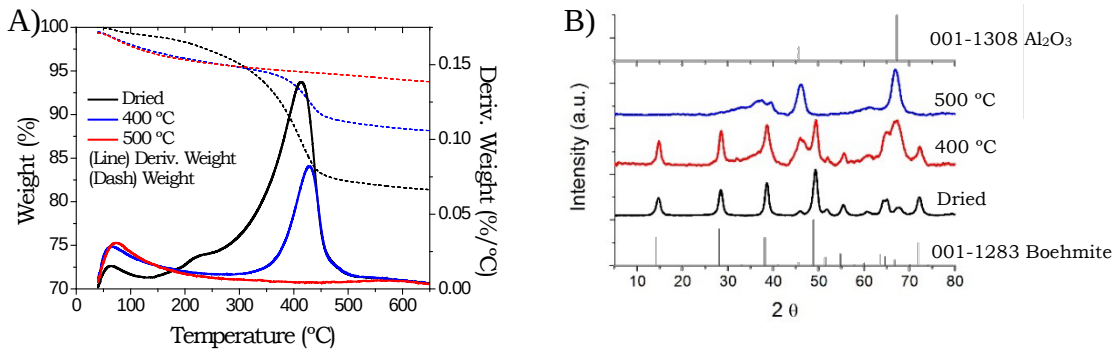

Figure 3.22. TG analysis (A) and XRD diffractograms (B) of the colloidal alumina calcined at different temperatures

3.2.1.3. Structured catalyst

Before carrying out the structuring of the catalyst, a compilation of the formulations that offered higher adherence (≥ 90%) with the three colloids and the corresponding catalytic results was made. After its analysis, the best formulation

was selected and structured systems were prepared on Fecralloy® monoliths with different cell density. The samples obtained were characterised and tested in the methanol synthesis reaction.

3.2.1.3.1. Selection of the best formulation

The activity results of the different slurried catalysts prepared with the different colloids presenting the highest adherence are compiled in *Figure 3.23*. It is noticeable that lower alumina content than zinc oxide or silica is required to obtain excellent adherence (>90%). However, as it was showed before, the CO conversion and the selectivity to different compounds changed with the colloid used:

- The addition of 10% of Al_2O_3 decreased selectivity to methanol in comparison to the parent catalyst and 0% slurried catalyst (*Figure 3.23*). However, the CO conversion increased.
- In contrast, 33.3% of colloidal ZnO presented a decrease in the CO conversion (*Figure 3.23)*.
- The addition of 33.3% of SiO_2 produced a decrease in selectivity to methanol as with colloidal Al_2O_3, but with lower selectivity to methanol than CZA_10%Al_2O_3 and similar CO conversion to the parent catalyst (*Figure 3.23*).

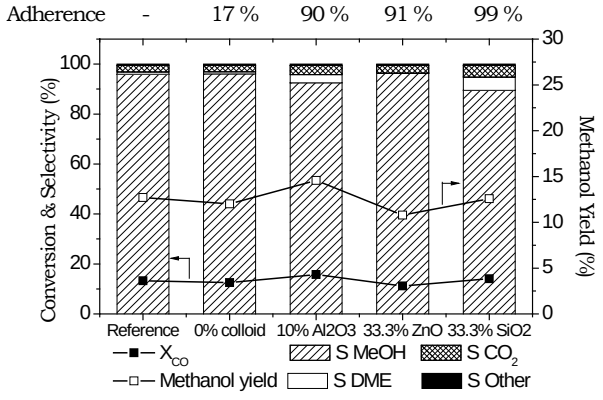

Figure 3.23. Activity results of slurried catalysts with the best adherence performance for each colloid in methanol synthesis reaction. Methanol yield (empty symbols), CO conversion (filled symbols) and selectivities (bars). Reaction conditions: 260 ºC, 40 bar and 2.55 Lsyn/g_{CZA}·h.

Furthermore, these changes altered the methanol yield (*Figure 3.23*). The addition of no colloid to the slurry did not show noticeable changes. The use of colloidal Al_2O_3 produced a slight increase in the methanol yield from 12 to 15% approximately. However, the addition of ZnO produced a decrease in the methanol yield and colloidal SiO_2 showed a similar methanol yield to the parent catalyst.

Therefore, CZA_10%Al_2O_3 was chosen as the best formulation and the structured catalysts for methanol synthesis were prepared on Fecralloy® monolith and characterised.

3.2.1.3.2. Physicochemical properties of structured catalyst

- **Textural properties**

The textural properties of the structured catalyst were measured by N_2 adsorption, and the corresponding isotherms are shown in *Figure 3.24*. Moreover, the desorption isotherm was used to calculate the pore size distribution (*Figure 3.25*). The BET surface area, the total pore volume and the equivalent pore diameter are calculated from the isotherm and the results are presented in *Table 3.6*.

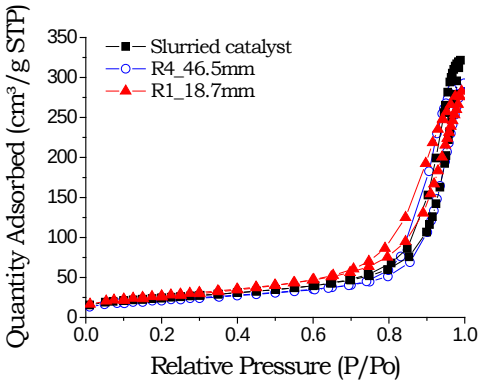

Figure 3.24. N_2 Isotherm of slurried catalyst and structured catalyst of CZA_10%Al_2O_3.

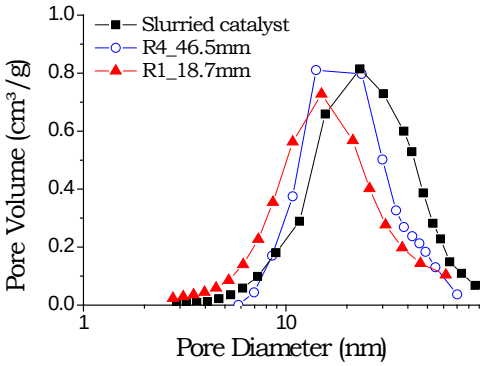

Figure 3.25. Pore size distribution of slurried catalyst and structured catalyst of CZA_10%Al_2O_3.

Table 3.6. Textural properties and reducibility of structured catalyst

Sample	Form	S. BET (m^2/g)	Total pore volume (cm^3/g)	Equiv. pore diameter (nm)	Cu surface area (m^2/g_{CZA})	H_2 cons. (cm^3/g_{CZA})	TPR Reducibility (%)
CZA_ 10%Al_2O_3	Slurried	86	0.50	23.3	30.7	175.7	104
	R4	87	0.45	20.7	33.1	173.8	103
	R1	92	0.44	19.1	34.1	177.6	105

The results showed similar textural properties between the slurried and the structured catalysts (*Figure 3.22-23 and Table 6*). Both slurried and structured catalysts presented type IV isotherms with a similar total pore volume and pore size distribution.

- **Copper metal surface area**

The copper metal surface area was measured by N_2O-RFC. The results were summarised in *Table 3.6*. It is noticeable that the Cu metal surface area of the structured catalysts were similar between them and 10-12% higher than that of the parent catalyst.

- **Reducibility**

The reducibility of the structured catalysts was measured by H_2-TPR (*Table 3.6 and Figure 3.26*). H_2 consumption was estimated by integrating the peaks of the TCD signal.

The results showed also no change in the maximum reduction temperature when the catalyst was coated on the metallic substrate (*Figure 3.26*). Similar reducibility was also measured, near to 100% (*Table 3.6*).

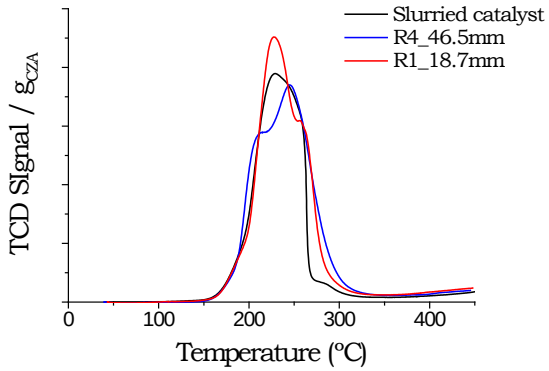

Figure 3.26. TPR of H_2 analysis of slurried catalyst and structured catalyst of CZA_10%Al_2O_3.

- **Activity Test**

The activity test of the structured catalyst was carried out in a Hastelloy reactor with 17 mm of internal diameter at 260 °C and 40 bar. The results are shown in *Figure 3.27.*

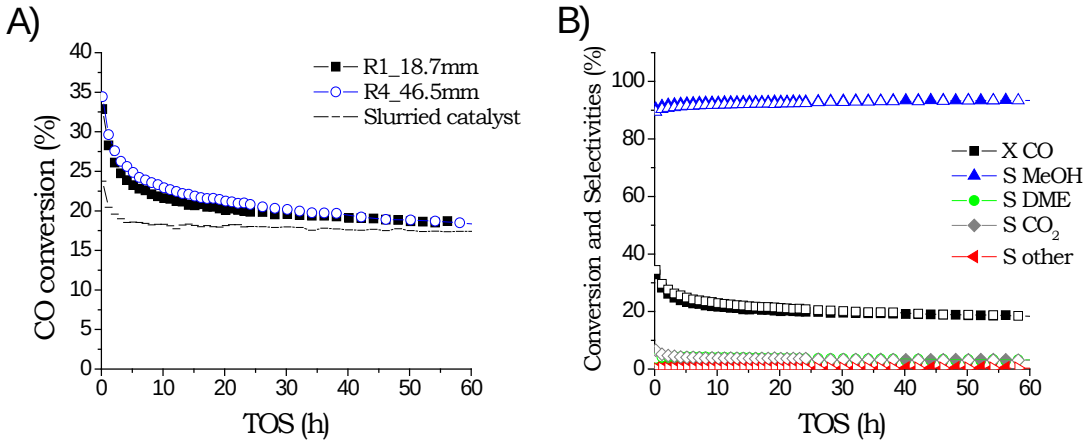

Figure 3.27. Activity test of structured catalyst of CZA_10%Al_2O_3 sample in Fecralloy® monoliths of R1_18.7µm (Filled symbols) and R4_46.5µm (empty symbols). Reaction conditions: 260 °C, 40 bar and 2.55 Lsyn/g_{CZA}·h. Coated catalyst 1 g.

Results showed that the structured catalysts present similar CO conversion and slightly higher CO conversion than the slurried catalyst. Furthermore, the selectivities to the different compound were also similar (*Figure 3.27*). In addition, radial temperature profile was also measured and shown in *Figure 3.28*. The results showed an almost isotherm profile in both studied monoliths of different cell density.

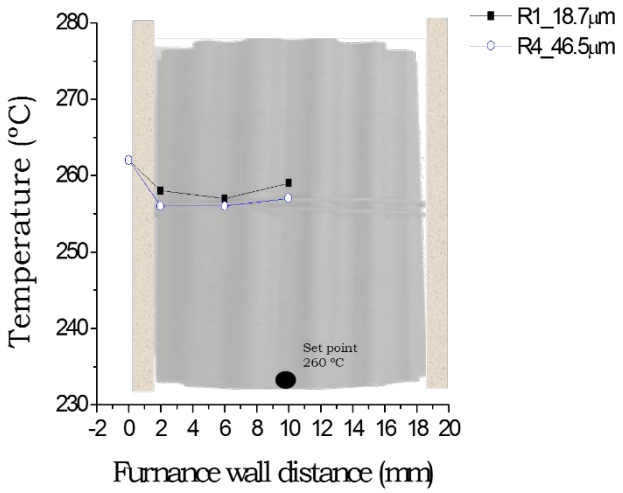

Figure 3.28. Temperature profile of monoliths R4 (289 cpsi) and R1 (2360 cpsi) in methanol synthesis reaction at 260 ºC y 40 bar with 2.55 L_{syn}/g_{CZA}·h. Coated catalyst 1 g.

3.2.2. Discussion

3.2.2.1. Slurried catalyst

When inorganic oxide colloids were added to the slurry, changes in the catalytic properties were observed (*Table 3.2*). On the one hand, textural properties of the slurried catalysts depend on the colloid properties. For example, in the case of the addition of colloidal Al_2O_3 occurred an increase in the BET surface area due to the additional surface area that alumina provides.

On the other hand, the Cu metal surface area and the catalyst reducibility decrease with the addition of colloids and it is more noticeable increasing the colloid content (*Table 3.2*). These additives could create interactions with active sites or cover the metallic phase, thus changing the catalytic properties of the

parent catalyst, such as activity, selectivity and stability [8,12,35]. Moreover, an increase in the Cu crystal size was observed with colloid addition by in-situ XRD analysis, agreeing with the decrease in the Cu surface area (Table 3.2).Therefore, the colloid nature and its content directly affect in copper surface area.

Regarding the methanol synthesis test, a decrease in methanol selectivity and an increase in dimethyl ether (DME) selectivity were observed when colloidal Al_2O_3 was added (*Figure 3.7*). It is widely known the ability of the alumina to dehydrate the methanol to DME [36- 42]. Alumina presents acid sites, which are detected by the NH_3-TPD analysis (*Figure 3.6A*), that can produce the methanol dehydration. Moreover, these changes in selectivity lead to an increase in the CO conversion (*Figure 3.7*). In the direct synthesis of DME, the thermodynamic equilibrium limitation of the methanol formation is removed due to the dehydration of methanol to DME while the first is formed [43,44]. Therefore, the equilibrium of the reaction is shifted to the right and the CO conversion increases.

Trying to avoid the dehydration capacity of the alumina without losing its ability to enhance the adherence of the catalyst layer in the monolith, the use of boron to neutralize the acidity of alumina was studied (*Figure 3.8-3.9*). Mineral acids such as H_3PO_4 or H_3BO_3 are used to modify alumina and reduce the strength of the Lewis acid sites that this compound presents [28]. These mineral acids are able to avoid the formation of strong Lewis acid sites or reduce the accessibility to adsorbate molecules [28]. The incorporation of different contents of boric acid showed a decrease in DME selectivity. Nevertheless, even with the highest content studied, 17.4 mmol of H_3BO_3/g Al_2O_3, DME selectivity (≈3%) did not reach the values of the parent catalyst (≈1%). Unfortunately, the CO conversion decreased as the boric acid content increased (*Figure 3.8*). These results agree with the decrease in methanol dehydration, which stops favouring the displacement of equilibrium. However, the metallic surface area of the catalyst also decreased when the H_3BO_3 is added to the slurry (*Figure 3.9*). Therefore, despite neutralizing the acidity of the Al_2O_3, the addition of H_3BO_3 by this method produce negative effects on the parent catalyst and this strategy was abandoned.

The addition of the colloidal ZnO produced a slight decrease in CO conversion (*Figure 3.10*). As it is shown in *Table 3.2,* the Cu metal surface area and the reducibility sharply decrease with the addition of ZnO (Table 3.2). T.A. Nijhuis *et al.* [12] suggested that this could be due to the coverage of the metallic phase by the colloids reducing the activity of the catalyst. As we said before, after in-situ XRD analysis the results showed that the decrease of the copper surface area was

related to an increase in the Cu crystal size (*Table 3.2*). However, the CO conversion did not decrease noticeably with the colloid content (*Table 3.3*)

There is a huge controversy in the mechanism of the methanol synthesis reaction and the role of the zinc in this reaction [45]. It is widely thought that the Zn is employed as promotor to improve the dispersion of the Cu and to reduce the sintering of Cu [45]. However, the yield of the reaction improvement has been observed when ZnO is added to Cu-based catalysts [45-47]. Burch *et al.* [46] attributed this improvement to the performance of the ZnO as H_2 reservoir. Hence, it would favour the hydrogenation of the reaction intermediates. On the contrary, Kanai *et al.* [47] mention that the improvement in activity is due to the migration of ZnO_x to the cooper surface. It could generate CuZn alloy or Cu-O-Zn sites, stabilising the Cu^+ ions.

In this study when the colloidal ZnO is added a double effect might be produced. First, the addition of colloidal ZnO decreases the Cu metal surface area. However, despite decreasing the Cu surface area of the catalyst, the addition of ZnO could also originate an increase in the specific activity that could mitigate the decrease in active area.

The interaction between the parent catalyst and the colloidal ZnO is also shown in the selectivity (*Figure 3.10*). The basic character of ZnO produce a reduction of catalyst acidity as it is shown in *Figure 3.6B*. Therefore, a decrease in the selectivity of DME was observed as the content of this colloid increases.

In addition, trying to understand the effect of the addition of ZnO different contact modes between colloidal ZnO and CZA catalyst were studied. The results showed that the selectivity to DME is only altered when both compounds are mixed with high interaction (slurried mixture) decreasing sharply (from 1.1 to 0.15%, *Figure 3.12*). However, the CO conversion also exhibited changes. Despite decreasing the Cu metal surface area due to a high contact between phases, the CO conversion slightly increased in the mechanical mixture (*Figures 3.11-3.12*). It seems that the interaction between CZA and colloidal ZnO plays an important role. This could suggest that in the physical mixture the contact is not enough to produce noticeable changes of activity and in the slurried mixture too much contact is presented. Therefore, in the latter the positive effect of ZnO is mitigated due to the sharp decrease of the Cu metal surface area. However, the mechanical mixture allows an intermediate contact, which produce a catalyst without too much decrease in Cu surface area that makes it noticeable the improvement in the CO conversion when the ZnO is added (*Figure 3.12*).

Finally, with the use of colloidal SiO_2, it has been observed that the CO conversion slightly increased (*Figure 3.13*). Moreover, the selectivity to methanol decreased and the selectivity to DME increased. Therefore, a dehydration of methanol to DME has been produced as when colloidal Al_2O_3 was used, but with less dehydration. Silica presents weak acidity due to formation of silanol groups [48]. In NH_3-TPD (*Figure* 3.6C) can be seen a slight increase in the acidity of the catalyst. This change in acidity could produce a slight dehydration of methanol to DME, and consequently, the thermodynamic equilibrium of methanol formation will be slightly shifted. However, the CO conversion did not increase significantly when colloidal SiO_2 content was increased. Due to a reduction of the Cu metal surface area with colloidal SiO_2 content (*Table 3.2*), the activity of methanol synthesis catalyst decreases.

3.2.2.2. Adherence

The adherence tests showed the need of the addition of inorganic colloids to the slurry formulation to obtain appropriate adherence (Figure 17-18). With the absence of colloidal particles, the slurried catalyst showed low adherence, around 20%. However, the use of different colloids shows that the nature of the colloid and its content in the slurry produce significant changes in adherence.

Alumina was the inorganic oxide that produced the best results in adherence. It must be taken into account that Fecralloy® substrates are treated thermally at 900 °C to obtain adequate roughness to improve the catalyst adherence [49]. But in this thermal treatment, the Al which is one of the Fecralloy® components migrates to the surface and react with the atmospheric oxygen producing whisker of alumina. Hence, the better result could be due to the chemical affinity of the substrate with the colloidal alumina.

Nevertheless, due to the binder role that these inorganic colloids play, the adherence improved when the colloid content increases (*Figure 3.21*). The small particle of the colloids (nanoparticles) could fill the interparticular spaces of the catalyst particles, and enter in the surface roughness of the substrate, which create anchorage points between the catalyst layer and the substrate [12,21]. Hence, the cohesion and adhesion of the coated layer improves until a certain content is reached from which the adherence do not show relevant changes.

On the other hand, a decrease in adherence with calcination temperature was observed with colloidal Al_2O_3 that did not appear with other inorganic oxide colloids (*Figure 3.21*). Firstly, it seemed that the used PVA could be the reason of these results because this compound is not removed completely at 400 ºC and it requires 500 ºC for it (*Figure 3.22A*). However, PVA was added to all the slurries, so formulations with colloidal ZnO and SiO_2 should have presented the same behaviour with calcination temperature.

By TG and XRD analysis of colloidal Al_2O_3 at different calcination temperatures (*Figure 3.23*), it could be shown that the commercial colloidal alumina (Nyacol AL20) is transformed into pseudo-boehmite (AlO(OH) or $Al_2O_3{\cdot}H_2O$) phase that changes to γ-alumina at 500 °C approximately (*Figure 3.23B*). Calcining at 400 ºC produces an intermediate state between them. J.F. Sánchez *et al.* [50] suggested that the $Al(H_2O)_4OH]_2^{4+}$ ions, which are presented in boehmite, could react and form chemical bonds that improve the adherence of the catalyst. Therefore, when the OH group are eliminated by increasing calcination temperature, the adherence obtained decreases (*Figure 3.21*).

3.2.2.3. Structured catalyst

Once the slurry formulation was selected, structured catalysts were prepared and tested. As it is shown in *Figure 3.27,* the structured catalysts (R1_18.7μm and R4_46.5μm) exhibited slightly higher CO conversion than slurried catalyst (powder) agreeing with the Cu metal surface area (*Table 3.6*).

To our knowledge, there is little bibliography about structuring $Cu/ZnO/Al_2O_3$ catalyst for methanol synthesis. A. Montebelli *et al.* [14] tried to coat $Cu/ZnO/Al_2O_3$ catalyst in metallic open cell foams, but a decrease in activity was observed which was assigned to the slurry preparation and/or calcination procedure. X.K. Phan *et al.* [51] studied different methods to coat Cu-based catalyst in Fecralloy® monoliths and concluded that washcoating is the method that produces the best performances for methanol synthesis. Moreover, a better activity of the structured catalyst than the powder catalyst was observed. The authors suggested that the best performance of structured catalyst could be related to the better thermal properties of the metallic substrates: the axial temperature gradient in fixed bed was up to 10 ºC and in the structured catalyst less than 1 °C.

In our system, a radial temperature gradient was measured in the structured catalysts (R1 and R4) and slight changes of 2-3 ºC along the monolith were observed (*Figure 3.28*). Moreover, a difference between the centre of the monolith and the bottom of 2-4 ºC was also shown (*Figure 3.28*). However, these results cannot be compared with that of the slurried catalyst tested in powder because the temperature profile in the fixed bed has not been measured.

3.2.3. Conclusion

The structuration of the methanol synthesis catalyst was successfully obtained by the washcoating method. The addition of inorganic colloids are crucial for obtaining good adherence between the catalyst layer and the substrate. Good adherence was obtained with three studied colloids (Al_2O_3, SiO_2 and ZnO) on Fecralloy® substrates. However, different content is required for obtaining good adherence. Al_2O_3 was the colloid showing the best results.

Nevertheless, the use of these inorganic colloids affects the catalytic properties of the parent catalyst. The addition of these inorganic oxide particles could change the copper active sites, so the amount used is an important parameter to be considered. Large amount of colloids (>33.3%) decreases notably parameters such as Cu surface area and reducibility of the catalyst. Moreover, the colloidal particle itself could participate in the reaction. The acidity of both the Al_2O_3 and SiO_2 dehydrates the methanol to DME, and this effect increases with the increase of the colloid content. The use of boron to neutralize the acidity of the alumina showed a decrease of methanol dehydration. However, in addition to not neutralise completely the acidity of the mixture, the H_3BO_3 decreased the Cu metal surface area of the catalyst.

Therefore, a compromise must be taken between adherence, dehydration capacity and Cu metal surface area. In that sense, we observed that the CZA catalyst slurried with 10% of colloidal Al_2O_3 shows the best correlation between good adherence and maintenance of catalytic properties. This formulation allowed the successfully structuration by washcoating method on metallic substrates.

3.3. Dehydration catalyst or solid acid

This section shows the results of the characterization of the parent zeolite, the slurried zeolites and the structured catalysts prepared on Fecralloy® monoliths. The catalytic activity was measured in the methanol dehydration reaction.

The slurry preparation was carried out with different formulations (*Table 3.7*), which were based on previous formulations studied in our group [52]. The effect of the zeolite form in the slurry preparation was studied as well as the calcination temperature. Moreover, the effect of colloid content and nature of the colloid used (SiO_2 or Al_2O_3) was also investigated.

Table 3.7. Zeolite slurry composition and pH

Sample	ZSM-5 (%)	Colloid (%)		PVA (%)	H_2O (%)	pH
		SiO_2	Al_2O_3			
HZSM-5_0%	35.0	0.0	0.0	0.0	65	3.5
ZSM-5_11.8%SiO_2	29.8	4.0	0.0	1.2	65	5.6
HZSM-5_6%SiO_2	31.7	2.0	0.0	1.3	65	4.1
HZSM-5_11.8%SiO_2	29.8	4.0	0.0	1.2	65	4.1
HZSM-5_23.6%SiO_2	26.0	8.0	0.0	1.0	65	4.3
HZSM-5_6%Al_2O_3	31.6	0.0	2.1	1.3	65	3.8

The slurried samples were referred to as ZSM-5 in the case of the commercial zeolite in ammonium form and HZSM-5 for the zeolite in the proton form (H-type). For the slurried catalysts, this reference was followed by the percent of colloid (after drying and calcining the slurries) and the colloid used (SiO_2 or Al_2O_3). For example: HZSM-5_6%Al_2O_3.

3.3.1. Results

In this section, the results of the slurried catalyst are presented first. Then, the structured catalyst results are analysed.

3.3.1.1. Slurried catalysts

Different physicochemical properties of the slurried catalysts were measured. The effect of calcination treatment, the type of colloid used and their content in the slurried catalysts were studied.

- **Textural properties**

The textural properties of the ZSM-5 zeolite and the slurried ZSM-5 were measured by N_2 adsorption (*Figure 3.29*). Properties such as the BET surface area, the total pore volume and the micropore volume are summarised in *Table 3.8*.

Table 3.8. Textural properties of acid solids

Sample	Zeolite form in slurry	Calcination Treatment	BET Surface (m^2/g)	Total pore volume (cm^3/g)	Micropore volume (cm^3/g)
ZSM-5 (parent)	-	-	375	0.19	0.14
	-	400 °C, 3 h	399	0.22	0.15
	-	500 °C, 3 h	389	0.22	0.15
	-	500 °C, 5 h	384	0.22	0.15
ZSM-5_11.8% SiO_2	NH_4^+	400 °C, 3 h	315	0.25	0.11
		500 °C, 3 h	340	0.28	0.12
HZSM-5_6% SiO_2	H^+	400 °C, 3h	378	0.24	0.14
HZSM-5_11.8% SiO_2	H^+	400 °C, 3 h	336	0.28	0.13
		500 °C, 3 h	344	0.29	0.13
HZSM-5_23.6% SiO_2		400 °C, 3h	318	0.27	0.11
HZSM-5_6% Al_2O_3	H^+	400 °C, 3 h	371	0.29	0.13
Colloidal Al_2O_3	-	-	204	0.31	0
Colloidal SiO_2	-	-	114	0.22	0

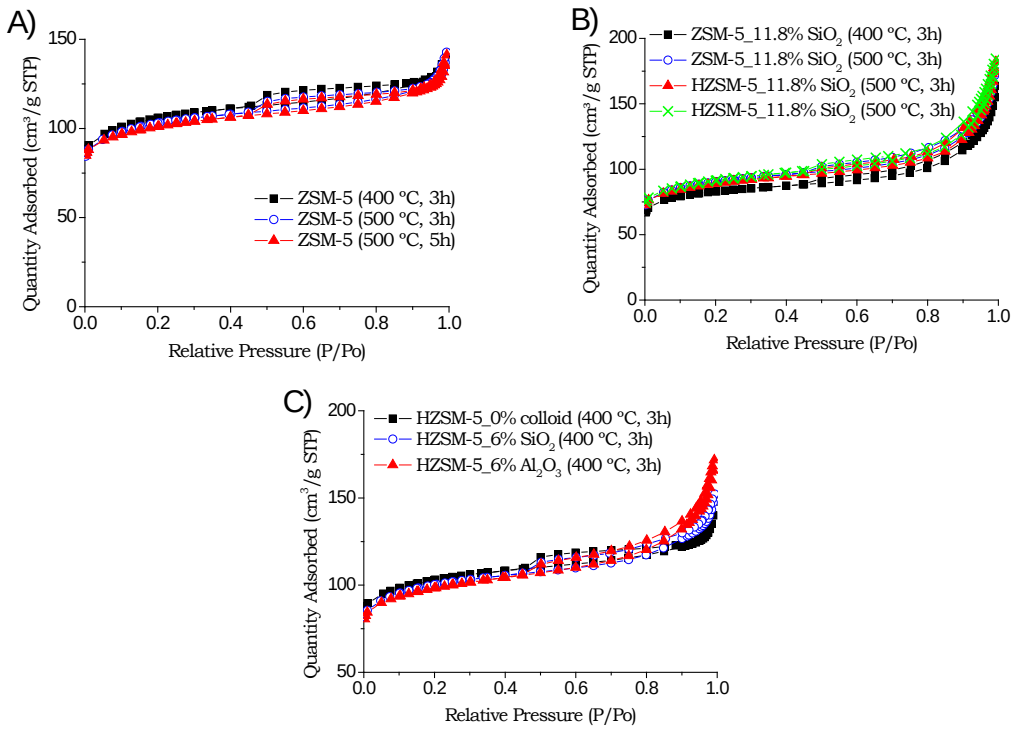

Figure 3.29. N_2 adsorption isotherm of a) commercial zeolite calcined at different conditions, b) slurried zeolite suspended in different forms and calcined at different temperatures and c) slurried zeolite with different colloid (Al_2O_3 or SiO_2)

The results showed type I isotherms for all samples (*Figure 3.29*). The commercial zeolite with different heat treatment presented similar textural properties (*Table 3.8*). However, the slurried zeolites presented a decrease in the BET surface area and the adsorbed N_2 increased at high values of P/P_0, probably due to aggregates of the zeolite crystals (*Table 3.8* and *Figure 3.29C*).

Preparing the slurry with zeolite in ammonium or proton form seemed to have no effect in the textural properties. Nevertheless, the sample with colloidal silica prepared with ammonium form zeolite and calcined at 400 °C presented lower surface area than the other samples.

The textural properties of the zeolites with different colloidal SiO_2 content are presented in Figure 3.30 and Table 3.8. All the zeolite samples showed a type I isotherm which is characteristic of microporous samples. Colloidal SiO_2 showed type IV isotherm. However, the sample with 23.6% of colloidal SiO_2 presented an

intermediate behaviour between type I and IV. At relative pressures around 0.8 a N_2 adsorption is observed related to the presence of mesoporosity in the sample.

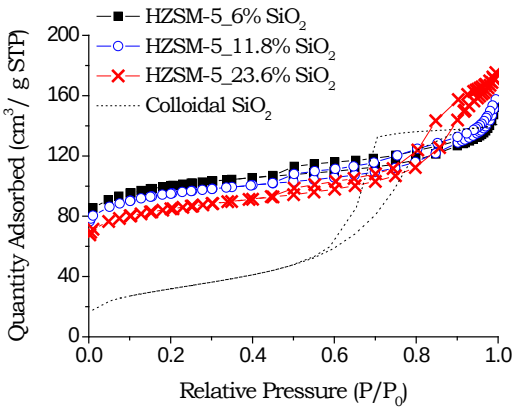

Figure 3.30. N_2 adsorption-desorption isotherms of slurried zeolite with different colloidal SiO_2 content

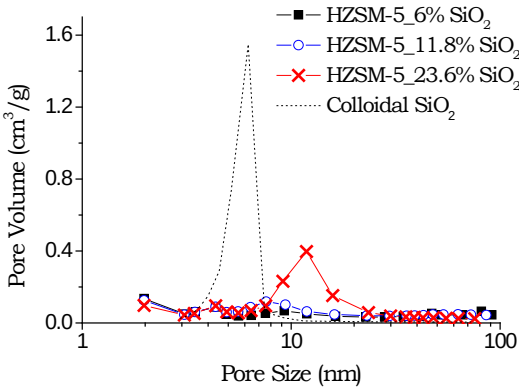

Figure 3.31. Pore size distribution of slurried zeolite with different colloidal SiO_2 content

The results showed a decrease in the BET surface area when colloidal SiO_2 is added to the slurried catalyst (Table 3.8). Moreover, the equivalent pore size increase with colloidal SiO_2 content. In the pore size distribution (Figure 3.31), it can be seen new pores at 10-12 nm approximately when 23.6% SiO_2 is used.

- **Crystallinity**

The zeolite crystallinity was studied by XRD analysis (*Figure 3.32*). The results showed no changes in the samples when different calcination treatments are used (*Figure 3.32A*). All the heat treatments preserved the ZSM-5 structure. Moreover, the slurried catalyst did not show significant changes. The zeolite form and the use of inorganic oxide colloids (Al_2O_3 or SiO_2) or the colloidal SiO_2 content did not alter the crystalline structure of the parent zeolite either (*Figure 3.32B-D)*.

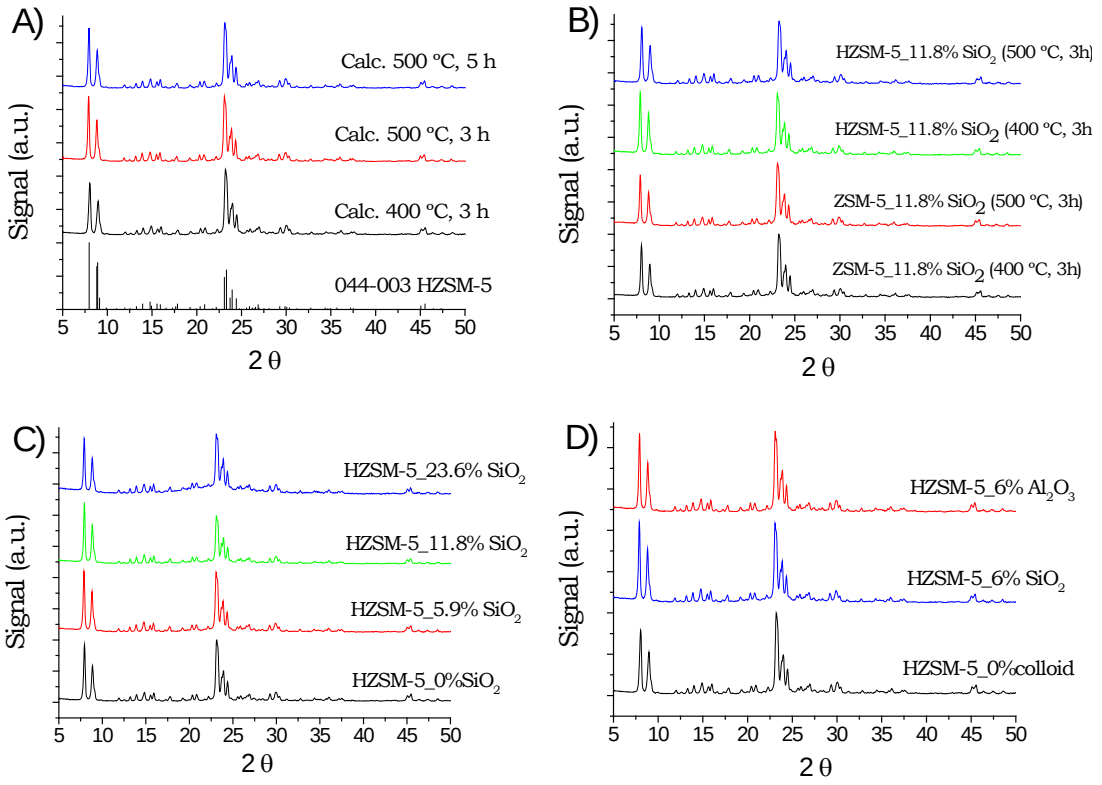

Figure 3.32. XRD analysis of zeolite samples: a) commercial zeolite CBV2314 with different heat treatments b) slurried catalyst suspended in different forms and calcined at different temperatures, c) slurried zeolite with different colloidal SiO_2 content and d) slurried zeolite with different colloid

- **Acid strength**

Acidity of the samples was measured by NH_3-TPD analysis and the signal was monitored by a TCD detector and a mass spectrometer (MS).

The effect of calcination temperature in acidity was presented in *Figure 3.33*. The results showed a decrease in acidity with calcination temperature in the TCD signal as well as in the 17 m/z signal.

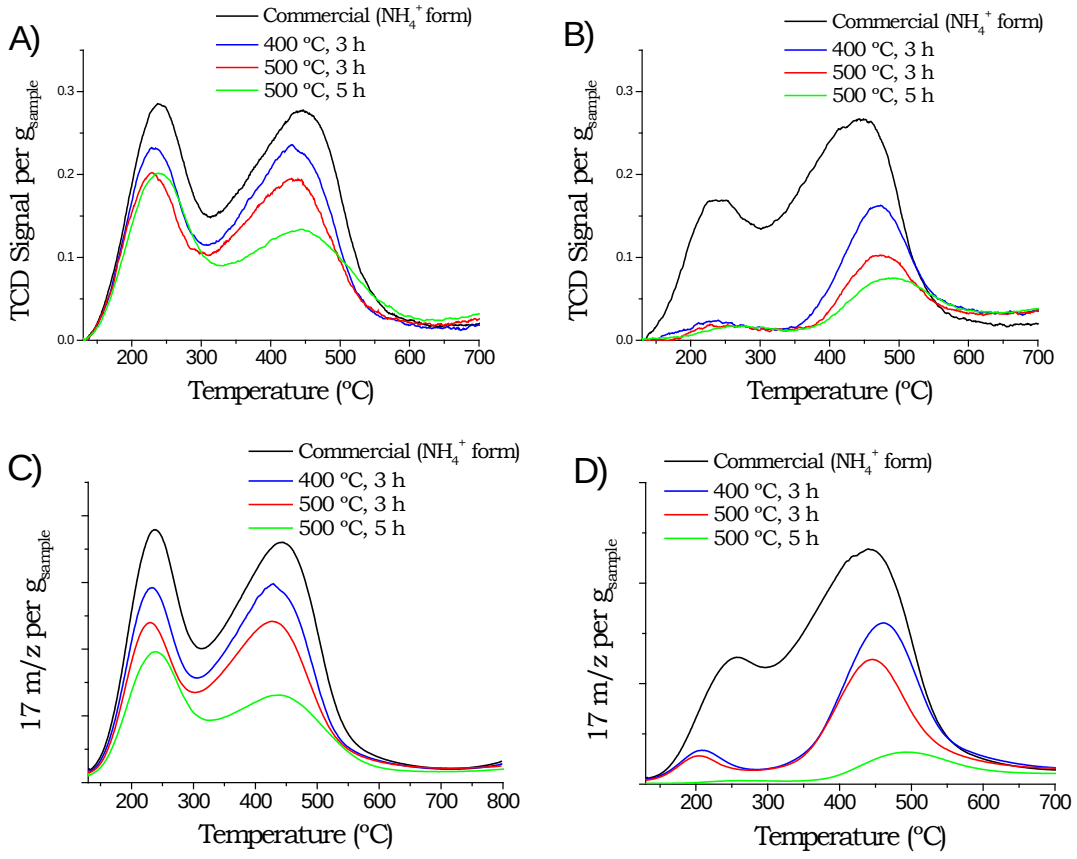

Figure 3.33. NH_3-TPD analysis monitored by A) TCD Signal and C) MS 17 m/z signal of zeolite samples with different thermal treatment. And blank analysis without preliminary ammonia saturation monitored by B) TCD Signal and D) MS 17 m/z signal of zeolite samples with different thermal treatment.

Surprisingly, the commercial zeolite in NH_4^+-form presented the highest apparent acidity. Ammonium form zeolites are thermally treated to decompose the ammonium cation, which is presented in the zeolite vacancies, obtaining the proton form, and consequently, an acid solid [53,54]. Therefore, the results obtained in NH_3-TPD analysis do not make sense because the proton form should be the most acid form [53-56].

To check if the ammonia detected corresponded to the adsorbed in the saturation of the sample, or if it was from the sample itself, samples were tested without preliminary ammonia saturation, which was referred to as blank analysis

(*Figures 3.33B and D*). In this analysis, only He flow was passed through the sample with the same temperature programme as NH_3-TPD. These results showed that the amount of ammonia remaining in the zeolite is significant and decreases with the calcination temperature. Therefore, the acidity results of these samples measured by NH_3-TPD should be analyzed with caution to avoid erroneous conclusions.

Thus, an estimation of the acid density was obtained by the difference between the NH_3-TPD and blank analysis *(Table 3.9 and Appendix A.2.2.*). The results showed low acidity of the commercial zeolite without thermal treatment (NH_4^+ form) and similar acidity of the other samples.

Table 3.9. Acidity estimation of zeolite with different thermal treatment

Sample	Thermal treatment	mmol NH_3/g sample		
		NH_3-TPD	Blank	Difference
ZSM-5	-	2.15	1.82	0.33
	400 ºC, 3h	1.72	0.54	1.18
	500 ºC, 3h	1.42	0.28	1.14
	500 ºC, 5h	1.24	0.19	1.05

When the zeolite in different zeolite form (NH_4^+ or H^+ form) was dispersed in aqueous media (slurry), TPD curves showed some differences (*Figure 3.34*). ZSM-5_11.8%SiO_2 samples (suspended in ammonium form) showed higher desorbed ammonia signal than HZSM-5_11.8%SiO_2 samples (suspended in proton form). This tendency was similar in TCD and 17 m/z signal (*Figure 3.35*). Nevertheless, as it was said before it must take into account the remaining ammonia in zeolite structure after calcination. Therefore, *Table 3.10* presents an estimate of the acidity, which was quantified with TCD by the difference of the NH_3-TPD and the blank analysis. They showed a slight lower acidity of the ZSM-5_11.8%SiO_2 calcined at 400 ºC than that of the other samples.

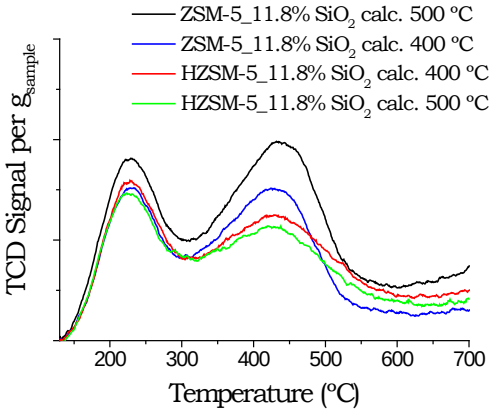

Figure 3.34. TCD signal of NH_3-TPD analysis of zeolites suspended in different forms (Ammonium or proton) and calcined at different temperatures.

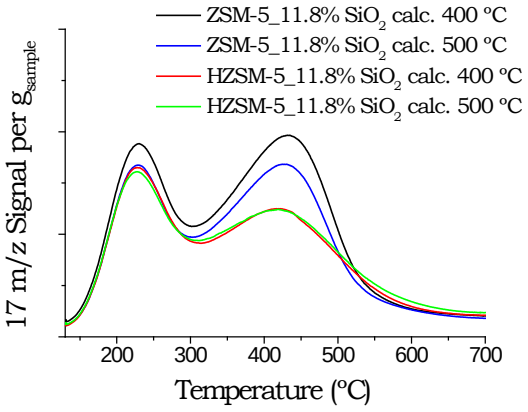

Figure 3.35. MS 17 m/z signal of NH_3-TPD analysis of zeolites suspended in different forms (Ammonium or proton) and calcined at different temperatures.

Table 3.10. Acidity of slurried zeolite samples

Sample	mmol NH_3/g zeolite		
	NH_3-TPD	**Blank**	**difference**
ZSM-5_11.8%SiO_2 400	1.34	0.54	0.80
ZSM-5_11.8%SiO_2 500	1.16	0.28	0.88
HZSM-5_11.8%SiO_2 400	1.06	0.19	0.87
HZSM-5_11.8%SiO_2 500	1.06	0.19	0.87

The effect on acidity of the different colloidal SiO_2 content calcined at 400 °C is presented *in Figure 3.36* and *Table 3.11*. The results showed a similar acidity for colloidal SiO_2 content lower than 11.8%. Nevertheless, for a colloidal SiO_2 content of 23.6% a decrease in acidity density was observed.

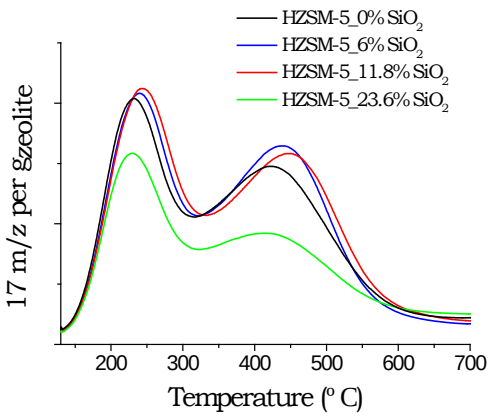

Figure 3.36. NH_3-TPD of slurried zeolite with different colloidal SiO_2 content

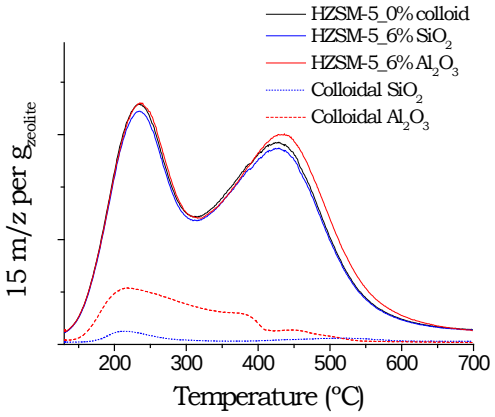

Figure 3.37. NH_3-TPD analysis of slurried zeolites with different colloids.

Table 3.11. Acidity of slurried zeolite with different colloidal SiO_2 content calcined at 400 ºC for 3 h. Data obtained after subtracting the blank test.

Sample	mmol NH_3/g zeolite
HZSM-5_0% colloid	0.88
HZSM-5_6% SiO_2	0.86
HZSM-5_11.8% SiO_2	0.87
HZSM-5_23.6% SiO_2	0.77

The addition of colloidal Al_2O_3 instead of colloidal SiO_2 was also studied. Results showed that despite the acidity presented by colloidal alumina or silica, the addition of colloidal Al_2O_3, like colloidal SiO_2, does not modify the overall acidity significantly (*Figure 3.37*).

- **Thermogravimetric analysis**

The effect of calcination temperature in the slurried zeolites was studied by TG analysis and results are presented in *Figure 3.38*.

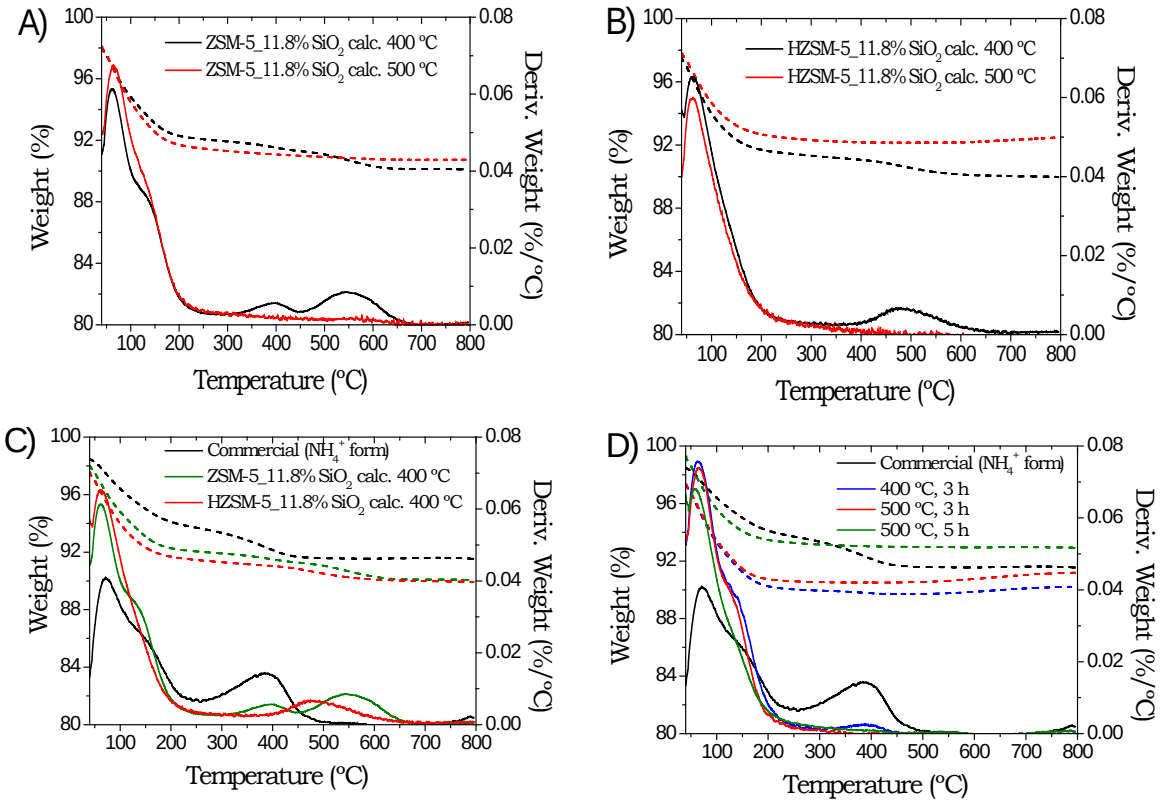

Figure 3.38. TG analysis of the slurried zeolites suspended: A) ammonium form, B) proton form and C) comparison of commercial zeolite and slurried ammonia and proton form. And D) TG analysis of commercial zeolite calcined at different temperatures. *Weight* is presented in dashed lines and *Deriv. Weight* is presented in solid lines.

The results showed that samples calcined at 500 ºC did not present weight-loss from 200 to 800 ºC (*Figure 3.39*). However, when the slurried catalysts were calcined at 400 ºC, samples showed a weight-loss. ZSM-5_11.8%SiO_2 (*Figure 3.39A*) included two peaks of weight-loss at 400 and 500 ºC approximately. However, HZSM-5_11.8%SiO_2 (*Figure 3.39B*) presented only one weight-loss peak at 500 ºC. Furthermore, the commercial zeolite showed a weight-loss at 400 ºC when it is in her ammonium form (*Figure 3.39D*), which could be connected to the remaining ammonia in the zeolite structure as it was shown in NH_3-TPD. This weight-loss decreases with calcination treatment (*Figure 3.39D*) and a weight-loss is still appreciable when the zeolite is calcined at 400 ºC for 3 h.

- **Activity Test**

After characterising, the activity for methanol dehydration was measured in a fixed bed reactor at 260 ºC and atmospheric pressure.

Different zeolite calcination temperatures were studied to obtain their proton form (H-form). In *Table 3.12*, it can be observed that the ZSM-5 zeolite presented similar activity when it is calcined at 500 ºC for 3 or 5 h, around 46% of methanol conversion. However, when the zeolite was calcined at 400 ºC, a decrease in methanol conversion was observed. All the samples showed DME selectivity near to 100%.

Table 3.12. Methanol conversion of zeolites subjected to different heat treatments.

	Calcination Treatment	X MeOH (%)
ZSM-5 (parent)	400 ºC, 3h	41.5
	500 ºC, 3h	45.9
	500 ºC, 5h	45.9

The slurried zeolites were also tested in a fixed bed reactor and the results are presented in *Figure 3.39*. When the slurry was prepared with the zeolite in its proton form (HZSM-5), similar methanol conversion to the commercial zeolite was observed. However, when the slurry was made with the ammonium form zeolite (ZSM-5) and then calcined at 400 °C, a decrease in methanol conversion was observed. Nevertheless, when it is calcined to 500 °C the methanol conversion is similar to the commercial zeolite (parent).

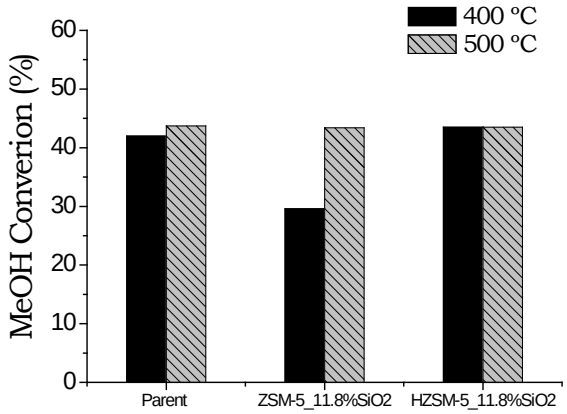

Figure 3.39. Methanol conversion of commercial zeolite (parent) and slurried catalysts (ZSM-5 and HZSM-5_11.8%SiO_2) at different calcination temperature. Reaction conditions: atmospheric pressure and 600 L/$g_{zeolite}$·h

The effect of the colloidal SiO_2 content was also studied in the methanol dehydration reaction (*Figure 3.40*). Results showed a decrease in the methanol conversion as the colloidal SiO_2 content increased. In all samples, the selectivity to DME was near 100%.

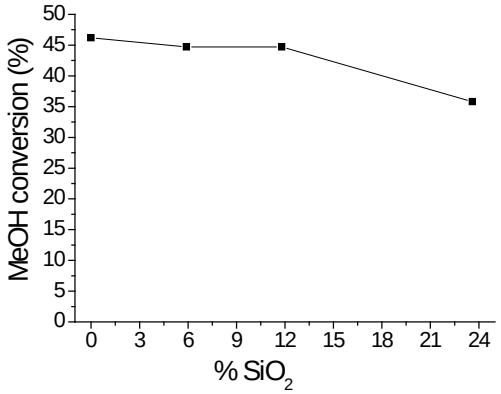

Figure 3.40. Methanol conversion of slurried zeolite with different colloidal SiO_2 content.

Finally, knowing the good performances of colloidal Al_2O_3 leading to adherent layers of the CZA catalyst (*see section 3.2.2*), the effect of changing the additive from SiO_2 to Al_2O_3 was studied. The results showed similar activity to the parent catalyst with the use of both colloids (*Table 3.13*).

Table 3.13. Effect of the nature of the colloid in methanol conversion and adherence. Reaction conditions: Atmospheric pressure and 600 L/$g_{zeolite}$·h

Sample	Colloid	Colloid content (%)	X MeOH
HZSM-5_0%colloid	-	0	46.2
HZSM-5_6% SiO_2	SiO_2	6	44.7
HZSM-5_6% Al_2O_3	Al_2O_3	6	45.1

3.3.1.2. Coating process

The particle properties of the dehydration catalyst for slurry preparation such as zeta potential and particle size were measured in aqueous media.

- **Zeta potential**

The zeta potential of HZSM-5, colloids and slurries at different pH are presented in *Figure 3.41*. Results showed negative zeta potential for the HZSM-5 zeolite and the colloidal SiO_2 with values higher than /-20 mV/ in all the studied range (*Figure 3.41A*). However, the colloidal Al_2O_3 presented positive charges at pH lower than 8.5 and negative charges at higher values (*Figure 3.41B*).

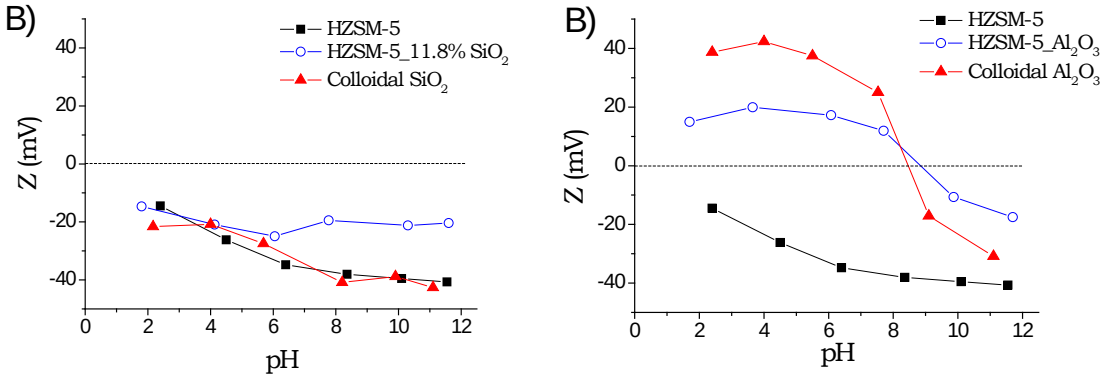

Figure 3.41. Zeta potential at different pH of a) commercial zeolite HZSM-5 and colloids employed, as well as of prepared slurries with these colloids b) SiO_2 and c) Al_2O_3

The zeta potential of the zeolite slurries with different colloids (*Table 3.7*) were also analysed (*Figure 3.41*). The use of colloidal SiO_2 with zeolite showed similar zeta potential to the individual compounds (*Figure 3.41A*). However, when the colloidal Al_2O_3 is added to the zeolite slurry, the zeta potential of the slurry is closer to the colloidal Al_2O_3 than to the zeolite (*Figure 3.41B*). This can be attributed to the fact that small colloidal particles of Al_2O_3 are surrounding the zeolite particles.

In *Table 3.7* pH values of different slurry formulation are shown. All of them presented pH values with high zeta potential, which is suitable for suspension stability. Therefore, the slurries pH was not modified trying to avoid changes in the catalyst acidity.

- **Particle size distribution**

The particle size distribution in aqueous media was measured by light scattering (*Figure 3.42)*. Results showed a particle size average D [4,3] of 4.8 µm and 90 % of the particles, d(0.9), are lower than 7.8 µm. Therefore, the zeolite did not required milling because the particle size is adequate for stable slurry preparation [5,6,11].

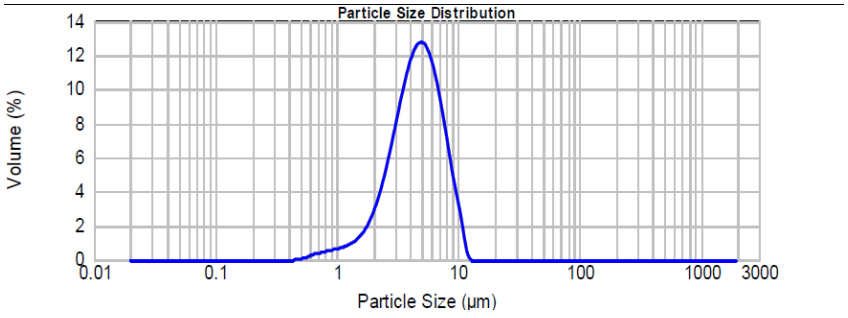

Figure 3.42. Particle size distribution in aqueous media.

- **Viscosity**

The viscosity measured at a share rate of 1000 s^{-1} is presented in *Table 3.14*. All the slurries presented a solid content of 35% (*Table 3.7*). The different formulation exhibited different viscosity as a function of the form of the zeolite (ammonium or proton form) and the colloid used (SiO_2 or Al_2O_3) (*Table 3.14*). The

ammonium form presented lower viscosity than proton form. Moreover, the use of colloidal Al_2O_3 instead of colloidal SiO_2 increased the viscosity.

Table 3.14. Coating properties of different slurry formulation of zeolite.

Sample	Viscosity (mPa·s)	Calc. temp. (ºC)	Adherence (%)
HZSM-5_0%colloid	3.5	400	31
ZSM-5 _11.8%SiO_2	5.6	400	96
		500	96
HZSM-5_ 11.8%SiO_2	5.9	400	94
		500	98
HZSM-5_ 6%Al_2O_3	18.8	400	94

- **Washcoating process**

Metallic monoliths were coated with zeolite by washcoating. The amount of catalyst loaded as a function of the immersions was presented in *Figure 3.43*. Addition of colloidal Al_2O_3 required less number of immersions to obtain the same amount of catalyst loaded (*Figure 3.43*). Moreover, in line with the viscosity, the number of immersions increased when viscosity decreased. All the studied formulation showed homogeneous coatings without plugging channel (*Figure 3.44*).

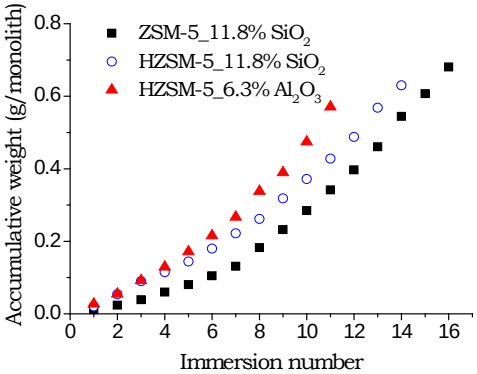

Figure 3.43. Graph of coated amount per immersion

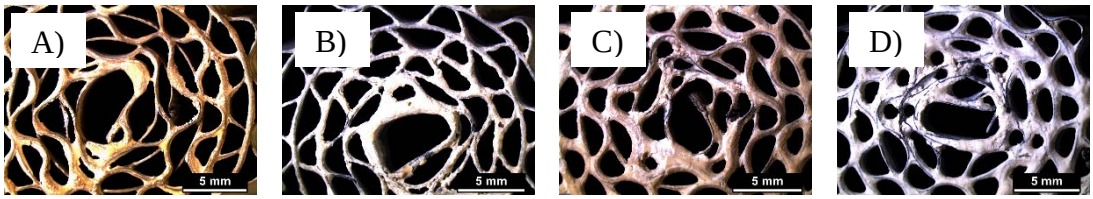

Figure 3.44. Images of coated monoliths of Fecralloy® with ZSM-5_11.8%SiO_2 calcined at a) 400 ºC and b) 500ºC and HZSM-5_11.8%SiO_2 calcined at c) 400 ºC and d) 500 ºC

- **Adherence Test**

The adherence test of the zeolite coatings was tested by sonication method and results are presented in *Table 3.14*. All the formulation showed excellent adherence above 90% as it was expected from a previous research [52], whereas the slurry without the addition of inorganic oxide colloid had a poor adherence (31%).

3.3.1.3. Structured catalyst

Taking into account the above-mentioned results, the zeolite in proton form with colloidal Al_2O_3 was chosen for the structured catalyst preparation.

The N_2 adsorption was used to measure the textural properties of the structured catalyst. The adsorption-desorption isotherms are presented in *Figure 3.45* and the main textural parameters such as the BET surface area and the total pore volume are summarised in *Table 3.15*.

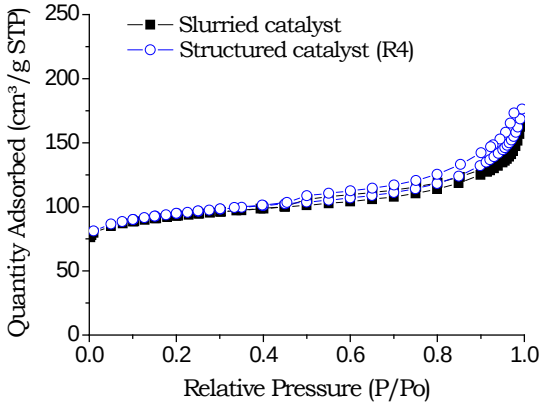

Figure 3.45. N_2 isotherm of slurried and structured catalyst (R4) of HZSM-5_6%Al_2O_3.

Table 3.15. Textural properties of slurried and structured catalyst HZSM-5_6%Al_2O_3

Sample	Physical form	S. BET (m^2/g)	Total pore volumen (cm^3/g)	Micropore volumen (cm^3/g)
HZSM-5_6%Al_2O_3	Slurried	351	0.29	0.13
	Structured (R4)	358	0.29	0.13

The results showed similar textural properties to the slurried catalyst when the zeolite is coated in the metallic substrate and the isotherms showed a type I isotherm, which confirms that the microporous character of the parent zeolite is preserved after structuration.

3.3.2. Discussion

In the structured catalyst preparation, a final calcination is needed to obtain compact layers of the catalysts and to improve the adherence to the structured substrate [12]. Hence, catalysts must be thermally treated twice if the slurry is prepared with the catalyst pre-formed.

In this way, the zeolite slurry could be prepared in its proton (thermaly pretreated) or ammonium form (without thermal pretreatment). If the slurried catalysts (in proton HZSM-5_11.8%SiO_2, or ammonium form ZSM-5_11.8%SiO_2)

are calcined at 500 ºC, both samples have similar methanol dehydration behaviour to the parent catalyst (*Figure 3.39*). However, in the following chapters, the zeolite was mixed with CZA catalyst for direct synthesis of DME. Therefore, trying to avoid possible Cu sintering of CZA catalyst, a lower zeolite slurry calcination temperature was also studied (400 ºC). At this temperature HZSM-5_11.8%SiO_2 sample exhibited higher dehydration capacity than ZSM-5_11.8%SiO_2. Moreover, the latter also presented lower surface area (*Table 3.8*) and an additional peak of weight-loss was shown by TG analysis related to remaining ammonia in the zeolite structure (*Figure 3.38C*).

The remaining ammonia was also detected in the TG analysis of commercial zeolite calcined at 400 ºC for 3h (*Figure 3.38D*) as well as in NH_3-TPD analysis (*Figure 3.33*). Moreover, lower methanol dehydration was also observed than in samples calcined at 500 ºC (*Table 3.12*). Nevertheless, the methanol conversion obtained with the slurried zeolite (ZSM-5_11.8%SiO_2) was lower than with the commercial zeolite. By TG analysis it was observed that the PVA of the slurried catalysts was not removed until 500 ºC (*Figure 3.21A*) being observed the weight-loss in both samples calcined at 400 ºC (Figure 3.38). Furthermore, the sample ZSM-5_11.8%SiO_2 presented two peaks of weight-loss related to the ammonia and PVA. However, the peak intensity of ammonia is higher in the slurried catalysts than in the commercial ZSM-5 calcined at 400 ºC. Therefore, it seems that remains of PVA in the slurried zeolite calcined at 400 ºC may produce a type of impediment, which could hinder the change of zeolite from NH_4^+ to H-type.

Trying to understand the behaviour of the structuration of zeolites with inorganic oxide colloid, the colloidal SiO_2 content was also studied. The results for methanol dehydration showed a decrease in methanol conversion with the colloidal SiO_2 content. Moreover, NH_3-TPD analysis showed a decrease in the acidity when large amount of this colloid was used. Just as it was said that inorganic oxide colloids could cover metallic phase of the catalyst [12,18,57], the excessive used of colloid could also probably cover acid sites of the parent zeolite. Therefore, the acidity of the catalyst and methanol dehydration to DME activity decreases.

Finally, the addition of colloidal Al_2O_3 instead of silica showed similar methanol conversion (*Table 3.13*). The NH_3-TPD analysis showed that the small content of these colloids (6%) does not affect the overall acidity of the final catalyst (*Figure 3.37*).

3.3.3. Conclusion

Zeolite slurries can achieve good adherence and activity. However, the form of the zeolite and the final calcination temperature are essential for attaining the methanol conversion of the parent zeolite.

- The PVA used as additive in the slurry seems to produce a type of impediment when low calcination temperatures is used, and higher temperature (above 500 ºC) is necessary to obtain H-form zeolite. Therefore, it was shown the necessity to prepare slurries with the zeolite in proton form or to calcine it above 500 ºC.
- High colloidal SiO_2 content could deactivate the acid catalyst. Colloid content higher than 11.8% produced a decrease in methanol conversion probably due to a coverage of the zeolite acid sites by the colloid.
- Colloidal Al_2O_3 is also a suitable colloid to use for structuring zeolites. There is no difference in activity between the use of low content colloidal SiO_2 or Al_2O_3.

3.4. References

[1] A. Montebelli, C.G. Visconti, G. Groppi, E. Tronconi, C. Cristiana, C. Ferreira, S. Kohler, *Catalysis Science & Technology*, 4 (2014) 2846-2870.

[2] V. Meille. *Applied Catalysis A: General*, 315 (2006) 1-17.

[3] P. Ávila, M. Montes, E. E. Miró. *Chemical Engineering Journal,* 109 (2005) 11-36.

[4] O. Sanz, F.J. Echave, F. Romero-Sarria, J.A. Odriozola, M.Montes. *Renewable Hydrogen Technologies Production, Purification, Storage, Applications and Safety*. Chapter 9 (2013) 201-224.

[5] C. Agrafiotis, A. Tsetsekou. *Journal of materials science*, 35 (2000) 951-960.

[6] O.H. Laguna, M.I. Domínguez, M.A. Centeno, J.A. Odriozola. *New Material for Catalytic Applications* (2016) 81-120.

[7] S. Vallar, D. Houivet, J. El Fallah, D. Kervadec, J.-M. Haussonne. *Journal of European Ceramic Society*, 19 (1999) 1017-1021.

[8] F.J. Echave, O. Sanz, M. Montes. *Applied Catalysis A: General*, 474 (2014) 159-167

[9] J.M. Zamaro, M. A. Ulla, E.E. Miró. *Catalysis Today*, 107-108 (2005) 86-93.

[10] O. Sanz, L.C. Almeida, J.M. Zamaro, M.A. Ulla, E.E. Miró, M. Montes. *Applied Catalysis B: Environmental*, 78 (2008) 166-175.

[11] J.R. González-Velasco, M.A. Gutierrez-Ortiz, J.L. Marc, J.A. Botas, M.P. González-Marcos, G. Blanchard. *Industrial & Engineering Chemistry Research*, 42 (2003) 311-317.

[12] T.A. Nijhuis, A.E. W. Beers, T. Vergunst, I. Hoek, F. Kapteijn, J.A. Moulijn *Preparation of monolithic catalysts, Catalysis Reviews*, 43:4 (2001) 345-380.

[13] X. Xu, J.A. Moulijn, Studies in surface science and catalysis 118 (1998) 845-854.

[14] A. Montebelli, C.G. Visconti, G.Groppi, E. Tronconi, S. Kohler, H.J. Venvik, R. Myrstad. *Applied Catalysis A: General,* 481 (2014) 96-103.

[15] G. Germani, A. Stefanescu, Y. Schuurman, A.C. van Veen. *Chemical Engineering Science,* 62 (2007) 5084-5091.

[16] N. R. Peela, A. Mubayi, D. Kunzru. *Catalysis Today,* 147S (2009) S17-S23.

[17] L.C. Almeida, F.J. Echave, O. Sanz, M.A. Centeno, G. Arzamendi, L.M. Gandía, E.F. Sousa-Aguiar, J.A. Odriozola, M. Montes. *Chemical Engineering Journal*, 167 (2011) 2-3.

[18] F.J. Echave, O. Sanz, I. Velasco, J.A. Odriozola, M. Montes. *Catalysis Today,* 213 (2013) 145-154.

[19] L. Lisi, R. Pirone, G. Russo, V. Stanzione. *Chemical Engineering Journal,* 154 (2009) 341-347.

[20] A.K. Mogalicherla, D. Kunzru. The *Canadian Journal of Chemical Engineering*, 88 (2010) 367-375.

[21] Juan M. Zamaro, Maria A. Ulla, Eduardo E. Miró. *Chemical Engineering Journal,* 106 (2005) 25-33.

[22] P.S. Dhillon, M.P. Harold, D. Wang, A. Kumar, S.Y. Joshi. *Chemical Engineering Journal*. https://doi.org/10.1016/j.cej.2018.08.120.

[23] M.A. Ashraf, O. Sanz, C. Italiano, A. Vita, M. Montes, S. Specchia. *Chemical Engineering Journal*, 334 (2018) 1792-1807.

[24] H. Pérez, P. Navarro, M. Montes. *Chemical Engineering Journal*, 158 (2010) 325-332

[25] V.G. Milt, S. Ivanova, O Sanz, M.I. Dominguez, A. Corrales, J.A. Odriozola, M.A. Centeno. *Applied Surface Science*, 270 (2013) 169-177.

[26] S. Sato, M. Kuroki, T. Sodesawa, F. Nozaki, G.E. Maciel. *Journal of Molecular Catalysis A: Chemical*, 104 (1995) 171-177.

[27] F.M. Bautista, J.M. Campelo, A. García, D. LunaJ.M. Marinas, M.C. Moreno, A.A. Romero. *Applied Catalysis A: General*, 170 (1998)159-168.

[28] R. I. Samoilova, S.A. Dikanov, A.V. Fionov, A.M. Tyryshkin, E.V. Lunina, M.K. Bowman. *Journal of Physical Chemistry,* 100 (1996) 17621-17629.

[29] F. J. Echave Lozano. *Tesis doctoral 2011*. Universidad del País Vasco.

[30] B.J. Hathaway, A.A.G. Tomlinson. *Coordination Chemestry Reviews,* 5 (1970) 1-43.

[31] J.W. Bae, S-H. Kang, Y-J. Lee, K-W. Jun. *Journal of Industrial and Engineering Chemistry*, 15 (2009) 566-572.

[32] I. Sierra, J. Ereña, A.T. Aguayo, J.M. Arandes, J. Bilbao. *Applied Catalysis B: Environmental,* 94 (2010) 108-116.

[33] R. Peláez, E. Bryce, P. Marín, S. Ordóñez. *Fuel Processing Technology,* 179 (2018) 378-386.

[34] A. Ateka, P. Pérez-Uriarte, I. Sierra, J. Ereña, J. Bilbao, A.T. Aguayo. *Reaction Kinetics, Mechanisms and Catalysis*, 119 (2016) 655-670.

[35] A. Galarneau, A. Sachse, B. Said, C-H. Pelisson, P. Boscaro, N. Brun, L. Courtheoux, N. Olivi-Tran, B. Coasne, F. Fajula. *Comptes Rendus Chimie,* 19 (2016) 231-247.

[36] S.S. Akarmazyan, P. Panagiotopoulou, A. Kambolis, C. Papadopoulou, D. Kondarides. *Applied Catalysis B: Environmental,* 145 (2014) 136-148.

[37] A. Bakhtyari, M.R. Rahimpour. *Methanol Science and Engineering* (2018) 281-311. ISBN: 978-0-444-63903-5 (Elsevier).

[38] K. Saravanan, H. Ham, N. Tsubaki, J.W. Bae. *Applied catalysis B: Environmental*, 217 (2017) 494-522.

[39] F. Hayer, H. Bakhtiary-Davijany, R. Myrstad, A. Holmen, P. Pfeifer, H.J. Venvik. *Chemical Engineering and Processing,* 70 (2013 77-85.

[40] F. Song, Y. Tan, H. Xie, Q. Zhang, Y. Han. *Fuel Processing Technology,* 126 (2014) 88-94.

[41] Z. Li, J. Li, M. Dai, Y. Liu, D. Han, J. Wu. *Fuel*, 121 (2014) 173-177.

[42] Y. Suwannapichat, T. Numpilai, N. Chanlek, K. Faungnawakij, M. Chareonpanich, J. Limtrakul, T. Witoon. *Energy Conversion and Management*, 159 (2018) 20-29.

[43] C. Arcoumanis, C. Bae, R. Crookes, E. Kinoshita. *Fuel,* 87 (2008) 1014-1030.

[44] T. A. Semelsberger, R. L. Borup, H. L. Greene. *Journal of Power Sources,* 156 (2006) 497-511.

[45] T. Matsuhisa, in *Catalysis: Volume 12* James J. Spivey (Ed.), UK, The Royal Society of Chemistry, 1996.

[46] R. Burch, S.E. Golunski, M.S. Spencer, *Journal of Chemical Society Faraday Transactions*, 86 (1990) 2683-2691.

[47] Y. Kanai, T. Watanabe, T. Fujitani, T, Uchijima, J. Nakamura, *Catalysis Letters*, 38 (1996) 157-163.

[48] A. A. Tsyganenko, E. N. Storozheva, O.V. Manoilova, T. Lesage, M. Daturi, J.C. Lavalley. *Catalysis Letters*, 70 (2000) 159-163.

[49] Lloyd R. Chapman, Powell, Tenn (1982) *U.S. Patent No. 4,318,828.*

[50] J.F. Sánchez M, O.J. González Bello, M. Montes, G.M. Tonetto, D.E. Damiani. *Catalysis Communications*, 10 (2009) 1446-1449.

[51] X.K. Phan, H. Bakhtiary-Davijany, R. Myrstad, P. Pfeifer, H.J. Venvik, A. Holmen. *Applied Catalysis A: General,* 405 (2011) 1-7.

[52] A. Eleta López. *Tesis doctoral 2008*. Universidad del País Vasco.

[53] E.G. Derouane, J.C. Védrine, R. Ramos Pinto, P.P. Borges, L. Costa, M.A.N.D.A. Lemos, F. Lemos, F. Ramôa Ribeiro. Catalysis Reviews: Science and Engineering 55 (2013) 454-515.

[54] J.J. Spivey. Chemical Engineering Communictaions 110 (1991) 123-142.

[55] A. Corma. *ARBOR Ciencia, pensamiento y cultura CLXXXVII EXTRA (*2011) 83-102.

[56] H. Mochizuki, T. Yokoi, H. Imai, R. Watanabe, S. Namba, J.N. Kondo, T. Tatsumi. Microporous and mesoporous materials 145 (2011) 165-171.

[57] A. Galarneau, A. Sachse, B. Said, C-H. Pelisson, P. Boscaro, N. Brun, L. Courtheoux, N. Olivi-Tran, B. Coasne, F. Fajula. *Comptes Rendus Chimie,* 19 (2016) 231-247.

CHAPTER 4

Two-phase catalysts: Direct synthesis of DME

INDEX

4.1. Introduction

The direct synthesis of dimethyl ether (DME) consists of synthesising methanol from syngas and dehydrate the methanol as it is formed, in the same reactor. Due to the consumption of the methanol, which is being dehydrated to DME, the thermodynamic equilibrium limitation of the methanol synthesis is removed and higher conversion of syngas is achieved [1-3]. Therefore, it will be necessary to be presented two catalytic phases, active for each of the reactions. Hence, the proximity of both active phases should play a crucial role in the reaction yield and 'a priori' the close proximity between phases must improve the catalyst performance [4-7].

Nevertheless, it has been reported that an excessive contact between both phases may create detrimental interactions and deactivate the catalyst [5,8,9]. The two phases mixing method may lead to a better or worse contact between phases, and consequently, to different interaction between them. A. García-Trenco *et al.* [5] observed that the activity decreases after increasing the phases contact by different mixing methods of the methanol synthesis catalysts (CZA) and the acid catalyst (ZSM-5). They concluded that the intimate contact between catalysts may produce interactions such as partial blockage of micropores or inter-cationic exchange of Cu^{2+}. Moreover, G. Bonura *et al.* [8] mentioned that in mechanical or grinding mixture, the mechanical stress favours the redistribution of the metal copper in the zeolite. Probably, this is why the physical mixture is one of the most employed way of mixing both catalysts, trying to avoid detrimental interactions [10-13]. On the contrary, there was discrepancies with other authors that showed better performances in the direct synthesis of DME by mixing dried a methanol synthesis catalyst and a solid acid in aqueous media, concluding that is the best preparation method to allow good contact between phases [4,6,14-16].

In principle, it seems that a slurried mixture of both catalysts would be an easy way to prepare structured catalysts with both phases. As the two phases are mixed in the same slurry, only one suspension would be required to coat the two catalysts on the structured substrate. However, as showed in the previous chapter (*Chapter 3*), it must be taken into consideration that to obtain homogeneous and adherent coatings different additives are required, in particular inorganic oxide colloids to improve the adherence of the catalyst layer on the substrate *(Figure 3.18*). Nevertheless, the use of these additives could also alter catalytic properties of the parent catalyst such as activity, selectivity and stability [17, 23].

In this chapter, the contact between both catalysts was studied using different bed architectures (sub-beds of different composition or uniform bed) and different mixing methods (physical or slurried mixtures). Finally, with the best contact mode, the effect of additives in the catalyst mixture slurry was also studied.

4.2. Results

4.2.1. Contact between CZA and HZSM-5 catalysts

The contact between both active phases was studied with different location of them in the catalytic bed by employing always the usual mass ratio CZA/HZSM-5 of 2, which is cited in bibliography as the appropriate ratio [24]. In *Figure 4.1* there is a diagram of the different studied architectures.

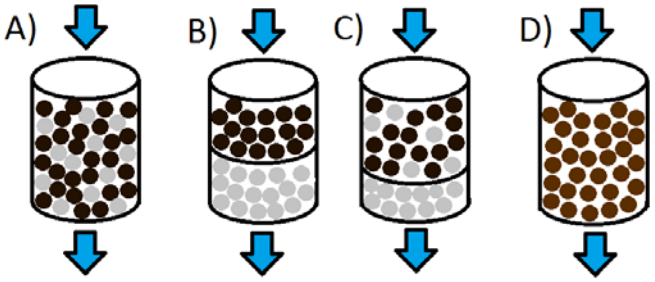

Figure 4.1. Scheme of different bed architectures studied. The CZA catalyst in dark brown, the HZSM-5 zeolite in grey and the slurried mixture of both catalysts in light brown.

The preparation method of these configurations are:

A) Physical mixture of the catalysts: the CZA catalyst and the HZSM-5 were pressed and sieved separately (300-500 μm), and then, mixed with spatula. This sample was called as C-Z_A.

B) Two separate beds of catalyst: the CZA catalyst and the HZSM-5 were pressed and sieved separately and located in two successive beds (300-500 μm), contacting the feed first with the CZA and then with the zeolite. It was called as C-Z_B.

C) Physical mixture of both phases with a thin layer of zeolite at the exit: a half of the zeolite was mixed mechanically with the CZA catalyst (both catalyst pressed and sieved separately to 300-500 μm) followed by the rest of the zeolite at the exit of the bed. It was called as C-Z_C.

D) Slurried catalysts mixture: the CZA catalyst and the HZSM-5 zeolite were dispersed in water, dried and calcined (without slurry additives). Then, the powder was pressed and sieved to 300-500 μm. This sample was called as C-Z_D.

- **Textural Properties**

The textural properties of the CZA catalyst, the HZSM-5 zeolite and the physical (C-Z_A) and slurried catalysts mixture of both (C-Z_C) (2:1 ratio of CZA:HZSM-5) were analysed by N_2 adsorption (*Figure 4.2*). Results showed a type IV isotherm for the CZA catalyst and type I for the ZSM-5 zeolite. Whereas, the physical mixture (C-Z_A) and the slurried mixture (C-Z_D) presented an intermediate behaviour between type I and IV. The BET surface area and the total pore volume are calculated from the isotherms and summarised in *Table 4.1*.

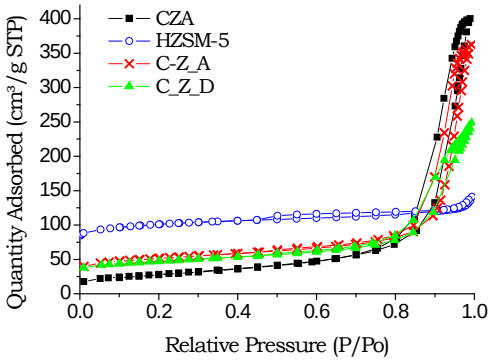

Figure 4.2. N_2-Isotherm of catalysts for direct synthesis of DME.

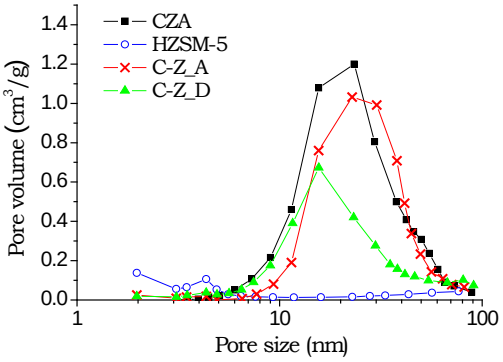

Figure 4.3. Pore size distribution of catalysts for direct synthesis of DME.

Table 4.1. Physicochemical properties of catalysts for direct synthesis of DME.

Sample	BET surface area (m^2/g)	Total pore volume (cm^3/g)	Equiv. pore size (nm)	CuO crystal size (nm)*	Cu surface area (m^2/g_{CZA})	TPR H_2 consumption (cm^3/g_{CZA})	TPR Reducibility (%)
CZA	100	0.62	24.5	3.8	35.9	168.6	100
HZSM-5	384	0.22	2.3	-	-	-	-
C-Z_A	186	0.53	12.0	3.8	34.8	174.6	103
C-Z _D	172	0.38	8.9	4.0	33.9	167.5	99.3

* Measured by XRD

The physical mixture showed a little bit higher BET surface area than the slurried catalysts mixture. Moreover, the pore size distribution of mixtures is similar to the CZA catalyst (*Figure 4.3*). Nevertheless, the slurried catalysts mixture exhibited lower total pore volume than the physical mixture, which presented a total pore volume closer to the CZA catalyst.

- **Crystallinity**

The crystallinity was studied by XRD analysis and diffractograms are shown in *Figure 4.4*. The physical (C-Z_A) and the slurried mixture (C-Z_D) showed peaks corresponding to both catalysts, CZA and HZSM-5. Furthermore, the CuO crystal size did not change when CZA catalyst is mixed in aqueous media with HZSM-5, and crystal size around 4 nm was estimated by Scherrer equation at 38.8 º (*Table 4.1*).

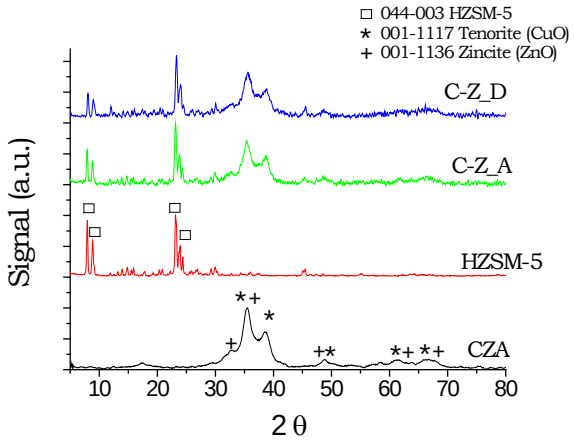

Figure 4.4. XRD results of catalysts for direct synthesis of DME.

- **Copper metallic surface area**

The Cu metal surface area was estimated by N_2O-RFC and the results are presented in *Table 4.1*. As it can be observed, the physical mixture (C-Z_A) and the slurried mixture (C-Z_D) presented similar Cu surface area to the CZA catalyst.

- **Reducibility**

The reducibility of the catalyst was measured by H_2-TPR. The results presented in *Figure 4.5* and *Table 4.1* showed that the physical mixture (C-Z_A) and the slurried mixture (C-Z_D) had similar reducibility to the CZA catalyst (*Table 4.1*). The maximum reduction peak is at around 230 °C in all cases (*Figure 4.5*).

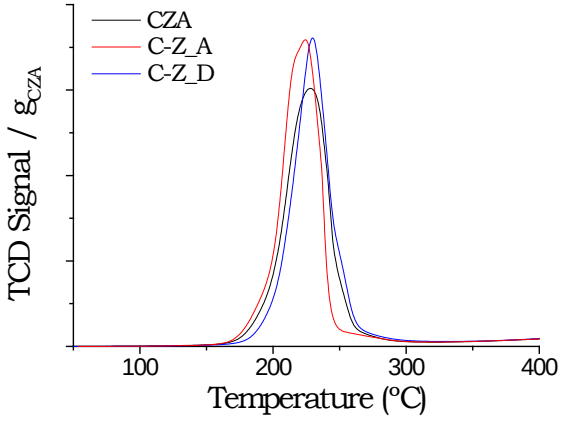

Figure 4.5. H_2-TPR analysis for catalyst for direct synthesis of DME

- **Acid strength**

The acidity of the samples was measured by NH_3-TPD. The results, which are monitored by mass spectrometer (*Figure 4.6*), showed low acidity of the CZA catalyst. In addition, the HZSM-5 zeolite presented two peaks of ammonia desorption at 250 and 450 °C approximately. However, when both catalysts are mixed together, the high temperature peak moves to lower temperatures (around

300-400 ºC). Furthermore, the physical (C-Z_A) mixture showed higher acidity than the slurried catalysts mixture (C-Z_D).

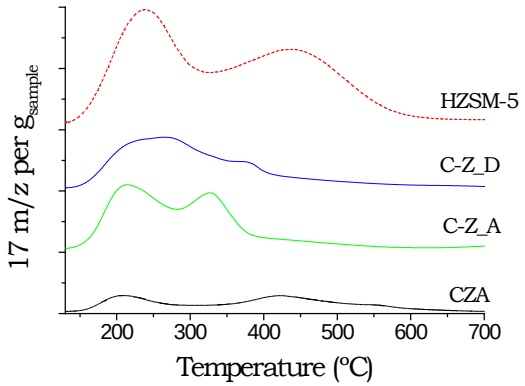

Figure 4.6. NH_3-TPD analysis for catalyst for direct synthesis of DME

- **Activity Test**

The activity test was carried out in a fixed bed reactor at 260 ºC and 40 bar with a space velocity of 2.55 L_{syn}/g_{CZA}·h. The results are shown in *Figure 4.7.*

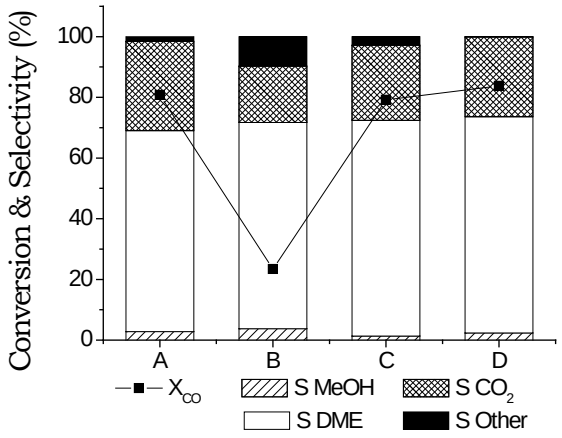

Figure 4.7. Activity test of the different bed architectures (*Figure 1*) for the direct synthesis of DME. Reaction conditions: 260 ºC, 40 bar and 2.55 L_{syn}/g_{CZA}·h with mass ratio of CZA/HZSM-5 of 2.

The results presented a low CO conversion of the two separated beds configuration (C-Z_B) (*Figure 4.7*). Whereas, other bed dispositions (C-Z_A, C and D) showed similar CO conversion around 80%. Nevertheless, changes in selectivities were observed.

The two separated phases (C-Z_B) depicted the highest selectivity to methanol and other compounds (light hydrocarbons) and the lowest CO_2 production (*Figure 4.7*). It was also observed that locating a physical mixture followed by a thin layer of zeolite (C-Z_C) instead of physical mixture in the whole catalytic bed (C-Z_A), allowed to decrease the selectivity of methanol from 2.8 to 1.4 %, but selectivity to by-products (S others) increased. However, the slurried mixture presented the highest selectivity to DME and the lowest selectivity to light hydrocarbons.

4.2.2. Study of additive incorporation to slurried mixture

As it was shown in *Chapter 3*, the preparation of structured catalysts by washcoating method uses additives such as inorganic oxide colloids to obtain homogeneous and adherent coatings. Therefore, in this section, a similar study has been done to deposit slurried catalysts mixture, C-Z_D. The effects of the nature of inorganic colloids (Al_2O_3, ZnO and SiO_2) and their content were studied. The samples were characterised after drying at 120 ºC (overnight) and calcining at 400 ºC (2 ºC/min) 3 h (slurried catalysts mixture).

The slurried catalysts mixtures with different colloids were referred to as C-Z followed with the colloid or colloids used and the percent of the colloid in the slurried catalyst (e.g. C-Z_23.3%ZnO+3.4%SiO_2).

4.2.2.1. Effect of colloid employed

Taking into account the results of the slurry formulations for the CZA catalyst and the HZSM-5 zeolite separately (*Chapter 3*), different slurry formulations were proposed to study (*Table 4.2*). All the formulation presented 20% of solid content and a mass ratio CZA/HZSM-5 of 2.

Table 4.2. Slurry formulations of mixtures of both catalysts

Sample	CZA (%)	HZSM-5 (%)	Colloid (%)			PVA (%)
			Al_2O_3	ZnO	SiO_2	
C-Z_D	12.7	6.4	0.0	0.0	0.0	0.9
C-Z_26.7%ZnO	9.3	4.7	0.0	5.3	0.0	0.7
C-Z_23.4%ZnO+3.4%SiO_2	9.3	4.7	0.0	4.6	0.7	0.7
C-Z_26.7%SiO_2	9.3	4.7	0.0	0.0	5.3	0.7
C-Z_11.7%Al_2O_3+3.6%SiO_2	10.8	5.4	2.4	0.0	0.7	0.7
C-Z_15.3%Al_2O_3	10.8	5.4	3.1	0.0	0.0	0.7

The slurries of catalysts mixtures were prepared by mixing two formulations (*see Chapter 2*):

1. Slurry formulation of the Cu/ZnO/Al_2O_3 catalyst (CZA) with the highest coating adherence:

    - For colloidal Al_2O_3: CZA_17.7%Al_2O_3
    - For colloidal ZnO: CZA_33.3%ZnO
    - For colloidal SiO_2: CZA_33.3%SiO_2

2. Slurry formulation of HZSM-5 zeolite (HZSM-5_11.8%SiO_2) with solid content of 20%.

4.2.2.1.1. Physicochemical properties

All the slurries were dried and calcined to obtain the powder (slurried catalysts mixture) and they were characterised by different methods. The physicochemical properties of the slurried catalysts mixtures are summarised in *Table 4.3*.

Table 4.3. Physicochemical properties of the slurried catalysts mixture for direct synthesis of DME

Sample	BET surface (m^2/g)	Total pore volume (cm^3/g)	Equiv. pore diameter (nm)	CuO size* (nm)	Cu surface area (m^2/g_{CZA})	TPR H_2 consump. (cm^3/g_{CZA})	TPR Reducibility (%)
C-Z_D	172	0.38	8.9	4.0	33.9	167.5	99
C-Z_26.7%ZnO	110	0.29	10.6	4.5	24.8	148.0	88
C-Z_23.4%ZnO+3.4%SiO_2	114	0.29	10.3	4.3	26.9	154.7	92
C-Z_26.7%SiO_2	138	0.39	11.2	4.3	24.7	157.3	93
C-Z_11.7%Al_2O_3+3.6%SiO_2	159	0.37	9.4	4.5	34.9	157.3	93
C-Z_15.3%Al_2O_3	160	0.43	10.8	4.4	32.6	161.9	96
Colloidal Al_2O_3	204	0.31	6.2	-	-	-	-
Colloidal ZnO	19	0.11	24.2	-	-	-	-
Colloidal SiO_2	114	0.22	7.6	-	-	-	-

*Measured by XRD

- **Textural Properties**

N_2 adsorption was used to measure textural properties of the slurried catalysts mixtures (*Figures 4.8-4.9 and Table 4.3*). The BET surface area decreased when colloids were included in the formulation and depended on the colloid employed in this order ZnO<SiO_2<Al_2O_3. This order was expected when analyzing the texture of the oxides obtained by drying and calcination of the colloids under the same conditions (*Table 4.3*). However, the pore size distribution did not show significant changes and a monomodal distribution was presented in all cases (*Figure 4.9*).

The colloidal ZnO presents a low BET surface area and total pore volume (*Table 4.3*). Therefore, the use of this colloid in the slurried catalysts mixture preparation produced much lower BET surface area and pore volume than the slurried catalysts mixture without colloids (C-Z_D) (*Figure 4.8 and Table 4.3*). Moreover, the addition of a small percentage of SiO_2 (C-Z_23.4%ZnO+3.4%SiO_2) to the slurried catalyst did not produce relevant changes.

When the colloidal SiO_2 and Al_2O_3 were used, it can be seen a similar pore size distribution to C-Z_D (*Figure 4.9*). However, the addition of colloidal Al_2O_3 in the slurried catalysts mixture produced samples with higher BET surface area than colloidal SiO_2 (*Table 4.3 and Figure 4.8*).

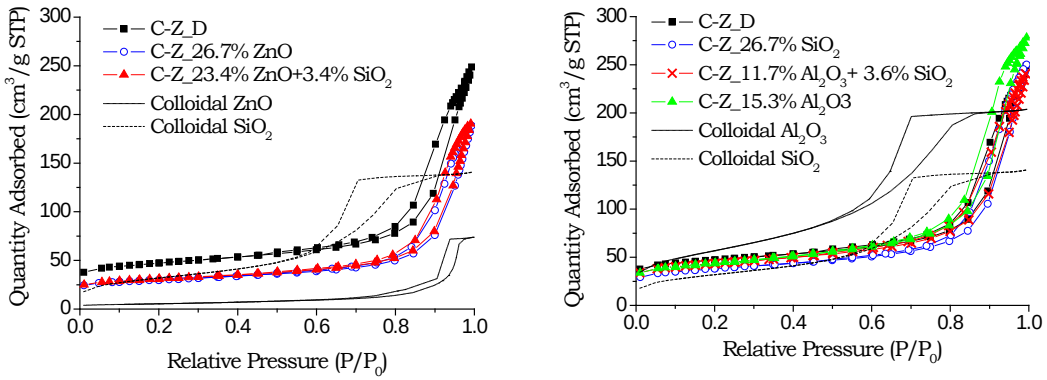

Figure 4.8. N_2 Adsorption-desorption isotherms of slurried catalysts with different colloids for the direct synthesis of DME.

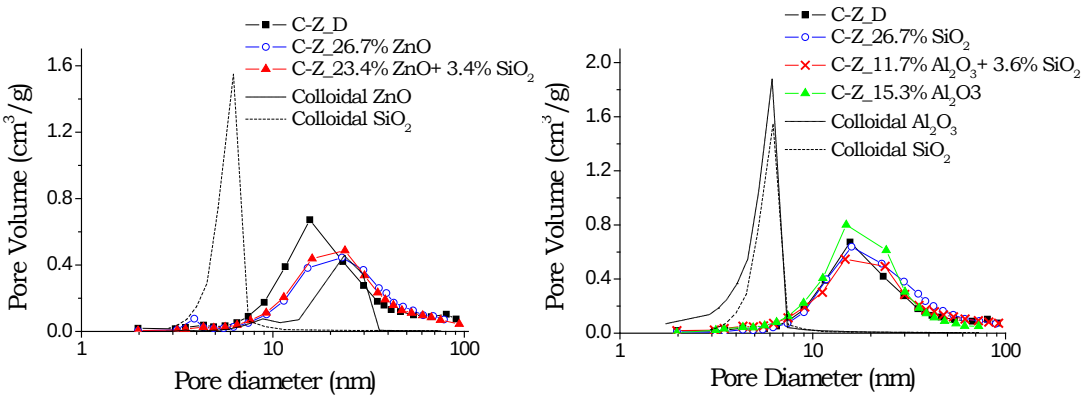

Figure 4.9. Pore size distribution of slurried catalyst with different colloids for the direct synthesis of DME.

- **Crystallinity**

The crystallinity of the samples was studied by XRD. The results showed the peak of CuO and ZnO of the CZA catalyst and the characteristic peaks of the ZSM-5 zeolite (*Figure 4.10*). Moreover, the ZnO peaks appeared when this colloid is used in the slurry. Nevertheless, the presence of Al_2O_3 or SiO_2 was not observed in the diffractograms when they are added in the slurry.

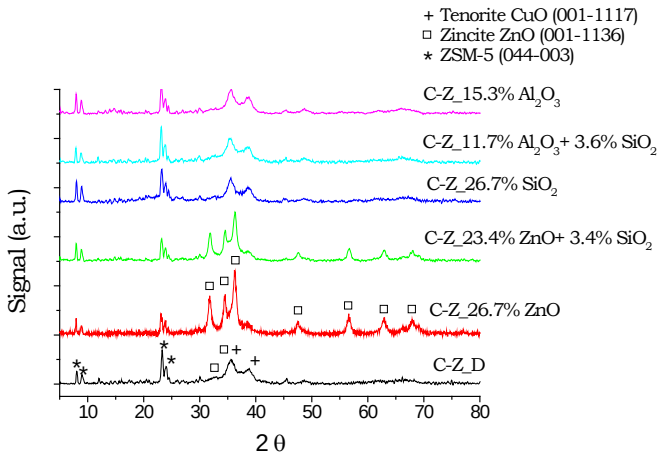

Figure 4.10. XRD of slurried catalysts with different inorganic oxide colloids

Scherrer equation was used to calculate the crystal size of CuO at 38.8 º (*Table 4.3*), and no relevant changes were observed when different colloids were used. Crystal size around 4.0-4.5 nm was estimated for all the samples.

- **Copper metal surface area**

The Cu metal surface area was estimated by N_2O-RFC and results are presented in *Table 4.3*. The results showed a decrease of the Cu surface area when ZnO and SiO_2 were used (*Table 4.3*). However, the addition of the colloidal Al_2O_3 to the slurry produced a Cu surface area close to the parent catalyst without colloids (C-Z_D).

- **Reducibility**

The reducibility of different slurried catalysts mixtures was measured by H_2-TPR (*Figure 4.11 and Table 4.3*). The results did not show relevant changes. All the samples presented a peak with a maximum reduction temperature around 230 °C (*Figure 4.11*). However, the H_2 consumption slightly change with the colloids used (*Table 4.3*). The addition of only ZnO (C-Z_26.7%ZnO) produced the highest decrease in reducibility. When ZnO is added with SiO_2 (C-Z_23.4%ZnO+3.4%SiO_2), the reducibility slightly increased. The addition of only SiO_2 (C-Z_26.7%SiO_2) or Al_2O_3+SiO_2 (C-Z_11.7%Al_2O_3+3.6%SiO_2) produced similar reducibilities, 93%. Using only colloidal Al_2O_3 (C-Z_15.3%Al_2O_3) produced

the highest reducibility (96%) and the closest to that of the slurried catalysts mixture without colloid (C-Z_D), around 99%.

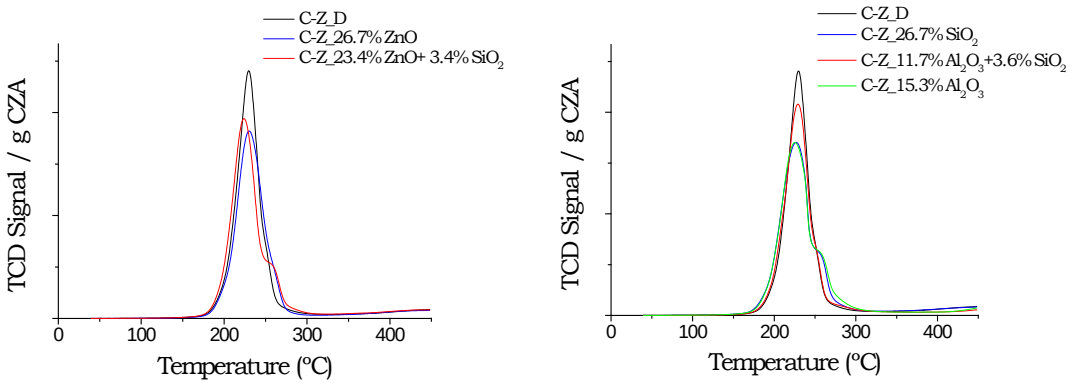

Figure 4.11. H_2-TPR analysis of slurried catalysts with different colloids for the direct synthesis of DME.

- **Acid strength**

The acidity of the slurried catalysts samples was measured by ammonia TPD analysis (*Figure 4.12*). The results showed that the addition of the colloids to the slurried catalysts mixture changes the acidity of the final catalyst. The use of ZnO produced a reduction of the acidity (*Figure 4.12A*). However, the addition of colloidal Al_2O_3 and SiO_2 did not affect in a greater extent the overall acidity of the samples (*Figure 4.12B*).

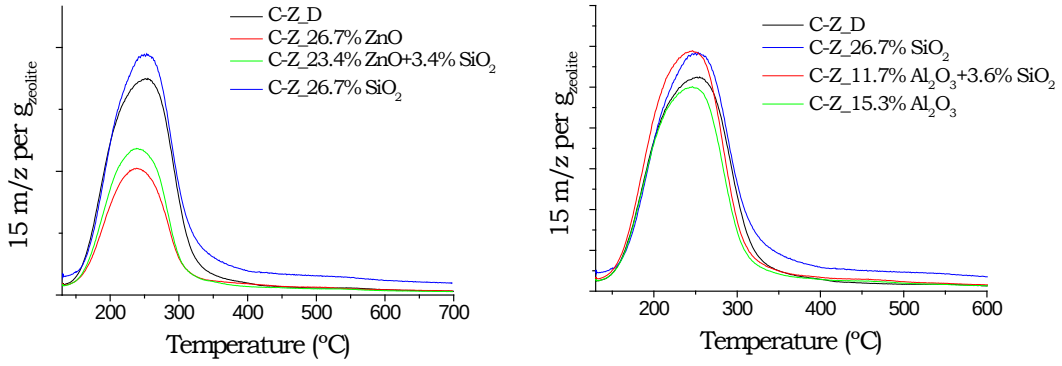

Figure 4.12. NH_3-TPD of the slurried direct synthesis of DME catalysts with different colloids

- **Activity Test**

The results of activity test of direct synthesis of DME in fixed bed rector at 260 ºC, 40 bar and 2.55 L_{syn}/g_{CZA}·h are presented in Figure 4.13, where are showed the changes produced in the CO conversion and the selectivity depending upon the nature of the inorganic oxide colloid used.

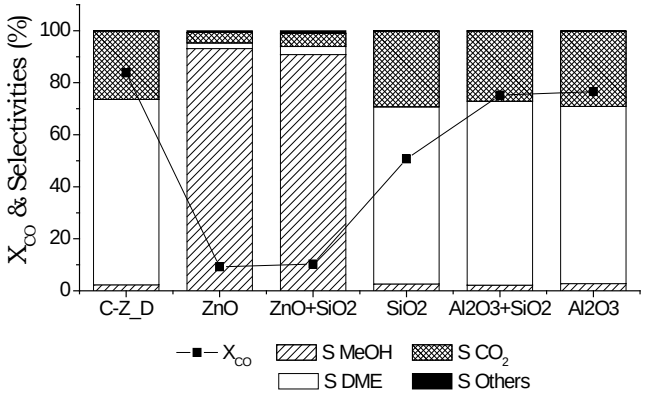

Figure 4.13. CO conversion and selectivities of slurried catalysts with different colloids for the direct synthesis of DME. Reaction conditions: 260 ºC, 40 bar and 2.55 L_{syn}/g_{CZA}·h

The addition of colloidal ZnO to the slurry produced a sharp decrease in the CO conversion and in the selectivity to DME (*Figure 4.13*). However, the selectivity to methanol increased. If ZnO and a small amount of SiO_2 were added (C-Z_23.4%ZnO+3.4%SiO_2) the CO conversion and DME selectivity slightly increased in comparison to the sample with only colloidal ZnO. In contrast, the use of colloidal Al_2O_3 and SiO_2 produced similar selectivities to the slurried catalyst without colloids. Nevertheless, the addition of only colloidal SiO_2 (C-Z_26.7%SiO_2) produced lower CO conversion than the samples with Al_2O_3 as additive (C-Z_15.3%Al_2O_3) or Al_2O_3 with a little SiO_2 content (C-Z_11.7%Al_2O_3+26.7%SiO_2).

4.2.2.1.2. Coating properties

The proposed slurry formulations were used to coat Fecralloy® monoliths of 289 cpsi (*Table 4.2*). The viscosity of slurries and the adherence obtained were measured (*Table 4.4*).

Table 4.4. Coating properties of different slurried mixtures

Sample	Viscosity (mPa·s)	Adherence (%)
C-Z_D	-	22
C-Z_26.7%ZnO	9.0	86
C-Z_23.4%ZnO+3.4%SiO_2	7.9	86
C-Z_26.7%SiO_2	7.2	86
C-Z_11.7%Al_2O_3+3.6%SiO_2	9.1	85
C-Z_15.3%Al_2O_3	15.7	81

The results showed that viscosity of the slurry changes depending on the colloid used (Al_2O_3, ZnO or SiO_2). The use of Al_2O_3 (C-Z_15.3%Al_2O_3) produced the highest value of viscosity despite using less content than with other colloids (*Table 4.2*). Colloidal SiO_2 (C-Z_26.7%SiO_2) produced the slurry with the lowest viscosity.

In the coating process, the number of immersions required for a certain load showed an inverse relationship with the viscosity of the slurry (*see Figure 4.14*). The lowest immersion numbers required to coat 1 g of catalyst was achieved with the slurry prepared with only colloidal Al_2O_3 (C-Z_15.3%Al_2O_3). On the contrary, the slurry with the colloidal silica (C-Z_26.7%SiO_2) required the highest number of coatings to load the same amount of 1 g of catalyst.

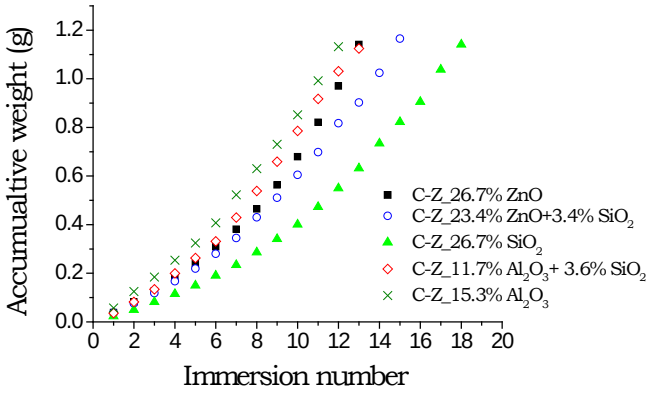

Figure 4.14. Coating process of slurried mixtures with different colloids

On the other hand, adherence was measured by sonication of the coated monoliths. The results summarised in *Table 4.2* showed that all the studied formulation exhibited good adherence above 80%. Nevertheless, when no colloidal additive was used in the slurry (C-Z_D), poor adherence was obtained.

4.2.2.2. Effect of colloid content

Due to the fact that the colloidal SiO_2 and Al_2O_3 presented good performance in selectivity, these colloids were chosen to study the effect of the colloid content in the mixture. The formulation of the slurries studied with different colloid content are presented in *Table 4.5*.

Table 4.5. Slurries formulation of catalysts with different colloid content.

Sample	CZA (%)	HZSM-5 (%)	Colloid (%)		PVA (%)	H_2O (%)
			Al_2O_3	SiO_2		
C-Z_D	12.7	6.40	-	-	0.90	80
C-Z_6.5%Al_2O_3	11.9	5.96	1.30	-	0.80	80
C-Z_8.6%Al_2O_3	11.7	5.83	1.72	-	0.79	80
C-Z_12%Al_2O_3	11.2	5.62	2.40	-	0.75	80
C-Z_15.3%Al_2O_3	10.8	5.41	3.05	-	0.72	80
C-Z_14.6%SiO_2	10.9	5.44	-	2.92	0.79	80
C-Z_26.7%SiO_2	9.33	4.67	-	5.33	0.67	80

4.2.2.2.1. Colloidal Al_2O_3

The physicochemical properties of the slurried catalysts mixture were measured by different methods and the main properties are summarised in *Table 4.6*.

Table 4.6. Physicochemical properties of the slurried catalysts with different colloidal Al_2O_3 content for the direct synthesis of DME

Sample	Al_2O_3 content (%)*	BET surface (m^2/g)	Total pore volume (cm^3/g)	Equiv. pore diameter (nm)	CuO size (nm)	Cu Surface area (m^2/g_{CZA})	TPR H_2 consumption (mL/g_{CZA})	TPR Reducibility (%)
C-Z	0	172	0.38	8.9	4.0	33.9	167	99
	6.5	171	0.37	8.8	4.2	34.7	167	99
	8.6	169	0.37	8.8	4.3	30.7	171	101
	12.0	168	0.38	9.1	4.3	30.1	172	102
	15.3	165	0.40	9.6	4.4	30.2	162	96
Colloidal Al_2O_3	100	204	0.31	6.2	-	-	-	-

*In powder after calcination at 400 ºC, 3h

- **Textural properties**

The textural properties of slurried catalysts mixtures with different colloidal Al_2O_3 content was measured by N_2 adsorption (*Figure 4.15)*. The BET surface area, the total pore volume and the equivalent pore size are presented in *Table 4.6*. The results did not show significant changes in textural properties when the content of colloidal alumina increased (*Table 4.6 and Figure 4.15*). In addition, a similar pore size distribution was obtained (*Figure 4.16*).

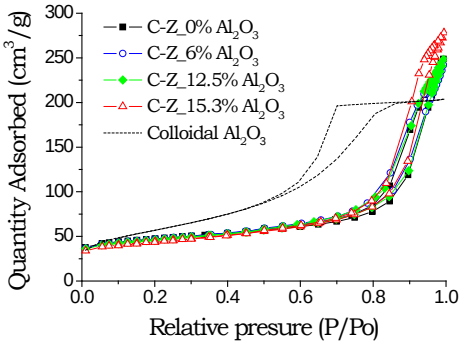

Figure 4.15. N_2 isotherm of slurried catalysts with different colloidal Al_2O_3 content.

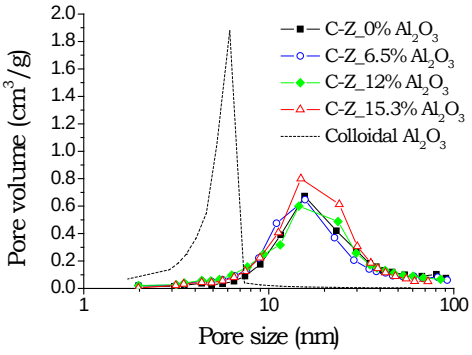

Figure 4.16. Pore size distribution of slurried catalysts with different colloidal Al_2O_3 content.

- **Crystallinity**

The crystallinity of the samples were measured by XRD and the diffractograms are presented in *Figure 4.17*. The results did not apparently show changes in crystalline phases (*Figure 4.17*). Furthermore, using the Scherrer equation, similar CuO crystal size were estimated (*Table 4.4*).

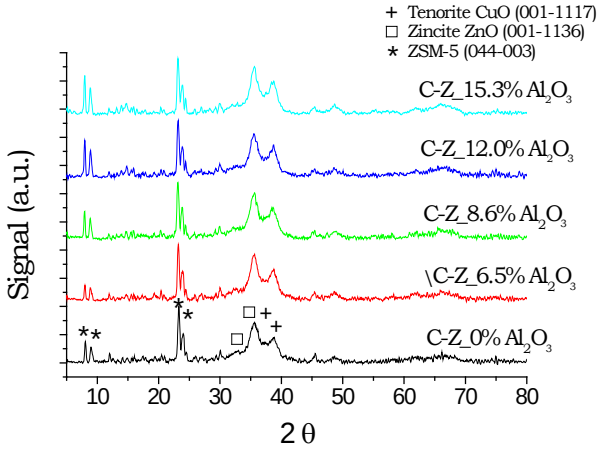

Figure 4.17. XRD analysis of different slurried catalysts with different colloidal Al_2O_3 content.

- **Copper metal surface area**

The Cu metal surface area was measured by N_2O-RFC (*Table 4.6*). The results showed that the addition of the lowest content of colloidal Al_2O_3 (C-Z_6.5%Al_2O_3) presents similar value to that of the slurried catalysts mixture without colloid. Nevertheless, higher colloidal alumina content than 6.5% showed a slight decrease in the Cu metal surface area, around 10-12%, that did not change by increasing the alumina content (*Table 4.6*).

- **Reducibility**

The reducibility of the slurried catalysts mixture was measured by H_2-TPR analysis (*Table 4.6 and Figure 4.18*). The results showed a maximum peak of reduction at 225-230 ºC (*Figure 4.18*). Moreover, the reducibility of the CZA catalyst was similar to the catalyst without colloids that was totally reduced at 400 ºC (*Table 4.6*).

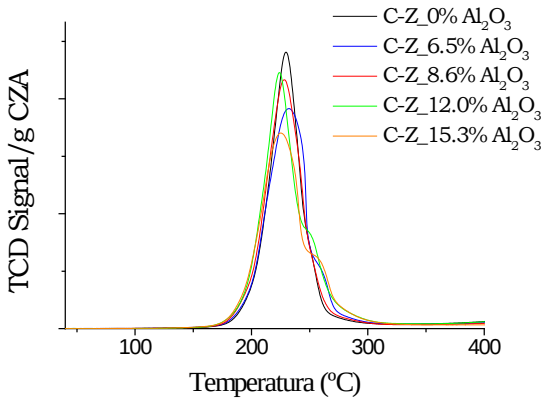

Figure 4.18. H_2-TPR analysis of slurried catalysts with different colloidal Al_2O_3 content for the direct synthesis of DME catalysts.

- **Acid strength**

The acidity of samples with different colloidal Al_2O_3 content were measured by NH_3-TPD. The results showed that colloidal Al_2O_3 presented a lower acidity than the slurried mixtures with different colloid content (*Figure 4.19A*). Furthermore,

the addition of this colloid did not seem to provide new acidity to the slurried catalysts mixture (sample), reducing the TPD peak when the colloid content increases. In addition, by normalising the signal per gram of zeolite (*Figure 4.19B*), the results did not show relevant changes in the acidity of the samples.

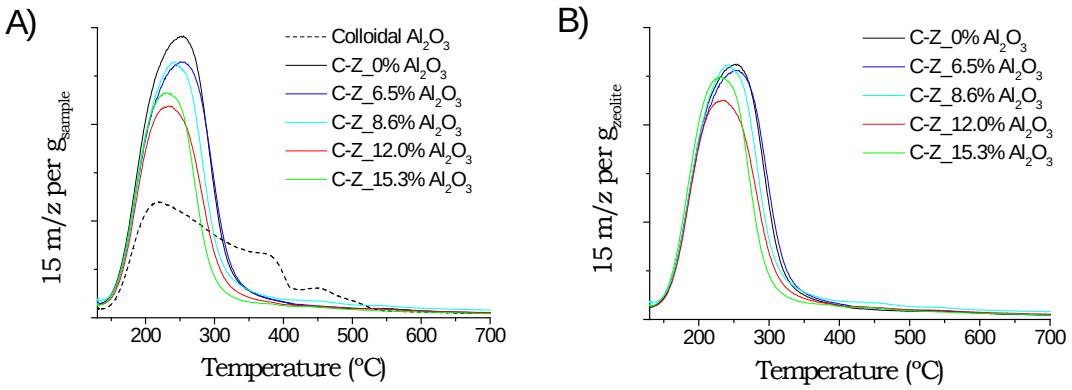

Figure 4.19. NH_3-TPD analysis of slurried catalysts for the direct synthesis of DME with different colloidal Al_2O_3 content: a) signal per gram of sample and b) signal per gram of zeolite.

- **Adherence Test**

Adherence test was carried out by sonication of the structured catalysts in petroleum ether. Good adherence was obtained for all the studied formulation using colloidal alumina, above 80% (*Table 4.7*).

Table 4.7. Adherence obtained of different slurries with different colloidal Al_2O_3 content

Sample	Adherence (%)
C-Z_0% Al_2O_3	22
C-Z_6.5% Al_2O_3	85
C-Z_8.6% Al_2O_3	80
C-Z_12.0% Al_2O_3	86
C-Z_15.3% Al_2O_3	81

- **Activity Test**

The activity test was carried out in a fixed bed reactor at 260 ºC and 40 bar. The results (*Figure 4.20*) showed that the increase of the colloidal Al_2O_3 content in the slurry formulation did not produce relevant changes in activity. CO conversions around 75-81 % were obtained (*Figure 4.20*). Moreover, selectivities to all compounds did not change with alumina content.

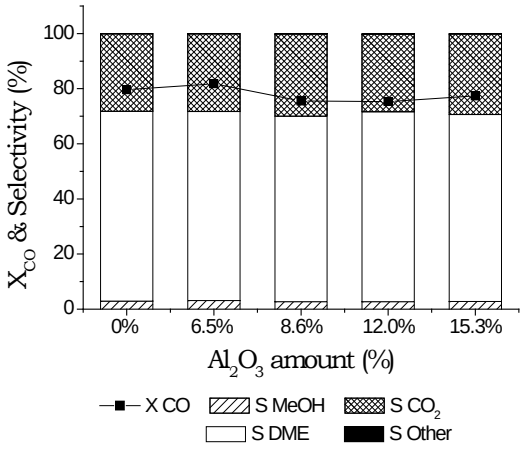

Figure 4.20. CO conversion and selectivities of direct synthesis of DME reaction with different colloidal Al_2O_3 content. Space velocity: 2.55 $L_{syn}/g_{CZA}·h$

On the other hand, the dehydration capacity of colloidal alumina was compared with HZSM-5 zeolite at 260 ºC (*Figure 4.21*). The results showed high selectivity to DME for both samples. However, the activity of colloidal Al_2O_3 is much lower (2%) than that of the HZSM-5 (46%).

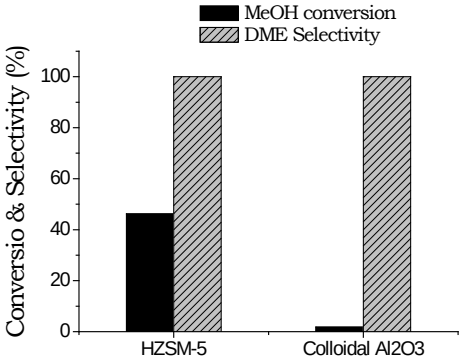

Figure 4.21. Activity test of methanol dehydration of HZSM-5 zeolite and colloidal Al_2O_3: Reactio conditions: 260 ºC, 1 atm and 10 $L/g_{zeolite}$·min

4.2.2.2.2. Colloidal SiO_2

In this section, the effect of the colloidal SiO_2 content in slurried catalysts mixture (CZA+HZSM-5) was studied. All the samples were characterised after drying and calcining the slurries and the physicochemical properties (summarised in *Table 4.8*) as well as the activity of the catalysts for direct synthesis of DME were measured.

Table 4.8. Physicochemical properties of slurried catalysts with different colloidal SiO_2 content for the direct synthesis of DME

Sample	SiO_2 content (%)	BET surface (m^2/g)	Total pore volume (cm^3/g)	Equiv. pore diameter (nm)	CuO size (nm)	Cu surface area (m^2/g_{CZA})	TPR H_2 consumption (mL/g_{CZA})	TPR Reducibility (%)
	0	172	0.38	8.9	4.0	33.9	167	99
C-Z	14.6	152	0.39	10.4	4.2	26.1	169	100
	26.7	138	0.39	11.2	4.3	24.7	157	93
Colloidal SiO_2	100	114	0.22	7.6	-	-	-	-

- **Textural properties**

The properties such as the BET surface area and the total pore volume of the slurried catalysts mixtures with colloidal SiO_2 as additive were measured by N_2 adsorption (*Figure 4.22*). The results are summarised in *Table 4.8*. The addition of the colloidal SiO_2 to the slurried catalysts mixture produced a decrease in the BET surface area with the silica content used (*Table 4.8*). However, the total pore volume and the pore size distribution remained similar to the catalyst without silica (*Figure 4.23 and Table 4.8*).

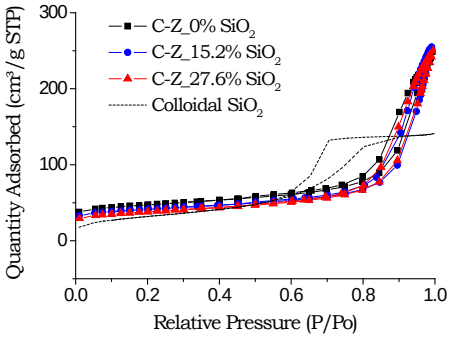

Figure 4.22. N_2 isotherm of C-Z samples with different colloidal SiO_2 content.

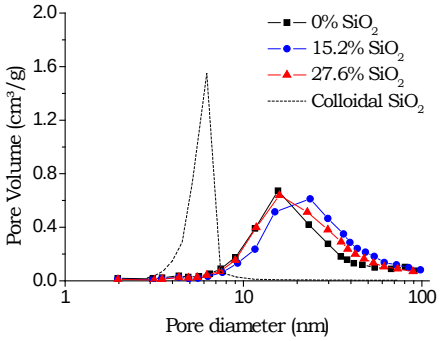

Figure 4.23. Pore size dsitribution of C-Z samples with different colloidal SiO_2 content.

- **Crystallinity**

The crystallinity of the samples was analysed by XRD. The diffractograms presented in *Figure 4.24* did not show relevant changes in structure. Moreover, crystal size of CuO obtained by XRD presented similar values around 4 nm (*Table 4.8*).

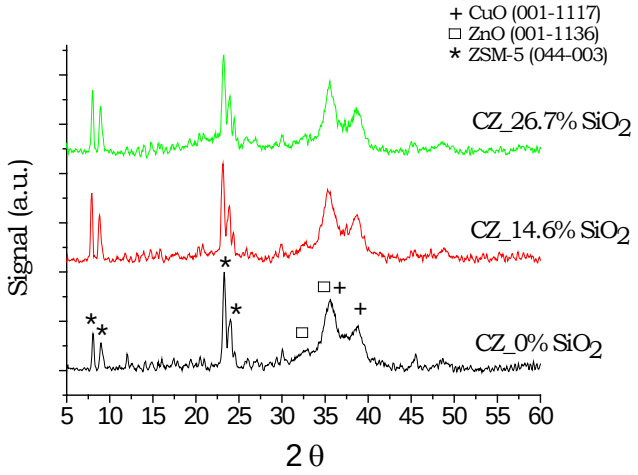

Figure 4.24. XRD of slurried catalysts with different colloidal SiO_2 content.

- **Copper metal surface area**

The Cu metal surface area of the samples was measured by N_2O-RFC. The results showed a decrease in the Cu surface area when the colloidal SiO_2 content increased (*Table 4.8*).

- **Reducibility**

The reducibility of the slurried catalysts mixtures with different colloidal SiO_2 content was measured by H_2-TPR (*Figure 4.25 and Table 4.8*). It can be observed that the reducibility when 14.6% of SiO_2 is used is similar to the catalyst without SiO_2. However, when 26.7% of SiO_2 is added a slight decrease of the reducibility (to 93%) was observed (*Table 4.8*). The maximum of the reduction peak was similar for all the samples at 230 °C approximately (*Figure 4.25*).

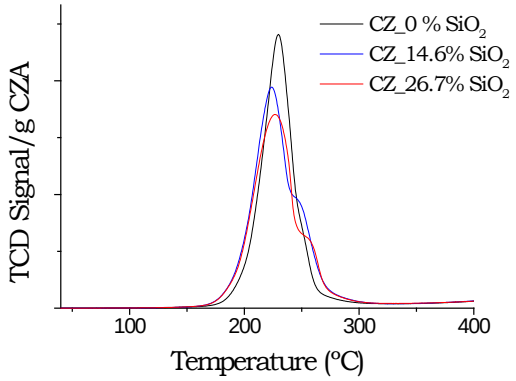

Figure 4.25. H_2-TPR analysis of slurried catalysts with different colloidal SiO_2 content for the direct synthesis of DME.

- **Acid strength**

The acidity of samples was determined by NH_3-TPD. Desorption curves of NH_3 are presented in *Figure 4.26*. The results showed that the addition of colloidal silica, which presented a very low acidity, did not affect significantly the overall acidity.

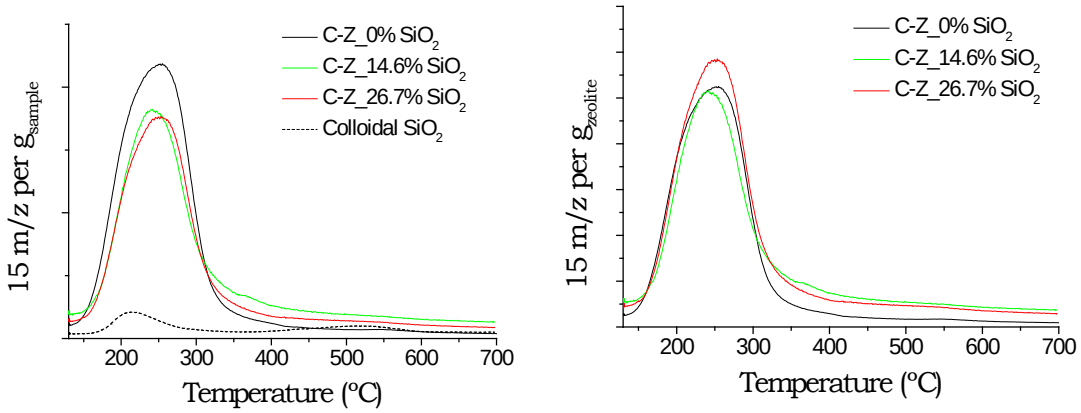

Figure 4.26. NH_3-TPD analysis of slurried catalysts with different colloidal SiO_2 content for the direct synthesis of DME: a) signal per gram of sample and b) signal per gram of zeolite.

- **Adherence Test**

The adhesion of the catalytic layer to the substrate was measured by sonication method. The results presented in *Table 4.9* showed a sharp increase in the adherence when the SiO_2 content increased, being good for 26.7% of silica content.

Table 4.9. Adherence of slurries with different colloidal SiO_2 content

Sample	SiO_2 content (%)		Adherence (%)
	In powder catalyst	In slurry	
C-Z_0% SiO_2	0	0	22
C-Z_14.6% SiO_2	15.2	2.92	39
C-Z_26.7% SiO_2	27.6	5.33	86

- **Activity Test**

The activity of slurried catalysts mixture was measured in a fixed bed reactor at 260 ºC and 40 bar. The addition of the colloidal SiO_2 to the slurried catalysts mixture produced a decrease in the CO conversion (*Figure 4.27*). Moreover, this decrease is more pronounced when the colloidal SiO_2 content increased. However, the selectivity to the different compounds is similar to the catalyst without SiO_2 (*Figure 4.27*).

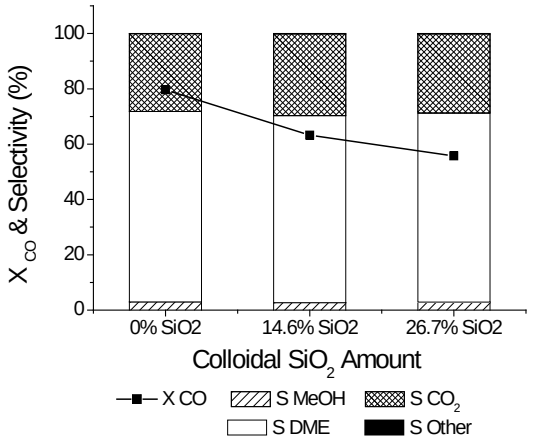

Figure 4.27. CO conversion and selectivities of slurried catalysts with different contents of colloidal SiO_2

4.3. Discussion

4.3.1. Architecture of the catalysts bed

When comparing the different disposition of the two catalysts for the direct synthesis of DME in the catalytic bed (*Figure 4.7*), it can be concluded that at the scale of millimetres that the bed has, the proximity of the two types of active sites is important. Indeed, the beds with the two phases mixed, independently of the preparation mode used, are always more active and selective than the separation of both types of active sites in two beds separated by a few millimeters.

The two separated beds of both catalysts (C-Z_B) showed the lowest CO conversion (Figure 4.7). This disposition only presented one plane of contact, so it performed similar to two independent reactors (one with CZA and the other with ZSM-5). The methanol synthesis reaction is thermodynamically limited [1-3]. However, according to this limitation, dehydrating the methanol meanwhile it is formed leads to a shift of the equilibrium to the right due to the methanol consumption. Therefore, the reaction would not be as favoured as if both phases were in contact such as in the physical mixture. Hence, the proximity of both phases is essential to favour the shift of the equilibrium of the methanol synthesis [4-7].

A thin layer of zeolite at the exit of a physical mixture bed (C-Z_C) showed similar CO conversion to that obtained when the whole bed is a physical mixture of catalysts (C-Z_A). Hence, in both cases the contact of both phases is adequate to favour the shift of the equilibrium. In addition, a more intimate contact of phases by dispersing the two catalysts in aqueous media (slurried mixture, C-Z_D) also presented good performances in the direct synthesis of DME. However many authors observed that a too high interaction between active phases may create detrimental interactions, which deactivate the catalyst [5,8,9]. A. García-Trenco *et al.* [5] observed a decrease in CO conversion with a slurry mixture of CZA and HZSM-5. However, it must be taken into account that in their study the methanol synthesis catalyst was dispersed in water after calcination. The dispersion of this catalyst in water produced the formation of hydrotalcite-like compounds due to a memory effect of this type of compounds, which led to a change in CuO crystal size [25,47]. In contrast, in our work all the slurries were prepared with the CZA catalyst before calcination, that is, with the original structure of the hydrotalcite intact. Hence, it seems that this situation prevents

the negative interactions between both catalytic phases and there was not observed a decrease in CO conversion.

Regarding the selectivities obtained, the slurried catalysts mixture presented lower selectivity to other compounds (mainly light hydrocarbons) than the other architectures (*Figure 4.7*). Two separated beds showed the highest selectivity to other compounds (S other). Moreover, when a thin layer of bare zeolite was located at the exit of the physical mixture bed (C-Z_C), DME and hydrocarbon selectivity were slightly higher than a bare physical mixture (C-Z_A). Therefore, it seems that the bed architecture also plays an important role in the selectivity.

In bibliography, there is a wide discussion about which type of acid sites dehydrates the methanol to DME or hydrocarbons. J. Xia *et al.* [26] suggested that Brønsted acid sited are responsible of methanol dehydration to DME, while the extra-framework alumina, which is associated to Lewis sites in zeolites, is responsible of the production of undesired hydrocarbons. However, other authors [27,28] concluded that the Lewis sites dehydrate the methanol to DME and that Brønsted sites are responsible of the dehydration of DME to hydrocarbons. On the other hand, A. García-Trenco *et al.* [29] after treating ZSM-5 zeolite and removing extra-framework alumina of it, they concluded that Brønsted sites are more active than Lewis sites for methanol dehydration to DME, but Lewis sites are also active in the reaction. In the same direction, M. Xu *et al.* [30], observed by adding water over different solid acids on the methanol dehydration reaction, that both sites (Brønsted and Lewis) are active for the reaction.

But not only the nature of acid sites is important in the methanol dehydration, the acid strength of solid acids is another factor to take into account. Acid strength measured by NH_3-TPD is divided generally in 3 types: weak (150-250 ºC), moderate or intermediate (300-400 ºC) and strong (450-550 ºC) [31-34]. The stronger the acid sites, the more activity of the catalysts [35]. However, strong acid sites promote hydrocarbon production due to an excessive dehydration of DME [36-38,39,40,41]. Thus, acid sites with weak-moderate strength are mainly desired to dehydrate methanol to DME [6,26,41-44].

In addition to that, the contact of both catalysts (architecture of the bed) add a new factor for the understanding of the process. The results showed a decrease in the acid strength of the zeolite when both catalysts are mixed (physical or slurried mixture, C-Z_A and C-Z_D respectively) (*Figure 4.6*). The NH_3-TPD analysis showed a shift of the high temperature peaks of the zeolite (400-500 ºC) to moderate temperatures (300-400 ºC), which decrease the formation of

hydrocarbon as by-products (*Figure 4.7*). However, the dispositions where the contact is minimum or negligible, such as in two separated beds (C-Z_B) or the thin layer of bare zeolite at the exit of the bed after a physical mixture (C-Z_C), would provide the strongest acid sites of the zeolite that promote the excessive dehydration of DME to hydrocarbons (*Figure 4.7*).

Furthermore, the slurried catalysts (C-Z_D) led to lower production of hydrocarbons than physical mixture (C-Z_A). As it can be seen in the NH_3-TPD analysis (*Figure 4.6*), the slurried mixture not only reduced the acid strength, but also reduced the number of active sites in comparison to the physical mixture (area under the curve). A. García-Trenco *et al.* [29] also studied by FTIR-Pyridine the effect of the contact of both catalysts by preparing them by different methods. They observed a sharp decrease of Brønsted sites when catalysts were mixed mechanically and in a slurry. This detrimental interaction due to the contact of catalysts was attributed to a migration of copper to the zeolite surface and the blocking of the zeolite pores. J.H. Flores *et al.* [4] and Z. Li *et al.* [45] also showed by NH_3-TPD the acidity change when both active phases were put in contact. The acid strength was reduced while increasing contact from physical mixture to slurried mixture. These acidity reduction was suggested to be due to a partial blockage of the porosity or acid sites of the zeolites [4,5,46,47]. As it has been shown in the textural properties of the samples in this work (*Table 4.1*), the slurried mixture presented a higher decrease in the total pore volume than the physical mixture, so a tighter contact between the two phases may probably generate an inaccessibility of the zeolite porosity by the CZA catalyst.

Therefore, the reduction of the acidity produced with an intimate contact (in the slurried mixture) prevents an excessive dehydration to form by-products. In this way, the slurried mixture not only produced a good contact that favour the shift of the equilibrium but also prevented the excessive dehydration due to its lower acidity.

4.3.2. Additive incorporation in the slurried catalyst

Structuring catalysts requires good adhesion between the catalyst layer and the substrate. However, as it is shown in *Table 4.4*, the slurried mixture requires the use of colloids to obtain adequate adherence. As it was shown in *Chapter 3*, inorganic oxide colloids act mainly as binder in slurry formulation. Therefore, with the use of different colloids (ZnO, SiO_2 and Al_2O_3), good adherence, above 80%,

was achieved. The small particle size of these colloids could fill the space between the catalysts particles and the substrate roughness and create anchoring points [17,20].

However, the nature of the colloid used changed the catalytic properties of the parent catalyst (*Figure 4.13*). The addition of the colloidal ZnO sharply decreased the DME selectivity and the CO conversion. The basic character of the ZnO leads to a decrease in acidity of the catalyst (*Figure 4.12*). Hence, the shift of the equilibrium is not favoured and the CO conversion decreased.

The use of different colloidal Al_2O_3 content, in contrast, did not show significant changes in activity (*Figure 4.19*). Cu metal surface area did not decrease noticeably (*Table 4.4),* so the methanol synthesis activity remained similar to the parent catalysts (CZA catalyst) and the obtained CO conversion did not change with different colloid contents. Moreover, similar selectivities to different compounds were obtained (*Figure 4.20*). NH_3-TPD analysis did not show an increase in acidity with colloidal Al_2O_3 addition (*Figure 4.19*), despite the fact that the colloidal alumina shows a certain acidity. The colloid content did not modify the acidy significantly, so the catalyst still presents enough acid sites to dehydrate all the methanol formed to DME shifting the thermodynamic equilibrium.

When colloidal SiO_2 is added to the slurry (C-Z_26.7%SiO_2), a decrease in CO conversion in the direct synthesis of DME reaction was shown (*Figure 4.13*). However, an increase in CO conversion was obtained when the colloidal SiO_2 content decreased (*Figure 4.27*), but leading to bad coating adherences on the monolith surface (*Table 4.9*). The use of larger amount of colloid helped to obtain good adhesion of the catalyst layer (*see Chapter 3*). Nevertheless, this content might produce detrimental effects to the catalysts [17,23]. N_2O-RFC measurements showed a decrease of copper metal surface area of the slurried catalysts mixtures when the colloidal SiO_2 increased. This effect was also observed when the effect of colloidal SiO_2 content was studied in the CZA catalyst (*Chapter 3*). In that case it was confirmed that the Cu surface area decreases with colloid content due to an increase in the Cu crystal size (*Table 3.2*).

4.4. Conclusion

The disposition of two catalysts involved in the direct synthesis of DME affects the reaction yield. A good contact of both phases by physical mixture or slurried mixture is required to favour the removal of the equilibrium limitation of the methanol formation.

The intimate contact of the slurried mixture offers better performance in the direct synthesis of DME reaction. Methanol synthesis catalyst (CZA) did not present significant detrimental interactions in this mixture and similar metal surface area and reducibility compared to the parent catalyst are achieved. In contrast, the contact of both catalysts alter the dehydration properties of the solid acid by reducing the acid strength. The production of by-products (hydrocarbon) due to strong acidity is avoided. Therefore, the slurried mixture provides better contact improving reaction yield because of the lower selectivity to undesired products than the physical mixture.

For structuring these catalysts the use of inorganic colloid as additives is required. Nevertheless, the nature of this colloid determine to the catalytic properties of the parent catalysts (methanol synthesis and dehydration catalyst).

The addition of colloidal ZnO to the slurry preparation produced the neutralisation of the acid sited of the zeolite. The basic character of the ZnO avoid the dehydration of methanol in the reaction. Hence, selectivity to DME lower than 3% is achieved while high production of methanol is observed.

On the other hand, the use of colloidal SiO_2 despite presenting similar selectivities to the slurried catalysts without colloids, lower CO conversion is achieved. The large amount of colloid required to obtain good adherence reduces the Cu surface area of the catalysts and consequently, the ability of the methanol synthesis catalyst to form methanol.

The use of colloidal Al_2O_3, in contrast, do not produce significant changes in the direct synthesis of DME yield. There were not observed detrimental interactions with the methanol synthesis catalyst and Cu surface area remained without significant changes. In addition, the use of colloidal Al_2O_3 did not modify in great extent the acidity of the catalyst. Therefore, similar CO conversion and selectivities to the slurried catalysts without colloids are achieved in the studied conditions.

4.5. References

[1] T. Ogawa, N. Inoue, T. Shikada, Y. Ohno. *Journal of Natural Gas Chemistry* 12 (2003) 219-227.

[2] C. Arcoumanis, C. Bae, R. Crookes, E. Kinoshita. *Fuel* 87 (2008) 1014-1030.

[3] T. A. Semelsberger, R. L. Borup, H. L. Greene. *Journal of Power Sources* 156 (2006) 497-511.

[4] J.H. Flores, M.I.P. da Silva. *Catalysis Letter* 146 (2016) 1505-1516.

[5] A. García-Trenco, A. Vidal-Moya, A. Martínez. *Catalysis Today* 179 (2012) 43-51.

[6] Q. Ge, Y. Huang, F. Qiu, S. Li. *Applied Catalysis A: General* 167 (1998) 23-30.

[7] S. P. Naik, H. Du, H. Wan, V. Bui, J.D. Miller, W.W. Zmierczak. *Industrial & Engineering Chemestry Research* 47 (2008) 9791-9794.

[8] G. Bonura, M. Cordaro, L. Spadaro, C. Cannilla, F. Arena, F. Frusteri. *Applied Catalysis B: Environmental* 140-141 (2013) 16-24.

[9] R. Peláez, E. Bryce, P. Martín, S. Ordóñez. *Fuel Processing Technology* 179 (2018) 378-386).

[10] J. Hu, Y. Wang, C. Cao, D.C. Elliot, D.J. Stevens, J.F. White. *Industrial & Engineering Chemestry Research* 44 (2005) 1722-1727.

[11] F. Song, Y. Tan, H. Xie, Q. Zhang, Y. Han. *Fuel Processing technology* 126 (2014) 88-94.

[12] F.S. Ramos, A.M. Duarte de Farias, L.E.P. Borges, J.L. Monteiro, M.A. Fraga, E.F. Sousa-Aguiar, L.G. Appel. *Catalysis Today* 101 (2005) 39-44.

[13] D. Mao, J. Xia, B. Zhang, G. Lu. *Energy Conversion and Management* 51 (2010) 1134-1139.

[14] A.T. Aguayo, J. Ereña, I. Sierra, M. Olazar, J. Bilbao. *Catalysis Today* 106 (2005) 265-270.

[15] R. Garoña, *Ph.D. Thesis* (2005) University of the Basque Country.

[16] J. Ereña, R. Garoña, J.M. Arandes, A.T. Aguayo, J. Bilbao. *International Journal of Chemical Reactor Engineering* 3 (2005) 1-15.

[17] F.J. Echave, O. Sanz, I. Velasco, J.A. Odriozola, M. Montes. *Catalysis Today* 213 (2013) 145-154.

[18] A.K. Mogalicherla, D. Kunzru. *The Canadian Journal of Chemical Engineering* 88 (2010) 267-375.

[19] O.H. Laguna, M.I. Domínguez, M.A. Centeno, J.A. Odriozola. *New Material for Catalytic Applications* (2016) 81-120.

[20] T.A. Nijhuis, A.E. W. Beers, T. Vergunst, I. Hoek, F. Kapteijn, J.A. Moulijn *Preparation of monolithic catalysts, Catalysis Reviews*, 43:4 (2001) 345-380.

[21] Juan M. Zamaro, Maria A. Ulla, Eduardo E. Miró. *Chemical Engineering Journal* 106 (2005) 25-33.

[22] F.J. Echave, O. Sanz, M. Montes. *Applied Catalysis A: General* 474 (2014) 159-167.

[23] P. Ávila, M. Montes, E. E. Miró. *Chemical Engineering Journal* 109 (2005) 11-36.

[24] N. Khandan, M. Kazemeini, M. Aghaziarati. *Catalysis Letters* 129 (2009) 111-118.

[25] I. Melián-Cabrera, M. López Cranados, L.G. Fierro. *Journal of Catalysis* 210 (2002) 273-284.

[26] J. Xia, D. Mao, W. Tao, Q. Chen, Y. Zhang, Y. Tang. *Microporous & Mesoporous Materials* 91 (2006) 33-39.

[27] É. Sarkadi-Pribóczki, N. Kumar, T. Salmi, Z. Kavács, D.Yu. Murzin. *Catalysis Letters* 93 (2004) 101-107.

[28] T. Takeguchi, K. Yanagisawa, T. Inui, M. Inoue. *Applied Catalysis A: General* 192 (2000) 201-209.

[29] A. García-Trenco, A. Martínez. *Applied Catalysis A: General* 411-412 (2012) 170-179.

[30] M. Xu, J.H. Lunsford, D.W. Goodman, A. Bhattacharyya. *Applied Catalysis A: General* 149 (1997) 289-301.

[31] S.D. Kim, S.C. Bek, Y-J. Lee, K-W. Jun, MJ. Kim, I.S. Yoo. *Applied Catalysis A: General* 309 (2006) 139-143.

[32] V. Vishwanathan, K-W. Jun, J-W. Kim, H-S. Roh. *Applied Catalysis A: General* 25 (2004) 251-255.

[33] J-H. Kim, M.J. Park, S.J. Kim, O-S. Joo, K-D. Jung. *Applied Catalysis A: General* 18 (2004) 37-41.

[34] P. Berteau, B. Delmon. *Catalysis Today* 5 (1989) 121-137.

[35] F.S. Ramos, A.M. Duarte de Farias, L.E.P. Borges, J.L. Monteiro, M.A. Fraga, E.F. Sousa-Aguiar, LG. Appel. *Catalysis Today* 101 (2005) 39-44.

[36] J. Xia, D. Mao, B. Zhang, Q. Chen, Y. Tang. *Catalysis Letters* Vol. 98 (2004) 235-240.

[37] M. Xu, J.H. Lunsford, D.W. Goodman, A. Bhattacharyya. Applie*d Catalysis A: General* 149 (1997) 289-301.

[38] T. Takeguchi, K. Yanagisawa, T. Inui, A. Inoue. *Applied Catalysis A: General* 192 (2000) 201-209.

[39] D. Mao, J. Xia, B. Zhang, G. Lu. *Energy Conversion and Management* 51 (2010) 1134-1139.

[40] M. Stiefel, R. Ahmad, U. Arnold, M. Döring. *Fuel processing Technology* 92 (2011) 1466-1474.

[41] J.J. Spivey. *Chemical Engineering communications* 110 (1991) 123-142.

[42] M. Stöcker. *Microporous and Mesoporous Materials* 29 (1999) 3-48.

[43] J.M. Campelo, F. Lafont, J.M. Marinas, M. Ojeda. *Applied Catalysis A: General* 192 (2000) 85-96.

[44] K.S. Yoo, J-H. Kim, M-J. Park, S-J. Kim, O.S. Joo, K.D. Jung. *Applied catalysis A: General* 330 (2007) 57-62.

[45] Z. Li, J. Li, M. Dai, Y. Liu, D. Han, J. Wu. *Fuel* 121 (2014) 173-177.

[46] J.H. Flores, M.I. Pais da Silva. *Colloids and Surfaces A: Physicochemical Engineering Aspects* 322 (2008) 113-123.

[47] Andrés García Trenco. *PhD Thesis* (2013) Universidad Politécnica de Valencia (UPV).

CHAPTER 5

Catalizadores estructurados para la síntesis directa de DME

ÍNDICE

5.1. Introducción

El carácter exotérmico de la síntesis directa de DME requiere sistemas capaces de un control adecuado de la temperatura sin disparos térmicos que aumenten la peligrosidad de los sistemas de reacción [1]. Además, el empleo común de catalizadores basados en cobre para la etapa de síntesis de metanol, aumenta la necesidad de un buen control de la temperatura en el reactor para evitar problemas de sinterizado del cobre, y consecuentemente, el pronto deterioro del catalizador [2-4].

Los sistemas estructurados pueden mejorar la transferencia de calor durante la reacción [5,6], sobre todo cuando se emplean sustratos estructurados metálicos, los cuales presentan mayor conductividad térmica que los cerámicos [6-8]. Los aceros ferríticos con aluminio son los más populares debido a las excelentes adherencias proporcionadas por la capa protectora de alumina generada tras el correspondiente pretratamiento [5]. No obstante, ha crecido el interés del uso de otros metales más conductores como el cobre o el latón [9-12] o el aluminio [13,14].

La forma más empleada para la preparación de estos monolitos metálicos es el enrollado o apilado de placas lisas y corrugadas de forma alterna [5,15]. La maleabilidad que presentan estos materiales permiten modificar la forma del sustrato y preparar sustratos con diferentes densidades de celda. De esta manera, una mayor densidad de celda proporciona un sistema con mayor superficie geométrica, pudiendo por una parte lograr un menor espesor de la capa catalítica, mejorando la transferencia de materia, y por otro lado, incrementar la conductividad térmica al disponer de unos sistemas con más material conductor y menor fracción hueca [6,7,16-20]. D. Merino *y cols.* [16] pudieron comprobar la mejora del control de temperatura en el sistema al utilizar monolitos de Fecralloy® de alta densidad de celda. En la síntesis de Fischer-Tropsch observaron como un monolito con una baja densidad de celda (289 cpsi) no permitía controlar el calor generado en dicha reacción produciendo un disparo térmico en el sistema. Sin embargo, aumentando entono a 10 veces la densidad de celda del monolito (2390 cpsi), la reacción pudo llevarse a cabo con un adecuado control térmico.

Por otro lado, el empleo de otras estructuras o geometrías con mayor tortuosidad como las espumas metálicas de porosidad abierta, también ha producido un aumento del interés en el estudio de sistemas estructurados para mejorar la transferencia de materia y calor. En este tipo de estructuras se

consigue un régimen de flujo turbulento, evitando el flujo laminar característico de los monolitos de canal longitudinal, y favoreciendo el contacto del gas con el catalizador mejorando, así, la transferencia de materia en el sistema [6,7,13,21]. Además, combinado con la ligereza que presentan y su elevada resistencia mecánica hacen de estos sistemas una alternativa prometedora para el diseño de componentes ligeros y rígidos [21,22]. A. Montebelli *y cols*. [23] simularon sistemas de espumas metálicas para la síntesis de metanol, donde vieron el gran potencial de estas estructuras para diseñar reactores compactos capaces de operar con una mejor transferencia de calor y menores relaciones de recirculación en comparación a los sistemas convencionales.

La síntesis directa de DME en reactores estructurados, según nuestro conocimiento, no ha sido muy estudiada en bibliografía. El grupo de H.J. Venvik en colaboración con el Instituto de Tecnología de Karlsruhe [1,24-27], y por otro lado J. Hu *y cols*. [28], realizaron estudios de la síntesis directa de DME en reactores de microcanales. No obstante, en todos ellos los catalizadores (el catalizador de síntesis de metanol y el catalizador ácido) eran previamente mezclados mecánicamente para posteriormente rellenar los canales con las partículas de los mismos.

Como se ha visto en capítulos anteriores, el contacto entre los catalizadores juega un papel importante en el rendimiento de la reacción. La búsqueda del diseño de catalizadores híbridos eficientes ha conducido al estudio de arquitecturas más complejas como la preparación de catalizadores núcleo-corteza (core-shell), dónde el catalizador de síntesis de metanol está rodeado (núcleo) del catalizador ácido (corteza). Este diseño cumpliría la disposición 'a priori' más eficiente para la ejecución de la reacción, sintetizándose el metanol en el núcleo del catalizador y deshidratándose a su salida [29-33]. Sin embargo, tanto las condiciones de hidrotratamiento como los reactivos utilizados en la síntesis del catalizador ácido, pueden desactivar el catalizador de síntesis de metanol, especialmente aquellos basados en cobre [31-33].

La gran versatilidad que ofrece el método de recubrimiento por inmersión (washcoating) en la preparación de catalizadores estructurados, permitiría diseñar arquitecturas organizadas (tipo tándem), localizando dos o más capas de catalizadores independientes para las reacciones que van a verse involucradas. Estos sistemas han sido estudiados en reacciones múltiples: como la NSR-SCR que combina la reducción catalítica selectiva de NOx (capa interna) con el almacenamiento y reducción de NOx (capa externa) [34,35] o el reformado autotérmico (ATR) de glicerol, colocando una capa de reformado al vapor y otra de

oxidación parcial [36]. La síntesis directa de DME, sería una reacción de interés también para estas arquitecturas, pudiendo localizar capas independientes de ambas fases sobre un sustrato, simulando la organización núcleo-corteza dónde la capa de zeolita recubriría al catalizador de síntesis de metanol.

En el desarrollo de tecnologías más compactas, seguras y eficientes (intensificación de procesos) es necesario el diseño de reactores compactos que permitan una mayor producción minimizando el coste. [13,37]. En general, los reactores catalíticos estructurados que se estudian en la literatura se caracterizan por una baja productividad volumétrica debido a que la mayoría de los trabajos usan reactores con baja carga de catalizador [11,38-41]. La mayoría de los autores trabajan con recubrimientos catalíticos de espesores inferiores a 50 μm debido a los resultados reportados por F. Kapteijn *y cols*. [42], que observaron problemas difusionales con espesores mayores en la síntesis de Fischer-Tropsch aumentando la selectividad a metano. Sin embargo, este estudio se realizó con monolitos cerámicos donde se pueden producir importantes gradientes de temperatura que pueden dar lugar a disparos térmicos [43]. En nuestro grupo se ha observado que en la síntesis de Fischer-Tropsch se puede trabajar con espesores de hasta 90 μm cuando se utilizan sustratos altamente conductores como el aluminio que permiten un buen control de temperatura y, por tanto, evitan la pérdida de selectividad por mal control térmico [16].

Como alternativa a esta limitación en la carga volumétrica de los sistemas estructurados, se ha propuesto rellenar con catalizador los sustratos estructurados conductores, obteniendo unos minilechos fijos, los cuales presentarían una mayor pérdida de carga que los monolitos recubiertos, pero menor que la presentada por los lechos fijos por el "efecto pared" [44-46]. Mediante estos sistemas B. Kaskes *y cols*. [44] consiguieron incrementar la productividad volumétrica de hidrocarburos en la síntesis de Fischer-Tropsch en comparación con un reactor de lecho fijo. Por otro lado, la síntesis directa de DME ha sido explorada rellenado reactores de microcanales (con tamaños de partícula entre 50-210 μm), donde se pudo observar el potencial de esta tecnología, que permite un excelente control de la temperatura, punto clave de este proceso, y por tanto una buena estabilidad del catalizador [1,28].

En este trabajo se ha estudiado la síntesis directa de DME en sistemas estructurados. Diferentes sustratos metálicos de diferente geometría y aleación han sido recubiertos con la formulación del catalizador C-Z_6,5%Al_2O_3 (*ver capítulo 4*), midiendo la actividad catalítica de estos catalizadores estructurados y sus propiedades fisicoquímicas. Además, la reacción con catalizadores

estructurados tipo tándem también ha sido estudiada, observando el comportamiento de la reacción frente a diferentes arquitecturas de los catalizadores en el monolito. Finalmente, se estudiaron diferentes variables, como la carga de catalizador y las condiciones de reacción, para poder incrementar la productividad volumétrica de DME en dichos sistemas (intensificación).

5.2. Resultados

En este capítulo, se presentan los resultados obtenidos de catalizadores estructurados para la síntesis directa de DME. Los resultados pueden dividirse en tres bloques:

- *Efecto del sustrato estructurado empleado*, dónde se variaron tanto aleación metálica (FeCrAl, latón y aluminio) del sustrato como la geometría o forma del mismo (monolitos de canal longitudinal de diferente densidad de celda y espumas de porosidad abierta).

- *Arquitectura del monolito.* Se estudió el efecto de la disposición de los catalizadores en un monolito de latón de 289 cpsi, depositando los dos catalizadores de la síntesis directa de DME tanto mezclados en una misma suspensión como depositados en capas independientes.

- *Intensificación de monolitos metálicos de latón*. Fueron estudiadas variables como velocidad espacial, temperatura de reacción y carga de catalizador.

5.2.1. Forma y aleación de los sustratos estructurados

Se emplearon monolitos de canales longitudinales paralelos de alta (R1=2360 cpsi) y baja (R4=289 cpsi) densidad de celda y espumas de porosidad abierta de dos densidades de poro E40 de 40 ppi y E60 de 60 ppi.

Se estudiaron aleaciones de FeCrAl (F), latón 63Cu/37Zn (L) y aluminio (A) de diferente geometría (*Tabla 5.1*). Los sustratos fueron recubiertos con la suspensión de los dos catalizadores para la síntesis directa de DME, C-Z_6,5%Al_2O_3 (*ver formulación en el Capítulo 2*). Todos los sustratos fueron cilíndricos de D = 16 mm y L = 30 mm (6 cm^3).

Tabla 5.1. Diferentes sustratos estructurados estudiados

	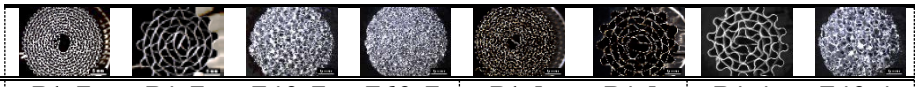							
Nombre	R1_F	R4_F	E40_F	E60_F	R1_L	R4_L	R4_A	E40_A
Aleación	FeCrAl				Latón		Aluminio	
Espesor lamina (μm)	50		-		50		80	-
Dimensiones Ø x L (mm)	16 x 30		16 x 25,4		16 x 30			
Densidad de celda/poro	2360 cpsi	289 cpsi	40 ppi	60 ppi	2360 cpsi	289 cpsi	240 cpsi	40 ppi
Superficie geométrica (cm^2)	528	213	115[a]	159[a]	528	213	142	105[a]
Ke,a[b] (W/m·K)	4,0	1,6	-	-	28,8	11,5	22,0	-
Ke,r[b] (W/m·K)	3,4	1,9	0,6-0,9[c]	-	18,4	7,2	12,9	7,7-7,9[c]

[a] Información del fabricante
[b] Conductividad efectiva axial ($k_{e,a}$) y radial ($k_{e,r}$) calculadas (*ver Anexo A.3*)
[c] Dato tomado de bibliografía [47][48]

5.2.1.1. Propiedades de recubrimiento

Los sustratos metálicos fueron recubiertos por el método de recubrimiento por inmersión (o washcoating). En la *Figura 5.1.* pueden observarse imágenes de diferentes sustratos recubiertos, y los resultados del recubrimiento se presentan en la *Figura 5.2*.

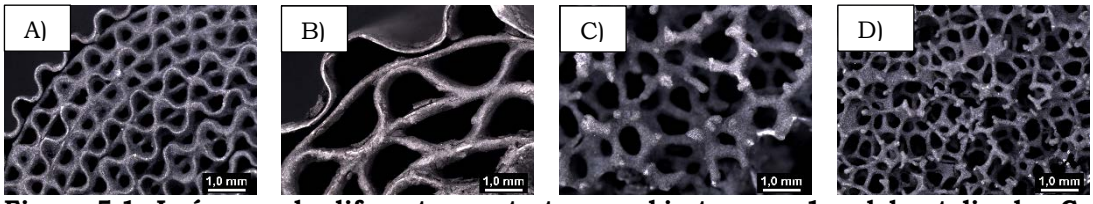

Figura 5.1. Imágenes de diferentes sustratos recubiertos con 1 g del catalizador C-Z_6,5%Al_2O_3: A) R1_F, B) R4_L, C) E40_F y D) E60_F

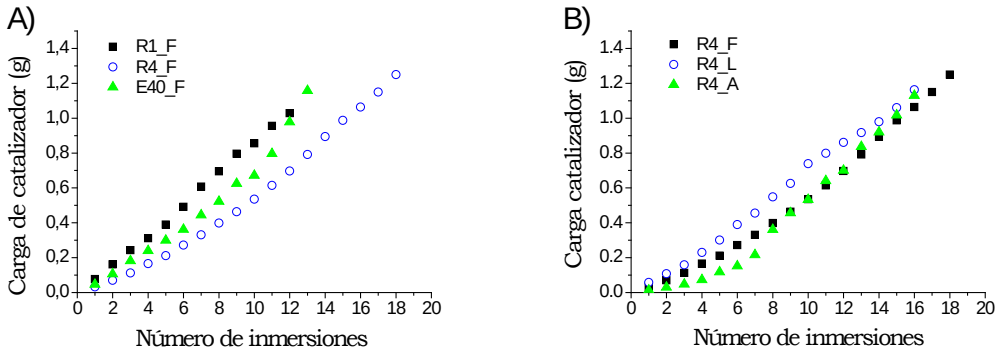

Figura 5.2. Proceso de recubrimiento de la suspensión C-Z_6,5%Al_2O_3 en A) sustratos de FeCrAl con diferente forma y B) sustratos de diferentes aleaciones.

Los resultados mostraron que para un mismo material (FeCrAl), debido a la diferente superficie geométrica y geometría del sustrato [41,49,50], el número de inmersiones o recubrimientos necesarios para depositar una misma carga de catalizador varía. Las espumas metálicas junto con los monolitos de 2390 cpsi permitieron depositar 1 g de catalizador con menor número de recubrimientos que un monolito de 289 cpsi (*Figura 5.2A*).

Por otro lado, se observó como el número de inmersiones requeridas para cargar una misma cantidad de catalizador depende poco de la aleación empleada (FeCrAl, aluminio o latón) (*Figura 5.1B*).

La adherencia de la capa catalítica en el sustrato metálico se determinó mediante la sonicación del catalizador estructurado en éter de petróleo. El valor de la adherencia se determinó mediante la cuantificación de la pérdida de peso de catalizador en el test. Los resultados se muestran en la *Tabla 5.2*, donde se puede observar unas buenas adherencias para todos los sustratos empleados. Además, se pudo observar una mejor adherencia para los monolitos de mayor densidad de celda y para las espumas debido a la geometría de los mismos, resultado también mostrado en numerosos estudios realizados en el grupo con diferentes catalizadores [49,41,50-52].

Tabla 5.2. Adherencia obtenida con el catalizador C-Z_6,5%Al_2O_3 sobre los diferentes sustratos estructurados

Muestra	Adherencia (%)
R1_F	91
R4_F	85
E40_F	98
E60_F	97
R1_L	93
R4_L	87
R4_A	80
E40_A	91

5.2.1.2. Propiedades físico-químicas

Los catalizadores estructurados fueron caracterizados por diferentes técnicas. Las principales propiedades fisicoquímicas se presentan en la *Tabla 5.3*.

Tabla 5.3. Propiedades fisicoquímicas de los catalizadores estructurados sobre diferentes sustratos

	Adsorción N_2			N_2O-RFC	H_2-TPR	
Muestra	Superficie BET (m^2/g)	V. total poros (cm^3/g)	Diámetro poro equivalente (nm)	Superficie metálica Cu (m^2/g_{CZA})	Consumo H_2 (cm^3/g_{CZA})	Reducibilidad (%)
Slurried	179	0,41	9,3	34,7	167	99
R1_F	180	0,48	10,6	31,2	181	107
R4_F	183	0,49	10,7	29,8	176	104
E40_F	174	0,46	10,5	28,8	166	98
E60_F	193	0,49	10,2	30,3	180	106
R1_L	181	0,43	9,5	29,8	177	105
R4_L	177	0,45	10,1	29,9	186	110
R4_A	174	0,52	11,9	29,0	172	101
E40_A	175	0,48	11,0	29,8	167	99

- **Propiedades texturales**

Las propiedades texturales de los catalizadores estructurados sobre diferentes soportes metálicos se midieron mediante adsorción de N_2. Las isotermas de

adsorción-desorción se muestran en la *Figura 5.3* y los resultados se presentan en la *Tabla 5.3*.

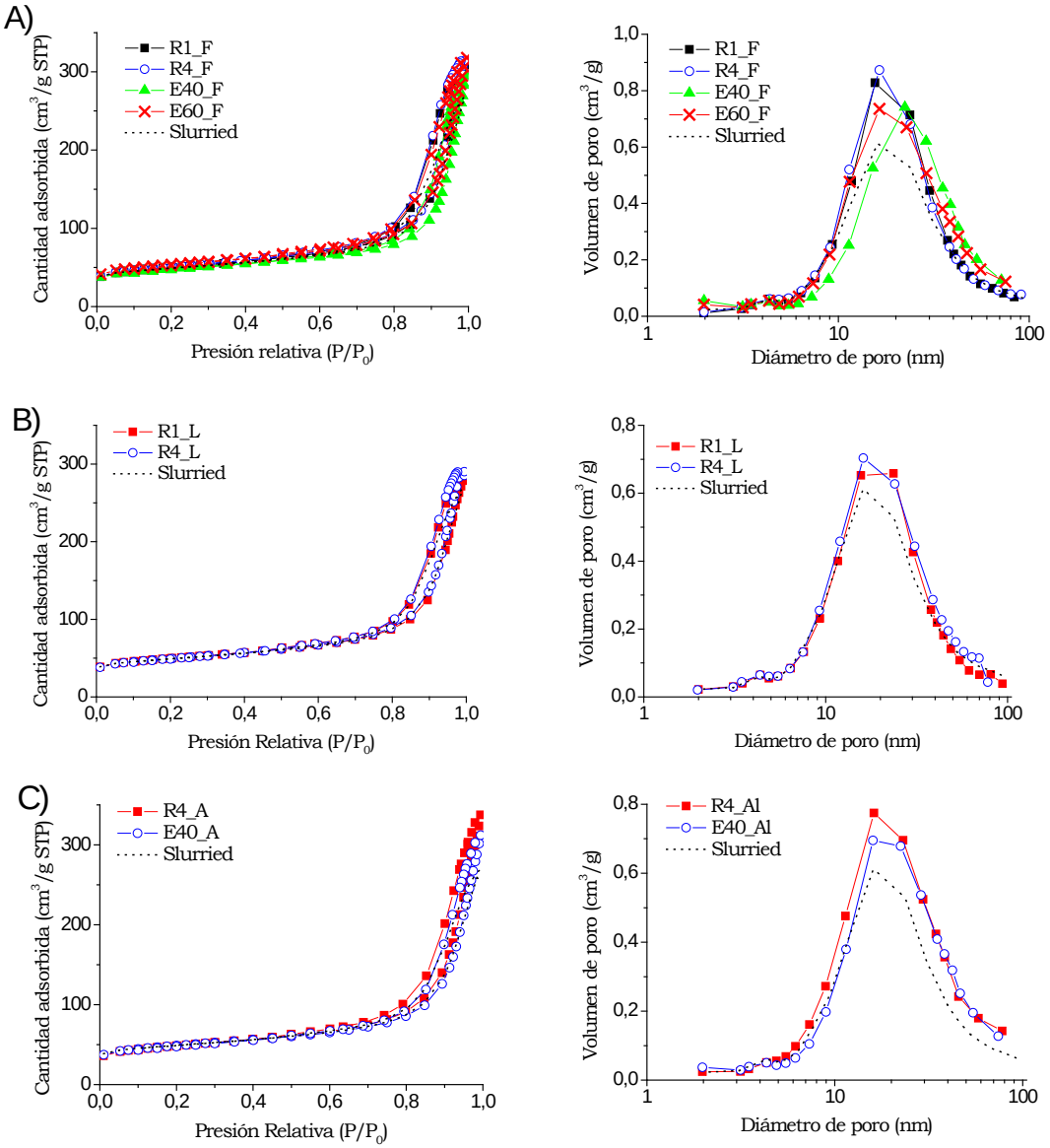

Figura 5.3. Isotermas de adsorción-desorción (izquierda) y distribución del tamaño de poro (derecha) del catalizador C-Z_6,5%Al_2O_3 depositado en diferentes sustratos metálicos A) FeCrAl B) Latón y C) Aluminio

Los resultados mostraron como la forma o geometría en los sustratos de la aleación FeCrAl no modificaba significativamente las propiedades texturales de la capa catalítica (*Figura 5.3A*), siendo similares a las del catalizador suspendido (slurried).

En cuanto a los monolitos de latón con diferente densidad de celda, se pudo observar el mismo comportamiento, dónde las propiedades texturales no se veían modificadas (*Figura 5.3B*). Del mismo modo, el monolito y la espuma de aluminio mostraron resultados similares (*Figura 5.3C*).

Por otro lado, la distribución de tamaño de poro tampoco se veía alterada por el empleo de un sustrato diferente, obteniéndose en todos los casos una distribución similar al catalizador suspendido o slurried (*Figuras 5.3*).

- **Superficie metálica de cobre**

La superficie metálica de cobre de los catalizadores estructurados se midió por cromatografía frontal reactiva de N_2O (N_2O-RFC). Los resultados se presentan en la *Tabla 5.3*.

Los catalizadores estructurados mostraron un ligero descenso de la superficie metálica de cobre con respecto al catalizador suspendido (*Tabla 5.3*). La forma y aleación de los sustratos estructurados, sin embargo, no mostró cambios significativos en los valores de superficie metálica de Cu.

- **Reducibilidad**

La reducibilidad de los catalizadores se midió mediante un análisis de temperatura programada de reducción con H_2 (H_2-TPR). El valor de reducibilidad se calculó a partir del volumen de H_2 consumido obtenido de la integración de la señal de TCD (previamente calibrada). Los resultados mostraron valores de reducibilidad similares al catalizador suspendido independientemente de la forma o aleación del sustrato empleado (*Tabla 5.3*). Además, el pico de reducción presentó su máxima temperatura alrededor de los 240 ºC en todas las muestras (*Figura 5.4*).

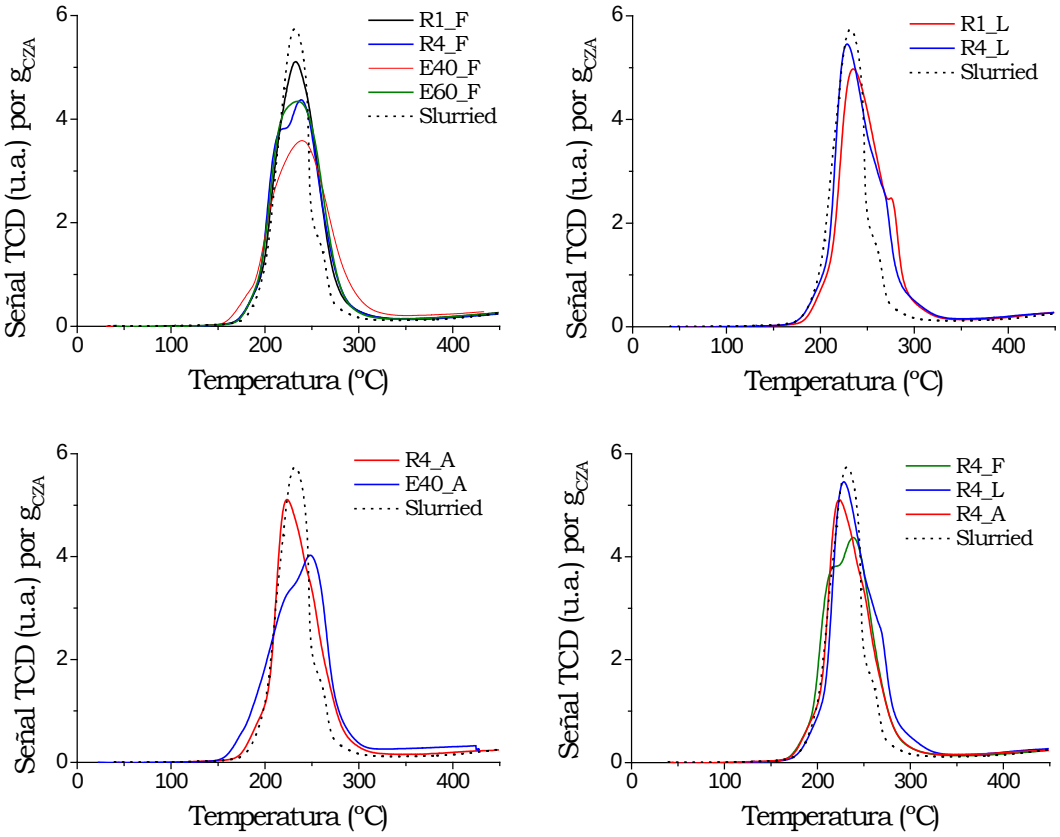

Figura 5.4. TPR del catalizador C-Z_6,5%Al_2O_3 en diferentes sustratos metálicos

Por otro lado, los sustratos metálicos sin recubrir también fueron analizados mediante H_2-TPR (*Figura 5.5*). Como se muestra en la Figura 5.5, el monolito de latón fue el único sustrato que mostró un consumo de hidrógeno apreciable en el rango estudiado. No obstante, este consumo no es significativo como para modificar la señal del sustrato recubierto. De este modo, podemos decir que las diferentes aleaciones estudiadas (FeCrAl, aluminio y latón) no afectan a la reducibilidad final del catalizador recubierto.

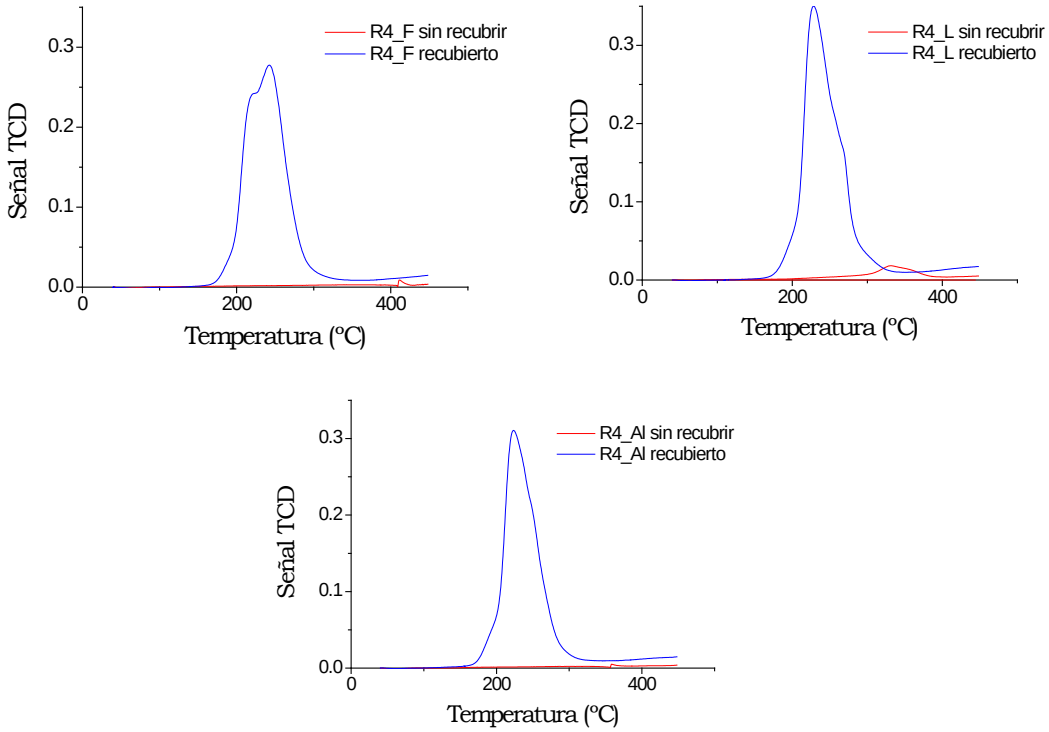

Figura 5.5. Resultados del H_2-TPR de los sustratos sin recubrir y recubiertos sobre las aleaciones estudiadas: a) FeCrAl, b) latón y c) aluminio

5.2.1.3. Test de actividad

La síntesis directa de DME se llevó a cabo en un reactor de Hastelloy® de 17 mm de diámetro interno a 260 ºC y 40 bar de presión. Durante estas medidas, también se monitorizó el perfil radial de los monolitos durante la reacción (*ver apartado 2.4.1 en capítulo 2*). Los resultados para una velocidad espacial de 1,7 L_{syn}/g_{cat}·h se muestran en la *Figura 5.6*. También se estudiaron diferentes velocidades espaciales para todos los casos y se presentan resumidos en la *Tabla 5.4*.

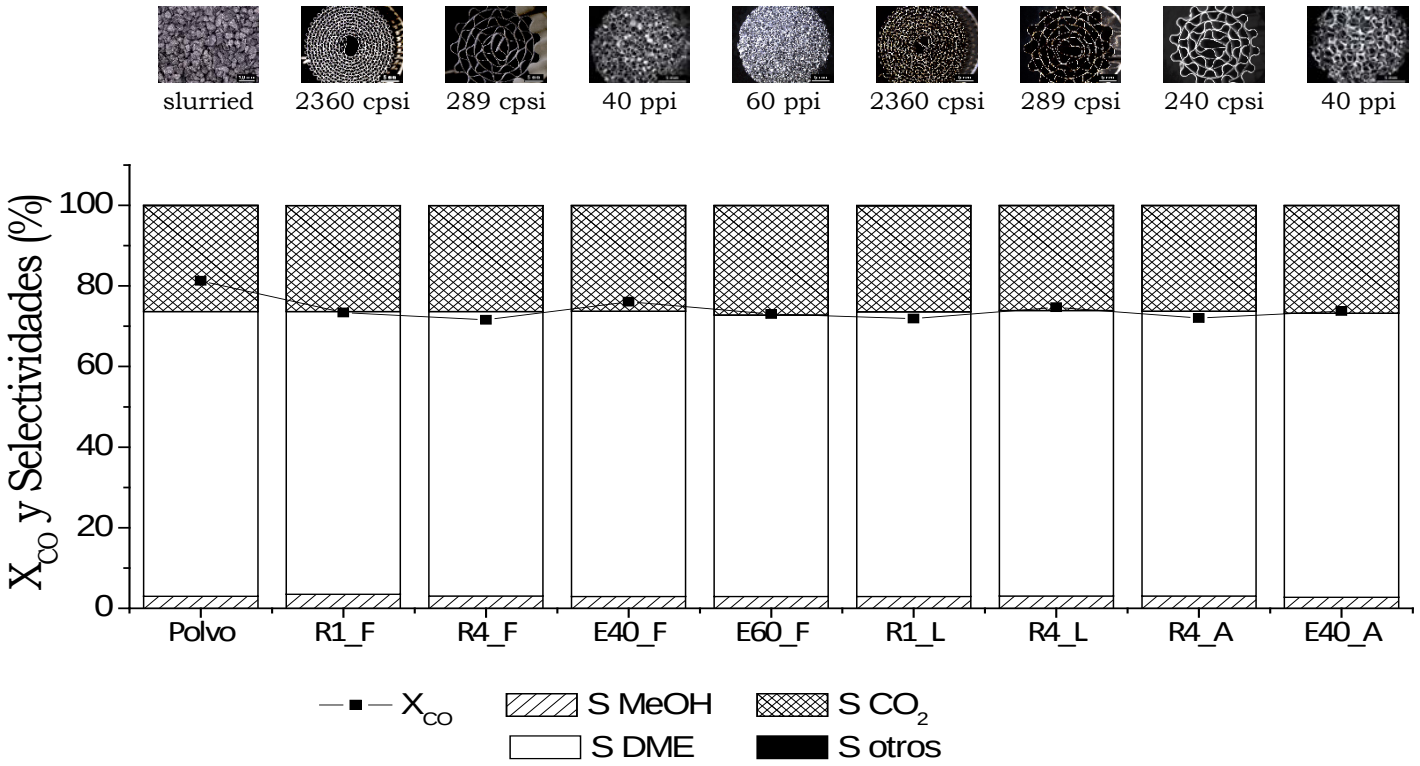

Figura 5.6. Resultados de conversión de CO y selectividad de los catalizadores estructurados (1 g) con diferentes sustratos para la síntesis directa de DME a 260 ºC, 40 bar y 1,7 L_{syn}/g_{cat}·h

Los resultados mostraron como la conversión de CO disminuía con el incremento de la velocidad espacial (*Tabla 5.4*). Sin embargo, las selectividades hacia los diferentes productos (DME, metanol, CO_2 e hidrocarburos ligeros) no se veía modificada con el cambio en la velocidad espacial.

Tabla 5.4. Datos de conversión de CO y selectividades obtenidas para la síntesis directa de DME a 260 ºC y 40 bar, a diferentes velocidades espaciales.

Muestra	Espesor nominal* (μm)	Velocidad espacial (L_{syn}/g_{cat}·h)	X_{CO} (%)	Selectividades (%)				ΔT_R [a] (ºC)
				MeOH	DME	CO_2	Otros	
Slurried	-	1,7	81,3	3,0	70,6	26,3	0,1	-
R1_F	19,9	1,7	75,5	3,1	70,7	26,1	0,1	1
		3,4	52,7	3,1	70,6	26,2	0,1	1
		6,8	26,6	3,5	70,7	25,7	0,1	2
R4_F	49,4	1,7	71,6	3,1	70,5	26,2	0,2	2
		3,4	52,2	3,3	70,3	26,3	0,1	2
		6,8	25,2	3,8	70,1	26,0	0,1	2
E40_F	91,6	1,7	76,1	3,3	70,6	26,0	0,1	0
		3,4	55,7	3,2	70,5	26,2	0,1	0
		6,8	30,5	3,5	71,0	25,3	0,2	0
E60_F	66,2	1,7	73,0	3,0	69,8	27,1	0,1	0
		3,4	51,3	3,0	69,5	27,4	0,1	0
		6,8	26,8	3,7	70,8	25,4	0,1	0
R1_L	19,9	1,7	71,9	2,9	70,7	26,3	0,1	2
		3,4	48,0	2,9	70,4	26,6	0,1	2
		6,8	24,0	3,3	71,7	24,9	0,1	2
R4_L	49,4	0,8	87,4	3,6	70,8	25,5	0,1	1
		1,7	75,8	3,6	71,1	25,2	0,1	2
		3,4	54,3	4,2	70,8	24,9	0,1	2
		6,8	30,0	4,0	69,2	26,6	0,2	2
R4_A	73,9	1,7	72,0	2,9	70,7	26,2	0.2	0
E40_A	99,8	1,7	73,8	2,8	70,5	26,6	0,1	0

*respecto a 1 g de catalizador

[a] ΔT_R= Temperatura centro monolito – Temperatura extremo monolito

Por otro lado, para una misma velocidad espacial (*Figura 5.5*), se observó un descenso de la conversión de CO en los catalizadores estructurados respecto al catalizador suspendido (slurried catalyst). Los catalizadores estructurados mostraron un descenso en la conversión de CO entorno al 7-13% con respecto al catalizador suspendido. No obstante, la forma y aleación de los sustratos estructurados no modificaron sensiblemente la conversión de CO y las selectividades obtenidas. Además, el gradiente de temperatura radial en todos los sistemas fue de 1-2 ºC.

5.2.2. Arquitectura del catalizador en los monolitos

En este apartado se estudió la disposición del catalizador en monolitos metálicos de latón de 289 cpsi. Se estudiaron 4 disposiciones o arquitecturas diferentes con 1 g de catalizador depositado, en las que se mantuvo la relación en peso CZA:HZSM-5 de 2:1 (*Figura 5.7*).

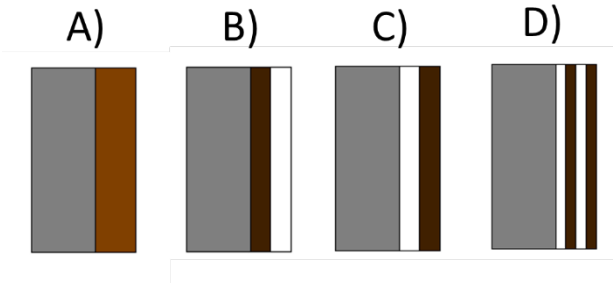

Figura 5.7. Esquema de las diferentes disposiciones estudiadas en el sustrato estructurado. Catalizador C-Z_6,5%Al_2O_3 (marrón claro), catalizador CZA_10%Al_2O_3 (marrón oscuro), zeolita ZSM-5_6%Al_2O_3 (color blanco) y sustrato metálico (color gris).

A) Mezcla en suspensión de los catalizadores (CZA + HZSM-5) con la formulación C-Z_6,5%Al_2O_3. Espesor de capa nominal de 50 µm.

B) Capa del catalizador HZSM-5 con la formulación HZSM-5_6%Al_2O_3 (0,333 g con un espesor de capa nominal de 18 µm) sobre una capa de catalizador de CZA con la formulación CZA_10%Al_2O_3 (0,667 g con un espesor de capa nominal de 32 µm).

C) Capa del catalizador CZA con la formulación CZA_10%Al_2O_3 (0,667 g con un espesor nominal de capa de 32 µm) sobre una capa del catalizador ácido HZSM-5 con la formulación HZSM-5_6%Al_2O_3 (0,333 g con un espesor de capa de 18 µm).

D) Disposición multicapa. 4 capas de catalizador en este orden (desde dentro hacia afuera) HZSM-5 (9 µm) + CZA (18 µm) + HZSM-5 (9 µm) + CZA (18 µm).

5.2.2.1. Propiedades de recubrimiento

Las diferentes suspensiones se recubrieron mediante el método de washcoating en monolitos de latón de 289 cpsi. El número de recubrimientos incrementó ligeramente cuando la capa del catalizador CZA está sobre la zeolita requiriendo mayor número de ciclos (*Tabla 5.5*).

Tabla 5.5. Adherencias de las diferentes arquitecturas

Muestra	Nº Recubrimientos	Adherencia (%)
A	15	87
B	16	85
C	22	90
D	23	86

La adherencia se midió mediante el cálculo de la pérdida en peso producida al someter a los catalizadores estructurados a una sonicación en éter de petróleo. Los resultados se presentan en la *Tabla 5.5*. Fueron obtenidas buenas adherencias para todas las disposiciones estudiadas de los catalizadores.

5.2.2.2. Propiedades físico-químicas

- **Propiedades texturales**

Las propiedades texturales tales como la superficie BET, el volumen total de poros y el diámetro de poro equivalente fueron medidos mediante adsorción de N_2 (*Figura 5.8*). Los resultados se presentan resumidos en la *Tabla 5.6*.

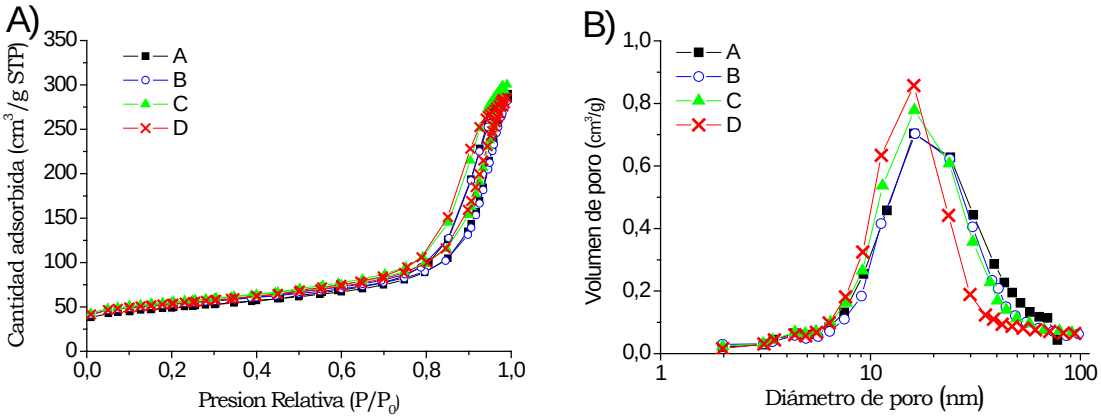

Figura 5.8. Isoterma de adsorción-desorción (A) y distribución del tamaño de poro (B) de las diferentes arquitecturas estudiadas en los monolitos

Tabla 5.6. Propiedades texturales de la capa catalítica de las diferentes arquitecturas

Muestra	Cantidad nominal depositada (g)	Superficie BET (m^2/g)	Volumen total de poro (cm^3/g)	Diámetro de poro equivalente (nm)
CZA__10%Al_2O_3	-	86	0,50	23,3
HZSM-5_6%Al_2O_3	-	371	0,25	2,7
C-Z_6,5%Al_2O_3	-	179	0,41	9,3
A	1	177	0,45	10,1
	2	185	0,46	10,1
B	1	192	0,44	9,0
	2	188	0,42	8,9
C	1	187	0,45	9,6
	2	182	0,40	8,8
D	1	193	0,44	9,1

Los resultados no mostraron diferencias relevantes en las propiedades texturales de las diferentes arquitecturas estudiadas. Además, una mayor carga de catalizador en el sustrato tampoco produjo cambios significativos.

- **Superficie metálica de cobre**

La superficie metálica de cobre se determinó mediante la técnica N_2O-RFC (*Tabla 5.7*). Los resultados mostraron valores similares entre las diferentes arquitecturas.

Tabla 5.7. Superficie de cobre y reducibilidad de los catalizadores depositados con diferentes arquitecturas

	N_2O-RFC	H_2-TPR	
Arquitectura	Superficie de Cu (m^2/g_{CZA})	Consumo de H_2 (cm^3/g_{CZA})	Reducibilidad (%)
A	29,9	186	110
B	28,5	169	100
C	28,9	167	99

- **Reducibilidad**

La reducibilidad se calculó mediante el consumo de H_2 producido por las muestras en un análisis de H_2-TPR (*Tabla 5.7*). Los resultados no mostraron cambios significativos en la reducibilidad, obteniéndose unos valores de reducibilidad completa del catalizador. Además, las diferentes arquitecturas mostraron una temperatura de reducción máxima de 230-240 °C (*Figura 5.9*)

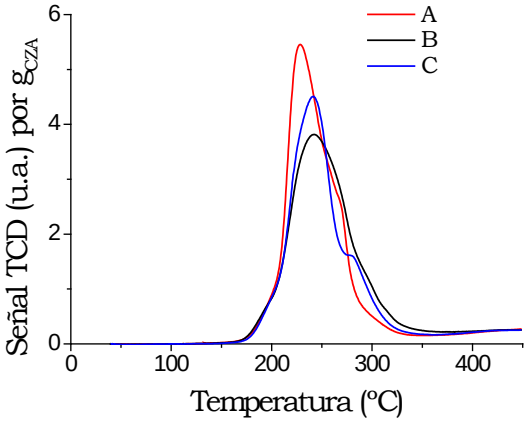

Figura 5.9. TPR de las diferentes arquitecturas estudiadas

5.2.2.3. Test de actividad

Las reacciones de síntesis directa de DME en sistemas estructurados se llevó a cabo a 260 ºC y 40 bar en un reactor de Hastelloy® de 17 mm de diámetro interno. Los resultados a dos velocidades espaciales diferentes con 1 g de catalizador depositado se muestran en la *Figura 5.10*.

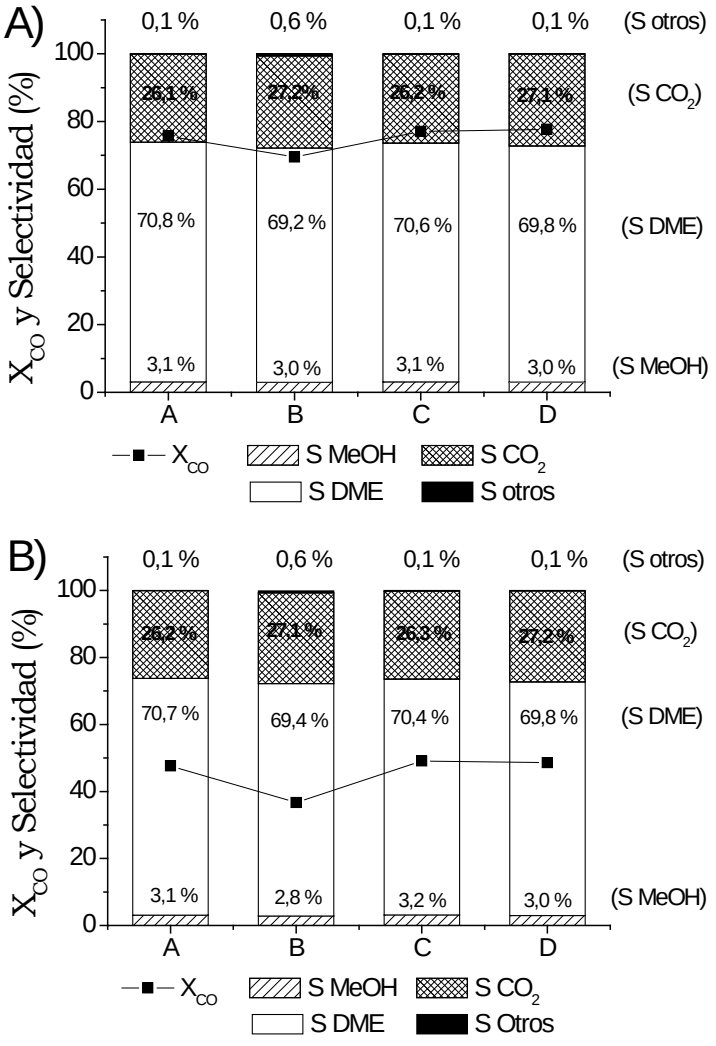

Figura 5.10. Resultados de actividad catalítica de los catalizadores estructurados (1 g de catalziador) con diferente arquitectura a 260 ºC, 40 bar con una velocidad espacial de A) 1,7 $L_{syn}/g_{cat}·h$ y B) 3,4 $L_{syn}/g_{cat}·h$

El catalizador estructurado con una capa de zeolita sobre una capa del catalizador CZA (B), mostró una disminución de la conversión de CO con respecto a la mezcla en suspensión C-Z_6,5%Al_2O_3 (A) anteriormente estudiada (*Figura 5.10*). Sin embargo, al cambiar la disposición de esas capas y localizando el catalizador de CZA sobre la capa de zeolita (C), la conversión de CO adquirió valores similares al de la mezcla en suspensión. Por otra parte, la disposición en multicapa (4 capas de los catalizadores en orden HZSM-5+CZA+HZSM-5+CZA) (D) mostró resultados de conversión de CO similares al de catalizador estructurado con 2 capas (C).

Los resultados mostraron este mismo comportamiento para las dos velocidades espaciales estudiadas, aunque con una conversión de CO inferior al emplear una velocidad espacial mayor (*Figura 5.10*). Además, la disminución de la conversión de CO observado en el caso B es más marcada cuanto mayor es la velocidad espacial.

Para todas las disposiciones estudiadas, no se apreciaron cambios significativos en la selectividad, salvo un ligero incremento de la selectividad a otros compuestos por parte de la arquitectura B (*Figura 5.10*).

También se estudió el efecto de duplicar la capa de catalizador (2 g catalizador) para las disposiciones A, B y C. Como se muestra en la *Figura 5.11*, el incremento del espesor de la capa depositada no modificó ni la conversión de CO ni las selectividades para los casos de la mezcla en suspensión (A) y la capa de catalizador CZA sobre la capa de zeolita (C). Sin embargo, la disposición del catalizador ácido sobre el catalizador CZA (B), mostró una reducción de la conversión de CO con el incremento de las capas de ambos catalizadores. Además, se observó un ligero aumento de la selectividad a otros compuestos (principalmente hidrocarburos ligeros) al aumentar las capas en esta última disposición (S_{otros}) de 0,6% a 1,2%.

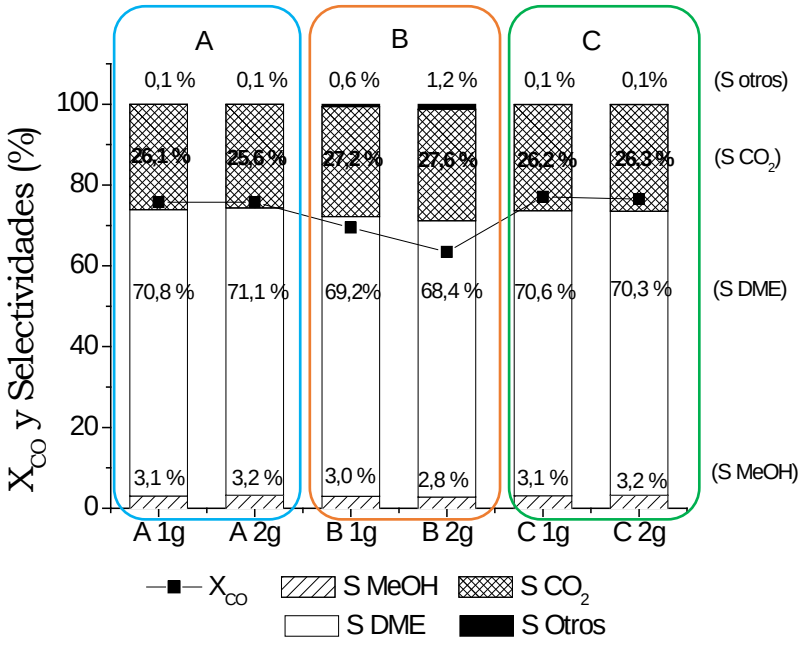

Figura 5.11. Resultados de conversión de CO y selectividad de diferentes arquitecturas de los catalizadores en el monolito con 1 g y 2 g de carga (diferente espesor) y velocidad espacial de 1,7 L_{syn}/g_{cat}·h

5.2.3. Intensificación con monolitos metálicos

En este apartado se estudiaron diferentes parámetros de la reacción con el fin de incrementar la productividad volumétrica de DME (intensificación):

- Variación de la carga volumétrica
- Variación de las condiciones de reacción
    - Velocidad espacial
    - Temperatura de reacción

5.2.3.1. Variación de la carga volumétrica

Monolitos de 289 cpsi (R4) de diferente aleación (FeCrAl y latón) fueron recubiertos con una carga nominal de 1 g (50 µm de espesor de capa) y 2 g de catalizador (100 µm de espesor de capa). Para ello, se empleó la formulación del catalizador C-Z_6,5%Al_2O_3 (*ver formulación en Capítulo 2*).

Los resultados presentados en la *Figura 5.12* muestran que la conversión de CO y selectividades a los diferentes compuestos no se ven sensiblemente modificados con el incremento de la cantidad de catalizador depositada, tanto para los monolitos de FeCrAl como de latón, duplicando la productividad volumétrica a DME al duplicar la carga en ambos sustratos metálicos (*Figura 5.12*).

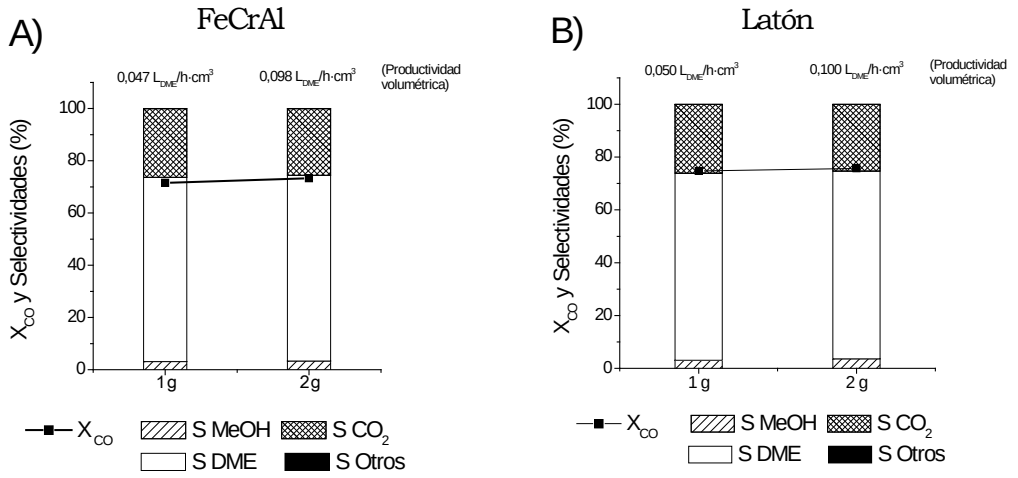

Figura 5.12. Resultados de actividad de catalizadores estructurados de A) Fecralloy® y B) latón con diferente carga y velocidad espacial de 1,7 L_{syn}/g_{cat}·h.

Por otro lado, con el fin de incrementar la carga volumétrica del catalizador en el sistema, determinados autores optan por rellenar los canales de los sustratos estructurados con catalizadores en polvo [44-46]. De este modo, en este estudio también se rellenaron monolitos de 289 cpsi de latón con el catalizador C-Z_6,5%Al_2O_3 (suspensión seca y calcinada y tamizada entre 300-500 µm). Se realizaron dos tipos de relleno:

- *3 g de catalizador*. El monolito metálico fue rellenado completamente con partículas del catalizador.

- *1 g de catalizador*. El monolito metálico fue rellenado con una mezcla de catalizador y carburo de silicio en relación 1:3.

La *Figura 5.13* muestra los resultados de actividad de los monolitos de latón rellenos con las partículas de catalizador. Los resultados muestran una disminución de la conversión de CO cuando el monolito está totalmente relleno con partículas del catalizador (3 g cat) con respecto a los monolitos recubiertos de la *Figura 5.12*. Sin embargo, las selectividades obtenidas fueron similares para los dos casos estudiados.

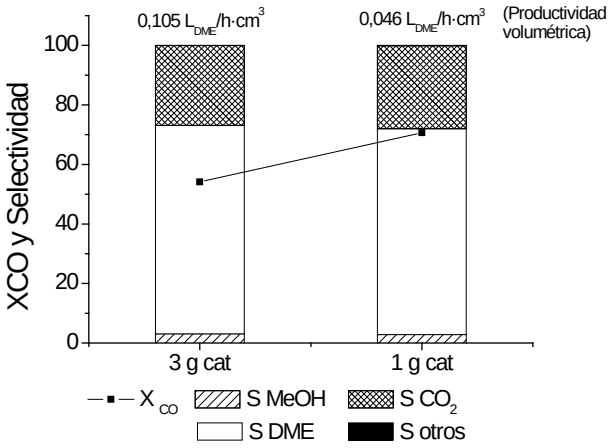

Figura 5.13. Resultados de actividad de monolitos de latón rellenos con el catalizador suspendido C-Z_6,5%Al_2O_3 y velocidad espacial de 1,7 L_{syn}/g_{cat}·h

Por otro lado, al rellenar con 1 g de catalizador diluido con SiC (1 g cat), se observó la misma conversión de CO y selectividad que en los monolitos recubiertos, con una productividad similar al del monolito recubierto con 1 g (*Figuras 5.12 y 5.13*).

En la *Figura 5. 14* se puede ver el comportamiento de la conversión de CO y la selectividad a DME frente al tiempo de reacción de los monolitos recubiertos y rellenos con catalizador en polvo. No se aprecian diferencias significativas en su

comportamiento frente al tiempo, lo que confirma la comparación basada en valores puntuales que se está haciendo.

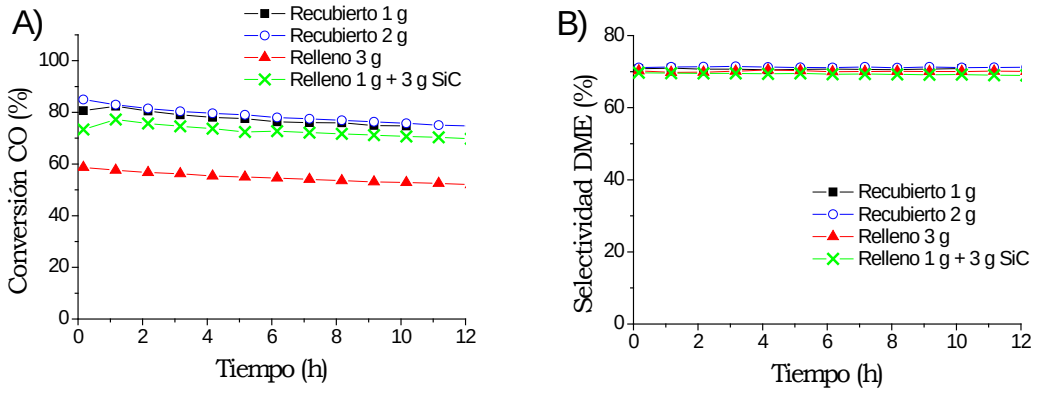

Figura 5. 14. Conversión de CO (a) y selectividad a DME (b) frente al tiempo de reacción. Condiciones de reacción: 260 ºC, 40 bar y 1,7 L_{syn}/g_{cat}·h

Los perfiles de temperatura radiales de los sistemas también fueron medidos, para ello se colocaron tres termopares en tres puntos del monolito (*ver sección 2.4.1 del Capítulo 2*). Los resultados, no mostraron cambios relevantes en los perfiles, pudiendo suponer un sistema isotermo tanto para los monolitos recubiertos como rellenos (*Figura 5.15*).

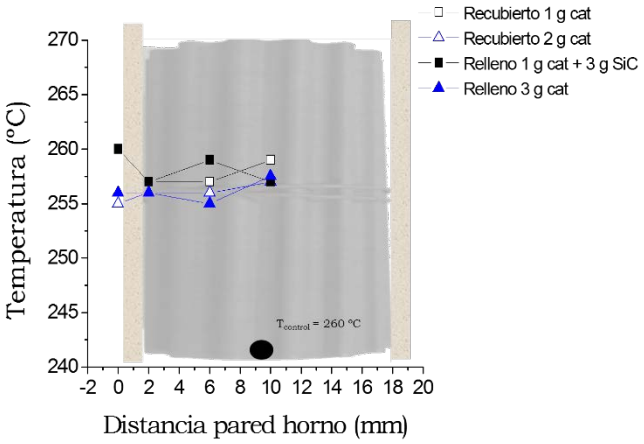

Figura 5.15. Perfil radial de temperatura en monolitos de 289 cpsi (R4) de latón recubiertos (símbolos huecos) y rellenos (símbolos sólidos)

5.2.3.2. Variación de las condiciones de reacción

Dos de los parámetros que afectan a las reacciones catalíticas fueron estudiados: la velocidad espacial y la temperatura de reacción empleada.

- **Velocidad espacial**

Diferentes velocidades espaciales fueron estudiadas a 260 °C y 40 bar de presión. Los resultados de actividad mostraron un descenso de la conversión de CO al aumentar la velocidad espacial (*Figura 5.16*). No se observaron cambios significativos en las selectividades de los compuestos.

La productividad a DME para las velocidades espaciales de 1,7 y 3,4 L_{syn}/g_{cat}·h presentan valores similares. No obstante, el empleo de una velocidad espacial de 0,85 L_{syn}/g_{cat}·h muestra una reducción de la productividad debido a que se trabaja en condiciones de limitación termodinámica.

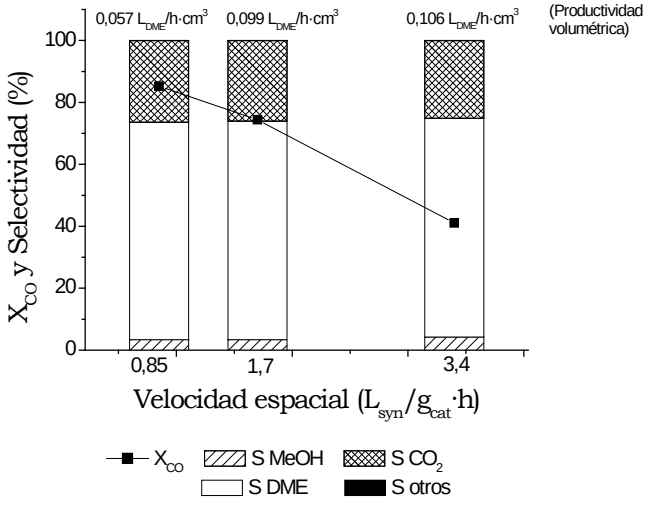

Figure 5.16. Resultados de actividad de catalizadores estructurados de latón (R4_L_2g) para la síntesis directa de DME a diferentes velocidades espaciales.

- **Temperatura de reacción**

Se estudiaron diferentes temperaturas de reacción para la síntesis directa de DME. Para ello, se seleccionó la mayor velocidad espacial estudiada anteriormente (3,4 L_{syn}/g_{cat}·h) y se recubrieron monolitos de 2 g de carga. Se llevaron a cabo siete experimentos independientes cada uno con un monolito fresco tomando los valores de conversión y selectividad a las 10 h de reacción donde los valores eran estables.

Los resultados catalíticos mostraron un aumento de la conversión de CO con la temperatura hasta los 300 ºC (*Figura 5.17*), temperatura a partir de la cual la conversión de CO disminuyó. Con ello, se pudo observar como la productividad volumétrica de DME incrementaba de la misma manera, alcanzando su máxima producción a 300 ºC.

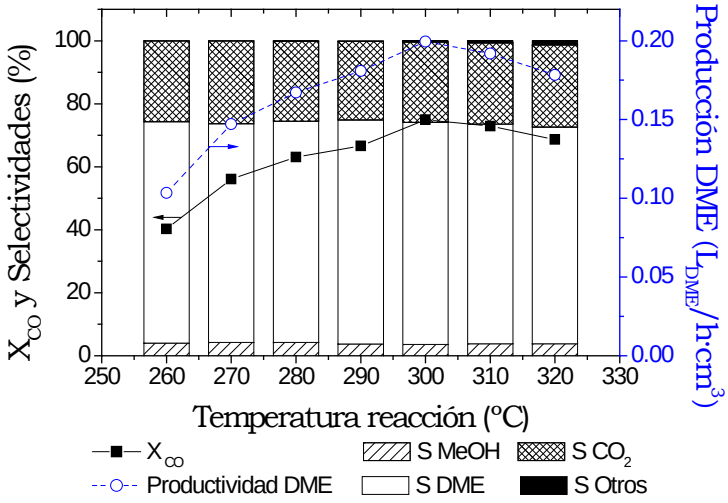

Figura 5.17. Resultados de conversión de CO, selectividad y productividad de DME para la síntesis directa de DME con 2 g de catalizador, a 40 bar y 3,4 Lsyn/gcat·h a diferentes temperaturas de reacción

Por otro lado, se observó una tendencia de crecimiento en los hidrocarburos formados (S Otros) con el incremento de temperatura. Como se muestra en la *Figura 5.18*, a partir de 300 ºC se aprecia un aumento exponencial de los hidrocarburos ligeros generados durante la reacción.

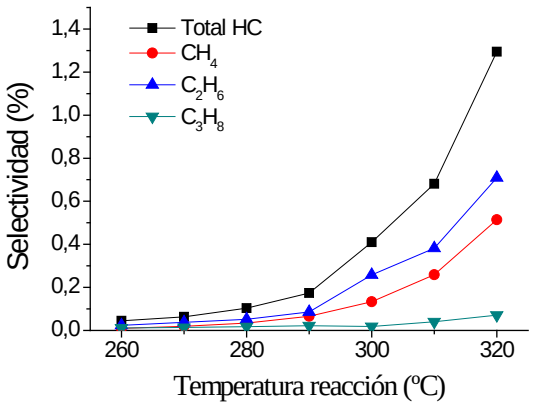

Figura 5.18. Resultados de selectividad a hidrocarburos ligeros en catalizadores estructurados de latón para la síntesis directa de DME con 2 g de catalizador, a 40 bar y 3,4 L_{syn}/g_{cat}·h a diferentes temperaturas de reacción

Finalmente, durante las reacciones de los catalizadores estructurados, también se monitorizó la temperatura radial dentro del monolito (*ver apartado 2.4.1 del Capítulo 2).* Los resultados mostraron un perfil prácticamente isotermo en todo el monolito, indistintamente de la temperatura de trabajo utilizada (*Figura 5.19*), viendo como la conductividad del latón fue suficiente para permitir un buen control de la temperatura en el sistema.

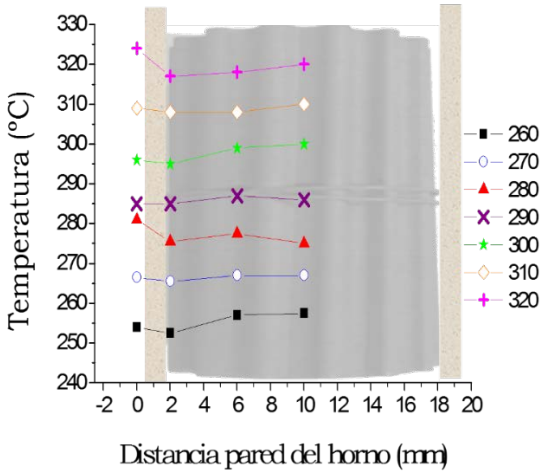

Figura 5.19. Perfil radial de los catalizadores estructurados de latón con 2 g de catalizador para la síntesis directa de DME con 2 g de catalizador, a 40 bar y 3,4 Lsyn/gcat·h a diferentes temperaturas de reacción

5.3. Discusión

5.3.3. Forma y aleación del sustrato estructurado

La estructuración del catalizador para la síntesis directa de DME en diferentes sustratos estructurados metálicos mostró valores similares de conversión de CO y selectividades a los diferentes compuestos (*Figura 5.5* y *Tabla 5.4*), aunque con una ligera bajada de la conversión de CO con respecto al catalizador suspendido (slurried) que puede estar relacionado con la disminución de la superficie metálica de Cu (*Tabla 5.3*).

Diferentes densidades de celda de los sustratos estructurados generan distintos espesores de capa para una misma carga de catalizador, pero espesores de capa catalítica elevados pueden generar problemas difusionales [6,7,38-40,42]. D. Merino *y cols*. [53] observaron como el incremento del espesor de capa suponía un descenso progresivo de la selectividad a hidrocarburos en la síntesis de Fischer-Tropsch, reacción conocida por presentar limitaciones difusionales con tamaños de partícula elevados [54,55]. Igualmente, F. Kaptjein *y cols*. [42] observaron también este efecto para la síntesis de Fischer-Tropsch en monolitos de cordierita y fijaron un espesor de capa máximo para evitar estas limitaciones de 50 μm, mientras que M.J. Stuts y D. Poulikakos [56] no observaron problemas difusionales con 70 μm de espesor en la oxidación parcial de metano en las condiciones estudiadas. Este efecto de restricciones difusionales con el espesor de capa catalítica ha hecho que otros autores tengan en consideración este parámetro y operen con bajos espesores de capas en otras reacciones. Así, B.M. Sollier *y cols*. [38] decidieron operar con 30 μm en el acoplamiento oxidativo de metano, mientas que S. Katheria *y cols*. [39] utilizaron espesores de 17 μm para evitar dicho efecto en el reformado de vapor de metano. Por otro lado, M.A. Ashraf *y cols*. [40] consiguieron operar sin limitaciones difusionales en el reformado con vapor de metano con espesores de capa de hasta 40 μm. En nuestro estudio, los diferentes sistemas estructurados permitieron depositar espesores de capa del catalizador comprendidos entre 20-100 μm sin que se observen limitaciones difusionales (*Tabla 5.4* y *Figura 5.5* y *5.12*). Sin embargo, cabe notar que un espesor de capa de 100 μm equivaldría a un tamaño de partícula esférica de 600 μm (*ver Anexo A.4*). Estos valores de tamaño de partícula son cercanos a los utilizados por determinados autores en la síntesis directa sin apreciar tampoco

problemas difusionales [57-59], permitiendo alcanzar así elevados espesores de capa sin detectar problemas de transferencia de materia.

La conductividad térmica de los materiales metálicos es varios órdenes de magnitud mayor a la de los catalizadores en polvo, lo que hace a estos sustratos interesantes para reacciones de elevada entalpía. Mientras que en un lecho fijo la transferencia de calor es controlada por convección (siendo la conducción despreciable), los sustratos estructurados aportan el mecanismo de conducción de calor a través de la matriz del material. Por lo tanto, cuanto mayor sea la conductividad del sustrato empleado, mayor será la transferencia de calor. La fracción hueca del sustrato también es un parámetro determinante en el proceso de transferencia de calor, ya que es complementaria de la fracción sólida o metálica que es la que conduce el calor (*Tabla 5.1*). E. Tronconi y G. Groppi [17-20] estudiaron el efecto de la fracción hueca y de la aleación metálica en sistemas estructurados proponiendo un modelo para determinar la conductividad térmica en función de su fracción hueca y la aleación metálica. En el mismo sentido, D. Merino *y cols*. [16], observaron como el empleo de monolitos de aluminio de 289 cpsi permitían un control adecuado del sistema en la síntesis de Fischer-Tropsch, mientras que similares monolitos de Fecralloy® producían un descontrol de la temperatura en el reactor, generándose un disparo térmico que impedía una operación adecuada. Esto es debido a la baja conductividad térmica del Fecralloy® respecto al aluminio. Pero este factor puede ser compensado aumentando la fracción sólida, como vieron D. Merino *y cols*. [16], que ocurría al aumentar la densidad de celda a 2360 cpsi con monolitos de Fecralloy®, lo que permitía un buen control de la temperatura.

En nuestro trabajo se han usado sustratos metálicos de alta y baja densidad de celda (2360 y 289 cpsi) de aleaciones con alta y baja conductividad térmica (latón y FeCrAl), así como monolitos de canales longitudinales paralelos y espumas de porosidad abierta (*Tabla 5.1*). En todos los casos se han observado mínimos gradientes de temperatura que indican un buen control térmico (*Tabla 5.4*).

Tabla 5.8. Calor generado en la síntesis directa de DME (ΔH= -246 KJ/mol DME) en monolitos con 1 g de carga

Muestra	Masa catalizador (g)	$T_{reacción}$ (ºC)	Velocidad espacial (L_{syn}/g_{cat}·h)	X_{CO} (%)	Calor generado (W)
R1_F	0,9073	260	1,7	75,5	0,39
R4_F	0,9840	260	1,7	71,6	0,40
E40_F	0,9087	260	1,7	76,1	0,40
E60_F	1,0296	260	1,7	73,0	0,43
R1_L	0,9268	260	1,7	71,9	0,38
R4_L	0,9319	260	1,7	75,8	0,40
	2,1228	260	1,7	75,7	0,92
	1,7546	300	3,4	75,0	1,51
R4_A	0,9305	260	1,7	72,0	0,39
E40_A	0,9087	260	1,7	73,8	0,39

Ahora bien, el calor generado en los monolitos de tamaño estándar (6 cm^3) en la síntesis de Fischer-Tropsch era superior en la mayoría de los casos a 0,9 W [16], mientras que en los sistemas estudiados en este trabajo para la síntesis directa de DME el calor generado para los diferentes sustratos oscila alrededor de 0,4 W (*Tabla 5.8*). Sólo dos experimentos superan claramente este valor, pero están realizados con monolitos de latón que son altamente conductores. Por lo tanto, en la síntesis directa de DME parece que el calor generado no es suficiente para producir diferencias en función de las diferentes conductividades de los sustratos estudiados (*Tabla 5.1 y 5.4*). Además, la mayor conductividad de los monolitos de latón permitió operar en condiciones más severas con un calor generado de hasta 1,5 W al variar parámetros como la masa de catalizador, velocidad espacial y temperatura, con un buen control de la temperatura también en esos casos.

Por otro lado, el empleo de espumas metálicas frente a los sustratos de canal longitudinal no mostró cambios significativos en la síntesis directa de DME (*Figura 5.5*). La tortuosidad característica de las espumas permiten una mejora en la transferencia de calor y materia [21,41]. F.J. Méndez *y cols*. [41] compararon monolitos de canal longitudinal con espumas de aluminio para la hidrogenación selectiva de 1,3-butadieno, y pudieron observar la ventaja de la geometría de la espuma frente a la de los monolitos de canal longitudinal, al mejorar la actividad

y selectividad al compuesto deseado. Esta misma mejora con el empleo de espumas metálicas frente a los monolitos metálicos también se observó en otras reacciones como la oxidación de tolueno [60], el reformado con vapor de metanol [11] y en la síntesis de Fischer-Tropsch [61,62], donde la conversión a CO incrementaba notablemente con el empleo de las espumas frente a los monolitos de canal longitudinal. Sin embargo, en la síntesis directa de DME, como se ha comentado anteriormente, no se observaron restricciones difusionales. Es probable que las espumas metálicas no muestren mejoras en la actividad catalítica en esta reacción, ya que son consideradas una buena alternativa para reacciones con una cinética rápida y que sufren ciertas limitaciones difusionales [63], cosa que no sucede en la síntesis directa de DME en las condiciones estudiadas.

5.3.4. Arquitectura de la capa catalítica

Las reacciones consecutivas de las que consta la síntesis directa de DME permiten desarrollar estructuras o arquitecturas tipo tándem, donde los catalizadores utilizados para cada reacción, se dispongan en el sustrato en capas independientes. De esta manera, con el estudio de diferentes arquitecturas tipo tándem en los monolitos (B, C y D de la *Figura 5.7*) se pudo estudiar el comportamiento de dicha reacción, al igual que compararla con la forma de depositar los catalizadores mediante su mezcla conjunta en una única suspensión (A). Los resultados mostraron como el rendimiento de la reacción variaba con alguna de la disposición empleada de los catalizadores (*Figura 5.10*).

La localización del catalizador ácido sobre la capa del catalizador de síntesis de metanol (B) mostró una bajada en la conversión de CO en comparación con la mezcla en suspensión de ambas fases (A) (*Figura 5.10*). Sin embargo, la disposición inversa de las capas (C, el catalizador de síntesis de metanol sobre la zeolita), presentó unos valores de conversión de CO similares al catalizador estructurado con la mezcla en suspensión de los catalizadores, al igual que ocurrió con la arquitectura multicapa estudiada (D). La diferencia del comportamiento mostrada por la configuración B respecto a las demás configuraciones fueron más marcadas cuanto mayor era la velocidad espacial, y por tanto, menor la conversión alcanzada (*Figuras 5.10B*).

Este comportamiento discrepa con el esperado para la disposición 'a priori' lógica, dónde ya que la reacción de deshidratación tiene lugar tras la síntesis de

metanol, parecería lógico localizar el catalizador ácido sobre la capa del catalizador de síntesis de metanol. De esta forma, tras producirse la reacción de síntesis de metanol, éste se deshidrataría a DME (*Figura 5.20 Arquitectura B*), lo que ha llevado a los estudios de catalizadores núcleo-corteza para la síntesis directa de DME a emplear esta disposición, es decir, el núcleo de catalizador de síntesis de metanol y la corteza de catalizador de deshidratación [29-33]. Sin embargo, G. Yang *y cols*. [30] observaron también como un catalizador de Cr/ZnO y ZSM-5 con esa disposición para la síntesis directa de DME sufría un descenso de la conversión con respecto a la mezcla física de ambos catalizadores. Estos autores sugieren dos posibles factores que podrían alterar el rendimiento de la reacción: una posible decoración de parte de los centros activos del Cr/ZnO al sintetizar la corteza de zeolita y posibles restricciones difusionales del gas de síntesis en la capa de zeolita.

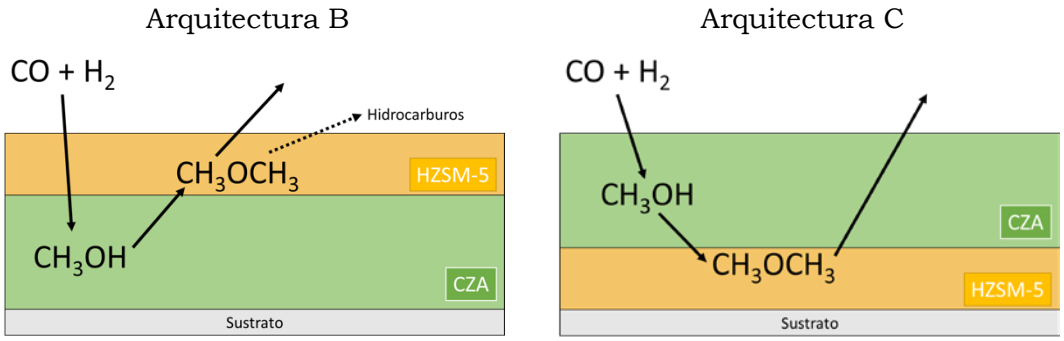

Figura 5.20. Esquema del concepto de la doble capa

Teniendo en cuenta que en nuestro trabajo no se apreciaron cambios en la superficie metálica de cobre para las diferentes arquitecturas (*Tabla 5.7*), el descenso de la conversión de CO en la arquitectura B (*Figura 5.10*) podría ser achacado a impedimentos difusionales por la capa de zeolita localizada en la parte exterior. Un análisis exhaustivo de las isotermas de adsorción no mostró cambios significativos entre las diferentes arquitecturas (*Figura 5.8* y *Tabla 5.6*). No obstante, al duplicar los espesores de capa en los catalizadores estructurados depositando el doble de carga, se observó cómo esa disminución de la conversión de CO se veía agravada (*Figura 5.11*). Estos problemas difusionales asociados al espesor de capa, también fueron observados para una estructura de doble capa

en monolitos de cordierita para las reacciones combinadas de la reducción catalítica selectiva de NOx y el almacenamiento y reducción de NOx (NSR-SCR) por U. de la Torre *y cols*. [64]. Un incremento del espesor de capa del catalizador Cu/Beta para la SCR, situado sobre otro de Pt-Ba/Al_2O_3 (catalizador NSR), suponía un descenso de la conversión de NOx al dificultar la llegada de los NOx a la capa inferior.

No obstante, la disposición inversa de las capas (*C en Figura 5.7*), donde el catalizador de CZA está sobre el catalizador ácido, no mostró cambios significativos con el aumento de espesor (*Figura 5.11*). En este caso, los reactivos (H_2 y CO) reaccionarían en la capa externa, generando únicamente metanol. Esta reacción no muestras problemas difusionales hasta valores de tamaño de partícula de milímetros [65], y como se vio en el *capítulo 3* tampoco mostró problemas difusionales en los catalizadores estructurados al comparar espesores de 20 a 50 μm. Del mismo modo, la arquitectura multicapa (*D en Figura 5.7*) no mostró cambios en la conversión (*Figura 5.10*). En este caso, al reducir el espesor de capa de la zeolita ZSM-5 a la mitad (9 μm) posiblemente se logre evitar los problemas de difusión anteriormente mencionados en la misma.

Por otro lado, cabe notar que la selectividad a otros compuestos secundarios incrementa al disponer la capa de zeolita sobre la de CZA (de 0,1% a 0,6%), y continúa incrementando con un mayor espesor de la capa (1,2%) (*Figura 5.11*). Como se muestra en la *Figura 5.20* la arquitectura B obligaría a los productos a recorrer toda la capa de catalizador ácido, lo que llevaría a favorecer la deshidratación de DME a hidrocarburos. Es por ello, por lo que la arquitectura con las capas localizadas de forma opuesta (capa de CZA sobre la zeolita) no generaría esa mayor productividad a estos compuestos indeseados al no forzar a los productos a pasar por el catalizador ácido (*Figura 5.20 Arquitectura C*).

5.3.5. Intensificación de monolitos metálicos

La variación de la carga volumétrica en los sustratos metálicos y las condiciones de operación, permiten incrementar la productividad volumétrica de DME en este tipo de sistemas. En este trabajo, se estudió la intensificación del proceso con monolitos de latón de 289 cpsi con el catalizador C-Z_6,5%Al_2O_3.

Un incremento de la capa catalítica, depositando el doble de catalizador en un mismo volumen, no mostró cambios relevantes ni en conversión de CO ni en

selectividades (*Figura 5.12*). De esta manera, la productividad volumétrica de DME se incrementó de 0,05 a 0,10 $L_{DME}/cm^3 \cdot h$ al duplicar la carga recubierta en el monolito (*Figura 5.12*). Esta carga volumétrica de 0,33 g/cm^3 es la máxima posible con estos sustratos, ya que cargas mayores comienzan a causar problemas de heterogeneidad con obstrucción de canales y pérdida de adherencia.

Otra alternativa al aumento de la carga volumétrica es el relleno de los monolitos con partículas de catalizador [1,28,44-46,], con lo que se pudo alcanzar una carga volumétrica de 0,5 g/cm^3 con partículas de 300-500 μm. Como se pudo observar, el hecho de rellenar un monolito completamente con el catalizador (3 g de catalizador) produjo un descenso de la conversión de CO entorno a un 25 % con respecto al monolito recubierto con 2 g usando la misma velocidad espacial (*Figuras 5.12B y 5.13*). Esta peor actividad no es debida a alteraciones del catalizador, ya que como se vio anteriormente la superficie metálica de cobre no se ve alterada (*Tabla 5.3*).

Otra posible causa de este comportamiento podría ser la exotermicidad de la reacción, que pudiera llegar a generar picos de temperatura que desactivaran el catalizador por sinterizado de cobre. Sin embargo, las curvas de conversión de CO frente al tiempo tampoco mostraron un comportamiento diferente (*Figura 5.14*), además de no observarse picos de temperatura a lo largo de todo el experimento (reducción y reacción) que pudieran provocar el deterioro del catalizador.

Por otro lado, el aumento de la carga de catalizador en los sistemas estructurados (para una misma velocidad espacial), suponen un aumento del caudal de gas alimentado. Este aumento de caudal podría generar una disminución de la temperatura de los gases a la entrada, como citan determinados autores, debido a un menor tiempo de residencia en el sistema de precalentamiento de los gases, generando un perfil axial [47,48,66]. Pero el perfil axial del sistema también depende de la exotermicidad de la reacción. L. Fratalocchi *y cols*. [67] estudiaron el efecto de una espuma metálica rellena con catalizador en la síntesis de Fischer-Tropsch (reacción exotérmica). Los resultados mostraron un perfil radial del sistema debido a un menor aporte de calor del horno (actuando como disipador de calor en vez de como fuente de calor). Además, ese menor aporte de energía del horno hace que los gases alimentados entren con menor temperatura, lo que hizo generar también un perfil axial a lo largo de la espuma metálica. En nuestro estudio, al disminuir la carga de catalizador en los monolitos rellenos, disponiendo 1 g de catalizador diluido en SiC, y por consiguiente alimentando el mismo caudal que en el monolito recubierto con 1 g de catalizador y mejorando la conductividad de los 'minilechos' al diluir el

catalizador con SiC, se observó que este monolito relleno recuperaba la conversión de CO con valores similares al recubierto (*Figura 5.12B y 5.13*). No obstante, en las medidas no se apreciaron cambios notorios en los perfiles radiales obtenidos para los diferentes casos con una variación de 2 ºC independientemente de la carga empleada (*Figura 5.15*). Del mismo modo, tampoco se observaron gradientes en el perfil axial estudiado (entre el punto de control situado a la salida del monolito, y el de medida situado a mitad de altura del monolito) que pudiesen justificar este cambio de actividad.

El análisis de todos estos resultados sobre la intensificación del proceso no arroja una conclusión clara que explique la pérdida de productividad cuando se llena el monolito con 3 g del catalizador en polvo. Parece que dicha pérdida de productividad no es debida al sinterizado del Cu por un mal control de temperatura y tampoco se observan gradientes significativos de temperatura ni radiales ni axiales que sugieran diferencias debidas a una falta de isotermicidad del lecho. Por tanto, será necesario incidir en un futuro próximo en este problema para encontrar una explicación satisfactoria.

Una vez incrementada la productividad con la carga volumétrica empleada, otra opción para continuar maximizando la producción de DME, es variando las condiciones de reacción. Como se muestra en la *Figura 5.15*, con unas velocidades espaciales de 3,4 $L_{syn}/g_{CZA}{\cdot}h$ se obtenían conversiones de CO lo suficientemente bajas para poder incrementar dicha conversión favoreciendo la cinética de la reacción con un aumento de la temperatura como se muestra en la *Figura 5.16*.

El aumento de la temperatura permitió incrementar la conversión de CO y por ende, la productividad volumétrica de DME hasta ~0,2 $L_{DME}/h{\cdot}cm^3$ a 300 ºC (*Figura 5.17*), temperatura a partir de la cual la conversión de CO comienza a disminuir debido a la termodinámica de la reacción [1,68]. Además, cabe notar que el incremento de la temperatura también supuso un incremento de la selectividad a hidrocarburos ligeros (*Figura 5.18*). Hay que tener en cuenta que la deshidratación del DME a hidrocarburos se agrava a elevadas temperaturas [69,70], particularmente a temperaturas superiores a 300 ºC [70-73]. En el proceso de deshidratación de metanol, las condiciones de operación y el catalizador empleado determinan la distribución de productos obtenida [70,74,75]. Por ejemplo, C.D. Chang *y cols*. [74,75], estudiaron diferentes condiciones que afectan a la deshidratación de metanol como la temperatura y la velocidad espacial empleadas, al igual que la relación SiO_2/Al_2O_3 del catalizador ácido. Este último parámetro afecta a la distribución de los hidrocarburos obtenidos (*Figura 5.21*), donde catalizadores con relación SiO_2/Al_2O_3 como el

empleado en este trabajo (relación SiO_2/Al_2O_3=23) generan más parafinas C_1-C_4, coincidiendo con los productos obtenidos en este trabajo.

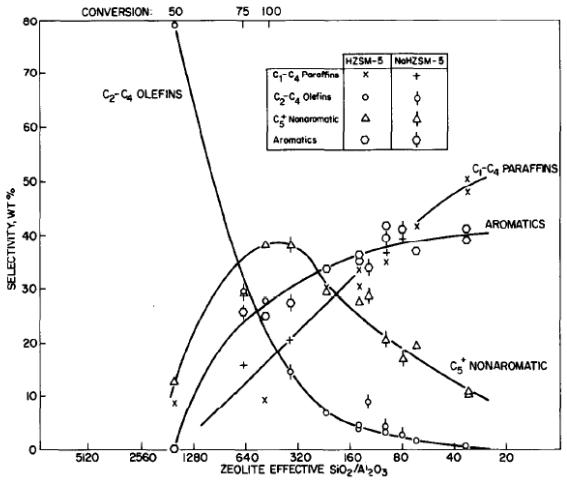

Figura 5.21. Distribución de la selectividad en la deshidratación de metanol a hidrocarburos con diferentes relaciones SiO_2/Al_2O_3 [74]

5.4. Conclusiones

Como se ha podido ver en este estudio, los catalizadores para la síntesis directa de DME han sido satisfactoriamente recubiertos en sustratos metálicos de diferente geometría y aleación, obteniendo unas buenas adherencias (>80%) en todos los casos, y con unos rendimientos en la reacción similares al catalizador suspendido (o slurried).

Además, mediante la preparación de diferentes espesores de capa se pudo comprobar que la reacción no muestra problemas de difusión en el rango estudiado (hasta 100 μm) y que las diferentes aleaciones metálicas (FeCrAl, latón y aluminio) proporcionan la conductividad suficiente para un buen control de temperatura en el sistema.

Por otro lado, el estudio de la arquitectura de la capa catalítica sobre el monolito, con las estructuras tipo tándem, permitió estudiar el comportamiento de la reacción frente a capas independientes de los catalizadores. En este trabajo se observó como la capa de zeolita (espesor ≥ 18 μm) genera problemas difusionales de los reactivos en las condiciones estudias disminuyendo la conversión a CO, siendo perjudicial su localización en la parte exterior (sobre la capa del catalizador CZA). Además, esta disposición también favorece la deshidratación del DME a hidrocarburos, incrementándose la producción a los mismos con el incremento del espesor de capa. Sin embargo, sorprendentemente la arquitectura de doble capa en la que el catalizador de CZA se encuentra sobre el catalizador ácido, mostró rendimientos similares a los de la mezcla en suspensión de ambas fases, permitiendo incluso incrementar el espesor de capa sin problemas difusionales ni cambios en la distribución de productos (DME, metanol y CO_2 principalmente).

Finalmente, se pudo aumentar la productividad volumétrica en los monolitos metálicos de latón doblando la cantidad de catalizador depositada y variando condiciones de reacción como la velocidad espacial y temperatura de reacción. Con el doble de carga y el doble de velocidad espacial en los monolitos de latón, la productividad volumétrica de DME pudo incrementarse 4 veces con respecto a los monolitos de partida (con 1 g de catalizador y 1,7 $L_{syn}/g_{cat}·h$), empleando una temperatura de reacción de 300 ºC. A partir de dicha temperatura la conversión se veía disminuida por la termodinámica de la reacción además de comenzar a incrementar la selectividad a compuestos indeseados (hidrocarburos).

5.5. Referencias

[1] F. Hayer, H. Bakhtiary-Davijany, R. Myrstad ,A. Holmena, P. Pfeifer, H.J. Venvik. *Chemical Engineering Journal* 167 (2011) 610-615.

[2] I. Sierra, J. Ereña, A.T. Aguayo, J.M. Arandes, J. Bilbao. *Applied Catalysis B: Environmental*, 94 (2010) 108-116.

[3] R. Peláez, E. Bryce, P. Marín, S. Ordóñez. *Fuel Processing Technology*, 179 (2018) 378-386.

[4] A. Ateka, P. Pérez-Uriarte, I. Sierra, J. Ereña, J. Bilbao, A.T. Aguayo. *Reaction Kinetics, Mechanisms and Catalysis*, 119 (2016) 655-670.

[5] P. Ávila, M. Montes, E. E. Miró. *Chemical Engineering Journal*, 109 (2005) 11-36.

[6] O.H. Laguna, M.I. Domínguez, M.A. Centeno, J.A. Odriozola. *New Material for Catalytic Applications* Capítulo 4. Ed. V.I. Parvulescu y E. Kemnitz (Elsevier) Amsterdam (2016) 81-120.

[7] O. Sanz, F.J. Echave, F. Romero-Sarria, J.A. Odriozola, M. Montes. *Renewable Hydrogen Technologies Production, Purification, Storage, Applications and Safety*. Capítulo 9. Ed. L.M. Gandía, G. Arzamendi y P.M. Diéguez (Elsevier) Amsterdam (2003) 201-224.

[8] C.G. Visconti, A. Montebelli, G. Groppi, E. Tronconi, S. Kohler. *Methanol: Science and Engineering*. Capítulo 19. Ed. A. Basile y F. Dalena (Elsevier) Amsterdam (2018) 519-538.

[9] A. Montebelli, C.G. Visconti, G. Groppi, E. Tronconi, S. Kohler, H.J. Venvik, R. Myrstad. *Applied Catalysis A: General* 481 (2014) 96-103.

[10] O. Sanz, S.A. Cruz, J.C. Millán, M. Montes, J.A. Odriozola. *Studies in Surface Science and Catalysis* 175 (2010) 661-664.

[11] F.J. Echave, O. Sanz, I. Velasco, J.A. Odriozola, M. Montes. *Catalysis Today* 213 (2013) 145-154.

[12] E. Tronconi, G. Groppi, T. Boger, A. Heibel. *Chemical Engineering Science* 59 (2004) 4941-4949.

[13] A. Egaña, O. Sanz, D. Merino, X. Moriones, M. Montes. *Industrial & Engineering Chemistry Research* 57 (2018) 10187-10197.

[14] G. Groppi, E. Tronconi, C. Cortelli, R. Leanza. *Industrial & Engineering Chemistry Research* 51 (2012) 7590-7596.

[15] Página Web: Continental Emitec GmbH disponible a Julio 2019 en www.emitec.com

[16] D. Merino, O. Sanz, M. Montes. *Chemical Engineering Journal* 327 (2017) 1033-1042.

[17] E. Tronconi, G. Groppi. *Chemical Engineering & Technology* 25 (2002) 743-750.

[18] G. Groppi, E. Tronconi. *Chemical Engineering Journal* 55 (2000) 2161-2171.

[19] G. Groppi, E. Tronconi. *Catalysis Today* 105 (2005) 297-304.

[20] C.G. Visconti, G. Groppi, E. Tronconi. *Chemical Engineering Journal* 223 (2013) 224-230.

[21] L. Giani, C. Cristiani, G. Groppi, E. Tronconi. *Applied Catalysis B: Environmental* 62 (2006) 121-131.

[22] Página Web: ERF materials & aerospace disponible a Julio 2019 en www.ergaerospace.com.

[23] A. Montebelli, C.G. Visconti, G. Groppi, E. Tronconi, C. Ferreira, S. Kohler. *Catalysis Today* 215 (2013) 176-185.

[24] F. Hayer, H. Bakhtiary-Davijany, R. Myrstad, A. Holmen, P. Pfeifer, H.J. Venvik. *Chemical Engineering and Processing* 70 (2013) 77-85.

[25] F. Hayer, H. BakhtiaryDavijany, R. Myrstad, A. Holmen, P. Pfeifer, H.J. Venvik. *Topics in Catalysis* 54 (2011) 817-827.

[26] F. Dadgar, R. Myrstad, P. Pfeifer, A. Holmen, H.J. Venvik. *Catalysis Letters* 147 (2017) 865-879.

[27] F. Dadgar, R. Myrstad, P. Pfeifer, A. Holmen, H.J. Venvik. *Catalysis Today* (2016) 76-84.

[28] J. Hu, Y. Wang, C. Cao, D. C. Elliot, D. J. Stevens, J. F. White, *Industrial & Engineering Chemistry Research* 44 (2005) 1722-1727.

[29] R. Nie H. Lei, S. Pan, L. Wang, J. Fei, Z. Hou. *Fuel* 96 (2012) 419-425.

[30] G. Yang, M. Thongkam, T. Vitidsant, Y. Yoneyama, Y. Tan, N. Tsubaki. *Catalysis Today* (2011) 229-235.

[31] G. Yang, N. Tsubaki, J. Shamoto, Y. Yoneyama, Y. Zhang. *Journal of the American journal society* 132 (2010) 8129-8136).

[32] Y. Wang, W. Wang, Y. Chen, J. Ma, R. Li. *Chemical Engineering Journal* 250 (2014) 248-256.

[33] R. Phienluphon, K. Pinkaew, G. Yang, J. Li, Q. Wei, Y. Yoneyama, T. Vitidsant, N. Tsubaki. *Chemical Engineering Journal* 270 (2015) 605-611.

[34] Y. Liu, M.P. Harold, D. Luss. *Applied Catalysis B: Environmental* 121-122 (2012) 239-251.

[35] P.S. Metkar, M.P. Harold, V. Balakotaiah. *Applied Catalysis B: Environmental* 111-112 (2012) 67-80.

[36] Y. Liu, R. Farrauto, A. Lawal. *Chemical Engineering Science* 89 (2013) 31-39.

[37] A.I. Stankiewicz, J.A. Moulijn. Proce*ss Intensification: Transforming Chemical Engineering.Chemical Engineering Progress* 96 (2000) 22-34.

[38] B.M. Sollier, L.E. Gómez, A.V. Boix, E.E. Miró. *Applied Catalysis A: General* 550 (2018) 113-121.

[39] S. Katheria, G. Deo, D. Kunzru. *Applied Catalysis A: General* 570 (2019) 308-318.

[40] M.A. Ashraf, O. Sanz, M. Montes, S. Specchia. *Intenational Journal of Hydrogen Energy* 43 (2018) 11778-11792.

[41] F.J. Méndez, O. Sanz, M. Montes, J. Guerra, C. Olivera-Fuentes, S. Curbelo, J.L. Brito. *Catalysis Today* 289 (2017) 151-161.

[42] F. Kapteijn, R.M. de Deugd, J.A. Moulijn. *Catalysis Today* 105 (2005) 350-356.

[43] A. M. Hilmen, E. Bergene, O.A. Lindvag, D. Schanke, S. Eri, A. Holmen. *Catalysis Today* 150 (2005) 357-361.

[44] B. Kaskes, D. Vervloet, F. Kapteijn, J.R. van Ommen. *Chemical Engineering Journal* 283 (2016) 1465-1483.

[45] C.G. Visconti, G. Groppi, E. Tronconi, *Catalysis Today* 273 (2016) 178-186.

[46] E. Tronconi, G. Groppi, C.G. Visconti. *Current Opinion in Chemical Engineering* 5 (2014) 55-67.

[47] E. Bianchi, T. Heidig, C.G. Visconti, G. Groppi, H. Freund, E. Tronconi. *Catalysis Today* 216 (2013) 121-134.

[48] E. Bianchi, T. Heidig, C.G. Visconti, G. Groppi, H. Freund, E. Tronconi. *Chemical Engineering Journal* 198-199 (2012) 512-528.

[49] Ion Velasco Ortiz. *Tesis doctoral* (2015). Universidad del País Vasco (UPV/EHU).

[50] S.A. Regenhardt, C.I. Meyer, O. Sanz, V. Sebastian, S. Ivanova, M.A. Centeno, J.A. Odriozola, M. Montes, A.J. Marchi, T.F. Garetto. *Molecular Catalysis*. https://doi.org/10.1016/j.mcat.2018.10.014 (In Press).

[51] L.C. Almeida, F.J. Echave, O. Sanz, M.A. Centeno, G. Arzamendi, L.M. Gandía, E.F. Sousa-Aguiar, J.A. Odriozola, M. Montes. *Chemical Engineering Journal* 167 (2011) 536-544.

[52] P. Brussino, J.P. Bortolozzi, O. Sanz, M. Montes, M.A. Ulla, E.D. Banús. *Catalysts* 8 (2018) 291-301.

[53] D. Merino, O. Sanz, M. Montes. *Fuel* 210 (2017) 49-57.

[54] E. Iglesia, S.C. Reyes, R.j. Madon, S.L. Soled. *Advances in catalysis*, 39 (1993) 221-302.

[55] D. Merino, I. Pérez-Miqueo, O. Sanz, M. Montes. *Topics in catalysis* 29 (2016) 207-218.

[56] M.J. Stutz, D. Poulikakos. *Chemical Engineering Science* 63 (2008) 1761-1770.

[57] F. Song, Y. Tan, H. Xie, Q. Zhng, Y. Han, *Fuel processing technology* 126 (2014) 88-94.

[58] K. Sun, W. Lu, M. Wang, X. Xu. *Catalysis communications* 5 (2004) 367-370.

[59] J.L. Li, X.-G. Zhang, T. Inui. *Applied catalysis A: General* 147 (1996) 23-33.

[60] O. Sanz, L.C. Almeida, J.M. Zamaro, M.A. Ulla, E.E. Miró, M. Montes. *Applied Catalysis B: Environmental* 78 (2008) 166-175.

[61] Ane Egaña Agote. *Tesis doctoral* (2018) Universidad del País Vasco (UPV/EHU).

[62] David Merino Bella. *Tesis Doctoral* (2016) Universidad del País Vasco (UPV/EHU).

[63] M.V. Twigg, J.T. Richardson. *Studies in surface science and catalysis* 91 (1995) 345-359.

[64] U. de la Torre, M. Urrutxua, B. Rereda-Ayo, J.R. González-Velasco. *Catalysis Today* 273 (2016) 72-82.

[65] G.H. Graaf, H. Scholtens, E.J. Stamhuis, A.A.C.M. Beenackers. *Chemical Engineering Science* 45 (1990) 773-783.

[66] C.G. Visconti, G. Groppi, E. Tronconi. *Catalysis Today* 273 (2016) 178-186.

[67] L. Fratalocchi, C.G. Visconti, G. Groppi, L. Lietti, E. Tronconi. *Chemical Engineering Journal* 349 (2018) 829-837.

[68] T. Ogawa, N. Inoue, T. Shikada, Y. Ohno. *Journal of Natural Gas Chemistry* 12 (2003) 219-227.

[69] A. García-Trenco, A. Vidal-Moya, A. Martínez. *Catalysis Today* 179 (2012) 43-51.

[70] J.J. Spivey. *Chemical Engineering Communications* 110 (1991) 123-142.

[71] F.J. Keil. *Microporous and Mesoporous Materials* 29 (1999) 49-66.

[72] G. Qi, Z. Xie, W. Yang, S. Zhong, H. Liu, C. Zhang, Q. Chen. *Fuel Processing Technology* 88 (2007) 437-441.

[73] J. Liu, C. Zhang, Z. Shen, W. Hua, Y. Tang, W. Shen, Y. Yue, H. Xu. *Catalysis Communications* 10 (2009) 1506-1509.

[74] C.D. Chang, C.T-W. Chu, R.F. Socha. *Journal of catalysis* 86 (1984) 289-296.

[75] C.D. Chang, A.J. Silvestri. *Journal of Catalysis* 47 (1977) 249-259.

CHAPTER 6

In a way of new Cu-based catalyst

for direct synthesis of DME

INDEX

6.1. Introduction

The need of two active phases in the direct synthesis of DME (methanol synthesis catalyst and dehydration catalyst) has driven the search of different ways of catalysts preparation to improve the performance in activity, selectivity and stability of the catalyst. As previously said, the role of the contact between phases was one of the parameters that researchers tried to elucidate [1-5]. Despite physical mixture is the common method of hybrid catalysts preparation [6-10], trying to maximize the metal dispersion (which controls of the activity in the reaction), G.R. Moradi *et al.* [4] reported a novel catalyst preparation for the direct synthesis of DME by the so-called sol-gel impregnation method, which showed high Cu dispersion. Different preparation methods were studied favouring high copper dispersion and a closer contact between components of the catalyst such as co-precipitation sedimentation, co-precipitation impregnation, sol-gel method, etc.

New catalysts designs based on encapsulation were also proposed in bibliography for direct synthesis of DME, specially, core-shell systems. These designs of a metal core surrounded by an acid catalyst shell present the possibility to separate the two active phases and, in general, protecting the metal core from deactivation by poisoning, coke deposition or sintering [11-13]. For example, H. Yang *et al.* [12] showed a good stability to sintering in the reduction as well as in the reaction step of Cu and CuZn particles encapsulated on SiO_2. However, the hydrothermal conditions and reagents used to synthesise the acid catalyst shell could deactivate the methanol synthesis catalyst, especially, those based in copper [14-17]. Thus, some authors (such as R. Phienluphon *et al.* [16], K. Pinkaew *et al.* [18] or M. Sánchez-Contador *et al.* [17]) developed a new way of preparing core-shell of $Cu/ZnO/Al_2O_3$ and SAPO-11 without hydrothermal treatment by using silica sol as adhesive between them.

On the contrary, other authors have oriented their work on ordered mesoporous material as an alternative to encapsulate copper particles [19-21]. The high surface area of these supports and the tailored ordered pores give the possibility to confine metal oxides in these pores with high metal dispersion [22-24]. X. Guo *et al.* [19] were managed to prepare copper particles highly dispersed in the mesoporous of SBA-15 with high load (up to 50%). In addition, the minimization of particles aggregation or sintering due to the encapsulation in narrow pores makes this a promising method of catalysts preparation. Thus, A. García-Trenco *et al.* [21], showed the better stability of this type of catalyst mixed

with ZSM-5 zeolite for the direct synthesis of DME than the most frequent $Cu/ZnO/Al_2O_3$+HZSM-5 catalytic system.

In this chapter, the results obtained in a 3 month-stay collaboration with Prof. Andrei Khodakov (Université de Lille - France) are presented. In this group, new ways of preparing bifunctional catalysts are being developed last years. They lead to highly dispersed metal particles in an acid matrix such as zeolites by encapsulating metal particles. Good results were obtained with cobalt, nickel and magnesium encapsulation in ZSM-5 zeolite by using CNT's impregnated with these metals as sacrificial template for producing additional porosity during the zeolite crystallization [25,26]. After synthesis, the organic templates (the one used to induce the structure of the zeolite and the one used to produce additional meso/macro pores) are removed from the zeolite structure by a heat treatment and new macro/mesoporosity is created, giving rise to a hierarchical porous structure with interconnected micro and meso/macropores. By dispersing a metal in the organic template before the zeolite growth, the metal particles can be dispersed in the zeolite structure and located in the porosity that the template produces when it is removed.

On the other hand, water-in-oil microemulsion also attracts great interest in this group. With this method, metal nanoparticles can be created in the micelles. Thus, the size of the micelles, and consequently, size of the metal particles, can be controlled by the emulsion preparation [27,28] achieving small particles of metal [29,30]. Later, a layer of silica can be growth around the particles, the so-called nanoreactors [27,31]. Due to their specific structure (core-shell-like structure), nanoreactors may present excellent catalyst stability preventing from metal aggregation or sintering [27,31]. Furthermore, the thickness of the shell could be also a control tool for selectivity. V. Subramanian *et al.* [31], who studied these systems in Fischer-Tropsch synthesis, showed a limitation of the hydrocarbons chain growth by the nanoreactor diameter. Therefore, the group cited this method as an important tool for efficient control of activity, selectivity and stability in this reaction.

In the presented work, different copper encapsulation synthesis methods were explored: namely, sacrificial template, carbon spheres, copper nanorector and copper confinement in SBA-15.

These methods of synthesis are in many cases elaborated and expensive, allowing small amounts to be obtained in most of the recipes used. This clashes

frontally with the objective of this thesis which is the preparation of structured systems for which significant amounts of sample are required as a starting point for the structuring study. Therefore, the samples that have been obtained have been subjected to basic characterizations that allow exploring their eventual interest in structuring. Only the most promising samples have been further characterized and their catalytic properties have been explored.

Samples were characterised by different techniques such as N_2 adsorption and XRD. In addition, the most interesting catalysts were also tested in the DME synthesis reactions.

6.2. Results

In this section, the results of the different methods of copper encapsulation studied were presented. Textural properties and crystallinity were analysed for each method following the different steps of synthesis. Then, the activity of some synthesised catalysts were tested for methanol synthesis or direct synthesis of DME reaction, and some physicochemical properties were measured, such as reducibility and copper metallic surface area.

The samples were referred to as:

- Sacrificial template method: ZSM-5 zeolite was referred to as xZSM-5, in which 'x' is the zeolite form: Na or H (sodium or proton form respectively). If the zeolite was synthesised with CNT's as sacrificial porosity template, the sample was referred to as NaZSM-5 with the size in nm of CNT's in brackets (NaZSM-5 (10-20) or NaZSM-5 (20-40)).

  Copper was introduced by two methods:

  - The conventional incipient wetness impregnation in the zeolite explained before (crystallized with and without CNT's). The samples were referred to as with a forward slash: Cu/NaZSM-5, Cu/NaZSM5 (10-20) or Cu/NaZSM-5 (20-40)
  - The sacrificial template method. The zeolite was crystallized in the presence of CNT's impregnated with copper. The samples were

referred to as Cu@xZSM-5 with the size in nm of CNT's size in brackets: Cu@xZSM-5 (10-20) and Cu/xZSM-5 (20-40)

- Carbon spheres: Samples prepared with this method were referred to as Cu@C_NaZSM-5 or Cu@C_HZSM-5 depending on the zeolite form (sodium or proton form respectively)

- Copper nanoreactors: Copper nanoreactors with silica were referred to as Cu@SiO_2. After zeolite growth the sample was referred to as Cu@SiO_2_NaZSM-5 and Cu@SiO_2_HZSM-5 when the zeolite was in sodium and proton form respectively.

- Confinement of copper in SBA-15: Copper and zinc were confined in mesoporous structures. The samples were referred to as CuZn/SBA-15 for SBA-15 support and CuZn/Al-SBA-15 for modified SBA-15 support with aluminium.

6.2.1. Sacrificial Template

The sacrificial template method consists of using CNT's impregnated with copper as sacrificial template in the zeolite crystallization. A detailed description of the preparation method can be found in *section 2.2.1.3.2* of *chapter 2* (page 42). The samples were studied by characterising their textural properties and crystallinity. The results are summarised in *Table 6.1*.

Table 6.1. Textural properties and crystal size of samples prepared by sacrificial template with CNT

Sample	BET surface area (m^2/g)	Total pore volume (cm^3/g)	Micropore volume (cm^3/g)	Cu0 crystal size (nm)*
NaZSM-5	417	0.18	0.17	-
NaZSM-5 (10-20)	435	0.20	0.17	-
NaZSM-5 (20-40)	440	0.21	0.19	-
Cu/NaZSM-5	353	0.16	0.15	24
Cu/NaZSM-5 (10-20)	369	0.17	0.15	20
Cu/NaZSM-5 (20-40)	348	0.16	0.14	25
Cu@NaZSM-5 (10-20)	363	0.17	0.14	33
Cu@NaZSM-5 (20-40)	394	0.20	0.15	30
Cu@HZSM-5 (10-20)	401	0.20	0.16	29
Cu@HZSM-5 (20-40)	433	0.22	0.14	34
HZSM-5	405	0.19	0.17	-

* Measured by XRD

- **Textural properties**

Textural properties of the samples were measured by N_2 adsorption. All the samples presented a type I isotherm, which is characteristic of microporous samples (*Table 6.1* and *Figures 6.1-6.2*).

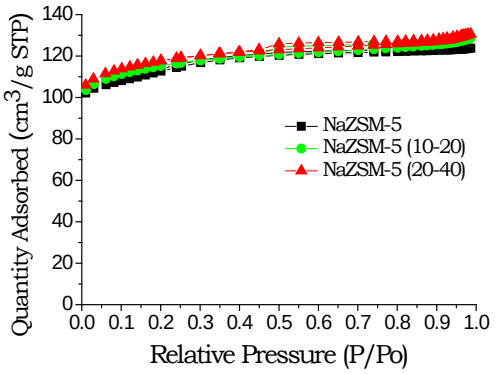

Figure 6.1. N_2 isotherms of the zeolites prepare with and without CNT

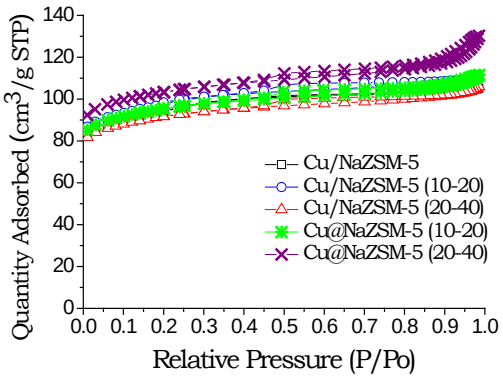

Figure 6.2. N_2 isotherms of the catalysts prepared by incipient wetness impregnation and sacrificial template

The zeolite crystallization with CNT's (@NaZSM-5 (10-20) and @NaZSM-5 (20-40)) did not present relevant changes in textural properties and the pore size distribution (*Figures 6.1-6.3* and *Table 6.1*), regardless of the CNT size used.

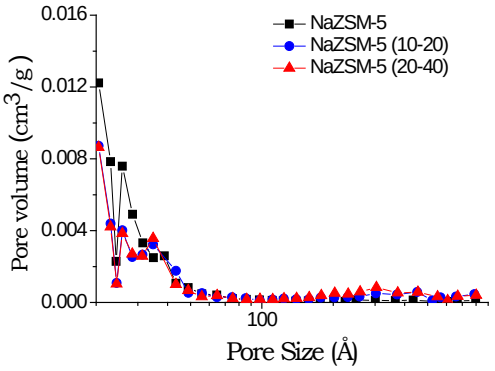

Figure 6.3. Pore size distribution of the zeolites prepare with and without CNT

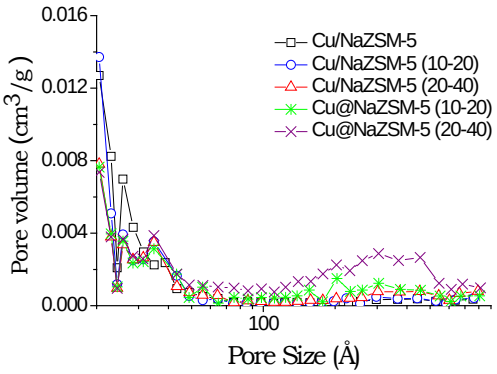

Figure 6.4. Pore size distribution of the catalysts prepared by incipient wetness impregnation and sacrificial template

When copper was impregnated in the CNT's, the samples showed a new mesopores in the range of 20-60 nm that did not appear in the zeolite growth with bare CNT (*Figures 6.3* and *6.4*). These pores are more noticeable in the sample prepared with 20-40 nm CNT's than those of 10-20 nm. Moreover, using CNT's of 20-40 nm lead to the highest BET surface area (*Figure 6.2* and *Table 6.1*). This effect was also observed by C. Flores *et al.* [26] with 3 different metals (Co, Ni, Mg).

They cited the essential role of metal in the synthesis and suggested that the zeolite nucleation only occurs on the metal oxide sites, allowing the growth of the zeolite around the CNT's and producing the mesoporosity by their removal (see the scheme in *Figure 6.5*).

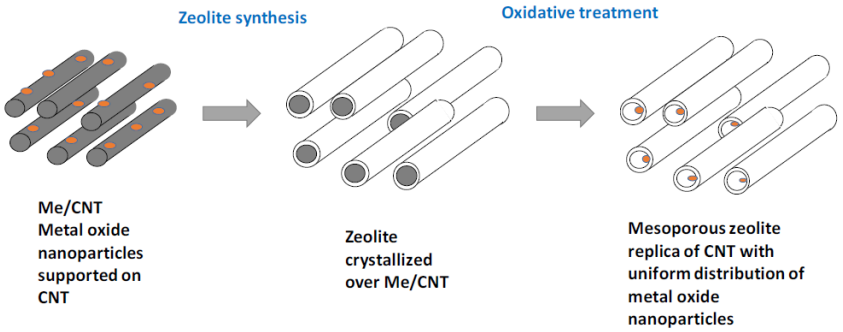

Figure 6.5. Scheme proposed about the zeolite growth around CNT with metal by C. Flores *et al.* [26]

On the other hand, the change of zeolite form from sodium (Na) to proton (H) form showed an increase in the BET surface area (*Figure 6.6* and *Table 6.1*), despite not showing significant changes in the pore size distribution (*Figure 6.7*).

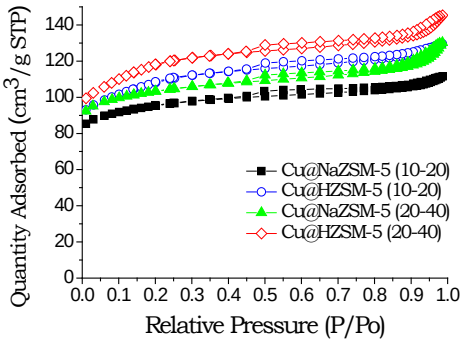

Figure 6.6. N_2 isotherms of the catalysts prepared by sacrificial template before and after ion exchange

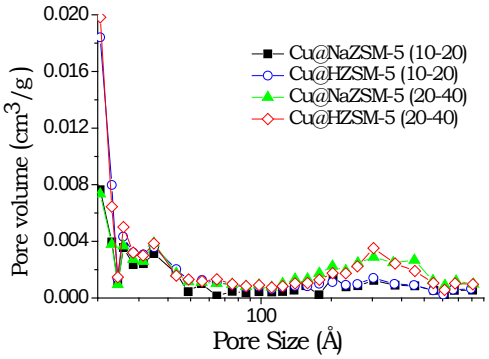

Figure 6.7. Pore size distribution of the catalysts prepared by sacrificial template before and after ion exchange

- **Crystallinity**

The crystallinity of the synthesised zeolites, as well as the copper oxide phase in the structure, was studied by XRD analysis.

It can be seen that the zeolite growth by the sacrificial template method was successfully carried out. All the samples presented a ZSM-5 structure and similar to the samples prepared by incipient wetness impregnation of Cu on ZSM-5 *(Figure 6.8*).

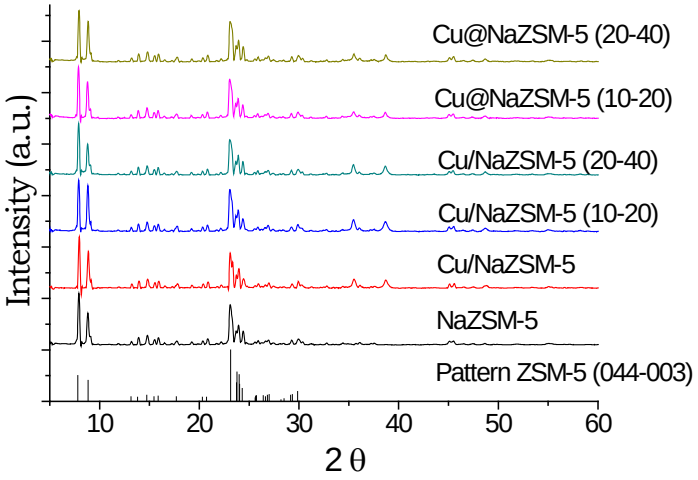

Figure 6.8. XRD analysis of catalysts prepared by incipient wetness impregnation and sacrificial template method.

Furthermore, the presence of copper in the sample could be observed in the diffractograms (*Figure 6.8*). The CuO peaks with the highest intensity appeared at 35.7 and 38.8 ° (*Figure 6.9*).

The CuO crystal size was estimated by the Scherrer equation applied at the 38.8° peak. *Table 6.1* presents the data obtained. Samples prepared by the sacrificial template method showed a similar particle size of CuO to samples prepared by the incipient wetness impregnation. However, the change of Na- to H-zeolite form, produced a decrease in the CuO peaks intensity (35.7 and 38.8°) in both used CNT's sizes of 10-20 (*Figure 6.9A*) and 20-40 nm (*Figure 6.9B*). The ion exchange required to obtain the intermediate ammonium form (before H-form) was carried out with NH_4NO_3 solution. In this treatment, part of the copper was dissolved due to the acidity of the solution (pH = 4) [32] along with the temperature

at which the samples are subjected (80 °C). This was verify with a blue solution obtained after the ion exchange, which prove the presence of Cu^{2+} ions. Therefore, this decrease in copper content produced a decrease of peak intensity.

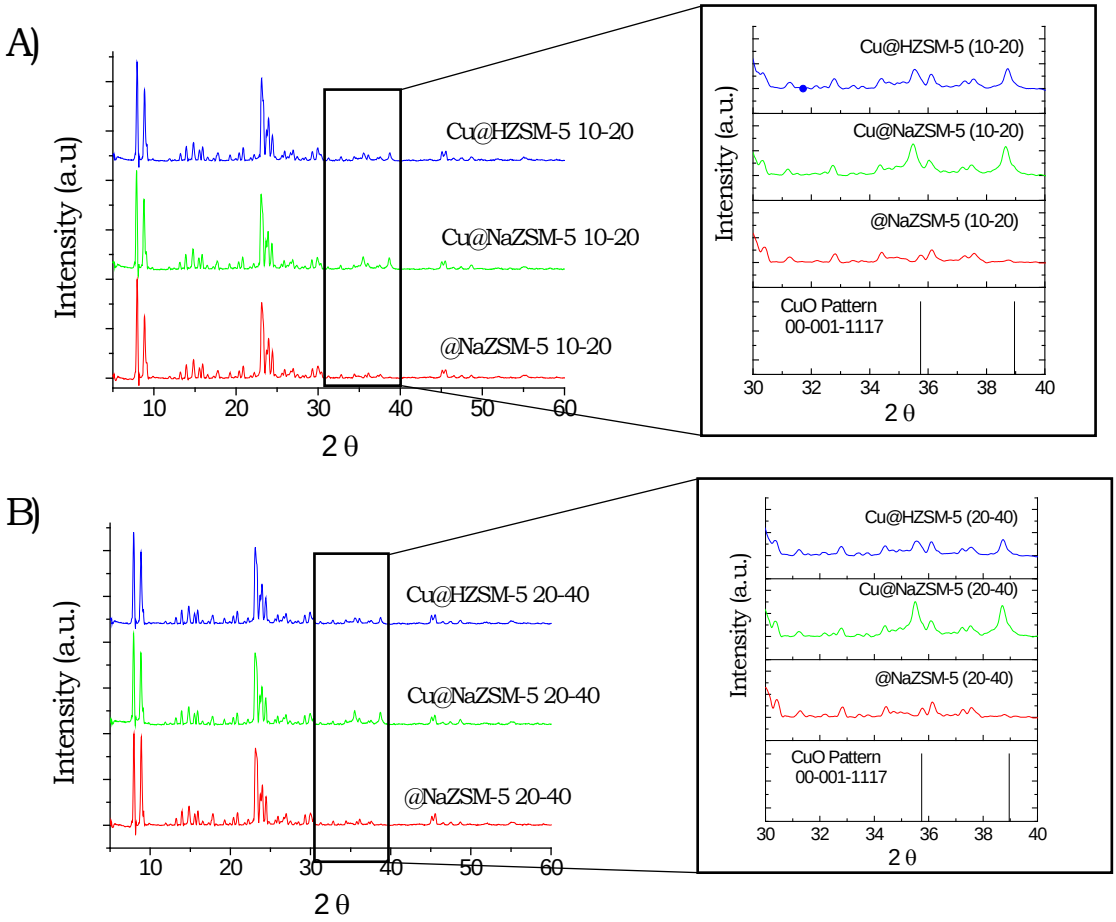

Figure 6.9. XRD of the samples prepared by sacrificial template method with CNT of A) 10-20 nm and B) 20-40 nm

6.2.2. Carbon spheres

Another synthesis method studied was referred to as carbon sphere method. Commercial copper nanoparticles were covered with a carbon layer, which is removed by calcination after the zeolite growth over these carbon on copper nanoparticles. A detailed description of the preparation method can be found in *section 2.2.1.3.2* of *chapter 2* (page 44). The textural properties of the sample and crystallinity of the zeolite synthesis steps were measured. The main results are summarised in *Table 6.2*.

Table 6.2. Textural properties and CuO crystal size of samples prepared by carbon sphere method

	BET surface (m^2/g)	Total Pore volume (cm^3/g)	Micropore volume (cm^3/g)	CuO crystal size (nm)*
NaZSM-5	417	0.18	0.16	-
HZSM-5	405	0.19	0.17	-
Cu@C_NaZSM-5	348	0.16	0.15	33
Cu@C_HZSM-5	357	0.18	0.16	35

* Measured by XRD

- **Textural Properties**

Textural properties of the samples were measured by N_2 adsorption. Type I isotherms corresponding to a of microporous solid are presented in *Figure 6.10*.

The zeolite in the proton form presented a BET surface area higher than the sodium form (*Table 6.2* and *Figure 6.10*). Moreover, the sample Cu@C_NaZSM-5 and Cu@C_HZSM-5 presented lower surface area than the bare zeolite due to the presence of copper.

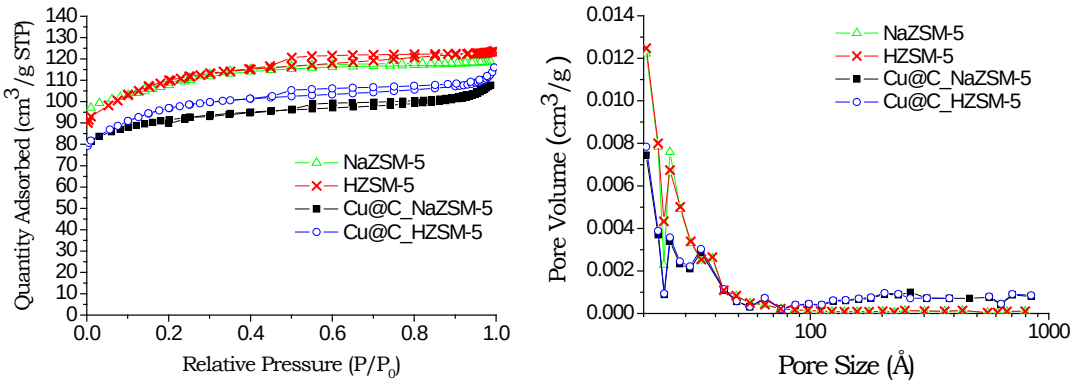

Figure 6.10. N_2 isotherm (A) and pore size distribution (b) of samples prepared by carbon spheres method A

- **Crystallinity**

Crystallinity was studied by XRD analysis. The results showed the synthesis of ZSM-5 zeolite successfully, as well as the presence of the copper oxide phase in the structure (*Figure 6.11*). Furthermore, CuO crystal size was estimated by Scherrer method at the 38.8 º line. The results showed similar CuO size for proton and sodium form samples. Nevertheless, a decrease in the intensity was observed in the proton form zeolite (Cu@C_HZSM-5). As said before, the ion exchange required to obtain the intermediate ammonium form (before obtaining the H-form) was carried out with NH_4NO_3 solution and it produced copper leaching [32]. Therefore, this decrease in copper content was translated into a decrease of peak intensity.

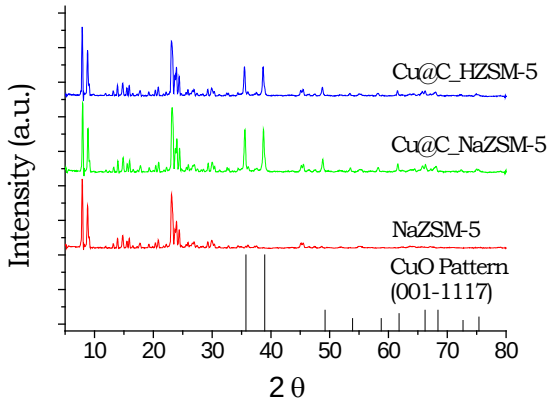

Figure 6.11. XRD analysis of the samples prepared by carbon sphere method

6.2.3. Copper nanoreactors

Copper nanoparticles with silica were synthesised by water-in-oil microemulsion. Then, these nanoreactors were used to grow a zeolite layer around them. A detailed description of the preparation method can be found in *section 2.2.1.3.3* of *chapter 2* (page 45). The sample of the different steps of the synthesis were characterised by N_2 adsorption and XRD.

- **Textural properties**

Textural properties were measured by N_2 adsorption and summarised in *Table 6.3*. The results showed an increase in the BET surface area, as well as the total pore volume, when the zeolite was grown (*Figure 6.12*). However, the sample in proton form (Cu@SiO_2_HZSM-5) presented an increase in the BET surface area in comparison with the sodium form (Cu@SiO_2_NaHZSM-5).

Table 6.3. Textural properties of the samples prepared by nanoreactors method

Sample	BET surface (m^2/g)	Total pore volume (cm^3/g)	Micropore volume (cm^3/g)
$Cu@SiO_2$	150	0.21	-
$Cu@SiO_2$_NaHZSM-5	424	0.43	0.09
$Cu@SiO_2$_HZSM-5	433	0.43	0.10

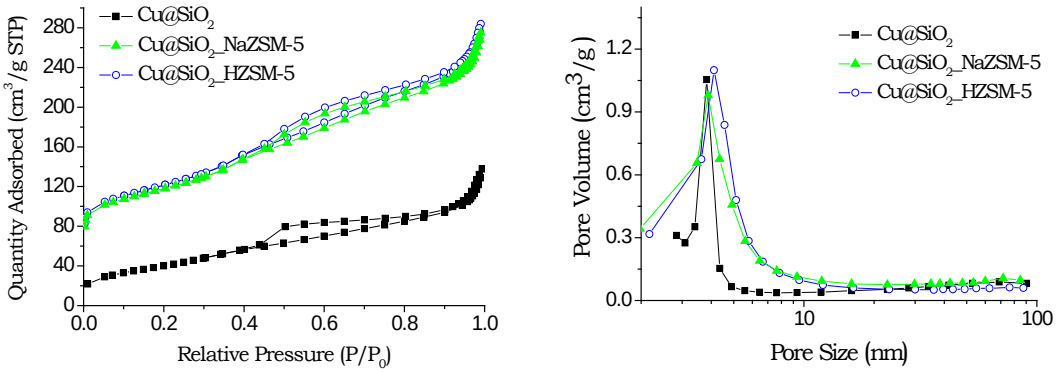

Figure 6.12. N_2 isotherms (a) and pore size distribution (b) of the bare $Cu@SiO_2$ nanoreactors and with zeolite growth.

- **Crystallinity**

The crystallinity of the samples was measured by XRD. The results showed an amorphous structure of the silica for nanoreactors $Cu@SiO_2$ (*Figure 6.13*). Moreover, the CuO was not visible in the diffractogram. After zeolite crystallization on the nanoreactors, the results showed the ZSM-5 structure (*Figure 6.14*). Thus, the zeolite was successfully synthesised over the copper nanoreactors.

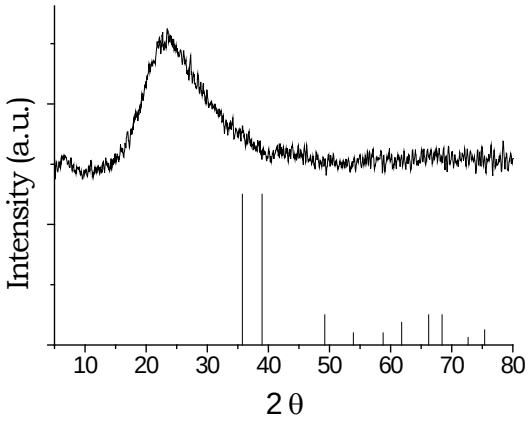

Figure 6.13. XRD pattern of Cu@SiO₂ sample

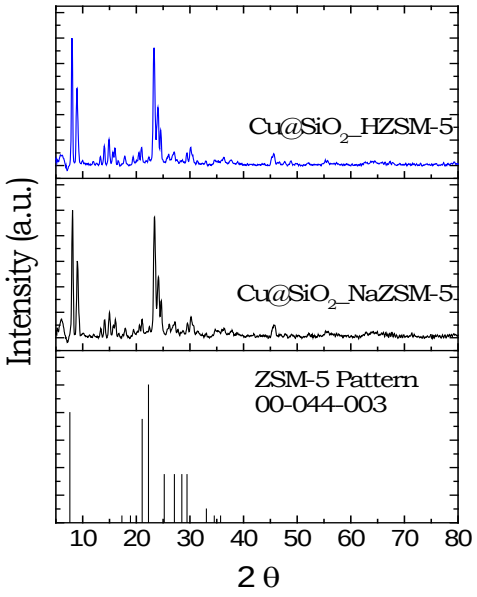

Figure 6.14. XRD results of the samples prepared by nanoreactors method after ZSM-5 zeolite growth

6.2.4. Confinement of copper in SBA-15

In this part, two supports were synthesised, a SBA-15 siliceous support and modified SBA-15 with aluminium (referred to as Al-SBA-15). After that, trying to confine copper and zinc particles in the supports, the reported ammonium-driving deposition-precipitation (ADP) method was used [19].

Textural properties, crystallinity and acidity of the bare supports and CuZn catalysts were analysed.

- **Textural Properties**

The textural properties of the samples were measured by N_2 adsorption and they are summarised in *Table 6.4*. The results showed a type IV isotherm, which is characteristic of mesoporous samples (*Figure 6.15*).

The incorporation of Al to the SBA-15 structure produced a decrease in both, the BET surface area and the total pore volume (*Figure 6.15* and *Table 6.4*). When Cu and Zn were incorporated to the support, a decrease in these textural properties was also produced in comparison to the bare support. In addition, CuZn/SBA-15 catalyst presented a decrease in the equivalent pore size (*Figure 6.15B*).

Table 6.4. Textural properties and crystal size of samples prepared by ADP method

	BET surface area (m^2/g)	Total pore volume (cm^3/g)	Equivalent pore size (nm)	CuO crystal size (nm)*
SBA-15	926	1.07	4.6	-
Al-SBA-15	614	0.91	5.9	-
CuZn/SBA-15	302	0.45	5.9	-
CuZn/Al-SBA-15	276	0.50	7.2	23

* Measured by XRD

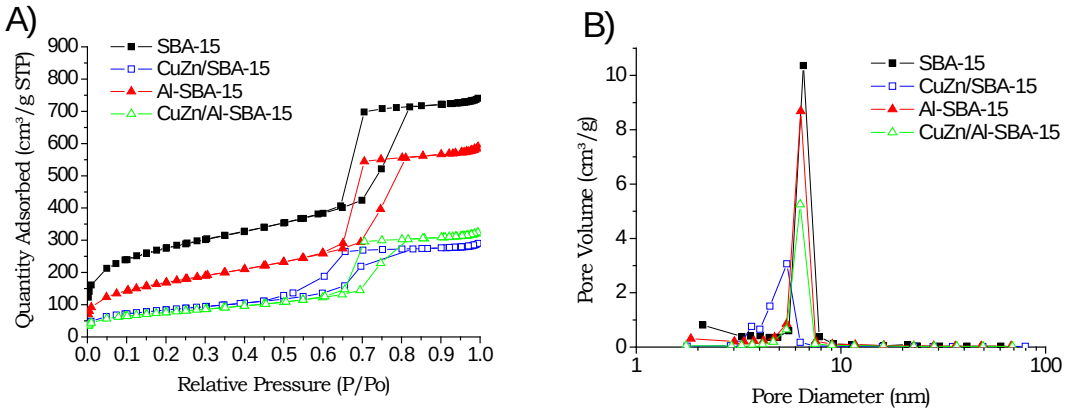

Figure 6.15. N_2 isotherms (a) and pore size distribution (b) of catalysts prepared by ADP method and the used supports.

- **Crystallinity**

The crystallinity of the samples was measured by XRD analysis. The results showed the characteristic peak of amorphous silica from 20-30 º in all the samples (*Figure 6.16*). On the other hand, CuZn catalysts presented the peaks of CuO phase. However, while CuZn/Al-SBA-15 sample showed intense peak of CuO, the CuZn/SBA-15 presented very low signal of CuO crystal.

Particle size of CuO crystal was estimated by Scherrer equation at 38.8º. However, due to the very low intensity of the peaks in the CuZn/SBA-15, it was only possible to calculate the crystal size in the CuZn/Al-SBA-15 sample, which presents a CuO crystallite size around 23 nm (*Table 6.4*).

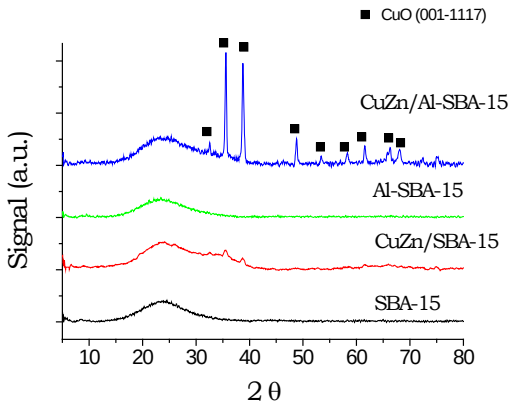

Figure 6.16. XRD analysis of the catalysts prepared by ADP method and their supports.

- **Acidity**

The acidity of the sample was measured by NH_3-TPD analysis of the synthesised supports. The results showed the lack of acidity in the SBA-15, whereas new acidity was generated with Al incorporation in the SBA-15 structure (*Figure 6.17*).

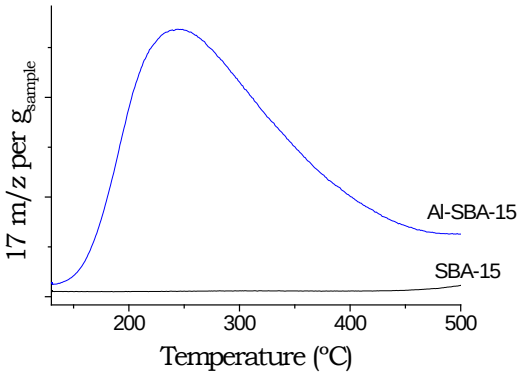

Sample	Acidity (mmol NH_3/g)*
SBA-15	~ 0
Al-SBA-15	0.41

* Calculated by TCD signal

Figure 6.17. NH_3-TPD of the SBA-15 and modified SBA-15 with Al

- **Scanning electron microscopy (SEM)**

The morphology of the samples was studied by scanning electron microscopy (*Figure 6.18*). The results showed the characteristic form of SBA-15, which consist of fibber-like structure [33]. The morphology was not affected by the Al incorporation in the SBA-15 structure. It can be seen that there are different segmental fibbers units with a length around 1,5-3 μm.

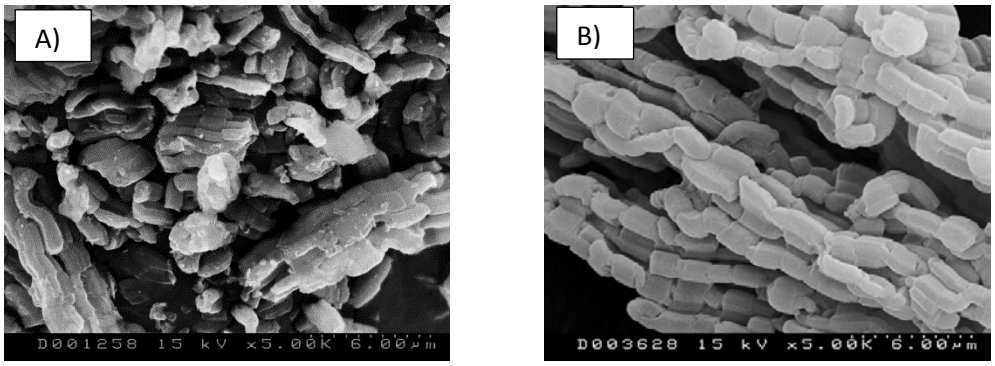

Figure 6.18. SEM images of the SBA-15 (a) and Al-SBA-15 (b)

6.2.5. Activity Test

Due to the complexity of above presented synthesis methods, only some of these catalysts could be tested in the reaction set-up. Before presenting the activity results, some additional characterisation were carried out for each catalyst. In *Table 6.5* the composition measured by X-Ray fluorescence (XRF) of the different catalysts is presented.

Table 6.5. Catalysts composition

Sample	Theoretical	XRF Composition (% wt.)				
	CuO (%)	CuO	ZnO	SiO_2	Al_2O_3	Na_2O
CZA	60	63.0	33.3	-	5.0	-
Cu@HZSM-5 (20-40)	10	5.0	-	91.2	3.7	-
Cu@SiO_2	24	15.0	-	79.3	-	5.7
CuZn/SBA-15	20	20.8	9.3	69.5	-	-
CuZn/Al-SBA-15	20	21.6	8.8	59.0	10.2	-

6.2.5.1. Copper surface area and reducibility

Properties of the catalysts such as copper surface area and reducibility are summarised in *Table 6.6*.

Table 6.6. Copper surface area and reducibility of Cu-based catalysts

Sample	Cu surface area (m^2/g_{CuO})	H_2 consumption (cm^3/g_{CuO})	TPR Reducibility (%)
CZA	54.2	281	100
Cu@HZSM-5 (20-40)	3.8	221	78
Cu@SiO2	0.8	212	75
CuZn/SBA-15	50.5	258	92
CuZn/Al-SBA-15	20.1	262	93

Copper surface area was measured by N_2O-RFC. The results showed similar metal surface area of the Cu/SBA-15 and CZA catalysts (used as reference) (*Table 6.6*). However, when copper was confined in SBA-15 modified with Al (CuZn/Al-SBA-15), the copper surface area decreased. On the other hand, the Cu@SiO_2 nanoreactors and Cu@HZSM-5 (20-40) samples showed a dramatic decrease in Cu surface area.

Reducibility of the samples was measured by H_2-TPR (*Figure 6.19*). The results showed lower reducibility of Cu@SiO_2 and Cu@HZSM-5 (20-40) samples than the CZA catalyst (*Table 6.6*). In contrast, samples with SBA-15 and Al-SBA-15 showed reducibility >90%.

On the other hand, there was no relevant changes in the reduction temperature of almost all samples (*Figure 6.19*). The samples presented a maximum reduction peak at around 250 °C. Nevertheless, the reduction temperature of Cu@SiO_2 sample shifted to higher temperatures (280 °C).

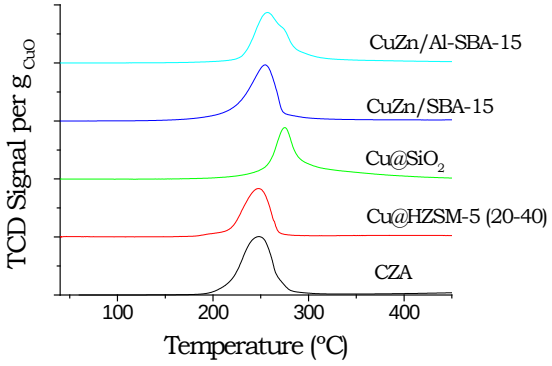

Figure 6.19. H_2-TPR of different Cu-based catalysts

6.2.5.2. CO conversion and Selectivity

Activity test was carried out in a fixed bed reactor at 260 °C and 40 bar with a space velocity of 4.25 L_{syn}/g_{CuO}·h (*Table 6.7*). The results showed really low or negligible CO conversion in the Cu@SiO_2 and Cu@HZSM-5 (20-40) samples. However, the Cu particles confined in the SBA-15 presented similar CO conversion to the CZA catalysts (as reference). Moreover, high selectivity (>90% to methanol) was achieved. In contrast, when the SBA-15 was modified with Al (CuZn/Al-SBA-15), the catalyst showed less CO conversion than when it is prepared with bare SBA-15. The selectivity to methanol, in this case, was negligible and high selectivity to DME and CO_2 were observed.

Table 6.7. Results of activity test of different catalysts at 260 ºC and 40 bar with 4.25 $L_{syn}/g_{CuO}·h$ (syngas of $H_2/CO=2$)

Sample	X_{CO} (%)	Selectivity (%)			
		MeOH	DME	CO_2	Other
CZA	17.0	95.9	0.9	2.7	0.5
Cu@HZSM-5 (20-40)	~0	~0	~0	~0	~0
Cu@SiO_2	1.0	77.5	1.7	15.4	5.4
CuZn/SBA-15	18.4	91.3	1.7	6.0	1.0
CuZn/Al-SBA-15	1.2	~0	63.4	32.9	3.7

6.3. Discussion

Different synthesis methods were used for the preparation of bifunctional catalysts. Mainly, Cu-based catalysts were prepared trying to obtain small copper particles dispersed in an acid catalyst. The methods used were:

- Sacrificial template
- Carbon spheres
- Copper nanoreactors
- Confinement of copper in SBA-15

The first three methods showed by XRD analysis the successful crystallization of ZSM-5 zeolite in the presence of copper particles, showing the characteristic peaks of ZSM-5 zeolite (*Figures 6.8,6.11,6.14*). Moreover, the CuO phase was detected by XRD at 35.7º and 38.8 º, which correspond to the most intense peaks of CuO (Tenorite 001-1117) (*Figures 6.9-6.11*). Nevertheless, the ion exchange conditions (at pH 4 and 80 ºC) produce a partial dissolution of copper, which produces a decrease in the XRD peak intensity from Na-form to H-form. Moreover, this copper loss in the final catalysts produced also changes in the textural properties (*Tables 6.1,6.2,6,3*), in which the BET surface area of the proton form sample increases in comparison to sodium form sample. Furthermore, this final catalyst showed lower CuO content than the theoretical one (*Table 6.5*).

In general, these three methods of preparation suffer from the same problem. The synthesis and activation of the zeolite is carried out with the Cu particles already present, which are therefore subjected to the ion exchange treatment to produce the zeolite proton form which is the one with acidic properties. During

this treatment, an important Cu leaching is produced, whereby the final solid obtained has a great deficit of active metal phase for the synthesis of methanol.

Consequently, the catalytic test showed the very low CO conversion of some catalysts prepared by these methods, in particular for the sacrificial template (Cu@HZSM-5 (20-40) catalyst) and nanoreactor method (Cu@SiO_2 catalyst) (*Table 6.6*). The results agree with the characterisation of these samples, in which the catalysts showed a very low copper surface area and a lower reducibility (*Table 6.6*). The treatment conditions during the hydrothermal synthesis and the reagent used in this synthesis method may deactivate the metal phase [14-17]. G. Yang *et al.* [14] showed a decrease in the activity when a core-shell catalyst was prepared by hydrothermal treatment. Dissolution of Cu by the formation of a coordinated compound between TPAOH and copper were suggested as possible reason of the methanol synthesis catalyst damage. In microemulsions, by contrast, V. Subramanian *et al.* [31] showed presence of boron in the nanoreactors due to the use of $NaBH_4$ in the process, and they suggested that this boron could negatively affect the reducibility and activity of the catalyst. By XRF analysis boron could not be identify due to the use of this compound as flux for the sample preparation. However, noticeable content of Na_2O was detected in the copper nanoreactor (Cu@SiO_2) (*Table 6.5*). The sodium is reported to affect the activity and stability of the Cu-based catalysts [34-37]. Z. Huang *et al.* [34] and K-W. Jun *et al.* [36] showed the detrimental effect in reducibility and copper dispersion due to an increase in Na content in Cu/SiO_2 and Cu/ZnO/Al_2O_3 catalysts respectively, which affect in great extent the final performance in activity and stability of the catalyst.

In the last synthesis method, we tried to confine copper particles in mesopores supports such a SBA-15. However, this siliceous support does not present acidity (*Figure 6.16*), which is required for methanol dehydration to DME. A modification in the SBA-15 by incorporating Al in the SBA-15 structure was studied to synthesise the bifunctional catalyst, which showed an increase in the acidity by NH_3-TPD (*Figure 6.17*). It is widely known that Si/Al ratio in zeolites or silica-alumina samples is an essential factor that controls the acidity of the samples. Thus, an increase in the Al atoms in the sample structure should lead to a solid with more acidity [38,39].

Al incorporation to SBA-15 produced a sample that presented the common type IV isotherm of mesoporous SBA-15 with H1 hysteresis loop [40] (*Figure 6.15*). Therefore, it can be seen that the incorporation of Al does not modify in great extent the mesoporous structure. However, the modification of the SBA-15

produced a sharp decrease in both, the BET surface area and the total pore volume. A decrease in the micropore volume was also observed from 0.11 to 0.02 cm^3/g when Al was introduced in the synthesis. Hence, after the pH-adjusting treatment, the textural properties of the sample change probably due to a filling of the micropores during this procedure as it was reported by S. Wu *et al.* [41].

The addition of metals (Cu and Zn) to the support produced a decrease in the BET surface area (*Table 6.4 and Figure 6.15A*), which could be attributed to the lower surface area of the metals and a partial blocking of the pores. In the pore size distribution a shift of the pores to a smaller size could be seen in CuZn/SBA-15 sample, whereas it was not produced in CuZn/Al-SBA-15 (*Figure 6.15B*). The pore size reduction of SBA-15 may be due to the location of copper and zinc particles in the pores of the support, partially blocking the pores mouth [19,21]. Therefore, it seems that the confinement of metal particles in the ordered porous of the support was achieved, whereas, in the Al-SBA-15 support, metal particles might be located in the external surface of the support. Moreover, the XRD analysis showed different particle size of CuO (*Figure 6.16*). Therefore, it seems that the Al-SBA-15 supports do not allow an adequate confinement of metal particles in its pores and big CuO crystal sizes are produced, while with the SBA-15 the copper particles are located in the support porous and small particle could be obtained. These results also agree with those of RFC-N_2O, where the copper surface area decreases from 50.5 to 20.1 m^2/g_{CuO} when Al is incorporated in the SBA-15 structure (*Table 6.5*).

Hence, the catalytic results showed much lower CO conversion of the CuZn/Al-SBA-15 catalyst than the CuZn/SBA-15 catalyst. On the other hand, it is noticeable that the use of Al-SBA-15 as support presented high selectivities to DME (*Table 6.7*) due to the higher acidity of this support than bare SBA-15 (*Figure 6.17*). Thus, the acid sites of the sample are able to dehydrate the formed methanol to DME, whereas the non-acid character of bare SBA-15 do not allow this reaction and high selectivities to methanol are obtained [42].

Finally, the good copper dispersion obtained on CuZn/SBA-15 catalyst produced similar catalytic behaviour to the standard methanol synthesis catalyst (CZA) (*Table 6.7*).

6.4. Conclusion

After studying different synthesis method for copper encapsulation in ZSM-5 zeolite, the results showed a growth of zeolite in the presence of copper particles successfully. However, a non-active catalysts were obtained for CO hydrogenation. The severe conditions of synthesis and regents used seem to deactivate the copper. Low copper surface area and a decrease in reducibility was observed. Moreover, the ion exchange step for zeolites partially dissolve the copper in the NH_4NO_3 medium, losing copper content of the final catalyst. On the whole, these synthesis methods can consider unsuitable.

In contrast, copper confinement in ordered mesoporous supports as SBA-15 performed excellent activities for methanol synthesis reaction. However, the incorporation of Al to the SBA-15 produced a worse copper dispersion than the bare SBA-15 and low CO conversion were obtained. Even so, a modification in the support to increase the acidity with aluminium presented an increase in acidity of the support and an increase in the DME selectivity was achieved.

In general, these new catalysts did not show promising results for the direct synthesis of DME due to the low copper surface area obtained (both due to loss of active phase and low metal dispersion). Moreover, the complexity and the cost of these syntheses reduce the viability of these methods for the main purpose of this work, which is the preparation of structured catalysts. Therefore, it was decided do not to advance further on these routes.

6.5. References

[1] J.H. Flores, M.I.P. da Silva. *Catalysis Letters* 146 (2016) 1505-1516.

[2] Q. Ge, Y. Huang, F. Qiu, S. Li. *Applied Catalysis A: General* 167 (1998) 23-30.

[3] S.P. Naik, H. Du, H. Wan, V. Bui, J.D. Miller, W.W. Zmierczak. *Industrial & Engineering Chemistry Research* 47 (2008) 9791-9794.

[4] G.R. Moradi, S. Noarsti, F. Yaripor. *Catalysis Communications* 8 (2007) 598-606.

[5] J-L. Li, X-G. Zhang, T. Inui. *Applied Catalysis A: General* 147 (1996) 23-33.

[6] A. García-Trenco, A. Vidal-Moya, A. Martínez. *Catalysis Today* 179 (2012) 43-51

[7] J. Hu, Y. Wang, C. Cao, D.C. Elliot, D.J. Stevens, J.F. White. *Industrial & Engineering Chemestry Research* 44 (2005) 1722-1727.

[8] F.S. Ramos, A.M. Duarte de Farias, L.E.P. Borges, J.L. Monteiro, M.A. Fraga, E.F. Sousa-Aguiar, L.G. Appel. *Catalysis Today* 101 (2005) 39-44.

[9] D. Mao, J. Xia, B. Zhang, G. Lu. *Energy Conversion and Management* 51 (2010) 1134-1139.

[10] F. Song, Y. Tan, H. Xie, Q. Zhang, Y. Han. *Fuel Processing technology* 126 (2014) 88-94.

[11] J. Zhang, F. Li. *Applied Catalysis B: Environmental* 176-177 (2015) 513-521.

[12] H. Yang, P. Gao, C. Zhang, L. Zhong, X. Li, S. Wang, H. Wang, W. Wei, Y. Sun. *Catalysis Communications* 84 (2016) 56-60.

[13] E. Baktash, P. Littlewood, R. Schomäcker, A. Thomas, P.C. Stair. *Applied Catalysis B: Environmental* 179 (2015) 122-127.

[14] G. Yang, N. Tsubaki, J. Shamoto, Y. Yoneyama, Y. Zhang. *Journal of the American journal society* 132 (2010) 8129-8136.

[15] Y. Wang, W. Wang, Y. Chen, J. Ma, R. Li. *Chemical Engineering Journal* 250 (2014) 248-258.

[16] R. Phienluphon, K. Pinkaew, G. Yang, J. Lie, Q. Wei, Y. Yoneyama, T. Vitidsant, N. Tsubaki. *Chemical Engineering Journal* 270 (2015) 605-611.

[17] M. Sánchez-Contador, A. Ateka, A.T. Aguayo, J. Bilbao. *Fuel Processing Technology* 179 (2018) 258-268.

[18] K. Pinkaew, G. Yang, T. Vitidsan, Y, Jin, C. Zheng, Y. Yoneyama, N, Tsubaki. *Fuel* 111 (2103) 727-732.

[19] X. Guo, A. Yin, W-L. Dai, K. Fan. *Catalysis Letters* 132 (2009) 22-27.

[20] H. Ham, J. Kim, S.J. Cho, J-H. Choi, D.J. Moon, J.W. Bae. *ACS Catalysis* 6 (2016) 5629-5640.

[21] A. García-Trenco, A. Martínez. *Catalysis Today* 15 (2013) 152-161.

[22] G. Prieto, A. Martínez, R. Murciano, M.A. Arribas. *Applied Catalysis A: General* 367 (2009) 146-156.

[23] Z-J. Wang, Y. Xie, C-J. Liu. *Journal of Physical Chemistry C* 112 (2008) 19818-19824.

[24] M. Zhang, S. Ji, L. Hu, F. Yin, C. Li, H. Liu. *Chinese Journal of Catalysis* 27 (2006) 777-782.

[25] C. Flores, N. Batalha, V.V. Ordomsky V.L. Zholobenko, W. Baaziz, N.R. Marcilio, A.Y. Khodakov. *Chemcatchem* 10 (2018) 2291-2299.

[26] C. Gomes Flores. *PhD Thesis* (2019) Federal University of Rio Grande do Sul (UFRGS) Brazil.

[27] Y. Chen, N. Batalha, M. Marinova, M. Impéror-Clerc, C. Ma, O. Ersen, W. Baaziz, J.A. Stewart, D. Curulla-Ferré, A.Y. Khodakov, V.V. Ordomsky. *Journal of Catalysis* 365 (2018) 429-439.

[28] M.P. Pileni. *Supramolecular Science* 5 (1998) 321-329.

[29] I. Lisiecki, M.P. Pileni. *Journal of Physical Chemistry* 99 (1997) 5077-5082.

[30] A. Kosak, D. Majovec, A. Znidarsic, M. Drofenik. *Journal of European Ceramic Society* 24 (2004) 959-962.

[31] V. Subramanian, K. Cheng, C. Lancelot, S. Heyte, S. Paul, S. Moldovan, O. Ersen, M. Marinova, V.V. Ordomsky, A.Y. Khodakov. *ACS Catalysis* 6 (2016) 1785-1792.

[32] F. J. Echave Lozano. *PhD Thesis 2011*. Universidad del País Vasco.

[33] H. Pérez, P. Navarro, M. Montes. *Chemical Engineering Journal* 158 (2010) 325-332.

[34] Z. Huang, F. Cui, H. Kang, J. Chen, C. Xia. *Applied Catalysis A: General* 366 (2009) 288-298.

[35] R. Raudaskoski, M.V. Niemelä, R.L. Keiski. *Topics in Catalysis* 45 (2007) 57-60.

[36] K-W. Jun, W-J. Shen, K.S.R. Rao, K-W. Lee. *Applied Catalysis A: General* 174 (1998) 231-238.

[37] C. Montassier, J.M. Dumas, P. Granger, J. Barbier. *Applied Catalysis A: General* 121 (1995) 231-244.

[38] I. Shirazi, E. Jamshidi, M.R. Ghasemi. *Crystal Research and Technology* 43 (2008) 1300-1306.

[39] P.L. Benito, A.G. Gayubo, A.T. Aguayo, M. Olazar, J. Bilbao. *Journal of Chemical Technology & Biotechnology* 66 (1996) 183-191.

[40] Hermicenda Pérez Vidal. *PhD Thesis* (2009). University of the Basque Country (UPV/EHU).

[41] S. Wu, Y. Han, Y-C. Zou, J-W. Song, L. Zhao, Y. Di, S-Z. Liu, F-S. Xiao. Chemistry of Materials 16 (2004) 486-492.

[42] J.J Spivey. Chemical Enigineering Communicatios 110 (1991) 123-142.

CHAPTER 7

General conclusions

The main objective of this thesis is to study metallic structured reactors for direct synthesis of DME by washcoating method. To achieve this aim, the adequate slurry formulation for the two catalysts selected for this reaction was investigated: the methanol synthesis catalyst ($Cu/ZnO/Al_2O_3$ or CZA) and the methanol dehydration catalyst (ZSM-5 zeolite), both of them studied separately (separate slurries of each catalyst) as well as mixed in the same slurry. In this section, the most relevant conclusions of this work are summarised:

- Methanol synthesis catalyst, $Cu/ZnO/Al_2O_3$ (CZA):

  - To obtain adherent coatings on the metallic substrate, the use of inorganic colloid oxides is needed.

  - The colloid nature and the colloid content are relevant in the layer adherence on the substrate. The colloidal alumina shows the best performance in obtaining good adherences with moderate contents.

  - The use of these colloids modifies the catalytic properties of the parent catalyst. The more colloid content the slurry has, the more the catalytic properties of the parent catalyst are damaged. The CZA_10%Al_2O_3 formulation is the one that shows the best compromise between obtaining good coating properties and few catalytic properties modifications of the parent catalyst.

- Methanol dehydration catalyst, ZSM-5 zeolite:

  - The zeolite slurry allows to coat the metallic substrates successfully with good adherence.

  - Nevertheless, due to the use of polyvinyl alcohol (PVA) in the slurry, the zeolite slurry must be prepared using the zeolite in the proton form (previously calcined) or the slurry zeolite must be calcined at temperatures higher than 500 ºC after coating process ensuring the removal of PVA to obtain similar methanol conversion to the parent zeolite.

  - Both, the colloidal silica and alumina, are adequate additives for obtaining adherent catalytic coatings without modifying the catalytic properties of the zeolite.

- Mixture of both catalysts in a slurry CZA+HZSM-5:

  - The slurried mixture of catalysts shows good performance for direct synthesis of DME with slightly higher yields than the common physical mixture of the powder of both components.

  - The mixture of two catalysts in the slurry allows to coat metallic substrates successfully by using inorganic colloid oxides as additives.

  - The nature of the colloids used affects to the final catalytic properties. The colloidal alumina shows the best results in a way of obtaining adherent coatings without modifying in great extent the catalytic properties of the methanol synthesis catalysts nor dehydration catalyst.

- Structured catalysts:

  - The structured catalysts show similar reaction yield for direct synthesis of DME to the slurried catalysts, which were tested in powder state.

  - The used substrate geometry and alloy do not modify significantly the CO conversion and selectivities to different compounds (mainly DME, methanol and CO_2).

  - It is achieved the preparation of tandem-type systems (dual-layer structured catalysts) with separate catalysts layers. Surprisingly, the architecture in which the methanol synthesis catalyst (CZA) is placed in the external layer presents better results than placing the zeolite layer above the CZA catalyst. The latter architecture favours the DME dehydration to hydrocarbons as well as decreases the global CO conversion.

  - The initial volumetric productivity of brass monoliths with a volumetric load of 0,16 g/cm^3 (1 g of coated catalyst) can be increased 4 times by doubling the catalytic load (0,33 g/cm^3) and by varying the reaction conditions (T_{reac} = 300 ºC and space velocity of 3,4 L_{syn}/g_{cat}·h).

- Bifunctional catalysts synthesis:

  - ZSM-5 zeolite can be synthesised around copper particles by 3 different methods. However, the catalysts obtained present really low copper surface area that produces really low or negligible activities for CO hydrogenation.

  - The confinement of copper particles in SBA-15 allows to obtain well dispersed copper particles on SBA-15 with good activity results for methanol synthesis reaction.

  - SBA-15 modification with aluminium produces new acidity to the support, which allows to dehydrate the methanol to DME. However, bad copper dispersion was achieved by the method reported in bibliography and copper surface area is noticeably alter producing low CO conversion.

ANEXOS
(APPENDIX)

ÍNDICE

A.1. Estudios previos de las condiciones de reacción para la síntesis directa de DME

Se realizaron estudios previos variando determinadas condiciones de reacción como la presión de trabajo, velocidad espacial y el catalizador ácido empleado con el fin de seleccionar unas condiciones de operación para la síntesis directa de DME.

En primer lugar, se realizó un estudio de la variación de la velocidad espacial. Como se muestra en la *Figura A.2.*, la conversión de CO disminuyó con la velocidad espacial de la forma esperada. Sin embargo, no se observaron cambios significativos en la selectividad. Por lo tanto, en este trabajo se seleccionó la velocidad espacial de 1,7 Lsyn/g·h en la que se obtienen elevadas conversiones de CO pero sin alcanzar las condiciones de equilibrio termodinámico.

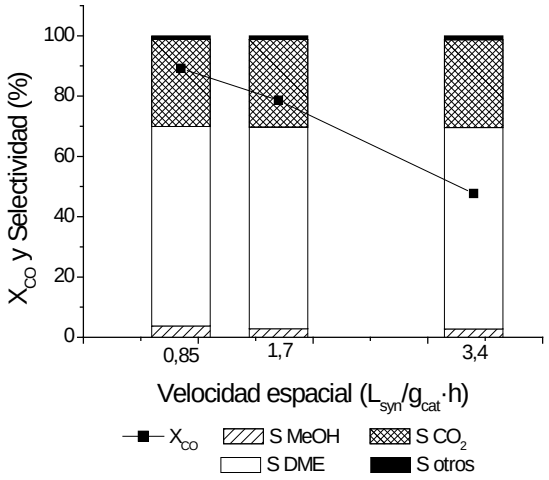

Figure A.1. Efecto de la velocidad especial en la síntesis directa de DME. Catalizadores: CZA + HZSM-5 (relación 2:1) a 260 ºC y 40 bar.

La síntesis directa de DME es una reacción exotérmica con reducción en el número de moles. Por lo tanto, la reacción se ve favorecida a elevadas presiones. Sin embargo, tras el estudio del efecto de la presión de trabajo (*Tabla A.1*), se decidió trabajar a 40 bar debido a que la diferencia en la conversión de CO no es tan elevada junto con la mayor facilidad que conlleva operar a menores presiones.

Tabla A.1. Efecto de la presión de trabajo en la síntesis directa de DME

Presión (bar)	conv. CO (%)	Selectividad (%)			
		MeOH	DME	CO_2	Otros
40	78,5	1,9	67,1	29,3	1,7
50	82,2	2,2	66,9	29,5	1,4

Por otro lado, se estudió el efecto de emplear dos catalizadores ácidos diferentes en la síntesis directa de DME: zeolita ZSM-5 (*Zeolyst International*) y alúmina (*Spheralite SC505)*. Sin embargo, los resultados mostraron la menor capacidad de deshidratar el metanol de la alúmina (*Tabla A.2*), por lo que se eligió la zeolita ZSM-5 como el catalizador ácido más relevante para este trabajo.

Tabla A.2. Efecto del catalizador ácido empleado en la síntesis directa de DME

Catalizador ácido	Relación CZA/cat. acido	conv. CO (%)	Selectividad (%)			
			MeOH	DME	CO_2	Otros
HZSM-5	2	78,5	1,9	67,1	29,3	1,7
Alúmina	2	67,8	19,0	56,5	24,4	0,1

A.2. Desorción a temperatura programada de NH_3 (NH_3-TPD)

A.2.1. Búsqueda de condiciones de análisis

Con el fin de elegir unas condiciones de análisis para este método, durante este trabajo se estudió el efecto de la variación de dos de las condiciones de análisis que suelen fijarse: el tiempo de purga para eliminar el amoníaco fisisorbido y la temperatura de saturación del amoníaco.

La variación del tiempo de purga mostró en primer lugar la necesidad de realizar una purga con He tras la saturación de amoníaco para poder obtener una línea base desde el inicio del registro de datos (*Figura A.2*). Por otro lado, el aumento del tiempo de purga mostró un descenso del pico de baja temperatura. Es por ello, que se eligió la purga de 60 min, para poder asegurar la eliminación adecuada del amoníaco fisisorbido y obtener una línea base desde el inicio sin modificar en exceso el primer pico de desorción.

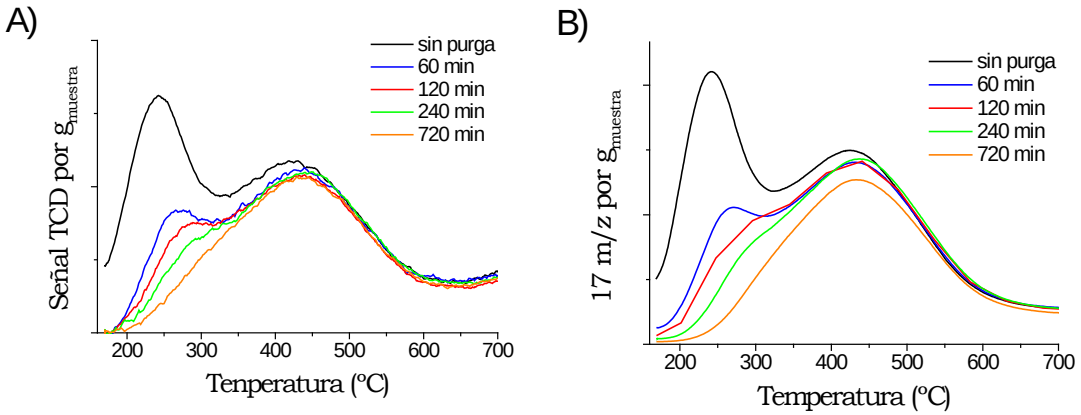

Figura A.2. Resultados del análisis de NH_3-TPD de la zeolita comercial CBV2314 para diferentes tiempos de purga con He a) señal TCD y b) señal masa 17 m/z

Por otro lado, el tiempo de saturación también mostró cambios en el primer pico de desorción correspondiente a la acidez débil (*Figura A.3*). El pico de baja temperatura disminuyó con la temperatura de saturación. De modo, que al igual que en el caso anterior, para evitar la modificación en exceso del pico de baja temperatura, el cual daría información de la acidez débil, se optó por fijar la temperatura de saturación del amoníaco a 130 ° C.

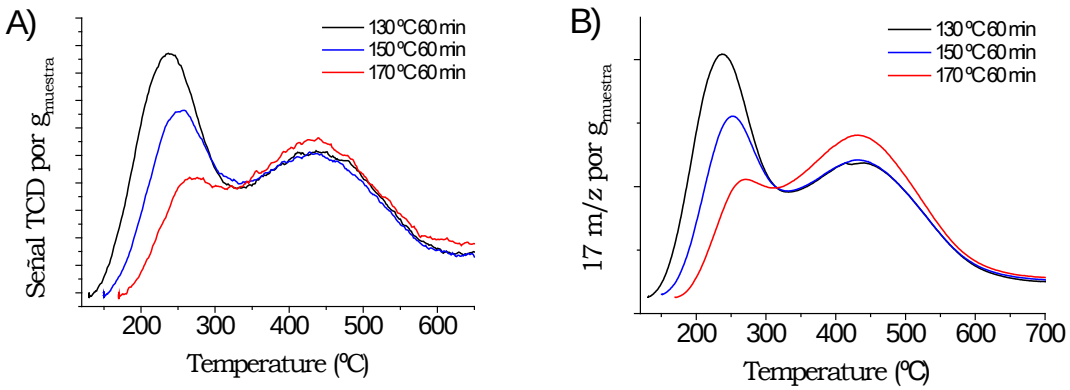

Figura A.3. Resultados del NH_3-TPD de la zeolita comercial CBV2314 para diferentes temperaturas de saturación de NH_3 a) señal TCD y b) señal masa 17 m/z

A.2.2. Cálculo de la acidez de la zeolita

Como se observó en el *Capítulo 3*, la calcinación de las zeolitas a diferentes temperaturas suponía la presencia de amoníaco remanente en las muestras que pudo ser observado mediante un análisis en blanco de las mismas (*ver apartado acidez en la sección 3.3.1.1. pág. 45*). Este análisis "blanco" supone realizar el mismo proceso realizado en los TPD de NH_3 pero sin la etapa de saturación del mismo. Para poder estimar un valor de acidez de las muestras se realizó la resta de las señales del análisis de NH_3-TPD y el blanco, obteniendo una curva corregida (*Figura A.4*).

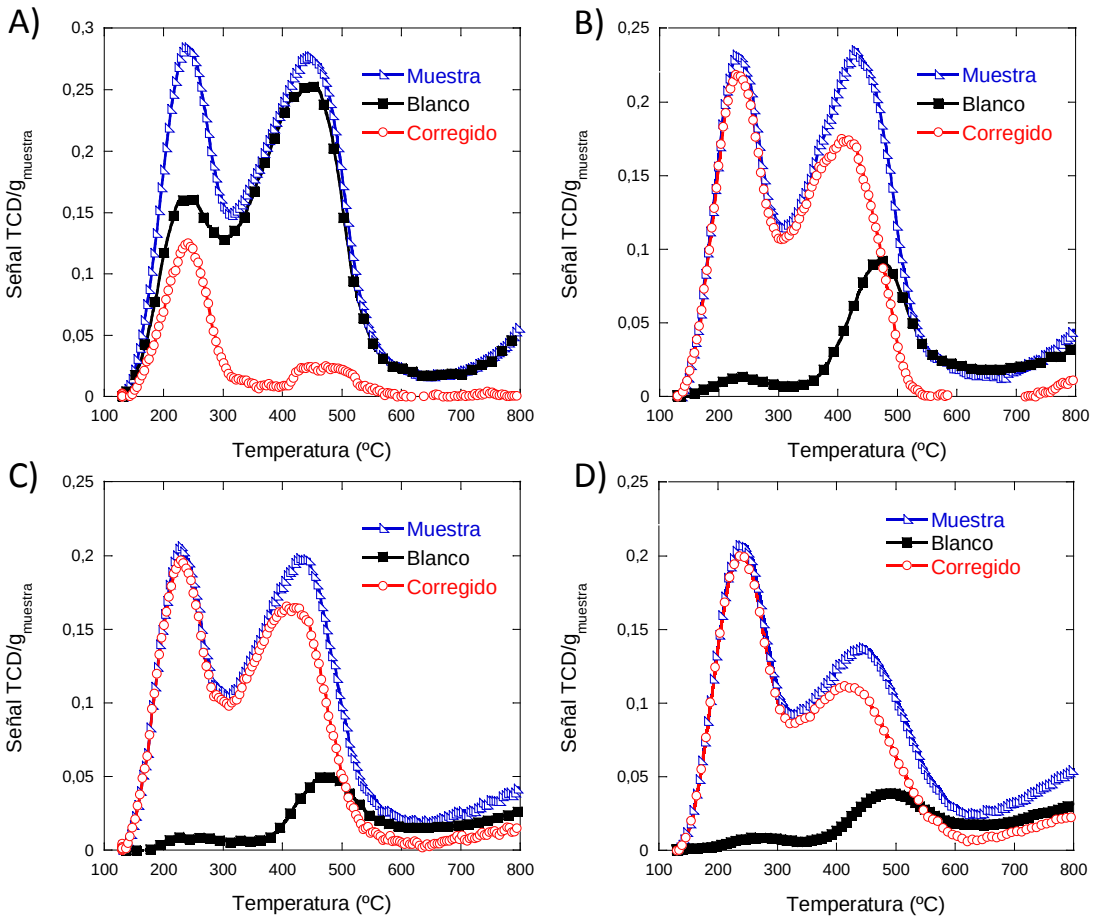

Figura A.4. Corrección de las señales del TCD para las muestras a) zeolita comercial NH_4^+, b) ZSM-5 calc. 300 3h, c) ZSM-5 calc. 500 3h y d) ZSM-5 calc. 500 5h

Por otro lado, integrando el área bajo la curva de las señales corregidas se pudo determinar la variación existente entre las muestras (*Tabla A.3*). Los resultados de la integración mostraron que las áreas de las muestras calcinadas con tratamientos térmicos diferentes no presentaban cambios tan significativos. Además, los resultados concordaban con la estimación realizada al restar los valores de acidez obtenidos en los análisis de TPD y blanco con la calibración del TCD.

Tabla A.3. Integración de la señal corregida de los TPD-NH_3

Muestra	Área bajo la curva	mmol $NH_3/g_{muestra}$ (TCD)
Zeolita comercial NH_4^+	15,11	0,33
ZSM-5 calc. 300 3h	48,49	1,18
ZSM-5 calc. 500 3h	48,76	1,14
ZSM-5 calc. 500 5h	45,18	1,05

A.3. Estimación de la conductividad efectiva de los monolitos

La conductividad efectiva de los monolitos, se estimó empleando las ecuaciones propuestas por C.G. Visconti y cols. [1].

La conductividad efectiva axial:

$$k_{e,a} = k_s \cdot (1 - \varepsilon)$$

La conductividad efectiva radial:

$$k_{e,r} = k_s \cdot (1 - \varepsilon)/(1 + \varepsilon)$$

donde k_S es el valor de la conductividad del sustrato metálico y ε es el valor de la fracción hueca.

A.4. Estimación del espesor de capa equivalente a una partícula esférica de catalizador

Para relacionar el espesor de capa a un tamaño de partícula equivalente, se empleó el concepto de tamaño característico (L) definido por O. Levenspiel [2], el cual relaciona el volumen de una partícula con su superficie externa abierta a la difusión. De esta forma, suponiendo una geometría esférica para las partículas de catalizador en polvo:

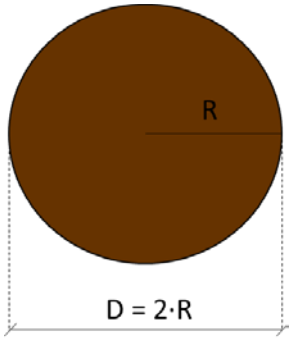

$$L = \frac{Volumen}{Superficie} = \frac{{}^{4}/_{3} \cdot \pi \cdot R^3}{4 \cdot \pi \cdot R^2} = \frac{R}{3} = \frac{D}{6}$$

Y para una capa catalítica depositada sobre un sustrato:

$$L = \frac{Volumen}{Superficie\ (S)} = \frac{S \cdot e}{S} = e$$

Por lo tanto, el espesor de capa catalítica podría relacionarse con el diámetro de una partícula mediante:

$$e = \frac{D}{6}$$

A.5. Calibración de los compuestos en cromatografía de gases (obtención del factor de respuesta)

Los compuestos de la reacción fueron identificados y cuantificados por cromatografía de gases (GC). Para realizar la calibración de los diferentes componentes, se empleó nitrógeno (N_2) como patrón interno.

Diferentes mezclas conocidas de cada componente (*i*) con N_2 fueron inyectadas en el cromatógrafo de gases obteniendo una recta de calibrado como la mostrada en la *Figura A.5*.

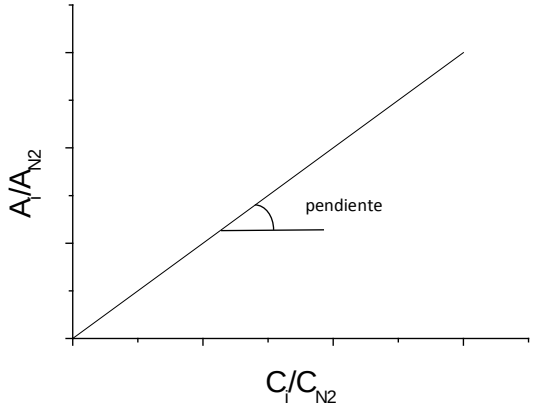

Figura A.5. Calibración de un compuesto i con patrón interno

Siendo A_i el área del compuesto a calibrar, A_{N2} el área del nitrógeno, Ci la concentración del compuesto a calibrar y C_{N2} la concentración de nitrógeno.

Así, el factor de respuesta para cada componente fue obtenido de la pendiente de la recta de calibrado

$$F_r = \frac{A_i / A_{N_2}}{C_i / C_{N_2}}$$

Los análisis cromatográficos han sido llevados a cabo en un GC Agilent 7890A con las columnas HP-PLOT/Q y HP-MOLESIEVE conectadas con el TCD y una columna HP-PLOT/Q en el FID. El método empleado presenta una duración de 55 min por cromatograma, dónde el horno se mantiene 20 min a 40 °C para

posteriormente ir incrementando la temperatura hasta 250 ºC con una rampa de 10 ºC/min. Todo ello combinado con los cambios de válvula indicados en la *Figura A.6* con el fin de separar todos los compuestos adecuadamente.

	Time (min)	Event Type	Position	Setpoint
1	0.05	Valve	Valve 3	On
2	0.05	Valve	Valve 1	On
3	1	Valve	Valve 3	Off
4	1	Valve	Valve 1	Off
5	5.75	Valve	Valve 2	On
6	13	Valve	Valve 2	Off
7	25	Valve	Valve 2	On
8	49	Valve	Valve 2	Off

Figura A.6. Tiempos de los diferentes cambios de válvula empleados en el método de análisis cromatográfico.

Los tiempos de retención para cada compuesto se resumen en la *Tabla A.4*.

Tabla A.4. Tiempos de retención y factores de respuesta de los compuestos analizados

Compuesto	Tiempo de retención (min)		Factor de respuesta	
	TCD	FID	TCD	FID
CO_2	6,3	-	1,19	-
H_2	16,5	-	0,04	-
N_2	20,5	-	-	-
CO	51,4	-	1,05	-
Metanol	32,6	25,4	0,77	1,34
DME	30,6	20,4	1,22	2,52
CH_4	23,2	1,0	0,72	2,80
Etano	11,5	2,3	1,10	5,40
Eteno	9,2	1,8	1,02	5,40
Propano	29,1	12,3	1,39	7,86
Propeno	28,4	10,6	1,32	7,97

A.6. Cálculo de la conversión de CO y selectividad

La conversión de CO se determinó mediante la ecuación:

$$X_{co}\ (\%) = \frac{moles\ CO\ convertidos}{moles\ de\ CO\ alimentados} = \frac{\left(\frac{A_{CO,0}}{A_{N_2,0}} - \frac{A_{CO,t}}{A_{N_2,t}}\right)}{\left(\frac{A_{CO,0}}{A_{N_2,0}}\right)} \cdot 100$$

Donde:

- $A_{CO,0}$ es el área de CO inicial
- $A_{N2,0}$ es el área de N_2 inicial
- $A_{CO,t}$ es el área de CO a un tiempo de reacción t
- $A_{N2,t}$ es el area de N_2 a un tiempo de reacción t

Y la selectividad a cada componente i se determinó mediante la ecuación:

$$Selectividad\ componente\ i\ (\%) = \frac{moles\ producidos\ de\ i}{moles\ reaccionados\ CO} \cdot \frac{1}{a} = \frac{\frac{A_{i,t}/A_{N_2,t}}{F_{r,i}}}{\frac{\left(\frac{A_{CO,0}}{A_{N_2,0}} - \frac{A_{CO,t}}{A_{N_2,t}}\right)}{F_{r,CO}}} \cdot \frac{1}{a} \cdot 100$$

Siendo a el número de moles del componente i producidos por cada mol de CO, $F_{r,i}$ el factor de respuesta del componente i y $F_{r,CO}$ el factor de respuesta del CO.

REFERENCIAS

[1] C.G. Visconti, G. Groppi, E. Tronconi. Chemical Engineering Journal 223 (2013) 224-230.

[2] O. Levenspiel, The Chemical Reactor Omnibook, OSU Book Stores Inc., Corvallis (USA) 1979.